UNIVERSITY OF CALIFORNIA
RIVERSIDE

Pyrolysis of Organic Molecules Relevant to Combustion as Monitored by Photoionization Time-of-Flight Mass Spectrometry

A Dissertation submitted in partial satisfaction
of the requirements for the degree of

Doctor of Philosophy

in

Chemistry

by

Kevin Howard Weber

August 2010

Dissertation Committee:
Dr. Jingsong Zhang, Chairperson
Dr. Yadong Yin
Dr. Chris Bardeen

The Dissertation of Kevin Howard Weber is approved:

_____

_____

_____

Committee Chairperson

ACKNOWLEDGEMENTS

Professor Jingsong Zhang
Professor Thomas Morton
Professor Eric Chronister
Jeff Lefler
Stan Sheldon
Dr. Dan Borchardt
Professor Fransisco Zaera
Professor Dave Bocian
Professor Leonard Mueller
Alan Nassimian
Wayne Kaylor
Daniel Adams
Dr. Kevin Simpson
Dr. David Hill
Dr. Rodney Jenks
Professor Yadong Yin
Professor Christopher Bardeen

DEDICATION

This work is dedicated to my family.

"In trust and believe that the time spent in this voyage…will produce its full worth in Natural History; and it appears to me the doing what little one can to increase the general stock of knowledge is as respectable an object of life, as one can in any likelihood pursue."

Charles Darwin, Voyage of the Beagle, 1799

…some few may devote themselves to increasing the stores of knowledge: the Lamp of Science must burn - "*Alere flammam*."

William Crookes, 1861

"It was a pleasure to burn."

Ray Bradbury, Fahrenheit 451

FIAT LUX

ABSTRACT OF THE DISSERTATION

Pyrolysis of Organic Molecules Relevant to Combustion as Monitored
by Photoionization Time-of-Flight
Mass Spectrometry

by

Kevin Howard Weber

Doctor of Philosophy, Graduate Program in Chemistry
University of California, Riverside, August 2010
Dr. Jingsong Zhang, Chairperson

Flash pyrolysis coupled to molecular beam extraction and single photon ionization time-of-flight mass spectrometry along with quantum chemical calculations are employed to study the pyrolysis of organic molecules with relevance to combustion processes. Branching ratios for the molecular elimination and bond fission pathways was achieved for ethyl and propyl iodides providing information about the nature of the mechanism with relation to chemical structure. Similarly, the decompositions of a series of alkyl methyl ethers, whose anti-knock ability in commercial fuels is attributed to the molecular elimination pathway, was investigated to examine the competition of primary and subsequent homolyses at higher temperatures, which tend to promote "knock". The isomerization/decomposition of isoprene was looked at in detail with special attention to the formation of soot precursor, most notably the "first ring" benzene. Cyclopentadiene and methylcyclopentadiene are known to be highly sooting fuels and were pyrolyzed to study the initial steps in aromatization. The pyrolysis of cyclohexene, cyclopentene, and 1,4-cyclohexadiene were conducted to facilitate interpretation of aromatic formation and

to compare experimental results with well established mechanisms. Finally, the pyrolysis of methylcyclohexane, an important component some jet fuels, was studied.

TABLE OF CONTENTS

LIST OF TABLES

LIST OF FIGURES

LIST OF SCHEMES

CHAPTER 1

INTRODUCTION

Radicals play an important role in variety of important processes such as pyroylsis/combustion, atmospheric chemistry, polymerization, and biochemistry. Unfortunately, they are typically highly reactive making their study difficult to achieve. Traditional experimental methods have made great advances in uncovering knowledge about such processes. Nevertheless, these methods are largely based on detection of stable end products and interpretation of intermediate steps of the mechanism with complex kinetics modeling.[1-3] Typical experimental methods include flow reactors and shock tubes, coupled with chromatographic and/or mass spectrometric detectors. Direct observation of intermediates using time-resolved spectroscopic methods has been the focus of more recent investigations.[4] Interpretation of the results from these methods is difficult due to the interference of other species in the spectral range of interest and the complexity of the reaction mechanisms. Computational methods have greatly aided the interpretation of these processes. Multi-reaction models can calculate concentration profiles if the rates of each reaction are known or can be estimated. Sensitivities of the concentration profiles to each reaction can be calculated and in this manner the most important reactions involved in the overall model can be elucidated. Accurate molecular geometries, heats of formation, and activation barriers can also be obtained from theory assisting identification of the lowest energy pathways available (thermal decompositions generally follow the lowest energy pathways). Ideally, direct and unambiguous detection

of all reaction intermediates and products and their concentration distributions in time would verify mechanistic details of the chemical reaction.

Characterization of the early stages of complex chemical reactions, particularly of the elusive "free" radical intermediates, can provide important information for verification of current models and discovery of previously unconsidered reaction mechanisms, thus providing a deeper understanding of the chemistry. In this work, the limitations of traditional methods are overcome with the employment of a high-temperature flash pyrolysis micro-reactor coupled with supersonic cooling and vacuum ultraviolet (VUV) photoionization mass spectrometry (TOFMS)[5,6] which enables the direct identification of the initial reaction intermediates, including the radical species. In order to understand the initial steps of a reaction it must be halted in a short amount of time with unequivocal detection of reactive intermediates and products. The approach described herein quenches the reaction by utilizing a fast-flow microreactor with a 20-100 μs residence time, followed by a "freezing" out of the reactive intermediates and products in a molecular beam. This results in the effectual isolation of the initial intermediates in a supersonic jet without any subsequent reaction and effects the decoupling of the key intermediates in the early time window from the rest of the reaction.

The technique was originally developed by Chen and co-workers[5] and has been demonstrated as a successful experimental approach. Briefly, the chemical moiety of

interest is “seeded” in an inert carrier gas which travels through a hot SiC tube where the thermal decomposition occurs. The heated mixture is then cooled upon expansion into a vacuum chamber from which a molecular beam is extracted where the intermediates, products and unreacted parent molecules can then be detected. With sufficient dilution in inert gas and short contact times, surface reactions can be minimized. A simple model indicates that under typical conditions <10% of the molecules (which are primarily carrier gas) in the heater would suffer surface collisions while the gas-phase collisions (~10^4-10^6 in the residence time) can efficiently transfer thermal energy inducing unimolecular dissociation of the precursors and limited bimolecular reactions, if the residence time is sufficiently long. Further studies at higher sample concentrations can be carried out to examine the bimolecular reactions.

The detection scheme in this work employs the usage of a time-of-flight mass spectrometer (TOFMS) that affords the determination of the molecular mass of each species produced by ionizing a chemical species and determining its mass/charge ratio. Most often mass spectrometers use a high-energy ionization source to maximize efficiency with broad applicability. The large amounts of internal (vibrational and electronic) energy installed in many resulting ions result in a significant amount of fragmentaion of the parent ion, thus complicating the spectra (while creating a “fingerprint”) and often the molecular ion in not the base peak or is not obvserved at all. In this work a vacuum ultra-violet (VUV) photoionization (10.5 eV) ionization source

imparts significantly less internal energy to the resulting parent ion (which is often the base peak or only significant peak observed) and allows the identification of free radicals produced upon thermolysis. This photon energy is sufficient to detect most of the polyatomic free radicals and all C3 and larger stable organic species with the exception of propane and butane.[7] This approach is powerful for the direct observation of reactive intermediates. This adventitious technique is herein employed to investigate the mechanisms for a variety of hydrocarbon pyrolyses.

Many chemical reactions are known to proceed to a significant extent by both radical and molecular processes. Such is the case in the thermal decomposition of alkyl iodides and alkyl methyl ethers. It is known that the nature of the alkyl group in these compounds can have tremendous influence on the degree of competition (branching ratios) for these processes. The true extent of one pathway versus another often remains unclear due the transient radicals. In the first portion of this dissertation the decomposition of ethyl and the propyl iodides are investigated to characterize the affect on branching ratios as a consequence of possessing a primary versus secondary alkyl group. Next, the pyrolysis of *tert*-amyl methyl ethers (TAME) and 2-methoxy trimethylbutane (MTMB) is explored to produce additional information on electronic versus field effects in thermolysis of tertiary methyl ethers. These experiments contribute valuable insight to the fundamental knowledge of how these reactions proceed as a function of the chemical structure and establish the reliability and utility of this technique.

The remainder of this work studies the production of aromatic compounds (particularly formation of the "first ring"), which are precursors of soot, from the pyrolysis of small fuel-like hydrocarbons, specifically isoprene (2-methyl-1,3,-butadiene), cyclohexene, 1,4-cyclohexadiene, cyclopentene, cyclopentadiene, and methyl-cyclopentadiene. Combustion has been a great ally for humans since we started kindling fires providing for heat in the cold, light in the dark, cooking of food, and more recently electricity. For a fuel to be desirable it must be high intensity, transportable, and controllable. Without question, the fossil fuels (hydrocarbons) best satisfy these descriptors. Today, with the incredible energy demands of the modern lifestyle, fossil fuels are the dominant source of energy to fill our need. In 2004 hydrocarbon combustion accounted for >80% of the total global energy budget and combustion will undoubtedly continue to be an important source of energy in the future. Unfortunately, the combustion of fossil fuels (hydrocarbons) produces pollution such as the greenhouse gas carbon dioxide, nitrogen and sulfur oxides (leading to acid rain, smog, and ozone), VOCs (volatile organic carbon compounds), and soot. The production of soot (and particulate matter) is of particular concern for several reasons. Although soot can be comprised of a complicated gallimaufry of compounds, at its core it is made up of polyaromatic hydrocarbons (PAHs) which can be carcinogenic (*e.g.* benzo (a) pyrene). The role of high exposure to soot as a cause of cancer in adolescent chimney sweeps was first noted by Percival Potts in London in 1775.[8] Recently, studies in the US[9-11] and UK[12] have found a range of carcinogenic PAH originating primarily from vehicle emissions.

Additionally, soot can strongly absorb solar radiation.[13] It was proposed in 2000 that the fastest way to fight global warming is the reduction of black carbon, methane, and other warming pollutants which can be more easily controlled than CO_2.[14] A recent assessment of the contribution to global warming from black carbon estimates the forcing to be 0.9 watts per square meter, which is a larger contribution than methane and about 55% of that from CO_2.[15] Jacobson contends that up to 30% of global warming could be controlled if you could control soot.[16] Lastly, soot formation represents an inefficient use of the fuel.

Despite extensive study, the fundamental mechanisms and basic chemistry of hydrocarbon combustion, even in the early stages of pyrolysis and oxidations, needs further improvement.[1-4,17-19] In this work the direct observation of initial reactive intermediates is accomplished by the powerful experimental approach of coupling flash pyrolysis of the compound of interest with subsequent cooling and isolation in a supersonic beam and analysis by VUV-MS, which can detect radicals and limits fragmentation.

REFERENCES

[1] W. C. Gardiner Jr. (Ed.), Combustion Chemistry, Springer-Verlag, New York, 1984.

[2] W.C. Gardiner Jr. (Ed.), Gas-phase Combustion Chemistry, Springer-Verlag, New York, 2000.

[3] J. Warnatz, U. Maas, R. W. Dibble, Combustion, Springer-Verlag, Berlin, 1996.

[4] J. A. Miller, G. A. Fisk, Chem. Eng. News 65 (1987) 22.

[5] D. W. Kohn, H. Clauberg, P. Chen, Rev. Sci. Instrum. 63 (1992) 4003.

[6] J. Boyle, L. Pfefferle, J. Lobue, S. Colson, Combust. Sci. and Tech. 70 (1990) 187.

[7] S. G. Lias, J. E. Bartmess, J. F. Liebman, J. L. Holmes, R. D. Levin, W. G. Mallard, Gas-Phase Ion and Neutral Thermochemistry, American Chemical Society, New York, 1988.

[8] R. F. Sawyer, Eighteenth Symposium (International) on Combustion (1981) 1.

[9] B. A. Benner Jr., G. E. Gordon, S. S. Wise, Environ. Sci. Technol. 23 (1989) 1269.

[10] L. M. Hildemann, G. R. Markowski, G. R. Cass, Environ. Sci. Technol. 35 (1991) 744.

[11] W. F. Rogge, L. M. Hildemann, M. A. Mazurek, G. R. Cass, B. R. T. Simoneit, Environ. Sci. Technol. 27 (1993) 636.

[12] R. M. Harrison, D. J. T. Smith, L. Luhana, Environ. Sci. Technol. 30 (1996) 825.

[13] J. Quaas, Science 32 (2009) 153.

[14] J. Hanson, M. Sato, R. Ruedy, A. Lacis, V. Oinas, Proc. Natl. Acad. Sci. USA 97 (2000) 9875.

[15] V. Ramanathan, G. Carmichael, Nature Geosci. 1 (2008) 221.

[16] M. Z. Jacobson, Science 409 (2001) 695.

[17] R. W. Walker, 22nd Int. Symposium on Combustion (Combustion Institute, Pittsburgh) (1989) 883.

[18] R. W. Walker, Sci. Prog. 74 (1990) 163.

[19] H. Brockhorn (Ed.), Soot Formation in Combustion, Springer-Verlag, New York, 1994.

CHAPTER 2

EXPERIMENTAL

Thermal decomposition experiments were accomplished in an apparatus that is schematically depicted in Figure 2.1. It makes use of a Wiley-MacLaren type linear time-of-flight mass spectrometer (TOFMS, model D-651, R. M. Jordan Company[1] to monitor pyrolysis products by means of 118.2 nm (10.48 eV) photoionization. A typical resolution (m/□m) obtained with this instrument has been assessed to be = 200 at *m/z* 150.[2] The main reactor chamber is pumped by a cryobaffled Varian VHS-6 diffusion pump, and the mass spectrometer is differentially pumped by means of a turbomolecular pump. Pyrolyses were carried out by expanding the parent molecules, seeded in inert carrier gas (typically helium or argon), via a heated silicon carbide tube (1 mm i.d., 2 mm o.d., Carborundum Corp) through a pulsed valve into the photoionization region of the mass spectrometer, similar to the apparatus described by Chen and coworkers.[3] The silicon carbide tubing was attached to a machinable piece of alumina by use of a high temperature ceramic adhesive (Cotronics Corporation) that had a 2 mm i.d. channel to allow the gas flow from the pulsed valve to the silicon carbide tube and was mounted to the faceplate of a General Valve series 9 pulsed valve operating at 10 Hz. The alumina isolates the silicon carbide microreactor both thermally and electronically from the pulsed valve and was sandwiched between the faceplate and a MACOR disk to provide additional stability. Two graphite electrodes (Poco Graphite) separated by ~1 cm were press-fitted onto the silicon carbide tubing and were heated resistively. The electrical

current was controlled by a Variac transformer and light bulbs hooked in parallel served as current limiters.

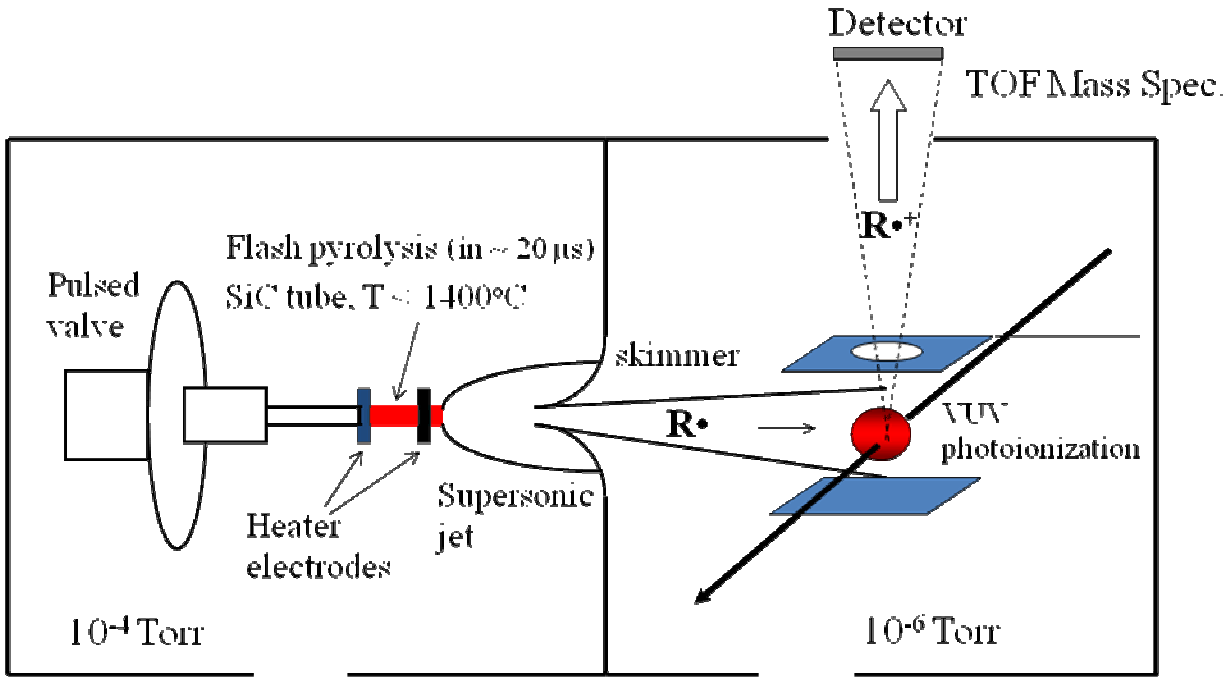

Figure 2.1 Schematic of the photoionization time-of-flight mass spectrometer.

Nominal temperature was measured using a type C thermocouple (Omega) wrapped around the outside of the heated portion of the silicon carbide nozzle. A temperature calibration curve was plotted by inserting a thermocouple insulated with ceramic adhesive into the heated nozzle and comparing that reading ($T_{internal}$) with the nominal temperature ($T_{nominal}$), which gives the empirical relation $T_{internal}$ (in ˚C) = 1.38 $T_{nominal}$ -200˚C for $T_{nominal} \geq$ 400˚C. Heat dissipation by the inserted thermocouple may have a greater cooling effect than the gas pulse, so the calibration equation represents

only a best approximation, and nominal temperatures reported are believed to be accurate to within 50 K. With a near sonic velocity of the sample within the nozzle, the residence time in the heater has been estimated to be approximately 20μs when helium is utilized as the carrier gas.[3]

The possibility of heterogeneous catalysis occurring on the SiC surface is a complication with flash pyrolysis nozzles of this type. The issue was addressed by Peter Chen with the pyrolysis of *t*-butyl nitrite,[4] $(CH_3)_3CONO$, which under homogeneous pyrolysis conditions decomposes to *t*-butoxy radical and NO by cleavage of an O-N bond. Heterogeneous decompositions can cleave the C-O bond producing *t*-butyl radical and NO_2, which were not observed. It was therefore concluded that the flash pyrolysis in the system proceeds primarily as a homogeneous process. Nevertheless, the contribution of heterogeneous processes cannot be neglected. For example, it was discovered that kinetic parameters are not reproduced accurately with this method.[2] Pyrolysis reactions with well-defined activation energies were investigated with this experimental apparatus and Arrhenius plots constructed in order to compare the experimental activation energies to literature values. The result of this investigation revealed that the experimentally obtained activation energies were ~60-70% of literature values. This result is a clear indication that heterogeneous catalysis on the SiC surface is attenuating the activation energies. Due to these considerations, the flash pyrolysis technique described in this body of work is best relied on for qualitative mechanistic insight.

Short residence times in the microreactor are achieved by maintainging a near sonic flow velocity throught the SiC tube. This occurs by supersonic injection of the gas pulse into the tube. This expansion occurs upon increase in the cross-sectional area between the pulsed valve faceplate orifice (0.75 mm) and the SiC tube (1.0 mm I. D.), similar to the nozzle and test section of a supersonic wind tunnel.[5] Supersonic flow cannot be maintained throughtout the SiC tube, but a series of expansions and compressions within the tube maintains an average flow velocity which is approximately sonic. With a high enough initial stagnation pressure, the pressure at the end of the tube is sufficient to expand into the vacuum chamber as a supersonic jet. The characteristics of this expansion resemble those occurring from a capillary tube, with a large length to diameter ratio, which has been found to be similar to a sharp edged orifice.[6] Although no cross-sectional change occurs at the tube exit, wall friction or heat transfer can achieve flow choking in a capillary nozzle, and sonic velocity is reached just before the tube exit.

Chen and coworkers[3] tested the difference in pulse width and velocity exiting both the bare pulsed valve faceplate and with a pyrolysis nozzle attached and found little or no difference between the two above 1.0 atmosphere stagnation pressure. From these results, they conclude that the flow velocity within the tube is near sonic, and the contact time within the tube can be easily estimated. The residence time within the pyrolysis region of our source was estimated to be ~ 20μs with helium as the carrier gas.

After exiting from the heated zone the unreacted precursor and its products are cooled by supersonic expansion. The degree of cooling increases with the mass of the carrier gas, and the rotational temperature of molecules in the jet after expansion has been ascertained to be ≤ 50 K by Chen and coworkers[7,8] by means of multiphoton ionization (the vibrational temperature tends to be higher). The present studies primarily utilize argon as the carrier gas providing the best balance of cooling and signal intensity/quality.

The use of a supersonic molecular beam coupled to flash pyrolysis in the apparatus used in these experiments allows for the isolation of the molecules under study. A molecular beam is extracted from an underexpanded, supersonic expansion from a high-pressure reservoir to a low-pressure region. The same type of expansion occurs from converging-diverging supersonic rocket nozzles. It is now possible to extract molecular beams from the core of expanding gas flow where the internal energy content of the molecules have been reduced to extremely low values without massive condensation. The molecular populations are then concentrated into one or a few internal states preparing coherent states excellent for characterization.

The unique properties of molecular beams are due to the supersonic nature of the gas resulting in an underexpansion described below. The gas starts from a negligible

small velocity, referred to as the stagnation state (P_0,T_0). The pressure gradient from the initial pressure (P_0) to the background pressure (P_b) causes acceleration of the gas flow towards the source exit. This flow can be approximated as isentropic, neglecting viscosity and heat conduction effects. The gas can reach the speed of sound at the source exit when the ratio of the reservoir pressure to background pressure, P_0/P_b, becomes greater than

$$G \equiv [(\gamma+1)/2]^{(\gamma/(\gamma-1))}$$

where γ is the ratio of heat capacities at constant pressure versus constant volume, C_p/C_v. Alternatively, if the pressure ratio is less than this critical value, the flow will exit subsonically, with an exit pressure nearly equal to P_b, without any further expansion. As the ratio P_0/P_b increases to be greater than G, the exit pressure becomes independent of the background pressure, P_b, and is therefore considered to be "underexpanded".

There are two characteristic features of supersonic flow. First, in a supersonic expansion beyond the source exit as the flow area increases so does the velocity of the flow, in contrast to subsonic flow. Second, supersonic flow cannot "sense" downstream conditions due to the supersonic nature. Essentially, particles traveling in the same direction with the same velocities do not interact with each other. Thus, the flow does not know the boundary conditions, yet it must adjust. Eventually, collisions with the background gas in the expansion chamber will reduce the molecular beam flow to subsonic velocity where in the flow can adjust to boundary conditions. This results in

shock waves, very thin nonisentropic regions of large density, pressure, temperature, and velocity gradients. The location of these shock waves depends on the P_0/P_b pressure ratio and the nozzle diameter, d. The region where the first shock wave appears downstream from the nozzle is known as the "Mach disk", and the region where the expansion creates supersonic flow is called the "zone of silence". The Mach disk is found at

$$x_m/d = (2/3)(P_0/P_b)^{\wedge}(1/2)$$

which is in units of nozzle diameters. To take advantage of the supersonic expansion properties a "skimmer", a hollow cone with a small aperture at the top, is placed in the zone of silence to isolate the supersonic portion of the beam before it collapses at the Mach disk. The skimmed portion of the beam is then directed into a differentially-pumped high-vacuum region where it is not significantly affected by the background gas and continues to be supersonic.

Products of thermolysis were analyzed by time-of-flight mass spectrometry. The analytical mass spectrometer consists of a sample inlet, ion source, mass analyzer, and detector connected to a data system to collect and process the data collected. Mass spectrometers cannot directly detect analyte molecules, only the ionized counterparts and therefore ionization methods are of particular importance to MS.[9] Analytes are ionized by single photon ionization (SPI) with a wavelength of 118.2 nm (10.5 eV) by using the third harmonic (355 nm) of a Nd:YAG laser with subsequent frequency tripling using a low pressure (20-80 Torr) Xe cell which was directly attached to the vacuum chamber.[10]

The vacuum ultraviolet (VUV) radiation was focused with a MgF_2 lens through an aperature into the photoionization zone while the fundamental 355 light diverged in that region. The intensity of the VUV light was maximized by measuring the photoionization current of NO (IE=9.2 eV) in an ionization cell located at the back of the chamber. The ion current produced was measured as a voltage drop between two electrode plates within this cell, biased at 0 and +180 volts. The molecular beam the incipient VUV photon we aligned and the signal optimized by adjusting the positions of the 355 nm focusing lenses and the molecular beam nozzle, and by varying the delay time from the initial gas pulse and the triggering of the laser so as to give a maximum intensity mass peak when running pure NO (*m/z*=30).

For ionization of a neutral molecule to occur an energy must be conferred that is equal to or greater than the ionization energy (IE) for that moiety. The IE is defined as the minimum amount of energy which has to be absorbed by an atom or molecule in its electronic and vibrational ground states by ejection of an electron.[11] Most molecules have an IE in the range of 7-15 eV. The IE is the bare minimum energy required for ionization of a molecule. Therefore, in the case of electron impact (EI) ionization, the classical ionization method for molecules having mass up to ~500 a.m.u., impacting electrons need to carry at least this amount of energy. Of course, for ionization to occur the energy of the electron would have to be transferred quantitatively. Such an event is of low probability and the ionization efficiency is close to zero when electrons have only

the energy of the analyte IE. Every molecule has an ionization efficiency curve of its own depending on the ionization cross section for that species. The ionization cross section (given in units of square-meters) describes the area through which the impacting particle must travel in order to effectively interact with the neutral of interest. When a molecule is ionized some of the energy transferred is transformed into external degrees of freedom, translational and rotational motion. Almost no molecular ions will be generated in the vibrational ground state. The preponderance of the ions created are vibrationally excited and many are above the dissociation energy level. Dissociation of the molecular ion leads to the formation of fragment ions.

To maximize ionization efficiency electrons of 70-eV of kinetic energy are commonly employed[12] in EI/MS. However, ionization with such as large amount of energy is a "hard" ionization technique as analytes tend to be heavily fragmented upon ionization. The molecular peak is often barely visible (if detected at all) which can impair the identification of unknowns. This occurrence resulted in a demand for fragmentation-minimized or "soft" ionization techniques such as single photon ionization (SPI). Photoionization is the photoinduced excitation of an electron into the ionization continuum and the escape of the electron thus freed from the atomic or molecular core. When photoionization occurs by absorbing a single photon, the photon energy of the applied intensity radiation must exceed the IE of the system. SPI with vacuum ultra-violet (VUV) radiation is capable of ionization of all organic compound classes,

including the saturated alkanes C3 or greater with the exceptions of propane and butane. The performance of VUV light sources is critical for SPI-MS as the average cross section for SPI is only 2-20 megabarn (Mb = $10^{-18}cm^2$) which is approximately 1/100 of the typical cross section for 70 eV EI MS. Despite this fact, the limits of detection (LODs) for SPI MS are similar to those observed with EI. This is the result of heavy fragmentation under EI with the most intense ion carrying a low fraction of the total ion current. In contrast, SPI shifts the signal intensity to the molecular ion peak, which can gain an order of magnitude in sensitivity. Additionally, high energy EI has a large amount of chemical noise. Multiple analyte fragment ions are generated with EI, as mentioned previously, and bulk gas matrix (carrier gas, air, etc.) is ionized. Low-energy mass spectra are typically easier to interpret due to the enhancement of the molecular ion, minimized fragmentations, and a fragmentation pattern dominated by a few characteristic primary fragmentations carrying large portions of structural information. Unfortunately, disadvantages include decreased ionization efficiency corresponding to loss of sensitivity and memory effects from slow desorption of sample from surfaces.

A potential limitation of this experimental apparatus is the occurrence of electron-impact ionization (EI) resulting from photoelectrons produced by scattered light within the photoionization region. Efforts to eliminate this occurrence have been made[10] such as minimizing the 355 nm spot size and masking the photoionization region from the diverging 355 nm beam. The efforts to completely eliminate the occurrence of EI

resulted in the loss of photoionization signal as well. A compromise was made to minimize the EI contribution while retaining sufficient photoionization signal. 1,3-butadiene was used to estimate the extent of EI in this system by comparison with the EI fragmentation pattern from Dannacher[7] and EI was assessed to contribute to ≤ 1% of the overall signal.

The extent of multi-photon ionization (MPI) has also been considered. Large fluencies are required to initiate a measurable MPI signal, thus due to the divergence of the 355 nm light in the photoionization region, multi-355 nm is not likely. MPE with 118 + 355 nm photons (14.0 eV) is also unlikely due to the negligible fragmentation of the room temperature spectrum of 1,3-butadiene.[2] Photoionization fragmentation of 1,3-butadiene at this energy would also result in the formaton of peaks such as *m/z* 28, 39, and 53 peaks,[13,14] with *m/z* 39 likely being the 100% ion peak (at 21.22 eV PI, *m/z* 39 is the molecular ion). All these factors indicate that the occurrence of EI and MPI are minimized in this experimental regime.

Upon ionization by the ion source an applied potential (V) accelerates the ion with charge = q into a field free drift region. The kinetic energy imparted to the ion is equal to the product of the voltage and the charge, K.E. = qV = $(1/2)mv^2$ (where m is mass and v is velocity). In the case of SPI, the charge will be unity, that is to say a positive charge with the magnitude of an electron. Considering that the velocity is

simply the distance (d) traveled per unit of time (t), it is easy to convert the signal ion current with time-of-flight (t_f) information to the mass of the ion, a Jacobian transformation. Including a small delay time delay (t_d) factor due to the time accelerating before entering the field free drift tube the observed time domain can be expressed by the simple equation, $t = t_f + t_d = \alpha m^{1/2}$. Ion current was monitored by a micro-channel plate detector and data was averaged with a Textronix TDS3032 digital oscilloscope (300MHz) averaged over 512 laser shots. The sampling rate was 10 Hz. and the molecular beam pulse width was 200 μs.

REFERENCES

[1] D. M. Lubman, R. M. Jordan, Rev. Sci. Inst. 56 (1985) 373.

[2] S. D. Chambreau, Free Radical Production and Thermal Decomposition Mechanisms of Small Molecules by Flash Pyrolysis, University of California, Riverside, Ph. D. Thesis (2002).

[3] D. W. Kohn, H. Clauberg, et al., Rev. Sci. Inst. 63 (1992) 4003.

[4] P. Chen, S. D. Colson, et al., Chem. Phys. Lett. 147 (1988) 466.

[5] H. Danseshyar, One-Dimensional Flow, Pergamon, New York 1976.

[6] G. Scoles, Atomic and Molecular Beam Methods, Oxford University Press, New York, 1988.

[7] P. Chen, S. D. Colson, et al., J. Phys. Chem. 90 (1986) 2319.

[8] H. Clauberg, D. W. Minsek, et. al., J. Amer. Chem. Soc. 114 (1992) 99.

[9] L. Hanley, R. Zimmermann, Anal. Chem. 81 (2009) 4174.

[10] S. D. Chambreau, J. Zhang, et al., Int. J. Mass Spec. 199 (2000) 17.

[11] J. H. Gross, Mass Spectrometry – A Textbook, Springer, New York, 2004.

[12] K. Vekey, J. Mass Specrom. 31 (1996) 445.

[13] J. Dannacher, J. Flamme, et al., Chem. Phys. 51 (1980) 189.

[14] L. Sellers-Hahn, R. E. Drailler, et al., J. Chem. Phys. 89 (1988) 889.

CHAPTER 3

ALKYL IODIDE PYROLYSIS

INTRODUCTION

The thermal decomposition of ethyl and propyl iodides, along with select isotopomers, up to 1300 K was performed by flash pyrolysis with a 20-100 μs time scale. The pyrolysis was followed by supersonic expansion to isolate the reactive intermediates and initial products, and detection was accomplished by vacuum ultraviolet single photon ionization time-of-flight mass spectrometry (VUV-SPI-TOFMS). The products monitored, such as CH_3, CH_3I, C_2H_5, C_2H_4, HI, I, C_3H_7, C_3H_6, and I_2, provide for the simultaneous and direct observation of molecular elimination and bond fission pathways in ethyl and propyl iodides. In the pyrolysis of ethyl iodide, both C-I bond fission and HI molecular elimination pathways are competitive at the elevated temperatures, with C-I bond fission being preferred; at temperatures ≥ 1000 K, the ethyl radical products further dissociate to ethene + H atoms. In the pyrolysis of *i*-propyl iodide, both HI molecular elimination and C-I bond fission are observed and the molecular elimination channel is more important at all the elevated temperatures; the *i*-propyl radicals produced in the C-I fission channel undergo further decomposition to propene + H at temperatures ≥ 850 K. In contrast, bond fission is found to dominate the *n*-propyl iodide pyrolysis; at temperatures ≥ 950 K the *n*-propyl radicals produced decompose into methyl radical + ethene and propene + H atom. Isotopomer experiments characterize the extent of surface

reactions and verify that the HI molecular eliminations in ethyl and propyl iodides proceed by a 1,2 elimination mechanism as opposed to a 1,1 elimination.

The dehydrohalogenation of alkyl halides have been extensively studied[1] and are initiated by either homolytic fission of the carbon-halogen bond or 1,2 intramolecular elimination (ε_i). Although alkyl fluorides are resistant to dehydrohalogenation, alkyl chlorides and bromides form alkene and hydrogen halide cleanly over intermediate temperatures, predominately by 1,2-ε_i, a process that continues to attract theoretical interest.[2-4] Alkyl iodide pyrolysis has proven more complicated than for other alkyl halides, long being known to produce a melange of alkene, alkane, and molecular iodine.[5] The saturated compound and iodine are formed by the fast reaction of hydrogen iodide and radicals with alkyl halide. The weaker C-I bond results in greater competition between bond fission and ε_i initiation events.

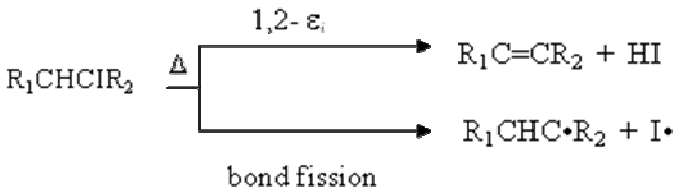

Scheme 3.1 Schematic depicting initiation events in the pyrolysis of alkyl halides.

The first quantitative kinetic measurements for the thermal decomposition of alkyl iodides were made by Ogg and Jones for *iso*-propyl[6] and *n*-propyl[7] iodides. *Iso*-propyl iodide was found to obey first order kinetics, and although both radical and molecular mechanisms were postulated, at that time the relative contributions of bond fission and molecular elimination were not accessible. However, in a subsequent study of bond dissociation energies for organic iodides, Butler and Polanyi[8] interpreted their results by considering both bond fission and molecular elimination pathways as partially rate determining. In contrast to *iso*-propyl iodide, *n*-propyl iodide decomposed with a rate law order of 1.5 (rate = $k[CH_3CH_2CH_2I][I]^{0.5}$) indicating the importance of radical chemistry. Later, Benson and co-workers[9-21] studied extensively the pyrolysis of alkyl iodides and believed the rate-determining step to be formation of hydrogen iodide. The rate law for *n*-propyl iodide being of order 1.5 was then understood as HI formation resulting from secondary hydrogen abstraction by an iodine atom following bond fission. They confirmed that *iso*-propyl iodide has a first order rate law[17] and undergoes elimination faster than iodine atom attack. The change in mechanism is explained in terms of (1) a stronger primary C-H bond, rendering H abstraction less facile and (2) attenuation of the activation energy for the molecular elimination. Although a true carbocation does not form in the gas phase, a strong correlation between heterolytic bond energies and activation energies for 1,2-ε_i has been demonstrated.[22] The semi-ion transition state[20,21] is highly polar and carbocation character is stabilized by polarizable alkyl groups, in a situation akin to the regioselectivity observed in (the reverse reaction) Markovnikov addition to alkenes. This is illustrated by the α-CH_3 effect,[20] where it was

documented that each additional α-CH_3 results in an ~25 ± 4 kJ/mol reduction of activation energy for dehydrohalogenation. Ethyl iodide also decomposes according to a first order rate law.[18] Benson et al. believed that, although "surprising" due to being a primary alkyl halide, the pyrolysis of ethyl iodide was completely consistent with the rate determining step being molecular elimination, yet they did not exclude the possibility of up to 20% radical dispropriation. It was argued at this time that the pyrolysis of alkyl iodides proceeded primarily by either one of two mechanisms, a radical mechanism, associated with primary iodides (except ethyl iodide), or 1,2-ε_i, associated with secondary and tertiary iodides.

Yang and Conway[23] attempted first to separate measurements of bond fission and molecular elimination rates for alkyl halides with ethyl iodide using a toluene flow technique over the temperature range of 660 – 794 K. They argued that ethyl radicals created immediately reacted with toluene in the flow system and by monitoring the production of ethene and ethane, both rates were elucidated. Their work indicated approximately 70% of the reaction proceeded via bond fission over this temperature range. The work was considered inconclusive,[24] and it was suggested that the bond fission pathway may contribute only ~2-20%. In comparison, more recently both Herzler and Frank[25] and Mertens et. al[26] considered the molecular elimination pathway to be negligible. The pyrolysis of ethyl iodide was recently studied by Kumaran et. al[27] with a shock tube coupled to atomic resonance absorption spectrometry (ARAS), directly

observing H atoms over the temperature range of 1080-2020 K and iodine atoms over the temperature range of 946-2046 K. Using the directly measured bond fission rates analyzed with RRKM statistical theory and available experimental data, they demonstrated that the reaction proceeds predominantly via the radical mechanism (C-I fission) with a branching fraction of 0.87 ± 0.11 in relation to molecular elimination. The resulting ethyl radical is unstable (in fact, this reaction has been used as a H atom source) and rapidly decomposes to ethene and H atom. The most recent study on the pyrolysis of ethyl iodide was by Miyoshi et. al,[28] also using a shock tube coupled to ARAS detection of I atoms in the temperature range of 950-1400 K with analysis by RRKM statistical theory. They reported a C-I fission branching fraction of 0.92 ± 0.06, in good agreement with that by Kumaran et. al.[27]

King,[19] under Benson, reported the very low pressure pyrolysis (VLPP) for *n*-propyl and *iso*-propyl iodides in 1971. In the VLPP experimental regime the *n*-propyl radicals rapidly decompose to form methyl radical and ethene. By monitoring the rates of propene and ethene formation kinetic parameters for both 1,2-ε_i and C-I bond fission were elucidated for *n*-propyl iodide, while the decomposition of *iso*-propyl iodide was considered to proceed completely by 1,2-ε_i. The decomposition of C3 and C4 alkyl iodides have been recently examined by Miyoshi et. al[28] using a shock tube coupled to ARAS detection of I atoms over the temperature range of 950–1400 K. They determined the C-I bond fission branching ratios of 0.6-0.9 for primary iodides, 0.2-0.4 for secondary

iodides, and <0.05 for tertiary iodides. Specifically for *n*-propyl iodide, the C-I fission branching fraction is 0.74 ± 0.05 and has no temperature dependence, while the value for *iso*-propyl iodide is in the range of 0.3-0.4, with a slight temperature dependence. Their results were consistent with the semi ion-pair model for the molecular elimination transition state.[28]

Despite the large amount of work on the pyrolysis of alkyl iodides, direct experimental observation of both the molecular elimination and bond fission pathways has not been reported. The experimental approach of flash pyrolysis coupled to supersonic expansion and vacuum ultraviolet (VUV) photoionization mass spectrometry provides short reaction times to examine the initial steps of pyrolysis, supersonic cooling to minimize recombination and reactions of products and intermediates, and minimized ion fragmentation due to the low ionization photon energy.[29-32] More importantly, the bond fission and molecular elimination pathways in the initial stage of pyrolysis can be directly observed *simultaneously* in this work, with minimum complication from subsequent reactions

EXPERIMENTAL

Ethyl iodide (99+%) was obtained from Aldrich, *n*-propyl iodide (99+%) and *i*-propyl iodide (98+%) were from Acros Organics. Perdueterated ethyl iodide (99+%) was obtained from Jansen Chimica and the mixed isotopomers of ethyl iodide (98+%) and

propyl iodide (99+%) from CDN Isotopes. The compounds studied were used without further purification and diluted to 1-4% in argon or helium by bubbling the noble carrier gas through the liquid at ethylene glycol/dry ice or ice/water bath temperatures. The backing pressure of the gas mixture was maintained at ~ 1.5 atm for all experiments.

RESULTS

(1) Ethyl Iodide (CH_3CH_2I, CH_3CD_2I, CD_3CH_2I, and CD_3CD_2I)

Stack plots of mass spectra for the low temperature pyrolysis of CH_3CH_2I, (2%) in argon carrier gas and (12%) in helium, are presented in Figures 3.1 (a) and 3.1 (b), respectively. Mass spectra for the high temperature pyrolysis of CH_3CH_2I in argon and helium (at the same concentrations) are presented in Figures 3.2 (a) and 3.2 (b). The mass spectra for the pyrolysis of isotopomers, CH_3CD_2I (2%) in argon, CD_3CH_2I (4%) in helium, and CD_3CD_2I (2%) in argon, are shown in Figure 3.3 (a), (b), and (c), respectively. In Figure 3.1 (a), the spectral traces have heater temperatures of 295, 645, 770, 790, 810, and 840 K. At room temperature a large peak at *m/e* 156 due to molecular ion of the parent C_2H_5I [ionization energy (IE) = 9.33 eV[35]] is observed, with a small photofragment peak at *m/e* 29. The reported appearance energy (AE) of the $CH_3CH_2^+$ photoionization fragment from C_2H_5I is 10.44 eV,[36] close to the VUV photon energy. At a temperature of 645 K an attenuation of signal is caused by a drop in number density upon heating. As the temperature is increased to 770, 790, 810, and 840 K, peaks at *m/e* 127 and 128 corresponding to iodine atom and hydrogen iodide are clearly discernible

and drastically rise in intensity. Since the appearance energy of I^+ at *m/e* 127 from C_2H_5I is 14.8 eV,[37] this peak is therefore a result of ionization of iodine atom (IE = 10.45 eV)[38] produced by homolytic cleavage of the C-I bond of C_2H_5I with a bond energy of ~52.0 kcal/mol.[27,39] The AE for HI^+ is 11.7 eV,[37] too large to be observed as a photofragment in this system, and therefore the peak at *m/e* 128 is also due to photoionization of neutral HI created by thermolysis of C_2H_5I. The peak at *m/e* 29 increases in

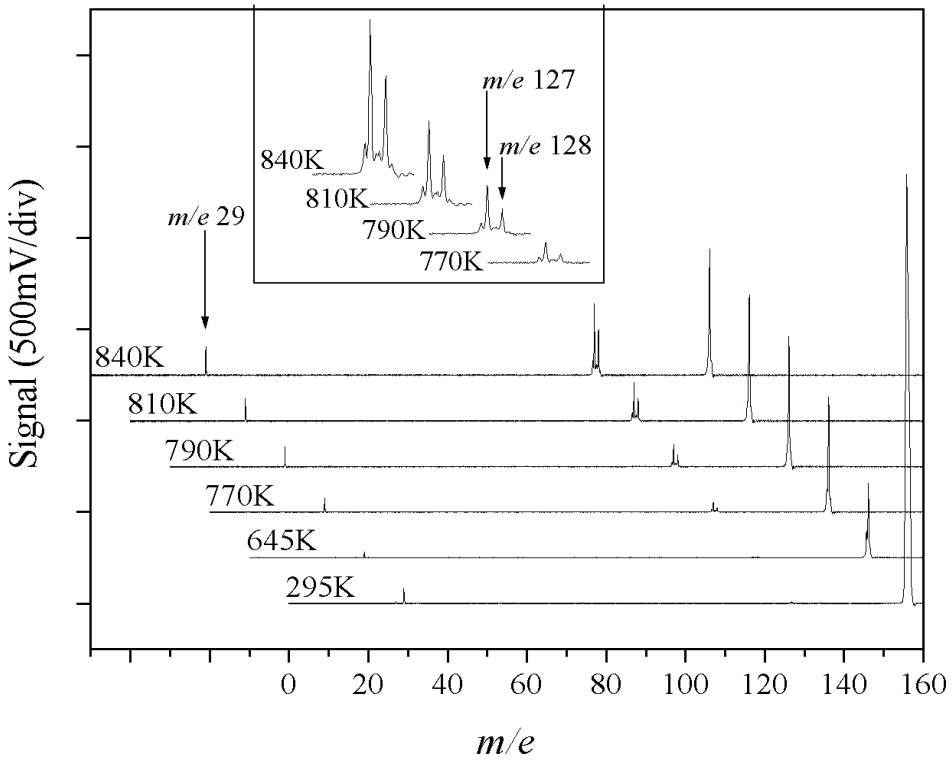

Figure 3.1 (a) Stack plot of mass spectra for pyrolysis of CH_3CH_2I (2%) in argon with internal nozzle temperatures from room temperature (295K) to 840K.

intensity over this temperature region. Direct photoionization of the neutral ethyl radical product in the C-I fission is readily accomplished in this system (IE = 8.12 eV[40]); however, $C_2H_5^+$ fragment due to photoionization fragmentation of C_2H_5I could also

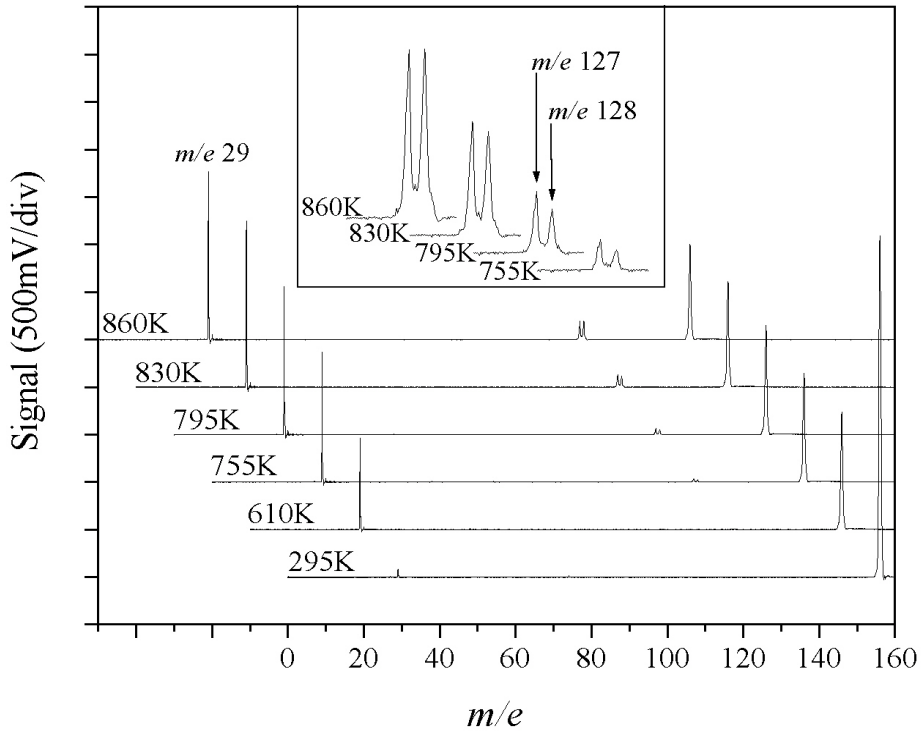

Figure 3.1 (b) Stack plot of mass spectra for pyrolysis of CH_3CH_2I (12%) in helium with internal nozzle temperatures from room temperature (295K) to 860K. The mass spectra are shifted for clarity.

contribute to the *m/e* 29 signal. An additional consideration is that ethyl radicals rapidly decompose[27] into H atom (not detectable in this apparatus) and ethene which has an IE = 10.514 eV,[41] slightly higher than the ionization photon energy and not detectable in this modest temperature range. Figure 3.1 (b) is for CH_3CH_2I (12%) in helium at heater temperatures of 295, 610, 755, 795, 830, and 860 K. At a temperature of 295 K, a strong molecular ion peak is detected at *m/e* 156 along with a small $CH_3CH_2^+$ photofragment at *m/e* 29 having a similar relative intensity to the molecular ion observed in the argon entrained sample (Figure 3.1 (a)). As the nozzle is heated to an internal temperature of 610 K, the molecular ion peak at *m/e* 156 decreases to less than half of the room temperature intensity with concomitant growth of the *m/e* 29 peak. The intensity of the *m/e* 29 peak is nearly equal to the *m/e* 156 peak in the helium data. In contrast, for the corresponding trace in argon carrier gas, *m/e* 29 is small. At the temperature of 755 K, the parent peak *m/e* 156 remains approximately the same intensity as in the 610 K trace while the peak at *m/e* 29 surpasses the *m/e* 156 peak. Small peaks at *m/e* 127 and 128 are now discernible, correlating to thermally produced I atom and HI. The peak at *m/e* 128 is approximately two thirds the intensity of *m/e* 127. As the nozzle is further heated to temperatures of 795, 830, and 860 K, the intensity of the *m/e* 156 parent decreases slightly. The peak at *m/e* 29, now comprised of the photoionization fragment of the hot parent molecule and thermally produced ethyl radical, is found to slightly increase while the peaks at *m/e* 127 and 128 exhibit significant increases in intensity. The peak at *m/e* 128 experiences a great increase in intensity and at 860 K it is slightly larger than the peak at *m/e* 127.

Figure 3.2 (a) presents the pyrolysis of CH_3CH_2I (2%) in argon at higher heater temperatures of 865, 925, 995, 1020, and 1115 K. At 865 K the molecular ion decreases in intensity while the signal at *m/e* 29, 127, and 128 all increase. The relative intensity of *m/e* 128 compared to 127 is observed to be approximately equal. As the temperature is raised to 925, 995, 1020, and then 1115 K, the parent peak continues to decrease, as does the *m/e* 29 signal. At these higher temperatures the parent compound rapidly

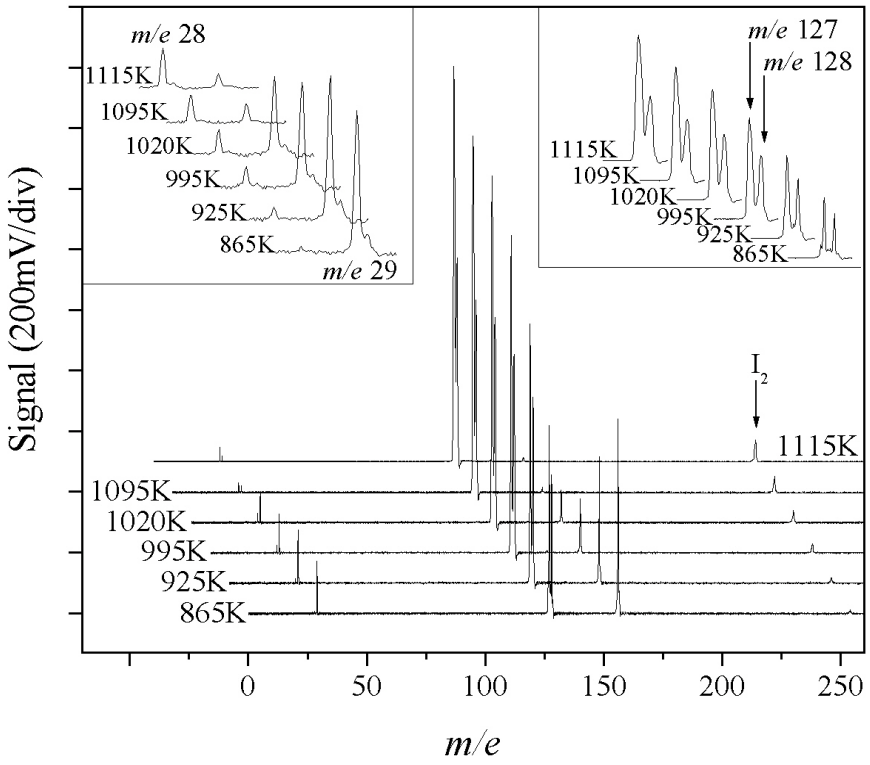

Figure 3.2 (a) Stack plot of mass spectra for pyrolysis of CH_3CH_2I (2%) in argon with internal nozzle temperatures from 865 K to 1115 K.

decomposes, and at temperatures of 1020 K or greater, none survives. As the parent compound is pyrolyzed, the contribution of photoionization fragmentation at *m/e* 29 is reduced, but that due to thermolysis ethyl products should increase. However, as mentioned previously, ethyl radicals rapidly decompose and at higher temperatures little *m/e* 29 is detected. Over this temperature range the intensity of *m/e* 128 relative to *m/e* 127 steadily decreases, and peaks at *m/e* 28 and 254 appear corresponding to products ethene and molecular iodine, respectively. Although the IE for ethene is slightly higher than the

photoionization energy, at these high temperatures cooling becomes less complete and enough internal energy content may remain for a "warm" molecule of ethene to be detected.

Figure 3.2 (b) is for CH_3CH_2I (12%) in helium at higher temperatures of 930, 975, 1030, 1090, 1140, and 1210 K. At 930 K the intensity of *m/e* 29 is approaching double that of the parent compound at *m/e* 156. The intensities of *m/e* 127 and 128 are now both approximately one third of the *m/e* 156 molecular ion. A small new peak at *m/e* 254 is detected, resulting from the formation of molecular iodine, I_2. With a nozzle temperature of 975 K the intensity of parent *m/e* 156 decreases slightly, the *m/e* 29 peak remains of similar intensity, and the peaks at *m/e* 127 and 128 display drastic increase in intensity. In the 1030 K trace both the parent *m/e* 156 ion and the *m/e* 29 peak noticeably

decreases in intensity. A small peak at *m/e* 28, C_2H_4, is now clearly observed. The peak at *m/e* 128 at this temperature has increased to almost twice the parent *m/e* 156 intensity with the *m/e* 127 peak being approximately 90% of the *m/e* 128 signal. The molecular iodine peak at *m/e* 254 once again more than doubles intensity in comparison to the

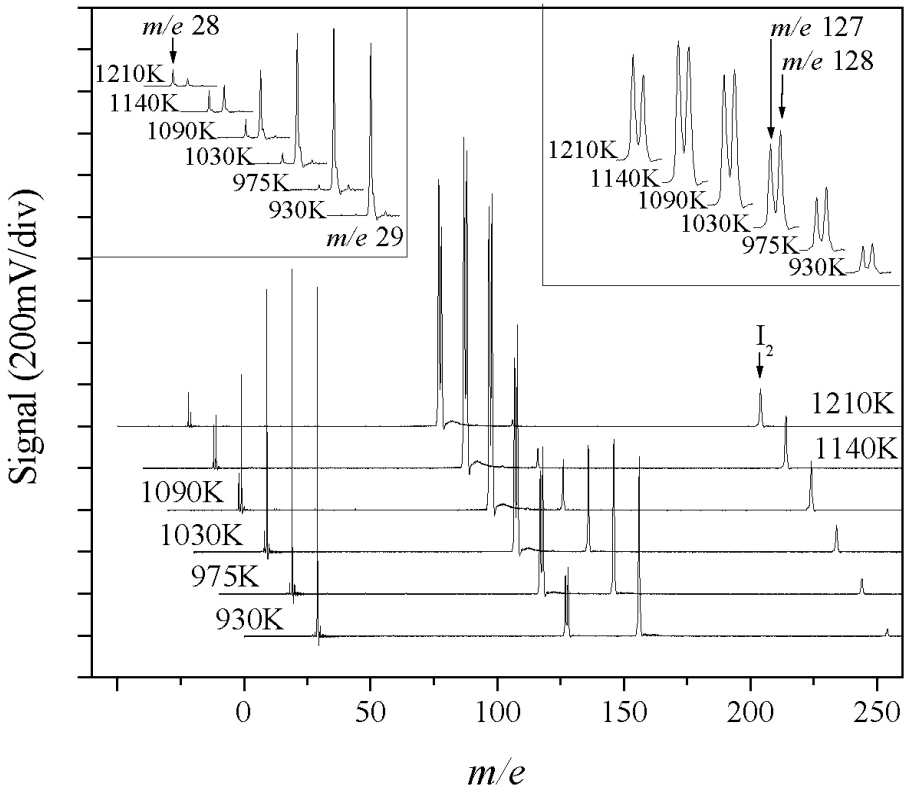

Figure 3.2 (b) Stack plot of mass spectra for prolysis of CH_3CH_2I (12%) in helium with internal nozzle temperatures from 930 K to 1210 K. The mass spectra are shifted for clarity.

previous trace. As the nozzle is heated to 1090 and then 1140 K, the peaks at *m/e* 156 and *m/e* 29 continue to decrease in intensity while the peaks at *m/e* 28, *m/e* 127, *m/e* 128, and *m/e* 254 all increase. Although the *m/e* 128 signal is increasing, over this temperature range the signal relative to *m/e* 127 is decreasing. At the highest temperature 1210 K the parent *m/e* 156 and ethyl *m/e* 29 are barely detectable, while a small C_2H_4 signal at *m/e* 28 and a significant I_2 peak at *m/e* 254 are observable. The peaks at *m/e* 127 and 128 are the dominant peaks and the relative intensity of *m/e* 128 compared to *m/e* 127 continues to decrease as the temperature increases.

Figure 3.3 (a) shows the pyrolysis of partially dueterated isotopomer CH_3CD_2I (4%) in helium at temperatures of 300, 710, 815, 910, and 990 K. At room temperature, a strong molecular ion is observed at *m/e* 158, accompanied by a minor $CH_3CD_2^+$ photofragment at *m/e* 31. As 710K, the *m/e* 31 peak increases relative to the parent *m/e* 158 peak, indicating production of CH_3CD_2 from thermolysis of CH_3CD_2I. At 815 K the *m/e* 31 peak is slightly more intense as peaks at *m/e* 127 and 128 are clearly discernible. With a nozzle temperature of 910 K the intensity of the molecular ion is drastically diminished with concomitant growth of I and HI peaks at *m/e* 127 and 128 that display comparable intensities. The *m/e* peak at 31 is less intense and a small I_2 peak at *m/e* 254 is observed. At the highest temperature 990 K, the molecular ion peak at *m/e* 158 is hardly detectable, while the peaks at *m/e* 127 and 128 continue to intensify, still having similar intensities. The peak at *m/e* 31 is now small and the peak at *m/e* 254 is observed

with similar intensity to the previous trace. Also, at 990 K, *m/e* 30 peak appears, indicating decomposition of the CH_3CD_2 radical to CH_2D_2.

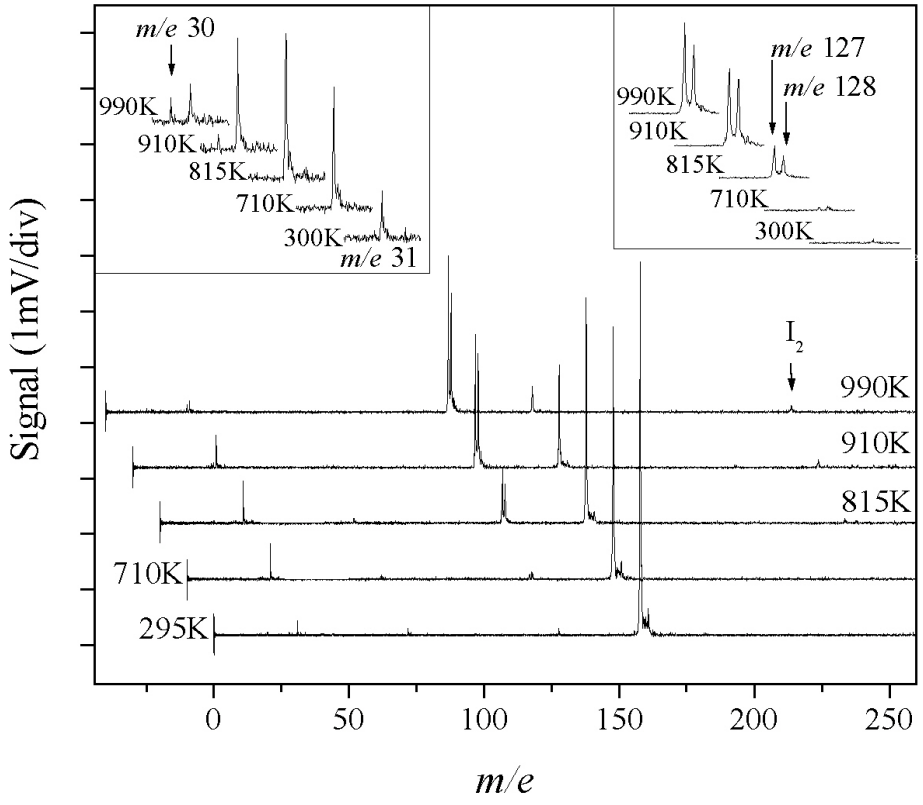

Figure 3.3 (a) Mass spectra for the pyrolysis of CH_3CD_2I (4%) in helium with heater temperatures of 300, 710, 815, 910, and 990 K.

The pyrolysis of CD_3CH_2I (2%) in argon at temperatures 295, 700, 850, 1000 and 1200 K is presented in Figure 33 (b). The molecular ion is observed at *m/e* 159 at room

temperature. At 700 K a CD_3CH_2 peak at *m/e* 32 is observed with approximately one third the intensity of the

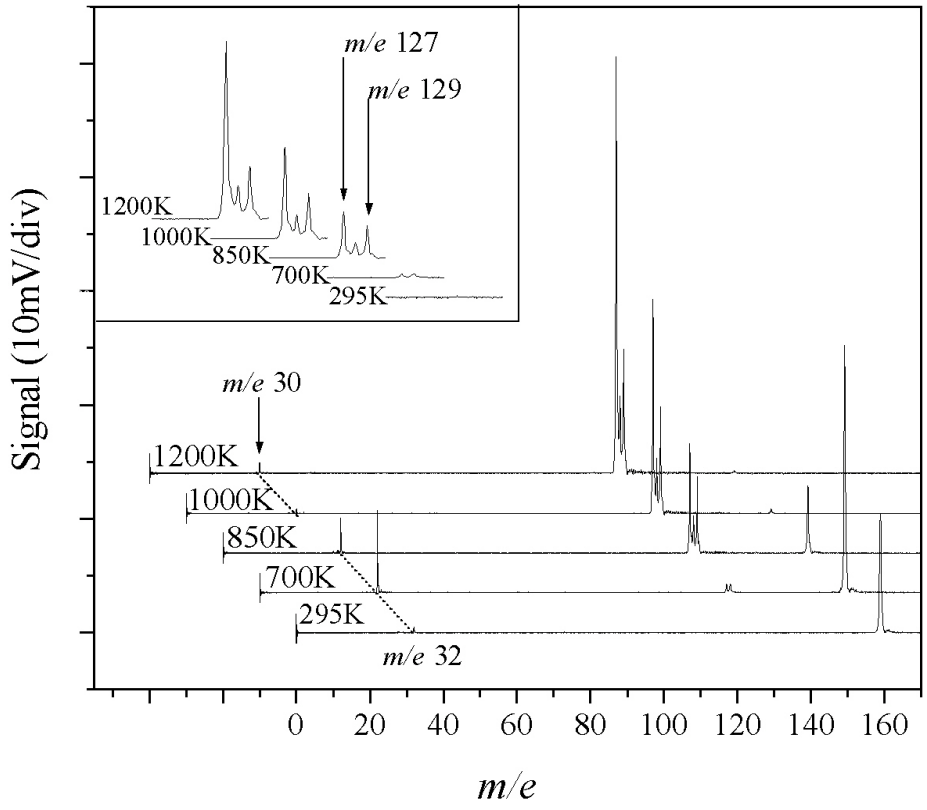

Figure 3.3 (b) Mass spectra for the pyrolysis of CD_3CH_2I (2%) in argon with heater temperatures of 295, 700, 850, 1000, and 1200 K.

molecular ion at *m/e* 159. Small peaks at *m/e* 127 and 129 are barely detected. At 850 K the parent peak at *m/e* 159 is significantly less intense, as is the *m/e* 32 peak. *m/e* 127 and

129 are the most intense peaks in this trace, with *m/e* 129 (DI) being approximately two thirds of *m/e* 127 (I). A small peak at *m/e* 128 is also observed. At 1000 K the parent peak is no longer detected and a small peak at *m/e* 30, corresponding to CD_2CH_2 from thermal decomposition of the CD_3CH_2 radical, is detected. Intense peaks at *m/e* 127 and *m/e* 129 dominate this spectral trace with *m/e* 129 having approximately half the intensity of *m/e* 127, along with a small *m/e* 128 peak. At 1200 K the *m/e* 127 peak continues to increase while the *m/e* 129 peak remains essentially the same intensity as observed at 1000 K. Again a small *m/e* 128 peak is detected while the peak of CD_2CH_2 at *m/e* 30 exhibits modest growth.

Figure 3.3 (c) shows the mass spectra of CD_3CD_2I (2%) in argon at nozzle temperatures of 300, 710, 815, 915, and 990 K. At room temperature a large molecular ion peak at *m/e* 161 is the only discernible peak. At 710 K the molecular ion is slightly diminished, and a peak is observed at *m/e* 34, along with small peaks at *m/e* 127 and 128. While the *m/e* 127 peak is I atom from homolysis, the peak at *m/e* 128 correlates to HI. Since no hydrogen is present in the fully dueterated sample (as the parent mass spectrum at room temperature indicates no impurity), it should come from surface exchange reactions of DI with the silicon carbide microreactor. The *m/e* 34 peak is largely due to the CD_3CD_2 radical, demonstrating again the production of ethyl radicals in ethyl iodide pyrolysis. At 815 K the peak at *m/e* 34 continues growth as the signals at *m/e* 127 and 129 drastically increase. The intensity of *m/e* 127 for the I atom is approximately half of

the signal at *m/e* 129, DI. A small peak at *m/e* 128 is still present and a peak at *m/e* 254 emerges corresponding to the molecular I_2. At temperatures 915 and then 990 K the peaks at *m/e* 34 and 161 quickly reduce in intensity and become barely detectable. A new peak arises at *m/e* 32, indicating the decomposition of CD_3CD_2 to CD_2CD_2, and the *m/e* 127 and 129 peak continue to increase while maintaining the same relative intensities.

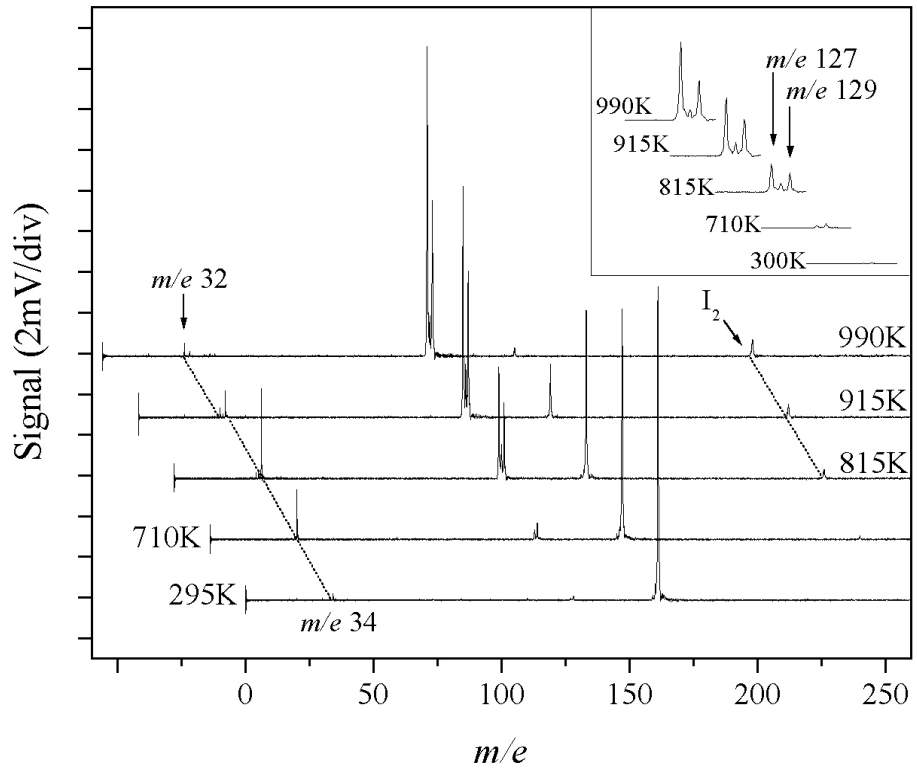

Figure 3.3 (c) Mass spectra for the pyrolysis of CD_3CD_2I with heater temperatures from 295 K to 990 K.

The peak at *m/e* 128 is still present, although, the relative intensity indicates the contribution of surface exchanged hydrogen iodide is minimal. The peak at *m/e* 254 is found to steadily increase in intensity.

(2) *n*-Propyl Iodide ($CH_3CH_2CH_2I$ and $CD_3CD_2CH_2I$)

Mass spectra for pyrolysis of *n*-propyl iodide (1%) in argon at temperatures 295, 760, 845, 975, and 1065 K are presented in Figure 3.4 (a). The spectrum at 295 K has a molecular ion peak at *m/e* 170 (IE = 9.26 eV)[42] and a photoionization fragment $CH_3CH_2CH_2^+$ at *m/e* 43 (AE = 9.8 eV).[42] At 760 K the parent peak decreases slightly with concomitant growth of the *m/e* 43 peak. At a nozzle temperature of 845 K the relative intensities of *m/e* 170 and 43 remain unchanged. A new peak at *m/e* 127 (I atom) is now clearly visible, while a small peak at *m/e* 128 (HI) is hardly detectable. At 975 K both the intensities of *m/e* 170 and 43 remain unchanged, while the peaks at *m/e* 127 and 128 grow dramatically. As HI^+ is not a reported photoionization fragment of *n*- propyl iodide, the *m/e* 128 peak is the HI product of thermal decomposition. A small *m/e* 254 peak is detected as molecular iodine. At the high temperature 1065 K, the peaks at *m/e* 170 and 43 slightly attenuate, while the *m/e* 127 and 128 peaks increase over three-fold from the 975 K data. New peaks at *m/e* 42, *m/e* 28, and 15 are detected correlating to propene, ethene, and methyl radical. The appearance of these peaks is consistent with decomposition of the *n*-propyl radical to ethene + methyl radical, which is known to occur in the conditions of very low pressure pyrolysis (VLPP) of *n*-propyl iodide,[19] and

propene + H atom. The *m/e* 254 peak of I_2 is now over twice the intensity of the previous trace. A new peak at *m/e* 142 is observed corresponding to methyl iodide, CH_3I. At higher temperatures (not depicted here) the relative amounts of *m/e* 127 and 128 remain nearly constant. Peaks at *m/e* 15 and *m/e* 42 are still detected as well as a small peak at *m/e* 28. The lack of a peak at *m/e* 43 indicates the complete decomposition of the *n*-propyl radicals and at these higher temperatures while the *m/e* 254 peak attenuates as I_2 undergoes secondary pyrolysis.

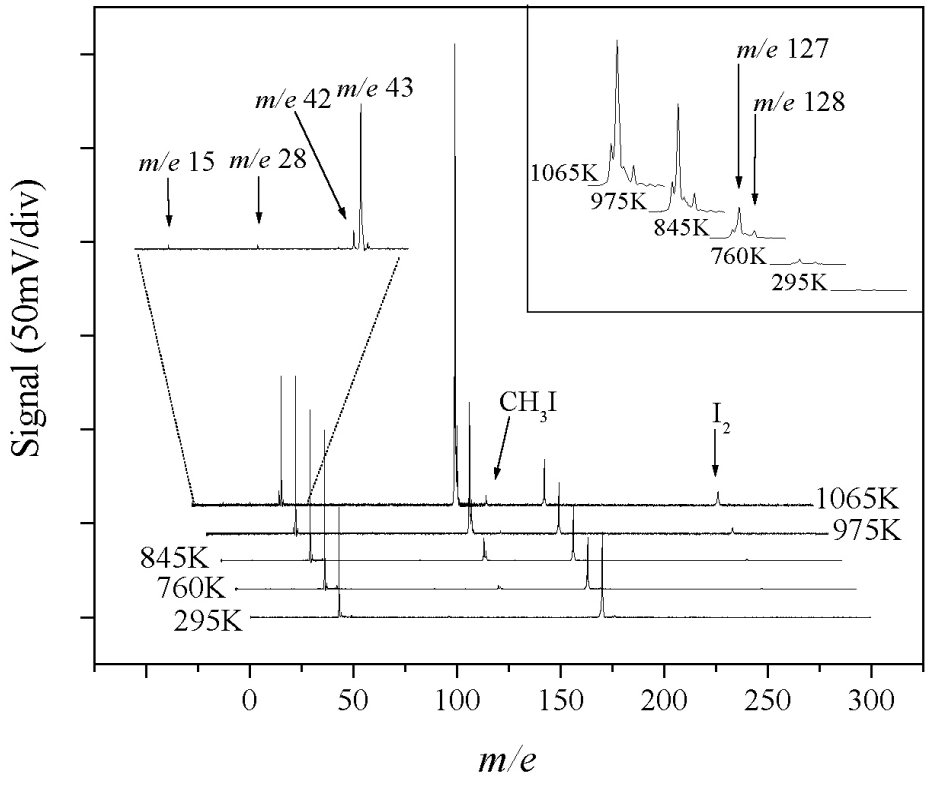

Figure 3.4 (a) Mass spectra for the pyrolysis of *n*-propyl iodide (1% in Ar) with heater temperatures from 295 K to 1065 K.

Figure 3.4 (b) displays the mass spectra of the pyrolysis of the isotopomer $CD_3CD_2CH_2I$ (1%) in argon at temperatures of 295, 720, 825, 965, and 1065 K. At 295 K the molecular ion peak *m/e* 175 is approximately 70% the intensity of the $CD_3CD_2CH_2^+$ photoionization fragment at *m/e* 48. The relative intensity of the parent ion to photofragment ion is similar to that observed in the undeuterated sample. At 720 K both peaks observed in the room temperature sample are found to be similar in intensity. At 825 K the intensity of *m/e* 48 is greater relative to the molecular ion peak at *m/e* 175. Also, a peak at *m/e* 127, approximately 40% the size of the parent peak is detected. Upon heating to 885 K the relative intensities of *m/e* 175, the molecular ion, and *m/e* 48 remain the same while the peak intensity at *m/e* 127 grows many times to an intensity comparable to *m/e* 48. Small peaks at *m/e* 18, 30, 46, and 254 are now barely detectable and correspond to CD_3, CD_2CH_2, CD_3CDCH_2, and I_2, respectively. At 965 K both the parent peak at *m/e* 175 and the *n*-propyl peak at *m/e* 48 are greatly reduced, while the *m/e* 127 peak grows and a peak at *m/e* 129, DI, arises to approximately 10% of the *m/e* 127 intensity. The peaks at *m/e* 18, 30, 46, and 254 are more prominent as the peak at *m/e* 48 decreases in intensity. At this temperature, a small peak at *m/e* 145 is observed corresponding to CD_3I. At the highest temperature 1065 K, the parent peak at *m/e* 175 and the *n*-propyl peak at *m/e* 48 drastically diminish. The peaks at *m/e* 127 and 129 continue to increase with the same relative intensity to each other, while the peaks at *m/e* 18, 30, 46, 145, and 254 exhibit modest growths. The peaks at *m/e* 18, 30, and 129 are more readily detected for the isotopomer than in the undeuterated pyrolysis. A peak at

m/e 128 is not observable which indicates a negligible contribution from the surface hydrogen exchange reaction of DI produced in the gas phase.

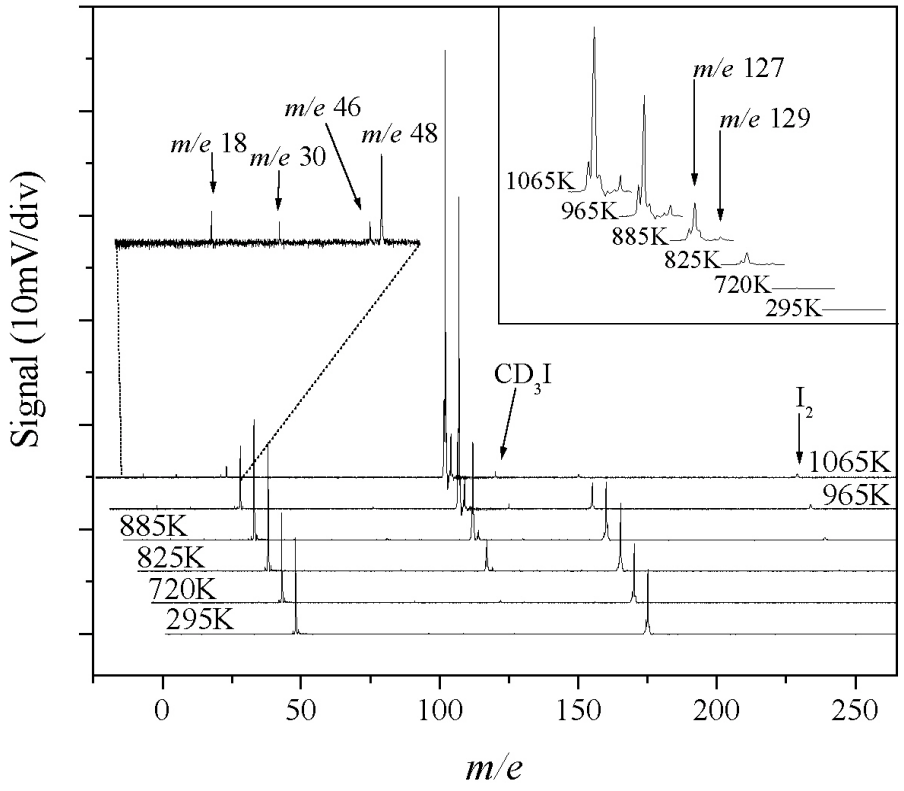

Figure 3.4 (b) Mass spectra for pyrolysis of the isotopomer $CD_3CD_2CH_2I$.

(3) *iso*-Propyl Iodide (CH_3CHICH_3 and CD_3CHICD_3)

The mass spectra of the pyrolysis of *iso*-propyl iodide (2%) in argon at temperatures of 295, 740, 840, 960, and 1065 K are presented in Figure 3.5 (a). The

parent peak, *m/e* 170 (IE = 9.18eV),[42] has approximately half the intensity of the photoionization fragment peak at *m/e* 43, $CH_3CHCH_3^+$ (AE = 9.70 eV).[42] At 740 K the

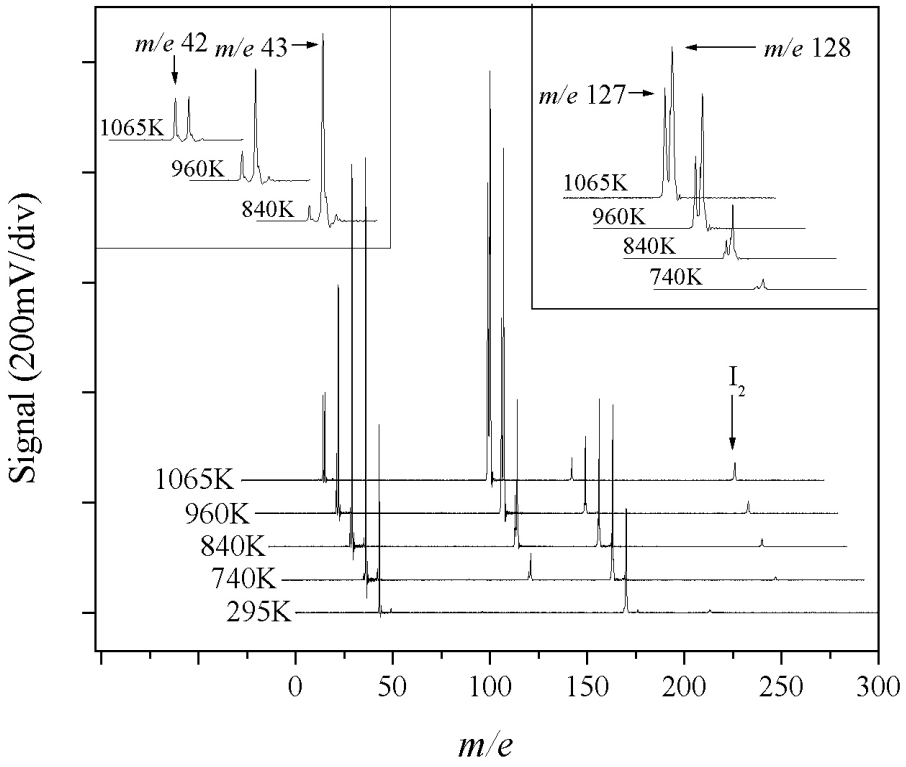

Figure 3.5 (a) Mass spectra for the pyrolysis of *iso*-propyl iodide with heater temperatures from 295 K to 1065 K.

m/e = 43 peak increases relative to the parent peak, and a new peak at *m/e* 128 appears corresponding to HI. At 840 K the signals at *m/e* 170 and *m/e* 43 remain essentially unchanged while the peak at *m/e* 128 increases over an order of magnitude in intensity.

A small peak at *m/e* 127, I atom, about 10% the intensity of the HI peak at *m/e* 128 is seen, and peaks at *m/e* 42 and 254 are visible correlating to product propene (IE = 9.73)[43] and I_2, respectively. At 960 K the *m/e* 170 and 43 peaks reduce in intensity as the peaks at *m/e* 42 and 254 slightly increase. At the same time the *m/e* 128 peak more than doubles while the *m/e* 127 peak becomes ~ 50% of the *m/e* 128 peak intensity. At 1065 K the *m/e* 170 molecular ion becomes very small. The *m/e* 43 peak is also reduced in intensity as the *m/e* 42 peak grows, becoming equal in intensity to *m/e* 43. At *m/e* 127, 128, and 254 the peaks continue to intensify. As found in the pyrolysis of *n*-propyl iodide, at higher temperatures the parent peak at *m/e* 170 and the *m/e* 43 peak are no longer detectable, and the peak at *m/e* 128 and 254 steadily decrease.

The mass spectra for the pyrolysis of CD_3CHICD_3 (2%) in argon at temperatures of 295, 720, 825, 920, 980, and 1075 K are shown in Figure 3.5 (b). At room temperature, the molecular ion at *m/e* 176 is a little more than half the size of the photofragment, $CD_3CHCD_3^+$, at *m/e* 49, similar to the unlabelled compound. At 720 K the *m/e* 49 peak increases relative to the *m/e* 176 peak, and small new peaks at *m/e* 127 and 129 are observed with *m/e* 129 being approximately double the intensity of *m/e* 127. At 825 K the molecular ion signal decreases significantly, the *m/e* 49 peak is of similar relative size in comparison to *m/e* 176, and new peaks at *m/e* 47 (isotopomer of propene, CD_3CHCD_2) and 254 (I_2) appear. The *m/e* 129 peak, DI, is now the largest one, growing by more than one order of magnitude, with a *m/e* 127 peak approximately a third of the

m/e 129 peak. As the temperatures of 920, 980, and 1075 K the molecular ion at *m/e*

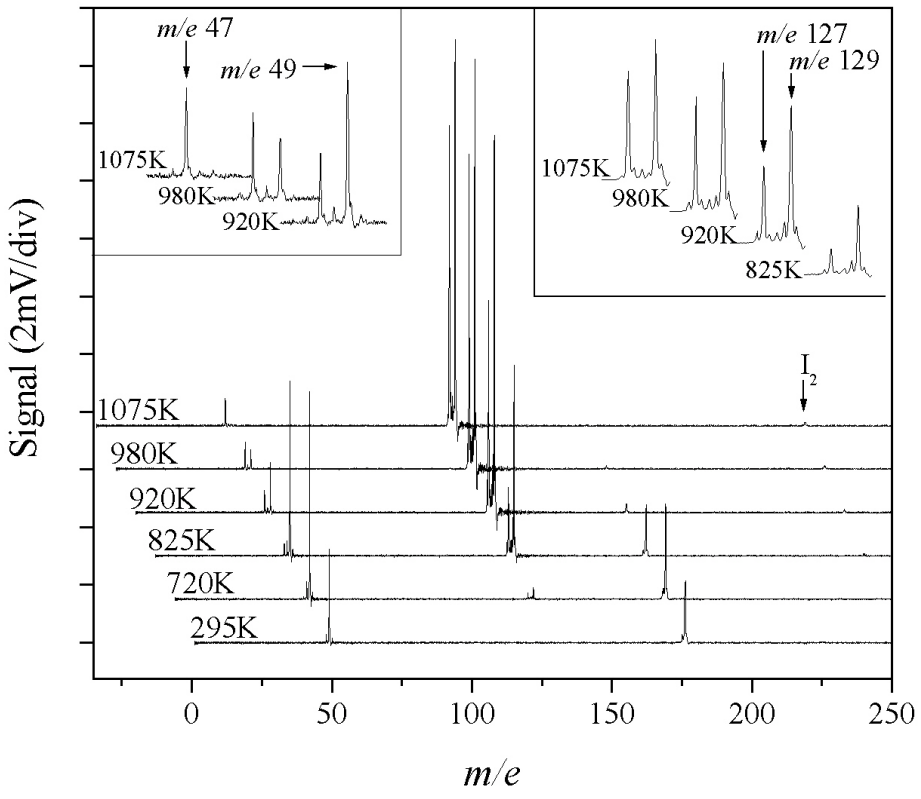

Figure 3.5 (b) Mass spectra for the pyrolysis of isotopomer CD_3CHICD_3 with heater temperatures from 295 K to 1075 K.

176 and the peak at *m/e* 49 disappear as the peaks at *m/e* 47, 127, and 129 increase in intensity. Over this temperature range a small I_2 peak at *m/e* 254 is detected.

DISCUSSION

Comparison of Figures 3.1 (a) and 3.1 (b) illustrates the effects of carrier gases in this experimental technique that has been described previously.[30] The carrier gas affects the photoionization mass spectra in two ways: (1) the efficiency of sample cooling and (2) the residence time in the microreactor. Photoionization fragmentation is sensitive to the internal energy content of the parent molecules, especially when the AEs of the fragments are close to the photon energy, and here ethyl iodide is such an example ($C_2H_5^+$ AE=10.44 eV[36] vs. 10.49 eV photon energy). Although helium will cool a room temperature sample to <50 K rotational temperature,[34] after pyrolysis the cooling is less efficient from the high temperature. The heavier argon gas provides for more efficient cooling which thereby results in the suppression of photoionization fragmentation. This effect is evident when comparing the relative signals at *m/e* 29 in Figure 3.1 (a) and 3.1 (b), which are due to both photoionization fragmentation of C_2H_5I and photoionization of neutral C_2H_5 from C_2H_5I thermolysis. For both the argon and helium entrained samples a photoionization fragment at *m/e* 29 is hardly detectable when the samples are expanded and cooled from the room temperature nozzle. As heat is applied the extent of photoionization fragmentation remains minimal in the argon sample, and the growth of the *m/e* 29 peak is modest and seems to be mainly due to the C_2H_5I thermolysis. In contrast, in helium (with also higher C_2H_5I concentration) the photofragment peak at *m/e* 29 has significant increases, being almost equal in intensity to the parent mass peak M^+ at a nozzle temperature of only 610 K. In both samples growth of the *m/e* 29 peak is observed concomitant with the growth of *m/e* 127 and 128 as the nozzle is heated up to ~

860 K. It may be that the amount of photoionization fragmentation over the 600-860 K temperature range is fairly consistent. If this is the case, the signal for thermally produced ethyl radicals that accompany the detected iodine atoms can be approximated by subtracting the intensity of the *m/e* 29 peak at the heater temperature of ~600 to 650 K from the *m/e* 29 signal at higher temperatures. One must also consider that the ethyl radical readily decomposes (ΔH = 34.8 kcal mol^{-1})[27] to H atom (not detectable in this study) and ethene (not detected at lower temperatures). The effectiveness of cooling is also evident by comparing the peak intensities at *m/e* 127 and 128 in Figures 1a and 1b. Note that the intensity of *m/e* 128 relative to 127 is smaller in the argon entrained sample in comparison to that in helium. I atom and HI have similar ionization energies (IE =10.43 eV[44] for I and 10.38 eV[45] for HI); however, the sensitivities for their photoionization detection at higher temperatures in these pyrolysis experiments could be different due to the different dependence on the internal energies. I atoms lack rotational and vibrational energy to be cooled by supersonic expansion and are essentially always in the ground state in both the argon and helium beams, while the ionization efficiency of HI is found to be sensitive to the extent of cooling of the internal energy. Helium provides less cooling for HI which results in a slightly more ionization in comparison with I atom whose ionization is not affected by cooling. In contrast, argon provides a greater degree of cooling for HI which results in a smaller peak with respect to I atom than in helium. The other factor affecting the sensitivity of I and HI detection is the residence time in the microreactor. The result of increased residence time is evident when comparing Figures 3.1 (a) and 3.1 (b). Note the intensity of *m/e* 127 is less than

10% the parent M^+ peak at *m/e* 156 at 860 K in the helium, while in the argon data at 840 K the *m/e* 127 peak is greater than half the M^+ intensity. The greater cooling ability of argon and the sensitivity for detection of HI at *m/e* 128 has been discussed above. From this one would expect less intense signals at *m/e* 127 and 128 in argon. The velocity through the microreactor is approximately sonic and therefore argon has a longer residence time, roughly three times that of helium. As a result, it is plausible that the difference is due to longer reaction time and more heat transferred to the pyrolysis sample in the flow of a heavier Ar carrier gas (with the same heat capacity or less). In summary, the mass spectra in argon carrier gas are less sensitive to the internal energy and are thus used for subsequent analysis and discussion.

The pyrolysis of ethyl iodide was long believed to proceed primarily via molecular elimination due to the inconsistency of first order kinetics with the rate laws observed for other primary alkyl iodides. However, the more recent studies indicated that in the temperature range of 950-1400 K bond fission is the dominant process,[27,28] which is consistent with the semi-ion pair transition state theory.[20,21] And based on the recently reported kinetic parameters,[27,28] the C-I fission branching fraction increases slightly with temperature over 950-1400 K. Our data clearly show both the HI and I production, and thus the HI + ethene and I + ethyl radical channels (Figure 3.1 and 3.2). In the temperature range of 770-1100 K in this study, the C-I fission is observed to be slightly more than the molecular elimination. The C-I fission branching fraction (from the argon

data) is plotted as a function of temperature in Figure 3.6 (a). The average C-I fission branching fraction is 0.7 ± 0.1 (1σ) in the temperature range of 770-1200 K, with a modest temperature dependence. Note that this fraction is based on an assumption that the ionization cross sections of I and HI are comparable (as they have nearly the same IE), which will be discussed further with the propyl iodide results. Also the fraction is an upper limit as there is a minor loss of I atoms due to the I_2 production or some undetected reactions of I atoms (although these are minimized by the short contact time). Our branching fraction is reasonably close to that by Kumaran et. al in Figure 3.6 (a)[27] and the value of 0.92 ± 0.06 in the temperature range of 950-1400 K by Miyoshi et. al,[28] with our values being smaller than these two previous studies and having a modest temperature dependence. The *m/e* 29 peak increases initially to the maximum around 900-1000 K, and then decays at the higher temperatures, while the parent mass peak M^+ steadily decreases for the entire range. It is difficult to access the relative contributions to the *m/e* 29 peak from photoionization fragmentation and thermolysis of C_2H_5I (the co-product of I atom); furthermore, at the higher temperature the ethyl radicals readily decompose to H + ethene. Nevertheless, the steady increase of the *m/e* 29 peak up to ~ 1000 K, concomitant with the decrease of the parent mass peak, especially in the argon spectra where the C_2H_5I concentration is lower and supersonic cooling is more efficient, implies a major contribution from the neural thermolysis and supports the direct observation of ethyl radical from thermolysis. The co-product of HI in the molecular elimination channel is ethene. At the temperatures below 840 K, no ethene *m/e* 28 peak is observed, possibly due to the slightly higher IE of ethene (10.514 eV)[41] than the photon energy and

cooling of the ethene product. At temperatures > 865 K, *m/e* 28 peak is detected, accompanying decreasing ethyl peak. This ethene product is more likely from decomposition of ethyl radical product rather than the co-product of HI molecular elimination. This is because that in the high temperature region the ethene peak increases with temperature much faster than the HI peak, while the ethyl radical is known to readily decompose to H + ethene and indeed its peak decreases with the increasing temperature and ethene peak concomitantly. For ethene to be detected in this system, a small amount of internal energy (≥ 0.02 eV) need remain after the supersonic expansion. It is plausible that the ethene produced from ethyl is hotter and the cooling at the high temperatures is less complete. A small amount of I_2 is observed at high temperatures; the possible sources are recombination of I atoms and/or abstraction reaction of I + C_2H_5I.

Molecular elimination in the pyrolysis of alkyl iodides is thought to proceed via a C1, C2 mechanism instead of 1,1 as the transition state energy barrier for 1,1 molecular elimination has been shown to be theoretically prohibitive for the alkyl chlorides and bromides.[2] The exclusive observation of HI in the pyrolysis of CH_3CD_2I (Figure 3.3 (a)) clearly illustrates that 1,1 molecular elimination is not occurring in the pyrolysis of ethyl iodide. The pyrolysis data of CD_3CH_2I and CD_3CD_2I in Figures 3.3 (b) and 3.3 (c) support this conclusion and also illustrate a small contribution of DI exchange with the surface of the microreactor. The perdeuterated ethyl iodide contains no hydrogen and therefore any HI detected here must be the result of DI exchange reaction with hydrogen

residing on the microreactor surface (which is known to occur readily). Since it is established from the early work[2] and our CH_3CD_2I result that the 1,1 molecular elimination is not feasible in ethyl iodide, the HI detected in the CD_3CH_2I experiment must come from another source such as the surface reactions (although a minor process); as the CD_3CD_2I data show that DI can produce HI via the surface exchange, the small HI signal in the CD_3CH_2I experiment can be readily explained by the surface exchange of DI (produced from 1,2 molecular elimination of CD_3CH_2I). These studies of the isotopomers also confirm the mechanisms of the ethyl iodide pyrolysis, which undergoes competitive bond fission and unimolecular decomposition, with the C-I fission being more abundant and ethyl radicals (CH_3CH_2, CH_3CD_2, CD_3CH_2I, and CD_3CD_2) produced decomposing further to H + ethene at higher temperatures.

In the pyrolysis of *n*-propyl iodide, $CH_3CH_2CH_2I$ has been known to primarily undergo bond fission and under low pressure conditions the resulting propyl radicals rapidly decompose into propene and CH_3.[19,28] The pyrolysis mass spectra of $CH_3CH_2CH_2I$ (Figure 3.4 (a)) show that the thermal decomposition onsets around 750 K, and proceeds essentially exclusively through bond fission (*n*-propyl + I), with a minor amount of HI (molecular elimination HI + propene). The C-I fission branching fraction of *n*-propyl iodide is shown in Figure 3.6 (b). The average value is 0.85 ± 0.06 (1σ) in the temperature range of 850-1100 K, with the fraction increasing slightly over the temperatures. Our results are compared with those by Miyoshi et. al[28] in Figure 3.6 (b),

and they are in reasonable agreement. The pyrolysis mass spectra of $CD_3CD_2CH_2I$ (Figure 3.4 (b)) are similar, with a predominant I atom peak, a minor DI peak, and no HI signal; this clearly indicates that the molecular elimination is mainly via the C1,C2 pathway in *n*-propyl iodide. A significant amount of photoionization fragmentation into *m/e* 43 $C_3H_7^+$ is due to the lower AE; nevertheless, the *m/e* 43 increases with the temperature, consistent with the *n*-propyl + I bond fission channel. Although difficult to detect, above ~1000K the *n*-propyl radical is observed to decompose into methyl radical at *m/e* 15 and ethene at *m/e* 28, as well as to propene at *m/e* 42 + H (not detected). This decomposition process is more clearly observed in the pyrolysis of isotopomer $CD_3CD_2CH_2I$ (Figure 3.4 (b)). A minor I_2 peak is observed similar to ethyl iodide. Interestingly, a small peak of CH_3I in the pyrolysis of $CH_3CH_2CH_2I$ and CD_3I in $CD_3CD_2CH_2I$ are identified, while these products are not detected in the pyrolysis of CH_3CHICH_3 and CD_3CHICD_3 (Figure 3.5). Several sources of the methyl iodide product are plausible: recombination reaction of CH_3 and I, CH_3 abstraction reaction with *n*-propyl iodide, or a (postulated) four-center elimination process in *n*-propyl iodide. These mechanisms are consistent with the fact that methyl iodide product are not detected in *iso*-propyl iodide, as CH_3 is not a secondary product of *iso*-propyl and *iso*-propyl iodide does not have the four-center elimination to produce methyl iodide. The four-center elimination process in *n*-propyl iodide might be possible, as the methyl iodide product appears at lower temperature before the secondary CH_3 product.

In contrast to the *n*-propyl system, the pyrolysis of *iso*-propyl iodide CH_3CHICH_3 is expected to primarily decompose into HI and propene via 1,2-ε_i.[28] The pyrolysis mass spectra of CH_3CHICH_3 in Figure 3.5 (a) indicate that the thermal decomposition onsets around 700 K, and molecular elimination is preferred over bond fission over the temperature range studied. The C-I fission branching fraction of *iso*-propyl iodide is shown in Figure 3.6 (b). The average value is 0.30 ± 0.05 (1σ) in the temperature range of 770-1100 K, with the fraction increasing slightly over the temperatures. Our results are in good agreement with those by Miyoshi et. al[28] in Figure 3.6 (b), and this implies that the ionization cross sections of HI and I at 10.49 eV are nearly the same. The pyrolysis mass spectra of CD_3CHICD_3 (Figure 3.5 (b)) are also similar, with competing I and DI product signals but no HI peak, further supporting that the molecular elimination in alkyl iodides is predominantly via the C1,C2 pathway. A significant amount of photoionization fragmentation into *m/e* 43 $C_3H_7^+$ is also seen due to the lower AE. The *m/e* 43 peak increases with the temperature up to ~ 800 K, consistent with the *iso*-propyl + I dissociation. The *iso*-propyl *m/e* 43 peak then falls significantly at temperatures > 850 K, and concomitantly the propene product at *m/e* 42 is detected above ~ 800 K and increases with temperatures. The production of propene are due to direct 1,2-ε_i of HI and/or secondary thermal decomposition of the *iso*-propyl radicals. The observation of CD_3CHCD_3 and CD_3CHCD_2 in the CD_3CHICD_3 sample also supports this mechanism.

Our C-I fission branching fractions of ethyl iodide and propyl iodides are based on the I^+ and HI^+ peaks assuming the same ionization cross sections for I and HI. The

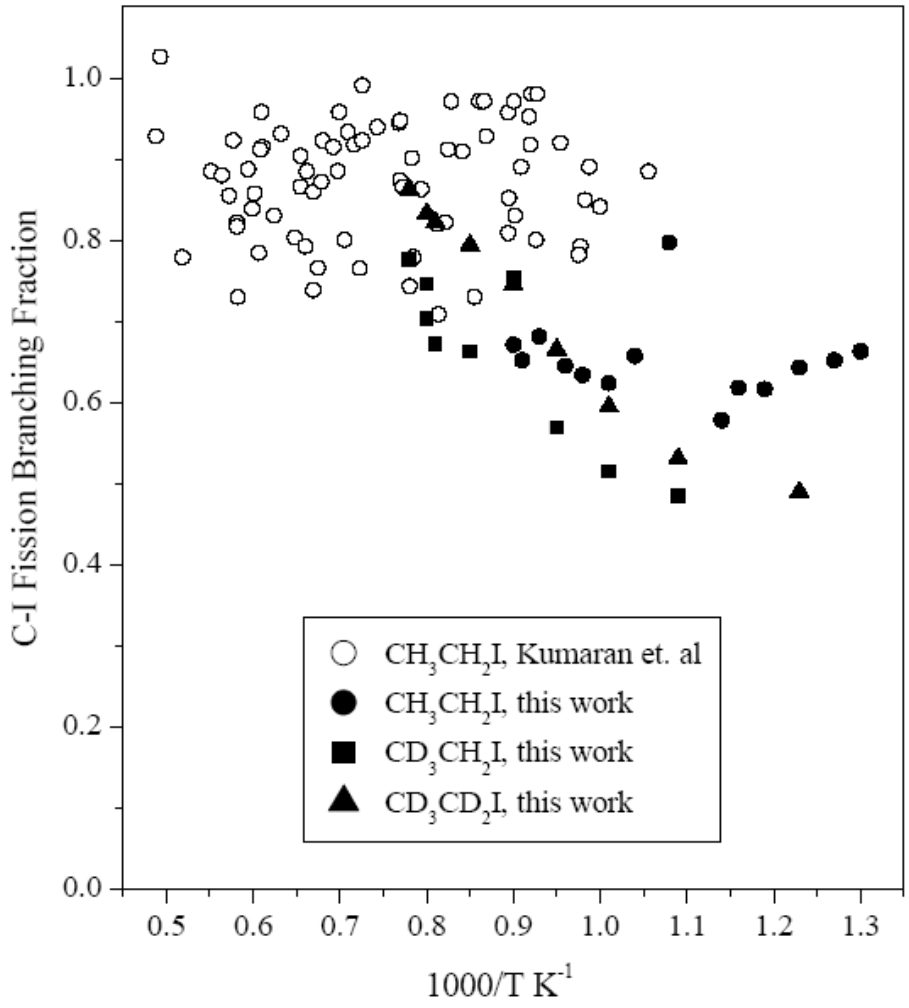

Figure 3.6 (a) C-I bond fission branching fractions for ethyl iodide: Kumaran (○, ref 27), CH_3CH_2I in this work (●),CD_3CH_2I in this work (■), and CD_3CD_2I in this work (▲).

agreement of our *iso*-propyl iodide results with those by Miyoshi et. al (Figure 3.6 (b)) would indicate that the ionization cross sections of I and HI are the same at 10.49 eV,

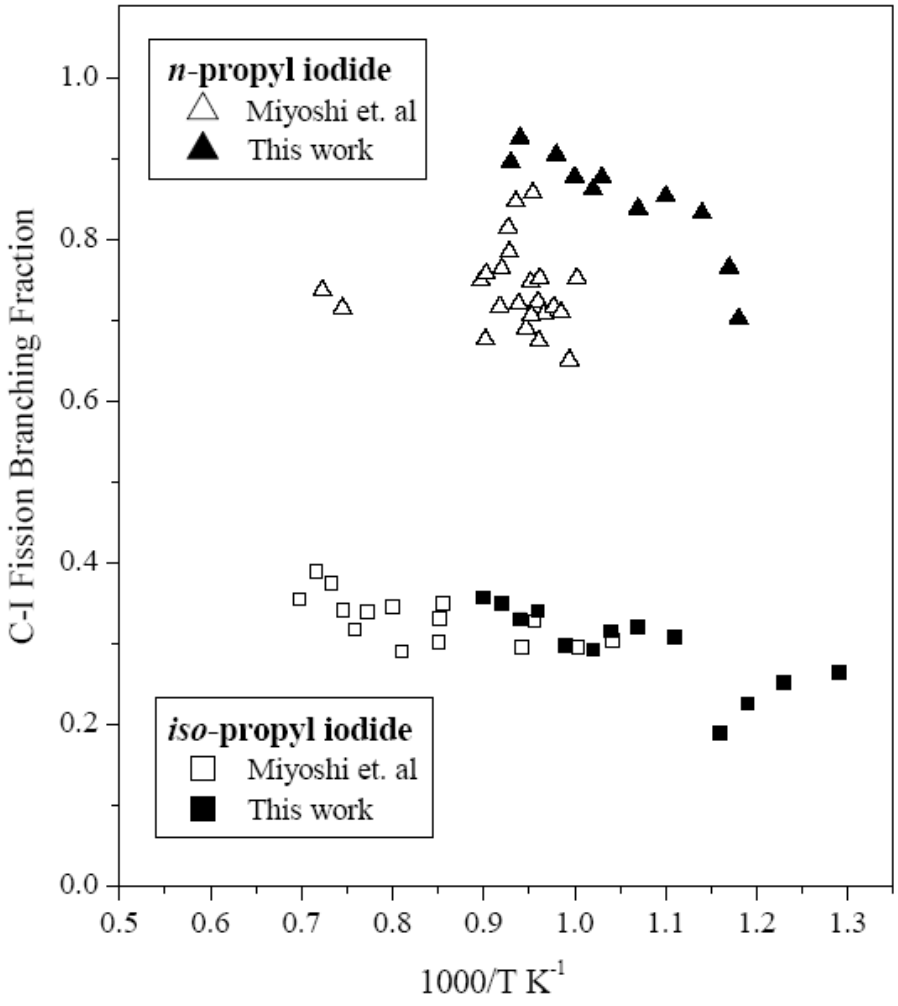

Figure 3.6 (b) C-I bond fission branching fractions for *n*-propyl iodide: Miyoshi et. al (Δ, ref 28) and this work (▲); branching fraction for *iso*-propyl iodide: Miyoshi et. al (□, ref 28) and this work (■).

while the comparison of ethyl iodide in Figure 6a would imply that the 10.49 eV ionization cross section of HI is ~ x4 of that of I. Since both the *n*- and *iso*-propyl iodide results are in better agreements with the previous studies by Miyoshi et. al,[28] it is plausible that the difference between our ethyl iodide results andthose by Kumaran et. al[27] and Miyoshi et. al[28] are not due to the ionization cross sections of I and HI. In the context of the semi-ion pair transition state theory it is interesting that for the data presented in this work ethyl iodide undergoes 1,2-ε_i to a large extent at the elevated temperatures, while the C-I bond fission is always dominant in *n*–propyl iodide. The C-I bond dissociation energies for ethyl, *n*-propyl and *iso*-propyl iodides are all nearly isoenergetic, being within ~0.5 kcal/mol of each other;[28] furthermore, ethyl, *n*-propyl and *iso*-propyl iodides have nearly the same pre-exponential A factors for the C-I bond fission. Consequently, the difference of the C-I fission branching fraction is determined by the relative rates of the 1,2-ε_i channel in the three compounds.

Although *n*-propyl iodide has a σ value (symmetry number) that is 2/3 of ethyl iodide, the presence of an α-methyl group should accentuate the rate of 1,2-ε_i.[1] However, when one compares the ratio of pre-exponential A factors for 1,2-ε_i versus bond fission from the recent calculations[27,28] a ratio of ~0.4 is found for both ethyl and *iso*-propyl iodides while for *n*-propyl iodide that ratio is only ~0.2. In ethyl iodide and *n*-propyl iodide, both primary alkyl iodides, the activation energies for the 1,2-ε_i process are lowered by ~15 kJ/mol compared to their C-I bond dissociation energies. For the

secondary *iso*-propyl iodide the activation energy for 1,2-ε_i is calculated to be 30 kJ/mol lower than the C-I bond fission. As a result, the 1,2-ε_i process is competitive with the C-I bond fission in the elevated temperatures for ethyl iodide despite being a primary alkyl halide, while the primary *n*-propyl iodide decomposes predominantly by bond fission and secondary *i*-propyl iodide decomposes primarily by 1,2-ε_i.

CONCLUSIONS

Pyrolysis of ethyl iodide onsets at ~750 K. The C-I bond fission and HI 1,2 molecular elimination pathways are competitive over the elevated temperature range from 750 – 1200 K, with the C-I bond fission being about ×2 of 1,2 molecular elimination pathway. The C-I fission branching fraction is in reasonable agreement with the previous studies and increases with the temperature. At temperatures above 1000 K, the ethyl radicals produced in C-I fission undergo further decomposition into H + ethene, consistent with the previous reports. Molecular iodine is detected at temperatures > ~850 K. The photoionization fragmentation of ethyl iodide is sensitive to cooling of its internal energy, as shown in the comparison of mass spectra in helium and argon carrier gases.

The pyrolysis of *n*-propyl iodide onsets at ~750 K, and the C-I bond fission dominates at the elevated temperature range of 700-1100 K. At temperatures greater than

~950 K *n*-propyl radicals from the C-I fission decompose to ethene and methyl radical and propene + H. The I_2 product is detected above ~850 K and the CH_3I product is detected above ~900 K. In contrast, the *iso*-propyl iodide pyrolysis onsets at ~700 K; both HI and I products are observed, and the 1,2 molecular elimination pathway is preferred to bond fission at all temperatures presented. The *iso*-propyl radicals from the C-I fission channel further decompose to propene + H at temperatures $\geq$ 850 K. The I_2 product is detected above ~850 K but no CH_3I is detected. The C-I fission branching fraction of both *n*-propyl iodide and *iso*-propyl iodide are in good agreement with the previous studies and increase slightly with the increasing temperature.

In all the three systems, isotopomer experiments verify that (1) the HI molecular elimination in ethyl and propyl iodides proceeds by a 1,2 mechanism as opposed to a 1,1 mechanism, which has been demonstrated as prohibitive for alkyl chlorides and bromides theoretically, and (2) a minimal surface exchange of DI occurs on the surface of the microreactor.

Acknowledgment

This work was supported by the University of California Energy Institute and by NSF grant CHE-0416244.

REFERENCES

[1] A. Maccoll, Chem. Rev. 69 (1969) 33.

[2] M. P. McGrath, F. S. Rowland, J. Phys Chem. A 106 (2002) 8191.

[3] S. Wolf, C. –K. Kim, Israel J. Chem. 33 (1993) 295.

[4] J. L. Toto, G. O. Pritchard, B. Kirtman, J. Phys. Chem. 98 (1994) 8359.

[5] J. V. S. Glass, C. N. Hinshelwood, J. Chem. Soc. (1929) 1815.

[6] J. L. Jones, R. A. Ogg, J. Am. Chem. Soc. 59 (1937) 1939.

[7] J. L. Jones, R. A. Ogg, J. Am. Chem. Soc. 59 (1937) 1931.

[8] E. T. Butler, M. Polanyi, Trans. Faraday Soc. 39 (1943) 19.

[9] S. W. Benson, J. Chem. Phys. 38 (1963) 1945.

[10] H. E. O'Neal, S. W. Benson, J. Chem. Phys. 34 (1961) 514.

[11] A. N. Bose, S. W. Benson, J. Chem. Phys. 38 (1963) 878.

[12] D. B. Hartley, S. W. Benson, J. Chem. Phys. 39 (1963) 132.

[13] P. S. Nangia, S. W. Benson, Chem. Phys. 41 (1964) 530.

[14] P. S. Nangia,S. W. Benson, J. Am. Chem. Soc. 86 (1964) 2773.

[15] D. M. Golden, A. S. Rodgers, S. W. Benson, J. Am. Chem. Soc. 88 (1966) 3196.

[16] S. W. Benson, H. E. O'Neal, Kinetic Data on Gas Phase Unimolecular Reactions, National Standard Reference Data Service, U. S. National Bureau of Standards, Washington D. C., 1970.

[17] H. Teranishi, S. W. Benson, J. Chem. Phys. 40 (1964) 2946.

[18] A. N. Bose, S. W. Benson, J. Chem. Phys. 37 (1962) 2935. A. Maccoll, P. J. Thomas, Nature 176 (1955) 392.

[19] K. D. King, D. M. Golden, G. N. Spokes, S. W. Benson, Int. J. Chem. Kinetics 111 (1971) 411.

[20] S. W. Benson, A. N. Bose, J. Chem. Phys. 39 (1963) 3463.

[21] S. W. Benson, G. R. Haugen, J. Am. Chem. Soc. 87 (1965) 4036.

[22] W. Tsang, J. Chem. Phys. 41 (1964) 2487.

[23] J. H. Yang, D. C. Conway, J. Chem. Phys. 43 (1965) 1296.

[24] G. Choudhary, J. L. Holmes, J. Chem. Soc. B (1968) 1265.

[25] J. Herzler, P. Frank, Ber. Bunsenges. Phys. Chem. 96 (1992) 1333.

[26] J. D. Mertens, M. S. Wooldridge, R. K Hanson, Eastern States Section Technical Meeting, The Combustion Institute, Pittsburg, PA 1994.

[27] S. S. Kumaran, M. -C. Su, K. P. Lim, J. V. Michael, Twenty-Sixth Symposium (International) on Combustion/ The Combustion Institute (1996) 605.

[28] A. Miyoshi, N. Yamauchi, K. Kosaka, M. Koshi, H. Matsui, J. Phys. Chem. A 103 (1999) 46.

[29] S. D. Chambreau, J. Lemieux, L. Wang, J. Zhang, J. Phys. Chem. A 109 (2005) 2190.

[30] K. H. Weber, J. Zhang, D. Borchardt, T. H. Morton, Int. J. Mass Spectrom. 249-250 (2006) 303.

[31] K. H. Weber, J. Zhang, J. Phys. Chem. A 111 (2007) 11487.

[32] D. W. Kohn, H. Clauberg, P. Chen, Rev. Sci. Instrum. 63 (1992) 4003.

[33] A. V. Friderichsen, J. G. Radziszewski, M. R. Nimios, P. R. Winter, D. C. Dayton, D. E. David, D. E.; G. B. Ellison, J. Am. Chem. Soc. 123 (2001) 1977.

[34] H. Clauberg, D. W. Minsek, P. Chen, J. Am. Chem. Soc. 114 (1992) 99.

[35] K. Watanabe, J. Chem. Phys. 41 (1964) 1469.

[36] J. C. Traeger, R. G. McLoughlin, J. Am. Chem. Soc. 103 (1981) 3647.

[37] A. P. Irsa, J. Chem. Phys. 26 (1957) 18.

[38] D. R. Lide (Ed.), Handbook of Chemical Physics 1992, 10-211.

[39] J. H. Sullivan, J. Phys. Chem. 65 (1961) 722.

[40] B. Ruscic, J. Berkowitz, L. A. Curtiss, J. Chem. Phys. 91 (1989) 114.

[41] B. A. Williams, T. A. Cool, J. Am. Chem. Soc. 94 (1991) 6358.

[42] J. C. Traeger, Int. J. Mass Spectrom. Ion Phys. 32 (1980) 309.

[43] J. C. Traeger, Int. J. Mass Spectrom. Ion Processes 58 (1984) 259.

[44] M. Grade, W. Rosinger, Sur. Sci. 156 (1985) 920.

[45] K. Watanabe, J. Chem. Phys. 26 (1957) 542.

CHAPTER 4

TAME

INTRODUCTION

At the onset of World War I in the early 20th century it became critical to augment the power of spark-initiated internal combustion engines to make aviation possible.[1] The fundamental limitation to increasing the compression ratio (and thus the power) for these engines was occurrence of "knock". Originally believed to occur during the compression stroke of the four-stroke engine, knocking or "pinging" was shown to result from pre-flame chain branching reactions during the power stroke.[1] When a fuel mixture decomposes in an uncontrolled manner ahead of the desired flame front, a sharp spike in pressure results, offset from the power stroke, which rapidly destroys the engine cylinder head and piston. Many molecules were found to prevent knocking (*e.g.* iodine). Although aniline was found to have superior anti-knock properties, the organolead compound tetra-ethyl lead (TEL) was found to be most practical[2] and was rapidly incorporated as an anti-knock additive to gasolines. The widely used octane number indicates the extent of antiknock properties of a motor fuel.

Over the years, concerns about automobile emissions have increased. As catalytic converters were introduced into automobiles in the 1970's, methyl *tert*-butyl ether (2-methoxy-2-methylpropane, MTBE) was employed as an anti-knock additive, being an affordable, compatible, cleaner burning replacement for TEL, which was not compatible

with catalytic converters. MTBE, *tert*-amyl methyl ether (2-methoxy-2-methylbutane, TAME), and ethyl *tert*-butyl ether (2-ethoxy-2-methylpropane, ETBE) have since been used as components of more modern gasolines due to their anti-knock properties, reduced volatile organic compound emissions, and cost-effectiveness.

Unfortunately, MTBE is somewhat soluble in water[3] and, because of its pungent odor,[4] can render a water supply unpalatable at low concentrations. Incidents of leakage from underground storage tanks into water supplies have caused MTBE to be outlawed in many locales. As a result, higher-order homologues such as TAME (being approximately three times less water soluble than MTBE[5]) have been employed. Compounds that are even less soluble such as *tert*-octyl methyl ether (2-methoxy-2,4,4-trimethylpentane, TOME),[6,7] *tert*-hexyl methyl ether (2-methoxy-2,3-dimethylbutane, MDMB), and other related compounds[8-13] have been seriously considered as replacements for MTBE. Nevertheless, the smaller *tert*-butyl ethers TAME, ETBE, and MTBE continue to be used because of the ease of manufacture and desirable properties.

The anti-knock ability of *tert*-alkyl ethers has been ascribed to a propensity for thermal decomposition into alkene plus alcohol *via* concerted 1,2-intramolecular elimination (1,2-ε_i). Both products themselves confer high octane. Scheme 1 depicts this process for the anti-knock compound TAME. The alkenes produced can prevent knock by intercepting reactive radicals, particularly OH, in the cool-flame region, forming

resonance-stabilized radicals (RSRs), which are less reactive.[14,15] The thermal decomposition of alkyl ethers has been studied.[16-18] Among primary alkyl ethers, dimethyl ether is found to decompose by a free-radical mechanism[19,20] while diethyl ether has both radical and molecular mechanisms operating.[21-25] Diisopropyl ether, a secondary alkyl ether, decomposes mainly by molecular elimination.[26] The tertiary alkyl ethers MTBE,[27-34] TAME,[31-34] and ETBE[31-34] are reported to react nearly exclusively *via* a molecular mechanism. The same trend is observed in the dehydrohalogenation of alkyl halides (which also can decompose by a molecular or radical mechanism), for which each alkyl substitution on an α-carbon results in an ~ 24 $kJmol^{-1}$ reduction of activation energy for molecular elimination.[35] This α -alkyl effect is the result of a highly polarized four-centered transition state, in which the alkyl substituent possesses a high degree of carbocation character. Additional α -alkyl substituents stabilize the transition state through hyperconjugation, giving rise to a situation similar to the regioselectivity observed in Markovnikov additions to alkenes. A smaller β-alkyl effect has been observed[36] causing, at least in some cases, doubling to tripling of kinetic rates. Semi-ion transition state theory[37,38] would predict molecular elimination from TAME to proceed at a rate up to several factors faster than MTBE. Experimentally, MTBE and TAME are found to decompose at similar rates,[32-34] and the situation is not clear cut. Consider that, for example, the thermal decomposition of *tert*-hexyl methyl ether (2-methoxy-2,3,3-trimethylbutane, MTMB) proceeds primarily *via* bond fssion,[39] as opposed to 1,2-ε_i, due to the highly sterically hindered tertiary center. Also, recent work on the pyrolysis of alkyl iodides indicate that molecular elimination of HI from ethyl iodide may be more

important over lower temperatures than would be predicted by semi-ion transition state theory.[40]

In this work we examine high temperature pyrolysis of the fuel oxygenate TAME, for which there is a relatively limited amount of published experimental data. Oxidation of TAME has previously been observed by static reactor,[31,32] high pressure jet-stirred reactor,[33] and in non-premixed flame.[34] The dominant decomposition reaction over intermediate temperatures (~700K-1000K) is believed to be the formation of 2-methyl-1-butene (2m1b) and 2-methyl-2-butene (2m2b) with concomitant production of methanol *via* the 1,2-ε_i process, while primary and secondary bond scissions become competitive at higher temperatures. The molecular

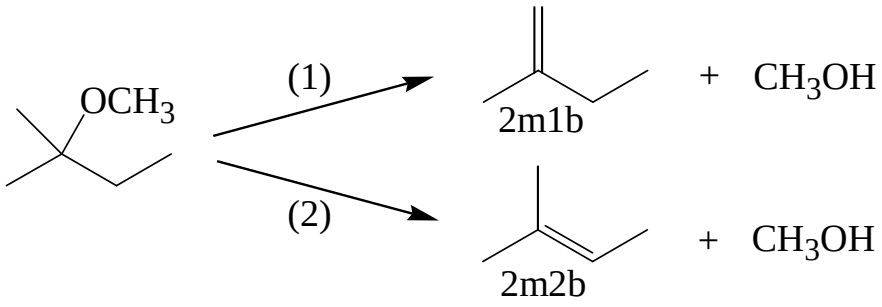

Scheme 4.1 The vicinal molecular elimination of methanol from TAME leads to 2-methy-1-butene (2m1b) or 2-methyl-2-butene (2m2b) both at *m/z* 70. The numbers in parens refer to the path numbers in Table 4.1.

elimination product branching distribution, treated thus far as completely statistical, is further investigated here. To determine the consequence of β-CH_3 substitution on MTBE, quantum chemical calculations along with experimental results are compared to previous work on MTBE pyrolysis by the present investigators,[41] Choo, Golden, and Benson,[29] and, most recently, Zhang *et al*.[42,43] Our experimental approach - flash pyrolysis coupled to supersonic expansion and vacuum ultraviolet (VUV) photoionization mass spectrometry - offers short reaction times to examine the initial steps of the thermal decomposition, supersonic cooling to quench the subsequent reaction and to minimize recombination of the initial products and intermediates, and "soft" VUV photoionization to minimize ion fragmentation allowing for direct detection of transient intermediates. Quantum chemical calculations of the transition state barriers for molecular eliminations of methanol and bond cleavage energies assist in elucidating the most likely reaction mechanisms.

EXPERIMENTAL

TAME (99+%) and 2-methyl-2-butene (99+%) were obtained from Sigma Aldrich. 2-Methyl-1-butene (99+%) was obtained from Columbia Organic Chemicals. Samples were used without further purification and introduced to the pyrolytic apparatus diluted in helium, argon, carbon tetrafluoride, or sulfur hexafluoride by bubbling the carrier gas through the liquid. The backing pressure of the gas mixture was maintained at ~ 1.5 atm for all experiments. The energetics of selected species involved in the

decomposition of TAME were calculated using quantum chemistry methods. Geometeries were optimized using the hybrid density functional theory method of Becke three-parameter functional with nonlocal correlation provided by Lee, Yang, and Parr (B3LYP) and the 6-31+G(2df,p) basis sets.[47,48] Vibrational frequencies were calculated at the same level of theory for characterizing the nature of the structures and for computing zero-point energy corrections. Numerical calculations for energies using CCSD were carried out on the DFT optimized structures. All calculations were conducted using the Gaussian 98/03 program package.[49] Relative energies of the compounds and pertinent transition states were listed on the basis of the enthalpies of formation at 0 K. The energetics of the molecular eliminations and simple bond dissociations are presented in Table 1.

RESULTS

(1) *tert*-amyl methyl ether (TAME)

Stack plots of mass spectra for the low temperature pyrolysis, up to ~1000 K of TAME seeded in argon and sulfur hexafluoride are presented in Figures 4.1 (a) and 4.1 (b), respectively. In Figure 4.1 (a), with the nozzle at room temperature, a molecular ion is barely detectable ($M^{+\bullet}$ = 102 for TAME). A large M-$CH_2CH_3^+$ ion base peak at *m/z* 73 is observed accompanied by a M-CH_3^+ peak at *m/z* 87 having 8% of the base peak intensity. The photoionization of TAME has been previously reported.[50] TAME fragments with preference for expulsion of the larger alkyl group, as has been observed

experimentally with other tertiary methyl ethers.[39,41]

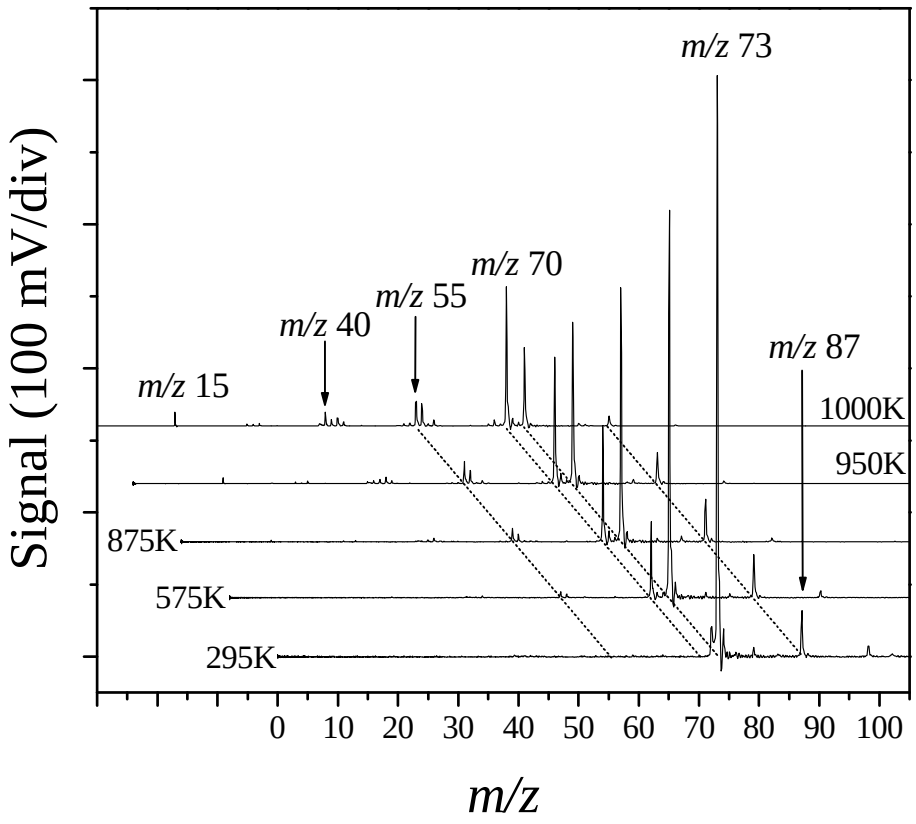

Figure 4.1 (a) Stack plot of mass spectra for pyrolysis of TAME in argon with internal nozzle temperatures from room temperature (~295 K) to 1000 K.

Scheme 4.2 depicts the photoionization fragmentation of TAME where *m/z* 73 has AE = 9.25 eV and *m/z* 87 has AE = 9.36 eV.[50] A trace amount of 2,3,3-trimethyl-1-butene used to facilitate mass calibration is observed as a small $M^{+\bullet}$ peak at *m/z* 98 and, as the nozzle temperature is increased, its M-CH_3^+ peak at *m/z* 83 is also discernible. A small peak at *m/z* 78 is also noted, residual C_6H_6 produced from these pyrolysis

experiments at higher temperatures. With a nozzle temperature of 575 K, the intensity of the *m/z* 73 peak from photoinonization of the parent TAME decreases, while the intensity

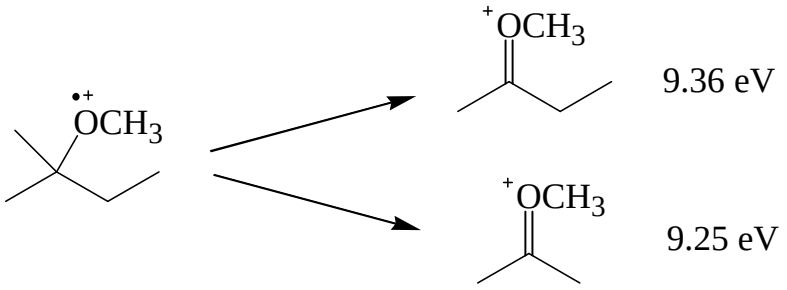

Scheme 4.2 Depiction of the observed photoionization fragments in the ionization of TAME (molecular ion at *m/z* 102 not observed). Appearance energies are from reference 50.

at *m/z* 87 (also from TAME) remains approximately the same. A new peak at *m/z* 70 with ~20% the intensity of the *m/z* 73 peak is now detected, corresponding to "isoamylenes" (C_5H_{10}): 2-methyl-1-butene (2m1b) and 2-methyl-2-butene (2m2b). These are the molecular elimination products of TAME (see Scheme 4.1). Methanol produced concomitantly by same process is not observed, due to its larger IE (10.85eV),[51] which exceeds the photoionization energy employed. The peaks associated with the trace impurities diminish in intensity except for the *m/z* 83 fragment from 2,3,3-trimethyl-1-butene, which now becomes visible. When the nozzle is further heated to temperatures of 875 and 950 K the intensities of *m/z* 73 and *m/z* 87 steadily decrease as the parent compound is consumed. The product peak at *m/z* 70 grows to roughly one half, then nearly equal intensities with respect to the base peak at *m/z* 73. Small peaks at *m/z* 55 and 56 become discernible, as well as small peaks at *m/z* 15, corresponding to CH_3

radical, and product acetone at *m/z* 58. At 1000 K, the M-CH_3^+ ion peak of TAME at *m/z* 87 is barely detectable and *m/z* 70 has increased to nearly double the intensity of M-$CH_2CH_3^+$ ion peak at *m/z* 73. The *m/z* 56 peak has grown in relative intensity to *m/z* 55. Small peaks at *m/z* 58 and *m/z* 72 are detectable, corresponding to the oxygenated products acetone (C_3H_6O) and 2-butanone (C_4H_8O), as well as at *m/z* 68 corresponding to isoprene, C_5H_8. A series of small peaks over *m/z* 40-43 are observed and the *m/z* 15 CH_3 peak intensity increases.

Figure 4.1 (b) presents a stackplot of mass spectra for the pyrolysis of TAME with sulfur hexafluoride as the carrier gas. Although not pictured here, the room temperature spectrum produces a M-CH_3^+ peak with 8% of the intensity of the M-$CH_2CH_3^+$, the same relative intensity observed in the argon entrained sample. At a nozzle temperature of 595 K the product peak at *m/z* 70 is barely discernible while at this nozzle temperature in argon, the *m/z* 70 peak is already ~20% of the *m/z* 73 base peak. The M-CH_3^+ ion peak at *m/z* 87 is found to have approximately 10% of the intensity of the *m/z* 73 M-$CH_2CH_3^+$ ion peak, similar to the argon data in Figure 4.1 (a). With the higher nozzle temperature of 875 K, the *m/z* 70 product peak grows to ~10% of the *m/z* 73 intensity while *m/z* 87 and *m/z* 73 peaks remain essentially unchanged. Nozzle temperatures of 975, 1000, and 1050 K do not significantly change the intensities of *m/z* 73 and *m/z* 87 while the isoamylene peak at *m/z* 70 increases to greater than half of the

m/z 73 peak. New peaks at *m/z* 15, 40-43, 55, 56, 58 are now clearly detected and at 1050 K a small peak at *m/z* 68 is observed.

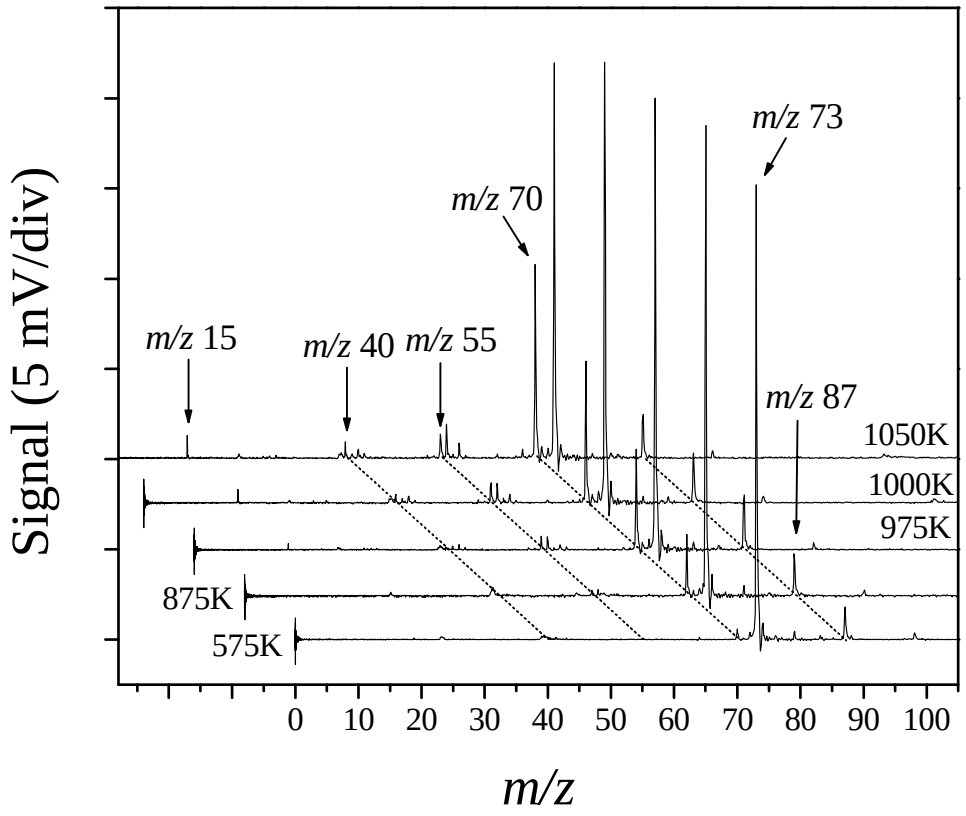

Figure 4.1 (b) Stack plot of mass spectra for pyrolysis of TAME in sulfur hexafluoride with internal nozzle temperatures from 575 K to 1050 K.

The carrier gas was changed to examine the effect on the pyrolysis due to (1) different residence times in the microreactor, (2) heat capacities of carrier gas, and (3) cooling efficiency of the gas. The velocity at the throat of the expansion is approximately

sonic, having an estimated residence time of 20 μs with helium as a carrier gas.[44] Since the speed tracks inversely with square root of mass, the residence times of argon, carbon tetrafluoride and sulfur hexafluoride should be approximately three, five, and six times longer, respectively. When helium is utilized as a carrier gas the pyrolysis of TAME onsets at temperatures > 600 K (not presented here); however, with argon carrier gas pyrolysis onsets below 600 K (Figure 4.1 (a)). At a nozzle temperature of 875 K the intensity of *m/z* 70 relative to *m/z* 73 is approximately 25% in helium and 50% in argon. The cooling efficiency for these gases are similar and, as their heat capacities are the same, the difference in the onset and extent of pyrolysis must be due to the different residence times. At temperatures > 950 K the spectra using helium or argon are indistinguishable. For the polyatomic fluorinated gases the presence of internal degrees of freedom increases heat capacities relative to the monoatomic gases. Residence times are longer, and the onset and extent of pyrolysis are significantly delayed compared to ideal gas carriers. With sulfur hexafluoride as a carrier gas the onset of pyrolysis does not start until temperatures > 600 K (Figure 1b), and at a nozzle temperature of 1050 K the *m/z* 70 product peak is only roughly one half the *m/z* 73 parent ion intensity, while in helium and argon *m/z* 73 peak is greatly reduced. The $[M\text{-}CH_3]^+$:$[M\text{-}CH_2CH_3]^+$ ion ratio (*m/z* 87 : *m/z* 73) for the pyrolysis in helium, argon, carbon tetrafluoride, and sulfur hexafluoride carrier gases was determined. Within experimental error all carrier gases resulted in the same ratio of photoionization fragmentation, with the $[M\text{-}CH_3]^+$ ion having 13 ± 4% the intensity of the $[M\text{-}CH_2CH_3]^+$ ion. This indicates that either all gases are cooling with equivalent efficiency or that the photoionization fragment is not

sensitive to internal energy content. Even though the observed photoionization fragmentation pattern of TAME is unaltered by the choice of carrier gas, the onset temperature for pyrolysis and the extent of reaction are significantly different. Argon was chosen for subsequent experiments to produce best quality spectra.

A stack plot for the high temperature pyrolysis (1110-1250 K) of TAME seeded in argon is presented in Figure 4.2. At 1100 K little *m/z* 73 is detected, being approximately 10% of the *m/z* 70 base (C_5H_{10}) peak. The intensity of the peak at *m/z* 40, C_3H_4, has increased drastically to nearly the same intensity as *m/z* 70 while the signals at *m/z* 15 (CH_3 radical), *m/z* 54 (C_4H_6), *m/z* 56 (C_4H_8), and *m/z* 68 (C_5H_8), have all increased in intensity. The production of C_4H_8 and a portion of the CH_3 signal is due to pyrolysis of TAME (discussed below in Scheme 4), while the other signals are known products from the pyrolysis of the isoamylenes, C_5H_{10} (vide infra).[34] As the heater is raised to the higher temperatures of 1160, 1200, and 1240 K the *m/z* 70 peak steadily decreases in intensity, and in the highest temperature trace, 1240 K, *m/z* 78 is detected corresponding to C_6H_6, presumably from the self combination of *m/z* 39 C_3H_3 radicals. The peaks at *m/z* 15, 28, and 40 continue to become more intense. The isobutylene peak at *m/z* 56 begins to slightly decrease in intensity while new peaks over the *m/z* range of 52-54 are observed. At these higher temperatures the *m/z* 68 peak remains relatively constant and the *m/z* 73 peak from TAME is hardly detectable. The half life for TAME[32,33] at a temperature of 1200 K is expected to be on the order of 70-150 μs, respectively, which is comparable to

the estimated residence time of ~60 μs for argon. Experimentally, TAME is found

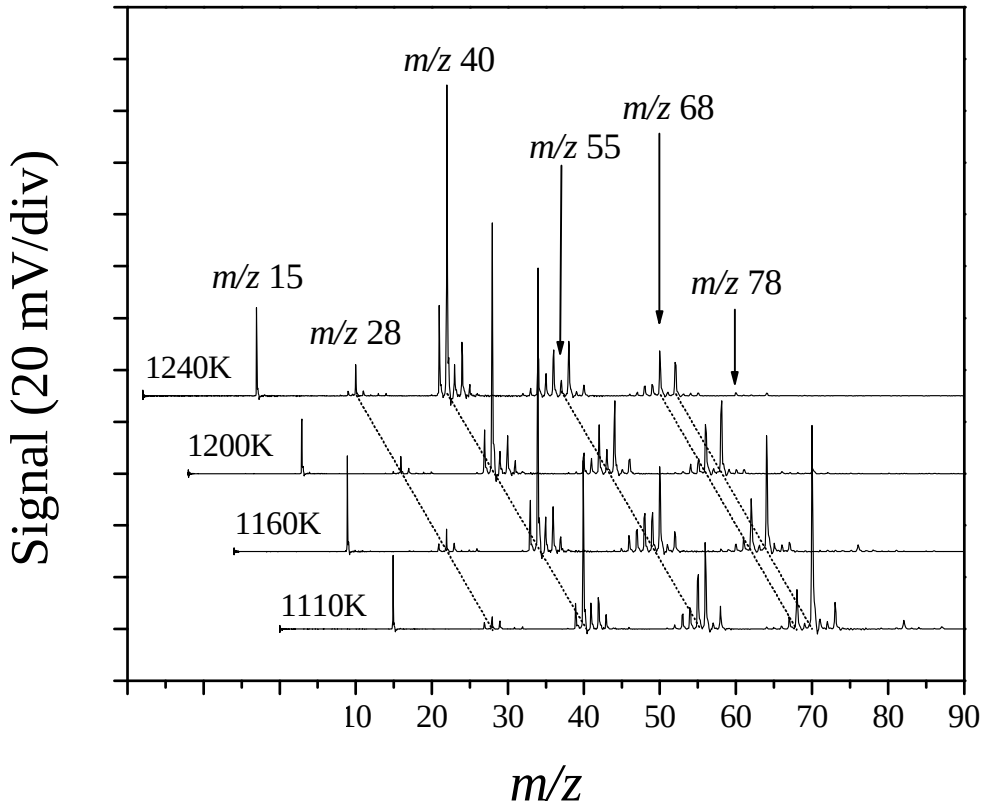

Figure 4.2 Stack plot of mass spectra for pyrolysis of TAME in argon with internal nozzle temperatures from 1100 K to 1240 K.

here to decompose completely at this temperature, the M-CH_3 ion at *m/z* 87 and M-CH_2CH_3 ion at *m/z* 73 corresponding to the photoionization fragments of TAME are not observed >1200 K. The reliability of the temperature measurement for the nozzle has

been investigated previously[39] and was determined to be accurate to ± 50 K. Four-center eliminations from tertiary centers have been reported as sensitive to wall effects[29,52] and surface catalysis must be considered, however, at higher temperatures they should not be significant.

(2) 2-methyl-1-butene (2m1b) and 2-methyl-2-butene (2m2b)

In attempt to evaluate the contribution of product fragmentation and investigate relative product yields, the pyrolysis of 2m1b and 2m2b in the argon carrier gas was conducted. Stack plots of mass spectra for temperatures from ~ 1100-1250 K are presented in Figures 4.3 (a) and 4.3 (b). When comparing Figure 4.3 (a) to 4.3 (b the mass spectra pattern of 2m1b and 2m2b undergoing pyrolysis are significantly di)fferent. Relative to the molecular ion signal at *m/z* 70 for these isomers, a large amount of *m/z* 68 is produced in the pyrolysis of 2m2b compared to 2m1b. This is explained by the propensity of 2m2b to undergo molecular decomposition to evolve hydrogen gas and produce 2-methyl-1,3-butadiene (isoprene) in preference to radical decomposition, as depicted in Scheme 4.3. This process is calculated by DFT to have an energy barrier of

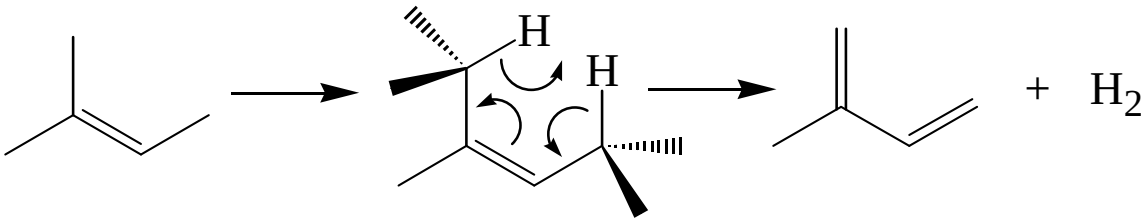

Scheme 4.3 The disrotary 1,4 elimination of molecular hydrogen from 2-methyl-2-butene to produce 2-methyl-1,3-butadiene (isoprene).

61.5 kcal/mol. The pyrolysis of 2m1b, on the other hand, produces a greater amount of signal at *m/z* 40, C_3H_4. Although these two alkene isomers have distinguishably different pyrolysis spectra, two difficulties prevented an accurate determination of the ratio of the product C_5H_{10} isomers in the pyrolysis of TAME: (1) differences in residence time for products compared to authentic samples and (2) interference from competing pyrolytic processes. In an attempt to determine the product isomer branching ratio from the TAME pyrolysis, the relative amounts of *m/z* 40 and *m/z* 68 in sample mixtures composed of 0%, 25%, 50%, and 100% 2m1b in 2m2b were monitored and compared with those of TAME at higher temperature (Figure 4.2). It was apparent that the majority of molecular elimination product is 2m1b, consistent with the previous study.[32] The comparison suggested a branching ratio value of 75 ± 20% 2m1b from TAME. Another noticeable delineation between the 2m1b and 2m2b spectra is the amount of *m/z* 78 observed. In Figure 4.3 (a), pyrolysis of 2m1b, a signal at *m/z* 78 is detected at temperatures ≥ 1190 K. In the pyrolysis of 2m2b presented in Figure 4.3 (b), a signal at *m/z* 78 is only barely detected in the hottest temperature trace at 1245 K. 2m2b undergoes molecular

elimination of H_2 in preference to C_3H_4 (*m/z* 40) production. Conversely, 2m1b prefers to decompose to C_3H_4 and likely rapidly loses H atom to form propargyl radicals, which then combine to form C_6H_6.

Comparing Figures 4.3 (a) and 4.3 (b) to Figure 4.2 it is apparent that the high-temperature pyrolysis of TAME produces mass spectra similar to those produced by pyrolysis of isoamylenes. The most noticeable differences distinguishing the TAME data from the isoamylene pyrolyisis experiments, however, are greater amounts of *m/z* 15, *m/z* 28, and *m/z* 56 in TAME. The elevated amounts observed indicate that these fragments are thermal decomposition products of TAME, due to additional product channels besides the molecular elimination channels (1) and (2). One must also consider that, due to longer residence times, the fragmentation patterns for the product isoamylenes in the TAME pyroylsis will not be as far progressed as in the neat pyrolysis. Also, in Figure 4.2, peaks at *m/z* 58 and *m/z* 72 corresponding to acetone and butanone are detected which can only come from the thermal decomposition of TAME. These additional bond homolysis channels are shown in Scheme 4 and will be discussed further below.

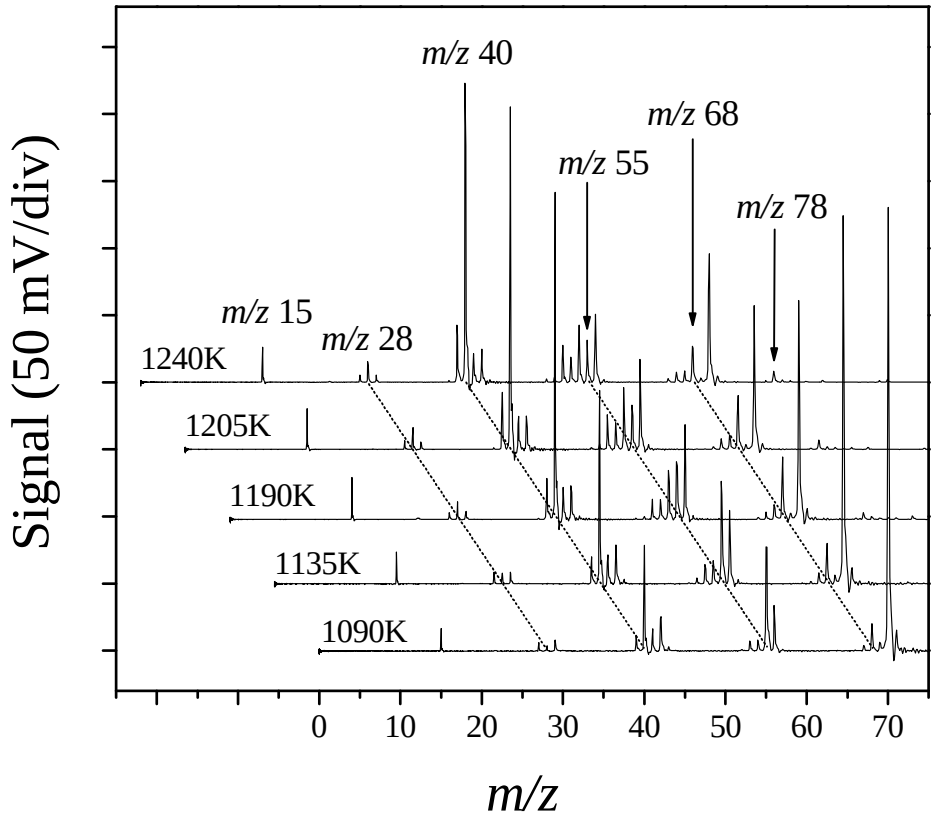

Figure 4.3 (a) Stack plot of mass spectra for pyrolysis of 2-methyl-1-butene in argon with internal nozzle temperatures from 1090 K to 1240 K.

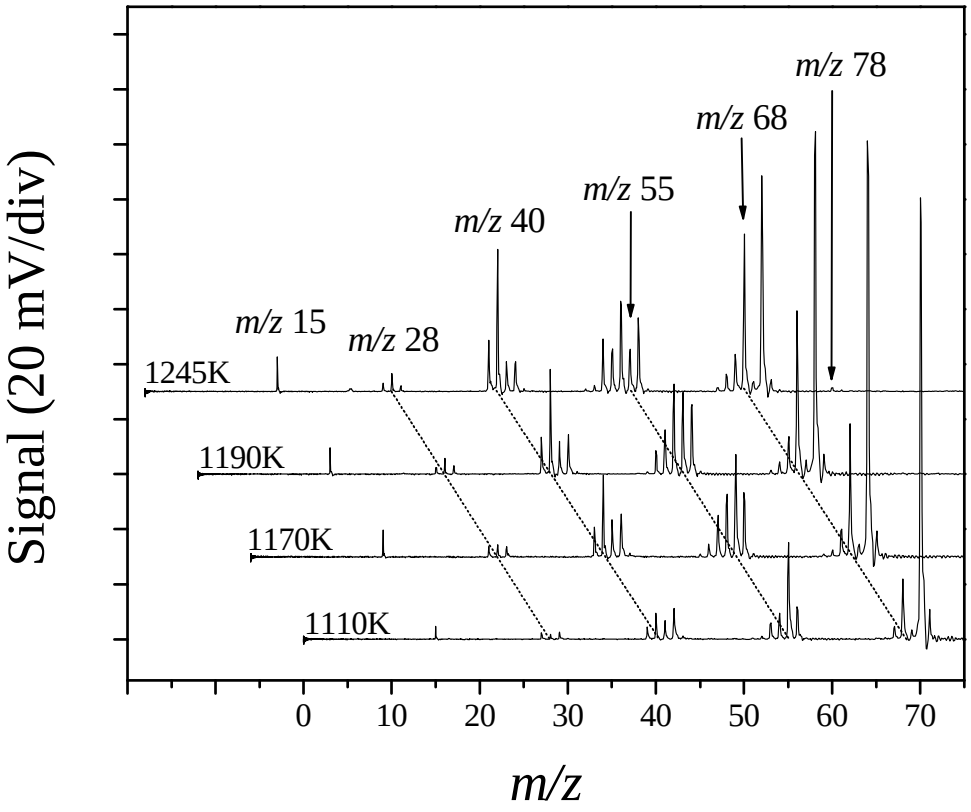

Figure 4.3 (b) Stack plot of mass spectra for prolysis of 2-methyl-2-butene in argon with internal nozzle temperatures from 1110 K to 1245 K.

CALCULATION

Potential energies for the 1,2-ε_i molecular eliminations of methanol to form isoamylene and simple bond fissions in the pyrolysis of TAME are reported in Table 4.1 and the bond fission pathways are presented graphically in Scheme 4.4 (in addition to the molecular elimination channels (1) and (2) in Scheme 4.1). CCSD calculations were

performed on structures optimized at the B3LYP/6-31+G(2df,p) level of theory. Reported activation energies[32,33] and values for the analogous processes reported for MTBE[29,43] are presented for comparison. The potential energy barriers for the molecular elimination of methanol and both the isoamylenes from TAME are calculated by DFT to be essentially isoenergetic, having a barrier of 53.7 kcal/mol to 2m1b and 53.8 kcal/mol to 2m2b. These values compare favorably with the calculated activation energy value of 55.0 kcal/mol reported by Kadi[31] and slightly lower than the 58.5 kcal/mol value reported by Goldaniga.[33] The molecular elimination process for MTBE, considered isoenergetic to TAME elimination by Goldaniga, is compared here in Table 4.1; its potential energy barrier was calculated to be 62.7 kcal/mol by Zhang et al. using the G3B3 method.[43] Our CCSD values predict that the molecular elimination activation energies of TAME are within 1 kcal/mol of one another; however, they are found to be grossly overestimated. Although the secondary H atoms are more readily abstracted than the primary H's, the DFT results predict that the energy barriers for path 1 and 2 are isoenergetic, implying that the molecular elimination product branching is basically statistical, as has been previously modeled.[33] With 6 H available to react to form 2m1b and 2 H to form 2m2b, thermal decomposition of TAME is expected to produce three times the amount of 2m1b compared to 2m2b, consistent with our observation (and consistent with the results of deprotonation of gaseous *tert*-amyl cation by strong base[53]). To evaluate the magnitude of β-effect, the transition state for molecular elimination of methanol from MTBE

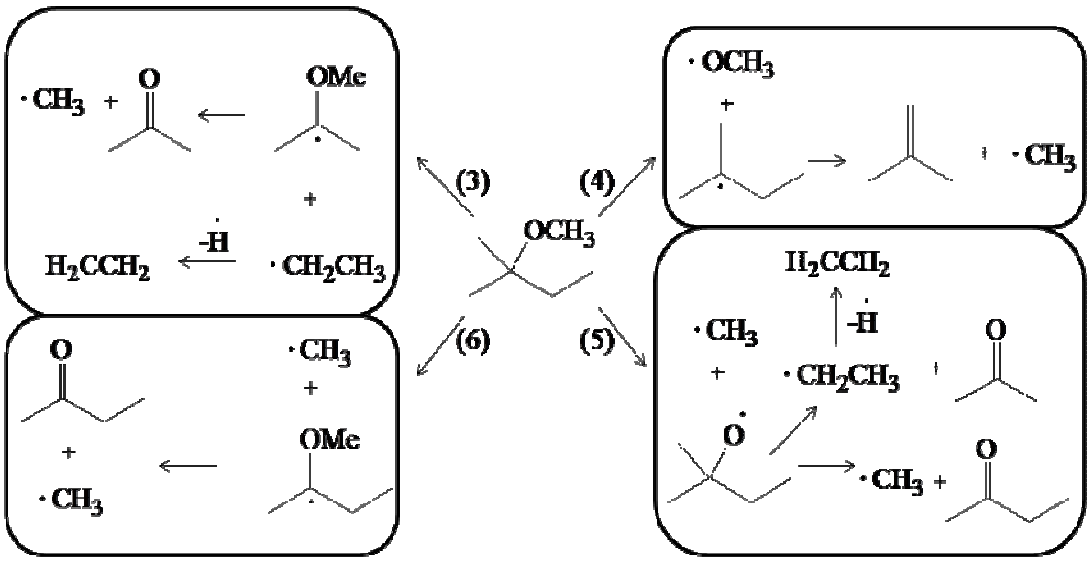

Scheme 4.4 Bond fission and radical decomposition in the pyrolysis of TAME. Values in parens refer to the pathways in Table 4.1.

was calculated in this work using the same DFT method and was found to be 54.4 kcal/mol (as compared to the value of 62.7 kcal/mol by the G3B3 method[43]); the DFT value is approximately 0.5 kcal/mol higher in energy than the molecular elimination calculated in this work for TAME. This attenuation of transition state energy barrier corresponds to a 65% increase in the rate of molecular elimination of TAME compared to MTBE.

Both CCSD and DFT predict the 3,4 C-C bond (path number not included in Scheme 4) to be stronger than other C-C bonds in TAME, being 6.3 and 8.5 kcal/mol stronger, respectively, than the predicted next strongest C-C bond, the 1,2 C-CH_3 bond

(path 6 in Scheme 4.4). The DFT bond homolysis values other than the 3,4 C-C bond are found to lie within the narrow range of 68.3 -71.6 kcal/mol. The magnitude of which agrees poorly with the reported kinetic parameters reported by Goldaniga,[33] which range

Process	path #	CCSD	B3LYP	TAME[a]	TAME[b]	MTBE[c]	MTBE[d]
Molecular Elimination							
$CH_3C(=CH_2)(C_2H_5) + CH_3OH$ (2m1b)	1	72.7	53.7	55.0	58.5	59.0	62.7
$(CH_3)_2C(=CHCH_3) + CH_3OH$ (2m2b)	2	73.7	53.8	55.0	58.5		
Simple Bond Fission							
$(CH_3)_2COCH_3 + C_2H_5$	3	85.8	68.3		82.0		
$(CH_3)_2C(C_2H_5) + OCH_3$	4	86.8	69.6		84.0		85.9
$(CH_3)_2C(C_2H_5)O + CH_3$	5	83.8	71.4		84.0		81.8
$CH_3C(C_2H_5)OCH_3 + CH_3$	6	87.0	71.6				84.9
$CH_2C(CH_3)_2OCH_3 + CH_3$		93.3	80.1				

Table 4.1 DFT zero point corrected (0K) and CCSD energy barriers for molecular eliminations (paths 1 and 2) and simple bond energy thresholds (paths 3-6) for TAME using geometries optimized at B3LYP/6-31+G(2df,p). Energies are in kcal/mol. For comparisons, (a) Ref. 32, from kinetic modeling. (b) Ref. 33, also from kinetic modeling. (c) Ref. 29. (d) Ref. 43 calculations based on the G3B3 theory.

from 82.0 – 84 kcal/mol (see Table 4.1). The CCSD values are found in the range from 83.8 – 87.0 kcal/mol with improved accuracy. Both of these results indicate that at higher temperatures all of the aforementioned paths could become competitive. It is interesting to note that both CCSD and G3B3[43] calculations predict that the O-CH_3 bond (path 5) is the weakest bond of these ethers. Although this agrees with G3B3 calculations for MTBE[43] it contradicts the experimental observervation that the C-CH_3 bond is the weakest bond in MTBE[41] (see discussion). The fission of the ethyl group to form ethyl and isopropyl radicals is predicted to be the most favorable homolytic process by DFT (path 3). Also interesting to note is that the relative strengths of the alkoxy-OCH_3 (path 4) and *t*-amyl-OCH_3 (path 5) bonds are different for CCSD than for DFT. DFT predicts that *t*-amyl-OCH_3 (path 4) homolysis is 1.8 kcal/mol weaker than *t*-amylO-CH_3 (path 5) homolysis while CCSD predicts path 4 to be 3.0 kcal/mol stronger. Consider that the reported bond strength of CH_3O-CH_3 of 80 kcal/mol.[54] Replacement of a methyl group for the electron withdrawing groups vinyl and aryl strengthen that bond (e.g. 87 kcal/mol CH_3O-$CHCH_2$[54] and 91kcal/mol for CH_3O-C_6H_5[54]). Although replacing ethyl with methyl does not produce a noticeable difference in bond strength (CH_3O-CH_2CH_3 = 80 kcal/mol[54]) one might suppose that if electron withdrawing groups strengthen that bond to oxygen then electron donating groups should weaken them. From this and the previous observation about C-C versus C-O bond strength it seems that DFT could place the relative bonds strengths properly.

DISCUSSION

The attractive feature of the *t*-alkyl methyl ether anti-knock compounds is the nearly exclusive vicinal molecular elimination of methanol with concomitant formation of corresponding alkene over intermediate temperatures such as found in an engine cylinder (~700-1000K). Over this temperature range TAME is found to primarily decompose by molecular elimination, with an approximate 3:1 branching ratio of 2m1b to 2m2b, via direct complex fission (1,2-ε_i) as opposed to a radical mechanism. This fact (both 2m2b and 2m1b are alkenes) is consistent with the notion that anti-knock properties are related to the production of alkenes, having the ability to intercept reactive chain branching radicals to form less reactive RSR's. Note that the blending research octane number (BRON), a measure of the ability of a fuel to resist "knock", for 2m2b (176) is much higher than the BRON for 2m1b (146) indicating an increased resistance to self ignition.

In our experiments the pyrolysis of TAME onsets at a slightly lower but comparable temperature than MTBE, ~600K compared to ~700K for MTBE (the accuracy of the temperature measurement has been determined to be ±50K). The magnitude of discrepancy between MTBE and TAME onset temperatures, barring any surface effects, could be indicative of an actual reduction in the reaction energy barrier. The observed attenuation of onset temperature for TAME compared to MTBE under the same experimental conditions can be explained, in part, by a α-CH_3 effect calculated by DFT to be on the order of a 0.5 kcal/mol. Previous work[31,33,34] has treated the rates of

molecular elimination of methanol for TAME and MTBE pyrolysis to be the same with reasonably good agreement with experiment. Pyrolysis of MTBE experiments performed in this work find an onset temperature of ~700K while previous work by this group[41] found the pyrolysis to onset at a higher temperature ~800K. These observations indicate that the condition of the nozzle indeed plays a role in this experimental regime. The semi-ionic transition states for molecular elimination of *t*-alkyl ethers are known to be sensitive to surface effects and they likely play a role in this system.

There are more possible bond fission pathways for TAME than with MTBE (Scheme 4.4). The 2m1b and 2m2b control experiments clearly demonstrate the elevated levels of methyl radical, ethene, and isobutylene from TAME at temperatures >950 K. Additionally, the oxygenated products acetone and butanone that are observed at these temperatures are characteristic of the TAME pyrolysis (see Scheme 4). The CCSD (this work) and other theoretical work on MTBE[43] predict the O-CH_3 bond (path 5) as the weakest bond. This is somewhat surprising as typically one would expect C-C bonds to be weaker than C-O bonds. The average C-C bond is 81 kcal/mol and average C-O bond is 84 kcal/mol.[55] That would be consistent with the experimental observation that the C-CH_3 bond in MTBE-d_3 is in fact weaker than the O-CD_3 bond implying that alkyl bond fissure should be the first observed homolytic process. From this previous observation plus the fact that ethyl bond cleavage is preferred over methyl bond (for example, the bond energy CH_3-CH_3 = 88 kcal/mol vs. CH_3-CH_2CH_3 = 85 kcal/mol),[54] which both

calculation methods correctly predict, it would be expected that ethyl cleavage to form isopropyl and ethyl radicals (path 3) as the most favored pathway. Both radicals thusly formed would rapidly decompose from ethyl to ethene + H and from isopropyl to acetone and methyl radicals (path 5, Scheme 4.4). In Figure 4.1 (a) and 4.1 (b) the first evidence of bond homolysis at ≥ 950 K is the observation of methyl radicals and acetone, along with very small amounts of ethene and ethyl. It should be noted that acetone and methyl radicals could also be produced by the homolysis of the O-CH_3 bond (path5) with subsequent decomposition of the alkoxy radical to either acetone and ethyl radical or butanone and methyl radical. Smaller amounts of butanone (compared to acetone) are observed and CCSD calculations predict that cleavage of the O-CH_3 bond (path 5) to be more favorable than cleavage of the C-CH_3 bond (path 6) by 3.2 kcal/mol. Isobutene is observed over this temperature range which can only be produced by cleavage of the C-OCH_3 bond (path 4). CCSD predicts path 6 to have an activation energy only 0.2 kcal/mol higher than path 4 while DFT predicts 2.0 kcal/mol higher energy. These results both indicate that at temperatures ≥ 950 K all of the reaction pathways examined in this work are significant yet the relative contribution of each pathway is unclear. The mass spectra are further complicated by the secondary pyrolysis of 2m1b and 2m2b, the primary molecular elimination products of TAME. The calibration experiments on the secondary pyrolysis of 2m1b and 2m2b indicate that 2m1b and 2m2b are less thermodynamically stable than the isobutylene produced from MTBE. This being the case, under harsher motor conditions TAME should not perform quite as well as an anti-

knock compound in comparison with MTBE. This is reflected in the higher BRON value of 116 for MTBE than the value of 111 for TAME.

Pyrolysis of 2-butanone (C_4H_8O)

2-butanone was obtained and introduced into the system with either helium or argon carrier gas while maintained at ice bath temperature. Figure 4.4 is a collection of mass spectra obtained from the pyrolysis of 2-butanone with helium as a carrier gas. With the nozzle unheated (RT) the spectral trace exhibits a large molecular ion peak, *m/z* = 72 (IE = 9.52 eV[56]). A photoionization fragment peak with ~12% relative intensity to the base parent peak is at *m/z* = 43, the acylium ion, $C_2H_3O^+$ (AE = 10.32 eV[57]). An additional fragment peak at *m/z* = 57 is observed, $C_3H_5O^+$ (AE = 9.90 eV[56]) with ~3% relative intensity. A signal slightly less intense compared with *m/z* = 57 is found at *m/z* = 29.

As the nozzle is heated to an internal temperature of 890 K the relative intensity increase of the *m/z* = 43 and *m/z* = 57 photoionization fragments is dramatic. At a nozzle temperature of 960 a small peak at *m/z* 15 is observed, the first indication of bond thermolysis. The *m/z* 29 peak is found to be slightly augmented in this trace. At a nozzle temperature of 1215 at *m/z* 15 is clearly discernible as is a *m/z* 28 peak, ethene, which results from the rapid loss of H atom from ethyl radical (discussed further below).

Similarly, the peak at *m/z* 43 has all but vanished as a strong peak at *m/z* 42 emerges. The peak at *m/z* 57 is now hardly detectable and a very small peak is observed at *m/z* 56. Based on the relative intensities of these peaks it seems plausible that the proprionyl radical is not only loosing H atom to form methyl ketene (*m/z* 56) but also

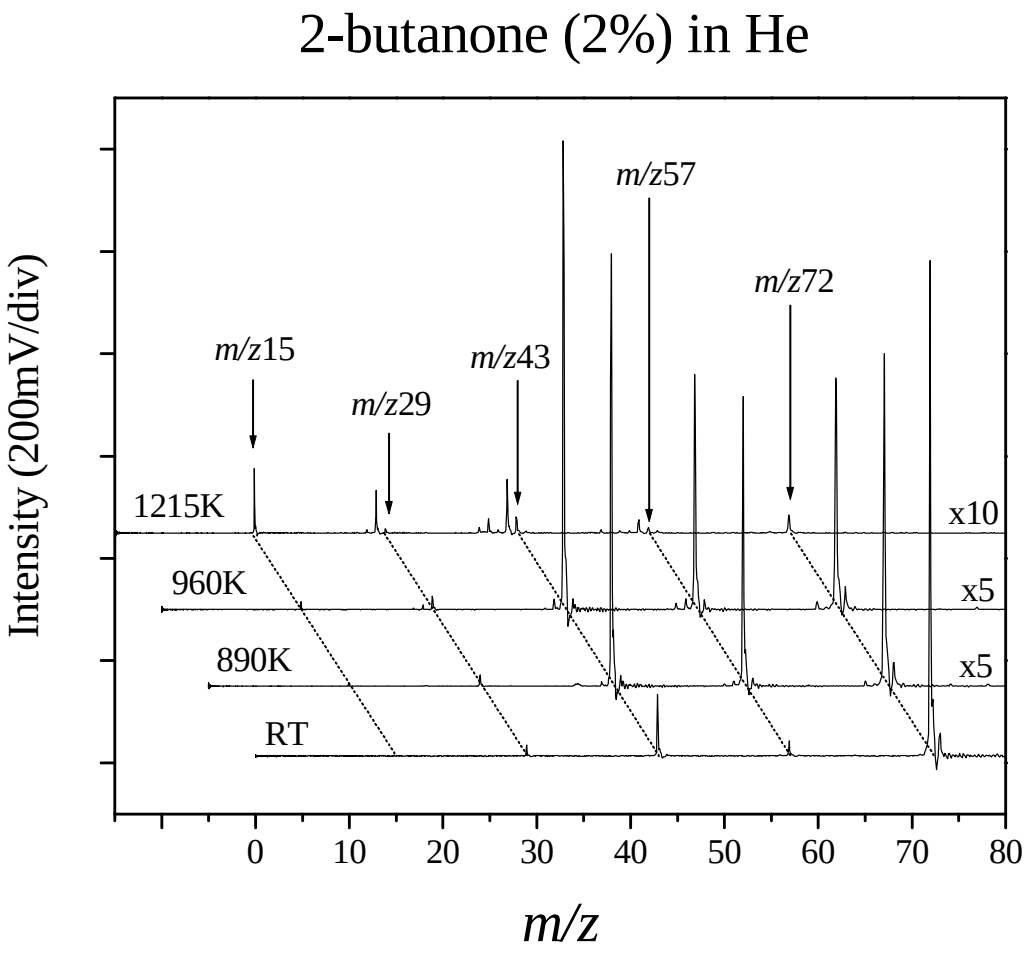

Figure 4.4 Stack plot of mass spectra for the pyrolysis of 2-butanone with unheated nozzle (RT) and over the temperatures from 890 – 1215 K in helium carrier gas. The traces are shifted for clarity.

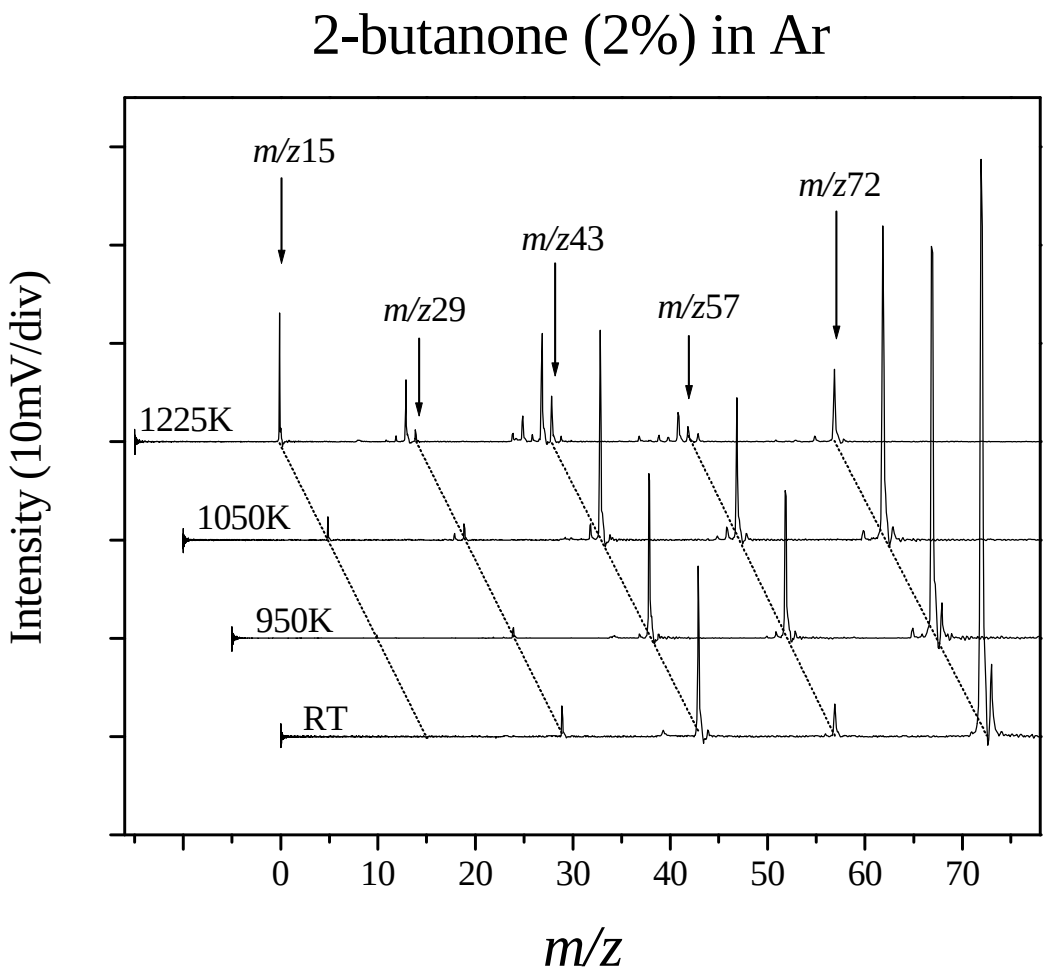

Figure 4.5 Stack plot of mass spectra for the pyrolysis of 2-butanone with unheated nozzle (RT) and over the temperatures from 950 – 1225 K in argon carrier gas. The traces are shifted for clarity.

expelling methyl radical, which would contribute to the signal at *m/z* 15, to form ketene (*m/z* 42). Calculations were carried out to further elucidate the potential energy landscape which are presented below. The acetyl radical is expected to lose H atom to form ketene.

A stack plot of mass spectra from the pyrolysis of 2-butanone entrained in argon is presented in Figure 4.5. In the trace with an unheated nozzle the spectral trace produced in very similar to the helium entrained sample. A large molecular ion peak is observed at *m/z* 72 accompanied by a prominent peak at *m/z* 43 from the acylium photoionization fragment. Small fragments are observed at *m/z* 29 and *m/z* 57. As the nozzle is heated to 950 K the rapid increase in the *m/z* 43 and especially *m/z* 57 is observed as in helium, however, the magnitude of the increase is markedly diminished in this argon sample. This is likely the result of more efficient cooling of the heavier argon carrier gas as has been observed previously. In the 1050 K spectral trace the fist evidence of homolysis is observed, approximately the same temperature observed in helium. At a nozzle temperature of 1225 K strong peaks at *m/z* 15, methyl radical, *m/z* 28, ethene, *m/z* 42, ketene are detected. The parent at *m/z* 72 is found to nearly be completely decomposed at this temperature as found in helium.

To assist the interpretation of the experimental results quantum chemical calculations were performed at the CCSD//B3LYP/6-31+G* level of theory using the Gaussian 98/03 program package. First, to investigate the preference for loss of ethyl versus methyl radial from the positively charged potential energy surface the single point energies calculated using the CCSD method from B3LYP/6-31+G* optimized geometries were accomplished. The resulting DE values for the loss of ethyl radical from $M^{+\bullet}$ is thermodynamically 26.0 kcal/mol while loss of methyl radical has a value of 22.8 kcal/mol. These values indicate that thermodynamically the loss of methyl radical is preferred which correlates well with the literature AE value of 9.90 eV as opposed to 10.32 eV for ethyl loss. The ΔDE for the two processes is ~.14 eV as calculated by CCSD while experimentally the energy difference in AEs are .4 eV. One must consider, however, that the AEs are representative of the transition state for expulsion of the alkyl radical which does not necessarily correlate with the thermodynamic value (for example TAME). The mass spectra for 2-butanone from the governmental database (http://webbook.nist.gov) reports a spectra where *m/z* 43 is the base peak. Although it may be that the *m/z* 43 fragment is preferred one might argue that due to the high ionization energies (~70 eV) employed subsequent fragmentation of the $–CH_3$ ion may be occurring. Contrary to this, experimentally at ~10.5 eV we observe to *m/z* 43 signal to be much larger than at *m/z* 57. Scheme 4.6 depicts homolytic pathways expected to occur in the thermal degradation of 2-butanone. From the neutral parent loss of ethyl versus methyl radical is calculated to be endothermic by 83.8 and 84.7 kcal/mol. These values are very similar and although a kcal/mol can result in a two-fold difference in rate

(assuming the same frequency factor) it is not know how reliable these values are. The subsequent decompositions of the radicals created was considered as well. For the loss of H atom from ethyl radical to form ethene was calculated to have a energy difference of 35.7 kcal/mol. The loss of H atom from acetyl radical was found to have a value of 47.4 kcal/mol while loss of H atom from proprionyl radical was placed at 48.4 kcal/mol. Loss of methyl radical from the proprionyl radical was calculated to have a DE = 38.0 kcal/mol. The value would predict that the preference for decomposition of proprionyl radical to form methyl radical and ketene is nearly exclusive. Overall, at temperatures > ~1000 K 2-butanone is found to decompose by both loss of methyl and ethyl radicals. The ethyl radicals rapidly expel H atom to produce ethene. The proprionyl and acetyl radicals are found to decompose to methyl radical with ketene and H atom with ketene respectively.

Pyrolysis of acetone-d_6 (C_3D_6O)

Acetone-d_6 was obtained from Aldrich (99%) and introduced into the system with either helium or argon carrier gas while maintained at ice bath temperature. Figure 4.6 is a collection of mass spectra obtained from the pyrolysis of acetone-d_6 with helium as a carrier gas. With the nozzle unheated (RT) the spectral trace exhibits a large molecular ion peak, *m/z* = 64 (IE = 9.70 eV[57]). A photoionization fragment peak is barely detected at *m/z* = 46, the deuterated acylium ion, $C_2D_3O^+$ (AE = 10.38 eV[57]). As the nozzle is heated to 650 K the fragment peak at *m/z* 64 has grown to approximately one third the

parent base peak intensity. This peak is entirely attributed to photoionization as no deuterated methyl radical at *m/z* 18 is observed. As the heat is increased bringing the nozzle to a temperature of 1025 K the parent peak at m/z 64 decreases in intensity as the the photoionization fragment peak at *m/z* 46 overtakes the parent peak signal and the first indications of bond homolysis are observed, very small peaks at *m/z* 18 and 44 are barely

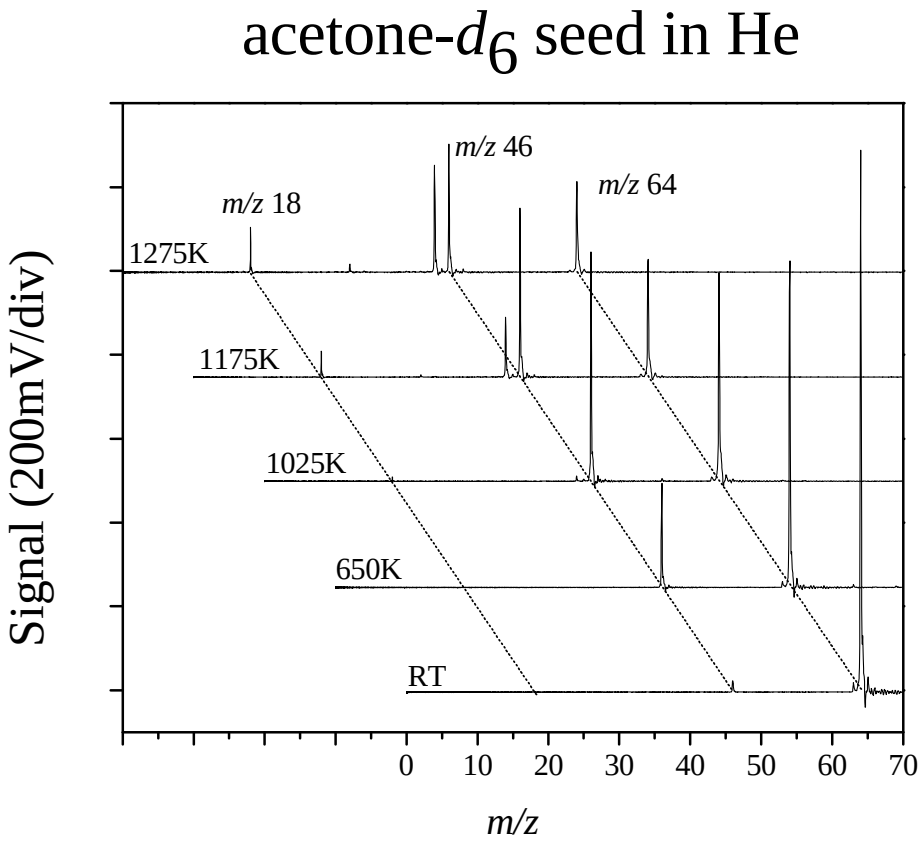

Figure 4.6 Stack plot of mass spectra for the pyrolysis of acetone-d_6 in helium carrier gas with nozzle temperatures up to 1275 K.

detectable at this temperature. At a nozzle temperature of 1175 K the *m/z* 18 and 44 peaks are clearly discernible as acetone-d_6 undergoes $_3$DC(O)C-CD$_3$ bond cleavage and the resulting deuterated acylium radical looses D atom to form deuterated ketene. At a temperature of 1275 K the trend continues as a new small peak at *m/z* 28 is observed, presumably carbon monoxide, CO, resulting from the decomposition of the acylium isotopomer.

Figure 4.7 presents a stack plot of mass spectra from the pyrolysis of acetone-d_6 in argon carrier gas. In the jet-cooled unheated nozzle trace (RT) the parent peak is a strong signal with the –CD$_3$ photoionization fragment being barely detected, as in the helium entrained sample. At a nozzle temperature of 675 K the photoionization fragment at *m/z* 46 increases to ~one fourth the intensity of the parent peak, slightly less than the increase observed in the helium sample. As the nozzle is further heated to 1050 K the first signs of homolysis are observed with a CD$_3$ radical starting at *m/z* 18 and the ketene isotopomer being formed at *m/z* 44. At 1175 K the signals at *m/z* 18 and 44 are more pronounced as the intensities of *m/z* 46 and 64 decline. At the hottest nozzle temperature presented here, 1250 K, a small peak at *m/z* 28 is observed.

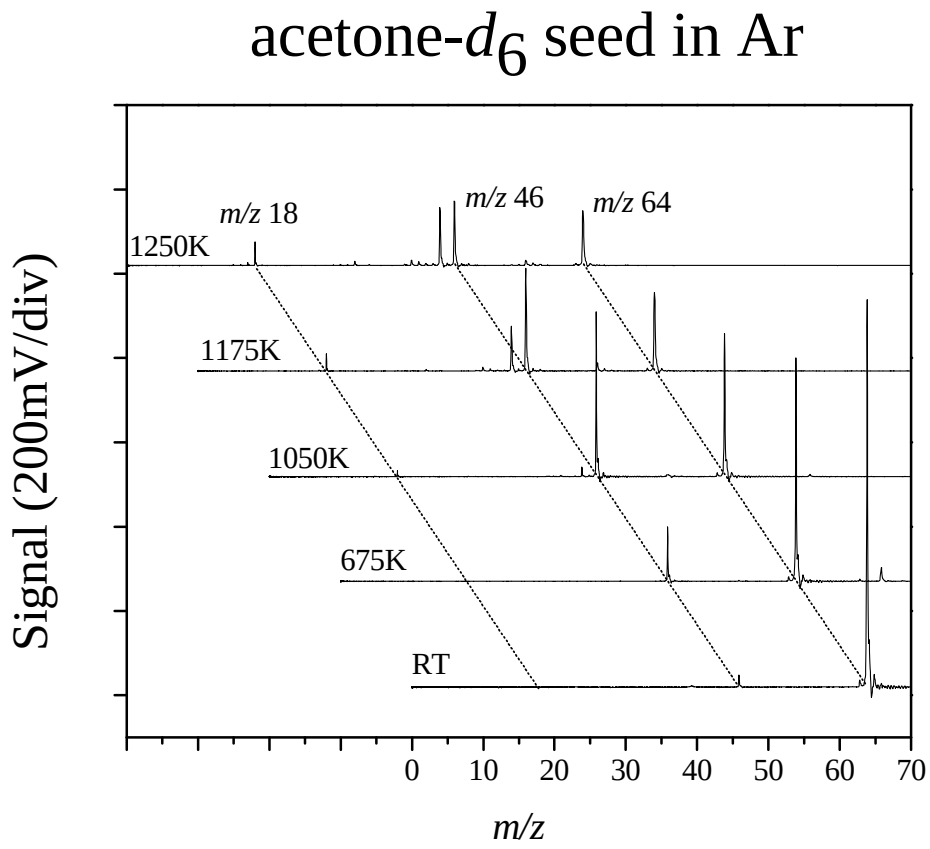

Figure 4.7 Stack plot of mass spectra for the pyrolysis of acetone-d_6 in argon in argon with nozzle temperatures up to 1250 K.

CONCLUSIONS - KETONES

The pyrolysis of 2-butanone and acetone-d_6 was accomplished on the 20-60 ms time scale in either helium of argon carrier gases. At temperatures > 1000 these compounds undergo C-C bond homolysis to form acetyl radicals and in the case of 2-butanone, competitive production of proprionyl radicals. The acetyl radicals rapidly lose H (or D as the case may be) either by photoionization or by thermolysis. The proprionyl

radical is found to prefer β-C-C decomposition to H (D) atom loss and the ethyl radical rapidly decomposes to H atom plus ethene. At temperatures > 1200 K acetyl radical is found to decompose by loss of methyl (or its isotopomer) to form carbon monoxide, CO.

CONCLUSIONS - TAME

The decomposition of TAME in argon was found to onset ~600 K which is slightly lower than the onset temperature for MTBE in argon (~700 K) with the same experimental set-up. A β-CH_3 effect is estimated to be ~0.5 kcal/mol by DFT. Over the temperature range applicable to an operating engine (700K – 1000K) molecular elimination of methanol to form isoamylenes 2m1b and 2m2b are the dominant reaction pathways. These eliminations are predicted to be essentially isoenergetic leading to a statistical distribution of products, which is consistent with experimental results of ~3:1 ratio of 2m1b to 2m2b. At temperatures >950 K primary bond homolysis is observed, which is similar to MTBE in this system which undergoes bond homolysis above 1000 K. In addition, secondary pyrolysis of the isoamylene alkenes, which are not as robust as the isobutene formed from MTBE, is found to occur.

REFERENCES

[1] T. Midgley Jr., Ind. Eng. Chem. 31 (1939) 504.

[2] T. Midgley Jr., T. A. Boyd, Ind. Eng. Chem. (1922) 14.

[3] A. Fischer, M. Muller, J. Klasmeier, Chemosphere 54 (2004) 689.

[4] A. F. Diaz, D. L. Drogos (Eds.), Oxygenates in Gasoline: Environmental Aspects, American Chemical Society (Oxford University Press), Washington, D. C., 1979.

[5] R. M. Stephenson, J. Chem. Eng. Data 37 (1992) 80.

[6] M. J. Papachristos, J. Swithenbank, G. H Priestman, S. Stournas, P. Polysis, E. Lois, J. Inst. Energy 64 (1991) 113.

[7] L. K. Rihko-Struckmann, R. S. Karinene, A. O. Krause, K. Jakobsson, J. R. Aittamaa, Chem. Eng. Process 43 (2004) 57.

[8] L. K. Rihko, A. O. I. Krause, Ind. Eng. Chem. 35 (1996) 2500.

[9] J. Liu, S. Wang, J. A. Guin, Fuel Process. Technol. 69 (2001) 205.

[10] D. E. Hendrickson, U.S. Patent Application W09516763.

[11] L. A. Smith, H. M. Putman, H. J. Semerak, C. S. Crossland, U.S. Patent 6,583,325, (2003).

[12] T. Evans, K. R. Edlund, U.S. Patent 2,010,356 (1935).

[13] J. Ignatius, H. Jaervelin, P. Lindqvist, Hydrocarbon Process 74 (1995) 51.

[14] C. K. Westbrook, W. J. Pitz, Energy and Technology Review Feb/Mar (1991) 1.

[15] C. K. Westbrook, Chemistry and Industry (UK) Aug 3 (1992) 562.

[16] P. J. Askey, C. N. Hinshelwood, Proc. Roy. Soc. 115A (1927) 215.

[17] A. Maccoll, Progress in Reaction Kinetics, Pergamon Press, Oxford, 4 (1967).

[18] K. J. Laidler, D. J. McKenney, The Chemistry of the Ether Linkage, Interscience, New York, 1967.

[19] K. H. Anderson, S. W. Benson, J. Chem. Phys 36 (1962) 2320.

[20] D. J. McKenney, K. J. Laidler Can. J. Chem. 41 (1963) 1984.

[21] G. R. Freeman, C. J. Danby, C. N. Hinshelwood, Proc. Roy. Soc. A245 (1958) 28.

[22] C. J. Danby, G. R. Freeman, Proc. Roy. Soc. A245, (1958) 43.

[23] G. R. Freeman, Proc. Roy. Soc. A245 (1958) 75.

[24] K. J. Laidler, D. J. McKenney, Proc. Roy. Soc. A278 (1964) 505.

[25] A. T. Blades, G. W. Murphy, J. Amer. Chem. Soc. 78 (1952) 1039.

[26] N. J. Daly, V. R. Stimson, Aust. J. Chem. 19 (1966) 239.

[27] N. J. Daly, C. Wentrup, Aust. J. Chem. 21 (1968) 1535.

[28] N. J. Daly, C. Wentrup, Aust. J. Chem. 21 (1968) 2711.

[29] K. Y.Choo, D. M. Golden, S. W. Benson, Int. J. Chem. Kinet. 6 (1974) 631.

[30] J. C. Brocard, F. Baronnet, Oxid. Comm. 1 (1980) 321.

[31] B. El Kadi, F. Baronnet, J. Chim. Phys. 92 (1995) 706.

[32] H. Bohm, F. Baronnet, B. El Kadi, Phys. Chem. Chem. Phys. 2 (2000) 1929.

[33] A. Goldaniga, T. Faravelli, E. Ranzi, P. Dagaut, M. Cathonnet, Twenty-Seventh Symposium (International) on Combustion/The Combustion Institute (1998) 353.

[34] C. S. McEnally, L. D. Pfefferle, Int. J. Chem. Kin. 36 (2004) 345.

[35] H. E. O'Neal, S. W. Benson, J. Phys. Chem. A 71 (1967) 2903.

[36] A. Maccoll, Chem. Rev. 69 (1969) 33.

[37] S. W. Benson, A. N. Bose, Chem. Phys. 39 (1963) 3463.

[38] S. W. Benson, G. R. Haugen, J. Am. Chem. Soc. 87 (1965) 4036.

[39] K. H. Weber, J. Zhang, D. Borchardt, T. H. Morton, Int. J. Mass Spec. 249-250 (2006) 303.

[40] K. H. Weber, J. M. Lemieux, J. Zhang, J. Phys. Chem. A 113 (2009) 583.

[41] S. D. Chambreau, J. Zhang, J. C. Traeger, T. H. Morton, Int. J. Mass Spec. 199 (2000) 17.

[42] T. Zhang, J. Wang, T. Yuan, X. Hong, L. Zhang, J. Phys. Chem. A 112 (2008) 10487.

[43] T. Zhang, L. Zhang, J. Wang, T. Yuan, X. Hong, F. Qi, J. Phys. Chem. A 112 (2008) 10495.

[44] D. W. Kohn, H. Clauberg, P. Chen, Rev. Sci. Instrum. 63 (1992) 4003.

[45] A. B. Friderichsen, J. G. Radziszewski, M. R. Nimios, P. R. Winter, D. C. Dayton, D. E. David, G. B. Ellison, J. Am. Chem. Soc. 123 (2001) 1977.

[46] H. Clauberg, D. W. Minsek, P. Chen, J. Am. Chem. Soc. 114 (1992) 99.

[47] C. Lee, W. Yang, G. Parr, Phys. Rev. B 37 (1988) 785.

[48] A. D. Becke, J. Chem. Phys. 109 (2001) 9287.

[49] M. J. Frisch, G. W. Trucks, H. B. Schlegel, G. E. Scuseria, M. A. Robb, J. R. Cheeseman, V. G. Zakrzewski, J. A. Montgomery, R. E. Stratmann, J. C. Burant, S. Dapprich, J. M. Millim, A. D. Daniels, K. N. Kudin, M. C. Strain, O. Farkas, J. Tomasi, V. Barone, M. Cossi, R. Cammi, B. Mennucci, C. Pomelli, C. Adamo, S. Clifford, J. Ochterski, G. A. Peterson, P. Y. Ayala, Q. Cui, K. Morokuma, D. K. Malick, A. D. Rabuck, K. Raghavachari, J. B. Foresman, J. Cioslowski, J. V. Ortiz, B. B. Stefanov, G. Liu, A. Liashenko, P. Piskorz, I. Komaromi, R. Gomperts, R. L. Martin, D. J. Fox, T. Deith, M. A. Al-Laham, C. Y. Peng, A. Nanayakkara, C. Gonzalez, M. Challacombe, P. M. W. Gill, B. G. Johnson, W. Chen, M. W. Wong, J. L. Andres, M. Head-Gordon, E. S. Replogle, J. A. Pople Gaussian 98/03, Gaussian, Inc., Pittsburgh, PA, 1998.

[50] J. C. Traeger, T. H. Morton, J. Phys. Chem. A 109 (2005) 10467.

[51] W. Tao, R. B. Klemm, F. L. Nesbitt, J. L. Stief, J. Phys. Chem. 96 (1992) 104.

[52] J. C. Brocard, F. Baronnet, H. E. O'Neal, Combust. Flame 52 (1983) 25.

[53] W. J. Marinelli, T. H. Morton, J. Am. Chem. Soc. 100 (1978) 3536.

[54] A. J. Gordon, R. A. Ford, The Chemists Companion, Wiley, New York, 1972.

[55] J. Waser, K. N. Trueblood, Chem One, McGraw-Hill, New York, 1976.

[56] J. C. Traeger, Org. Mass Spectrom. 20 (1985) 223.

[57] J. C. Traeger, R. F. McLouglin, A. J. C. Nicholson, J. Amer. Chem. Soc. 104 (1982) 5318.

CHAPTER 5

MTMB

INTRODUCTION

tert-Alkyl methyl ethers have seen wide use as fuel additives for nearly 40 years. As replacements for tetraethyllead, the simplest homologues – methyl *tert*-butyl ether (MTBE) and *tert*-amyl methyl ether (TAME) – present a new set of problems. Because of their water solubility, leakage from underground storage tanks and pipelines threatens to contaminate the water table with volatile compounds that can be smelled at part per billion concentrations.[1]

Higher homologues have been discussed as alternatives to MTBE and TAME, because they are expected to be much less soluble in water. More highly branched methyl ethers have attracted particular attention. *tert*-Octyl methyl ether (2-methoxy-2,4,4-trimethylpentane, TOME) exhibits excellent antiknock properties,[2] and approaches to its large scale production have recently been described.[3] Several patents and procedures outline the preparation and utilization of *tert*-hexyl methyl ether (2-methoxy-2,3-dimethylbutane, MDMB) along with other homologues and isomers.[4-9]

Conspicuously absent from this literature is the most highly branched example, 2-methoxy-2,3,3-trimethylbutane, which will be abbreviated below as MTMB. While general discussions of replacements for MTBE allude to this compound, very little

specific information has been provided.[4,9] MTMB has been the focus of NMR studies of internal rotation,[10] because of its high degree of internal steric hindrance, and has recently been studied (along with TAME, MDMB, TOME, and other homologues) by photoionization mass spectrometry.[11] However, the thermal decomposition of the neutral compound has not been discussed heretofore.

Two aspects of oxygenated fuel additives have become of paramount interest. The first is their antiknock activity in an automobile motor. The second is their solubility in water. Engine knock results from explosion of the fuel-oxygen mixture in front of the flame front during the power stroke.[12] If the fuel-air mixture at the far end of a hot cylinder ignites before the flame initiated by the sparkplug arrives, damage to the motor can result (not to mention loss of power and inefficient use of fuel). A definitive mechanism for the action of antiknock agents has not been described in the open literature, but there is no shortage of published hypotheses.[2] The behavior of oxygenated compounds at high temperatures provides a guide to how a compound might function when it comes in contact with a hot cylinder wall.

The second aspect addresses the fate of fuel that finds its way into the environment. Partition of fuel oxygenates into ground water has caused considerable alarm, regardless of whether they actually inflict environmental damage or have serious health effects. This paper addresses both aspects: the water solubilities of MDMB,

MTMB, and TOME are compared with those of TAME and MTBE, and the primary thermal decomposition channels of neutral MTMB at high temperatures are described, as monitored by photoionization mass spectrometry.

Traditional kinetic studies of bond homolyses have made use of scavenger techniques,[13,14] in order to assess the extent to which free radicals are formed. These methods examine the stable products derived from free radicals, rather than observing the radicals directly. In recent years, photoionization mass spectrometry has become a useful technique for interrogating free radicals.[15,16] In order for this approach to work, products of bond homolysis must give spectroscopic signatures that differ from those of the reactants or the products from other pathways. One of the most characteristic signatures is that of methyl cation (*m/z* 15), which arises uniquely from methyl radical at low photon energies. In the present study, 118 nm photoionization of the pyrolysis products of deuterated MTMB reveals the formation of methyl radicals, along with other products that are characteristic of bond homolysis.

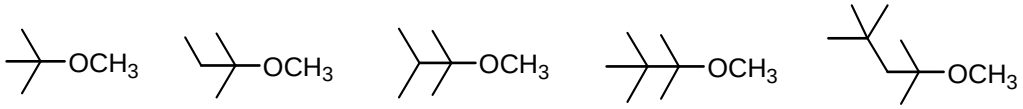

MTBE TAME MDMB MTMB TOME

The approach in these experiments presents several advantages: (1) a short reaction time to examine the initial steps of the thermal decomposition; (2) supersonic cooling, which quenches the reaction and minimizes recombination of products and intermediates; and

(3) minimal ion fragmentation by the use of the 10.48 eV "soft" photoionization source that imparts sufficient energy to ionize many closed-shell and free radical species. The supersonic cooling further reduces photoionization fragmentation by minimizing the internal energy of the parent molecules and the pyrolysis products.

Previous work from these laboratories has dealt with thermal decomposition of MTBE.[16] Molecular elimination represents the predominant mechanism, as Scheme 5.1 portrays. The published Arrhenius activation parameters, (E_a = 247 ± 4 kJ mol^{-1}; A = $10^{13.9}$ s^{-1})[17] correspond to dissociation of MTBE into methanol and isobutene, as the upper pathway in Scheme 5.1 depicts for an isotopically labeled analogue.

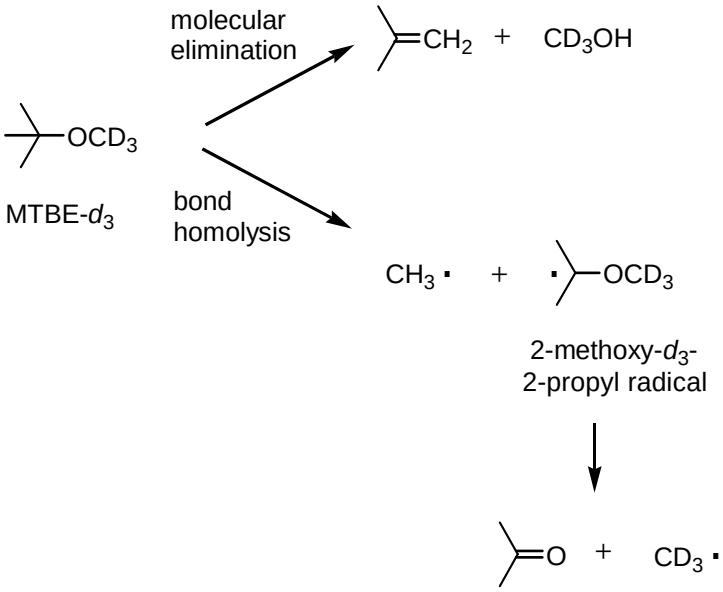

Scheme 5.1 Depiction of the expected molecular elimination and bond homolysis pathways expected in the pyrolysis of MTBE-d_6.

As we have previously reported in this journal, bond homolysis begins to compete with elimination at temperatures $\geq$1000K.[16] While the thermodynamic threshold for homolysis is much higher than the E_a for molecular elimination, the Arrhenius preexponential factors for bond homolyses are also much larger ($A > 10^{16}$ s^{-1} [17]). Consequently, at suitably high temperatures molecular elimination and homolysis proceed with comparable rates. As in the case of most thermal decomposition experiments with neutral molecules (except those performed in shock tubes or "wall-less reactors" [17]), it is difficult to rule out surface catalysis. However, the observed behavior is consistent with the activation parameters for homogeneous gas phase reactions.

Bond homolysis of MTBE initially forms a methyl radical and 2-methoxy-2-propyl radical, as illustrated by the lower pathway in Scheme 5.1. The 2-methoxy-2-propyl radical is unstable under the reaction conditions and dissociates to acetone plus a second methyl radical. Hence, bond homolysis of the deuterated MTBE shown in Scheme 5.1 yields a d_3-methyl radical and an undeuterated methyl radical, along with a molecule of acetone. At higher temperatures, acetone itself undergoes bond homolysis to produce acetyl radical and, ultimately, to yield two methyl radicals and carbon monoxide.

TOME undergoes the same sort of molecular elimination as does MTBE.[16] In those experiments, though, further decomposition of the olefinic products obscured the radicals that would be expected from bond homolysis. Thus, it remains unclear whether

the competition represented in Scheme 5.1 operates at elevated temperatures for the higher homologues of MTBE. Results presented here for MTMB show that homolysis competes effectively with molecular elimination in the case of this homologue.

EXPERIMENTAL

MTBE-d_3 was purchased from Cambridge Isotope Laboratories, acetone-d_6 from Aldrich Chemical Co., and 2,3,3-trimethyl-2-butene from ChemSampCo; these commercial products were used without further purification. Methoxy-2,3,3-trimethylbutane-d_6 (MTMB-d_6) was prepared as previously described[11] by addition of excess acetone-d_6 to a pentane solution of *tert*-butyllithium at –78° C followed by distillation of the recovered alcohol and conversion to the methyl ether in THF solution. The product ether was twice distilled at atmospheric pressure (bp 118º-121ºC). Other deuterated *tert*-alkyl methyl ethers were prepared in similar fashion, as previously described.[11,16]

Water solubilities of deuterated *tert*-alkyl methyl ethers were determined using ^{2}H NMR. An excess of the ether was sealed in a glass ampoule with deionized water, repeatedly mixed by shaking, and allowed to stand for at least 24 hours. The NMR spectrum of the aqueous layer was recorded and the peaks from CD_3 groups integrated relative to the natural abundance HOD peak (16.7 m<u>M</u>).

RESULTS

The impetus for studying multiply branched *tert*-alkyl methyl ethers derives from the water solubility of MTBE. As Table 5.1 summarizes, TAME (the replacement presently in use) is about one-third as soluble as MTBE on a mass basis. Further branching causes a sharp decrease in water solubility, as tabulated for MDMB, MTMB, and TOME. The biggest drop (more than a factor of 10) occurs with the increase in branching in going from MDMB to MTMB. On a mass basis, MTMB is nearly 200 times less soluble than MTBE, while TOME is 400 times less soluble than MTBE.

Scheme 5.2 illustrates the products expected from gas phase pyrolysis of MTMB-d_6. Molecular elimination of CH_3OD should yield 2,3,3-trimethyl-1-butene-d_5, as shown. Homolysis of the weakest bond of MTMB- d_6 ought to produce *tert*-butyl radical and a deuterated 2-methoxy-2-propyl radical. Both of those radicals should dissociate further under the reaction conditions. The *tert*-butyl radical is known to expel a hydrogen atom at elevated temperatures: the published kinetic parameters predict it should have a lifetime on the order of 10^{-6} sec at 1000K.[21] As noted above, the 2-methoxy-2-propyl radical is also unstable: the deuterated analogue should dissociate to methyl radical plus acetone-d_6.

Formula	Abbreviated	Molarity	mg/litre
$(CH_3)_3COCH_3$	MTBE [a]	403 m*M*	$3.55x10^4$
$CH_3CH_2C(CH_3)_2OCH_3$	TAME [b]	110 m*M*	$1.1x10^4$
$(CH_3)_2CHC(CH_3)_2OCH_3$	MDMB [c]	19 m*M*	2200
$(CH_3)_3CC(CH_3)_2OCH_3$	MTMB [c]	1.4 m*M*	180
$(CH_3)_3CCH_2C(CH_3)_2OCH_3$	TOME [c]	0.6 m*M*	90

[a] A. Fischer, M. Muller, J. Klasmeier, *Chemosphere* 54 (2004) 689.

[b] R.M. Stephenson, *J. Chem. Eng. Data* 37 (1992) 80.

[c] This work

Table 5.1 Solubilities of *tert*-alkyl methyl ethers in water at 20ºC.

The thermal decomposition of MTMB-d_6 was performed by seeding the sample both in argon and in helium passed through the pyrolysis tube, followed by supersonic expansion and 118 nm photoionization. With a heavier carrier gas, contact time is increased, while the jet expansion gives more effective vibrational cooling. The mass spectra of a sample in argon pyrolyzed in the temperature domain 575K to 900K is shown in Fig 5.1, in which a small amount of unlabeled 2,3,3-trimethyl-1-butene was included for comparison. For clarity, only the region above *m/z* 77 is shown in Fig 5.1.

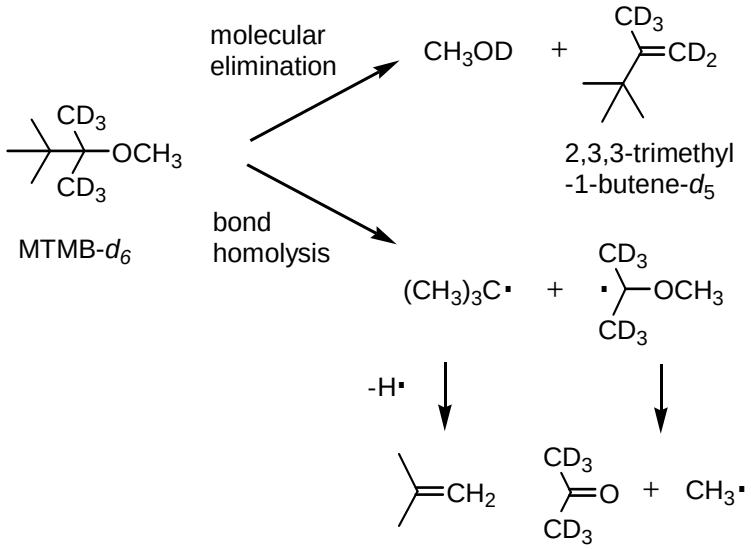

Scheme 5.2 Depiction of the molecular elimination and bond homolysis pathways expected in the pyrolysis of MTMB-d_6.

The bottom trace shows the mass spectrum of a room temperature sample cooled by supersonic jet expansion. Note that the base peak intensities (*m/z* 79 from MTMB and *m/z* 98 from the added alkene) drop sharply in going from room temperature to 575K. This is a consequence of the decrease in number density of the sample when it is heated.

Undeuterated 2,3,3-trimethyl-1-butene was examined separately as well as in a mixture with MTMB-d_6. Photoionization of this alkene produces two ions, *m/z* 98 (the molecular ion) and *m/z* 83, the M-CH_3 fragment ion. No *m/z* 15 ion is seen below 850K, which confirms that *m/z* 83 results from mass spectrometric decomposition of ionized

2,3,3-trimethyl-1-butene, rather than bond homolysis prior to ionization. At higher temperatures the *m/z* 83 intensity becomes larger than that of *m/z* 98, as bond homolysis of the neutral alkene starts to produce the allylic radical $(CH_3)_2C=C(CH_3)CD_2^{\cdot}$ (and *m/z* 15 begins to appear).

The ions at *m/z* 103 and *m/z* 88 in Fig 5.1 correspond to 2,3,3-trimethyl-1-butene-d_5 (from molecular elimination) and its M-CH_3 fragment. The ions at *m/z* 79 and *m/z* 118 come from the intact starting material: $(CD_3)_2C=OCH_3^+$, the M-$(CH_3)_3C$ ion from MTMB-d_6, and $(CH_3)_3CC(CD_3)=OCH_3^+$, the M-CD_3 ion from MTMB-d_6.[11] The extent of molecular elimination is comparable to what is observed for MTBE in this temperature domain. Methanol cannot be detected in these experiments because its IE is higher than 10.48 eV.[21] Fragments lighter than *m/z* 79 are not seen below 850K with argon as carrier gas.

Pyrolyses of samples of MTMB-d_6 seeded in helium are summarized by the stack plot of photoionization mass spectra in Fig 5.2. The carrier gas was changed in order to shorten the contact time, so as to minimize the contribution from pyrolysis of the alkene from molecular elimination. At 800K, in addition to the fragment ions from MTMB-d_6 (which does not exhibit a molecular ion), there is a peak at *m/z* 73 from a trace of MTBE ($(CH_3)_2C=OCH_3^+$, the M-CH_3 ion from MTBE), which was added to facilitate mass

calibration. The molecular ion of MTBE is too weak to detect under these conditions,[16] while MTMB-d_6 exhibits no molecular ion at all.

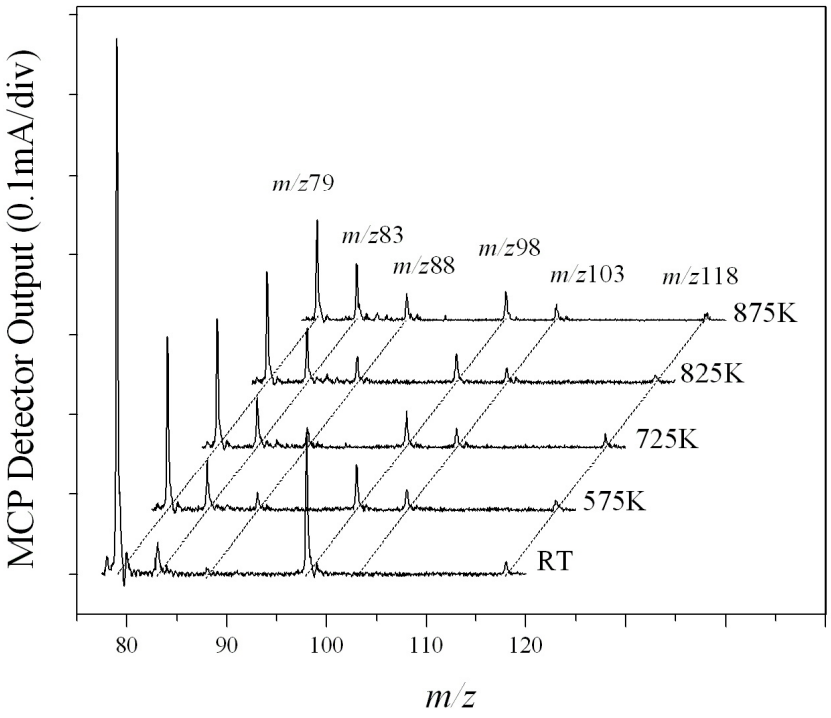

Figure 5.1 Stack plot of pyrolysis/supersonic jet expansion/118.2 nm photoionization TOF mass spectra of MTMB-d_6 seeded in argon (with a small amount of 2,3,3-trimethyl-2-butene as internal standard) as a function of nozzle temperature.

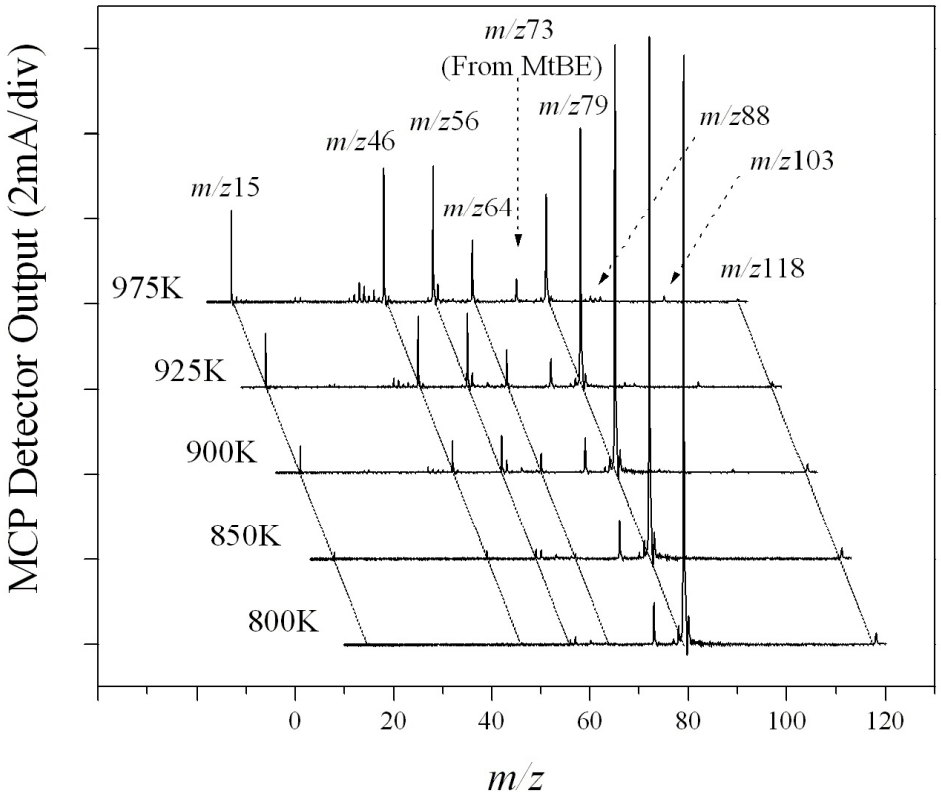

Figure 5.2 Stack plot of pyrolysis/supersonic jet expansion/118.2 nm photoionization TOF mass spectra of MTMB-d_6 seeded in helium (with a small amount of MTBE as internal standard) as a function of nozzle temperature.

As the temperature of the pyrolysis tube is raised above 850K, six new ions appear: *m/z* 15, *m/z* 46, *m/z* 56, *m/z* 57¸ *m/z* 64, as well as a very small *m/z* 88 peak. The lightest of these is methyl cation, which comes from photoionization of methyl radical. It is significant that no *m/z* 18 (CD_3^+) emerges until much higher temperatures. The

heaviest ion corresponds to photoionization of 2,3,3-trimethyl-2-butene-d_5 and of the allylic ion, $(CH_3)_2C{=}C(CD_3)CD_2^{\cdot}$, from its pyrolysis. The *m/z* 64 ion is the molecular ion from photoionization of the acetone-d_6 product, and *m/z* 46 is its M-CD_3 fragment. Photolysis of an authentic sample of acetone-d_6 in the experimental apparatus shows that the *m/z* 46 fragment always accompanies the molecular ion, providing a distinctive signature. Finally, *m/z* 57 comes from photoionization of the *tert*-butyl radical, while *m/z* 56 comes from photoionization of isobutene, the olefin produced by loss of a hydrogen atom from *tert*-butyl radical (as portrayed in Scheme 5.2).[18] The growth of the *m/z* 15, 46, 56, 57, and 64 peak intensities with increasing temperature demonstrates the dominance of the homolysis channel shown in Scheme 5.2.

The *m/z* 88 ion from 2,3,3-trimethyl-2-butene-d_5 has a very low intensity above 850K. At this temperature, 2,3,3-trimethyl-2-butene does begin to dissociate; the neutral alkene undergoes bond scission to $(CH_3)_2C{=}C(CD_3)CD_2^{\cdot}$ and methyl radical. From the control experiments on pyrolysis of the neutral, undeuterated alkene, however, it is clear that the *m/z* 15 peak seen in the MTMB-d_6 pyrolysis arises via the homolysis depicted in Scheme 5.2, rather than by dissociation of the alkene subsequent to molecular elimination.

The relative ion intensities in Fig 5.2 imply that molecular elimination (for which the signal occurs at *m/z* 88) is a minor pathway above 900K. For purposes of comparison, the stack plots in Fig 5.3 summarize the dissociation of MTBE-d_3 in the same

temperature domain. Isobutene (*m/z* 56) is the principal product from MTBE. As the intensity of *m/z* 56 increases with temperature, the photofragment at *m/z* 41 becomes visible (as confirmed by examination of an authentic sample of isobutene under the same conditions). As previously described, *m/z* 43 comes from thermal decomposition of acetone,[16] a product of the bond homolysis drawn in Scheme 5.1.

The pyrolysis/photoionization mass spectra in Fig 5.3 illustrate an additional complication in interpreting experimental results. Supersonic expansion in helium cools a room temperature sample down to <50K. Expansion of much hotter sample gives a jet with a correspondingly higher vibrational temperature. Some compounds show photoionization mass spectra that exhibit great sensitivity to vibrational energy content. MTBE is a case in point. An ion at *m/z* 57 appears upon heating, at temperatures below the onset of thermal decomposition, as indicated by its intensity relative to *m/z* 56 at 725K in Fig 5.3 (a). That ion contributes an intense peak in the published EI mass spectrum of MTBE at room temperature,[21] but this mass spectrometric fragmentation is effectively suppressed by cooling in a supersonic jet. When the temperature of the sample in the jet is elevated, the fragmentation of ionized MTBE to *m/z* 57 comes back.

One way of probing the temperature dependence of the photoionization mass spectrum is to examine supersonic expansions in argon carrier gas, which provides more effective cooling. Figures 5.3 (a) and (b) compare the pyrolysis/photoionization results

of MTBE-d_3 for these carrier gases. At room temperature, expansion of MTBE-d_3 in argon leads to a visible molecular ion peak at *m/z* 91. Expansion in helium gives a much smaller molecular ion peak, which is barely detectable. As noted above, MTBE-d_3 gives rise to *m/z* 57 ion when it is heated prior to super- sonic expansion in helium, even when no thermal decomposition is taking place. By contrast, pyrolysis/photoionization using argon as carrier gas gives greatly reduced intensities of *m/z* 57.

A

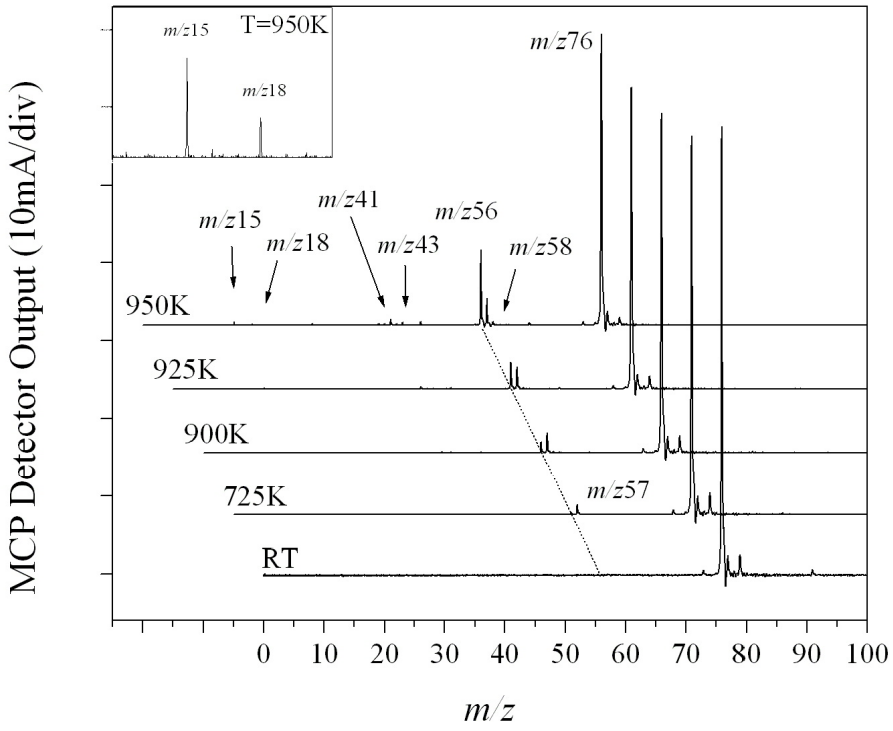

Figure 5.3 Stack plots of pyrolysis/supersonic jet expansion/118.2 nm photoionization TOF mass spectra of MTBE-d_3 seeded in helium with inset showing low mass fragments at 950K, intensity x40).

B

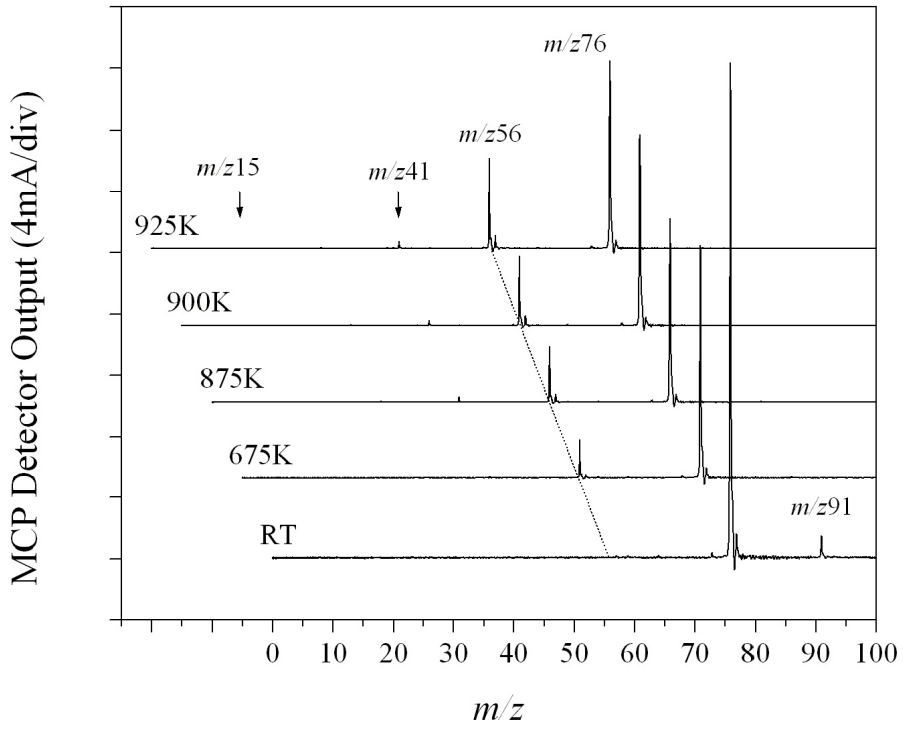

Figure 5.3 Stack plots of pyrolysis/supersonic jet expansion/118.2 nm photoionization TOF mass spectra of MTBE-d_3 seeded in argon as functions of nozzle temperature.

Following supersonic cooling, acetone, MTMB-d_6, and 2,3,3-trimethyl-2-butene display much less dependence of their photoionization mass spectra upon vibrational energy content (at least, as can be assessed by comparing expansion in helium versus argon). Thus the following inferences may be drawn:

(1) comparison of Fig 5.1 with Fig 5.3 (b) indicates that molecular elimination from MTMB-d_6 (as signaled by *m/z* 103 and its *m/z* 88 fragment ion) and MTBE-d_3 (as signaled by *m/z* 56) exhibit similar dependence upon pyrolysis temperature: alkene peaks become apparent around 600K. In Fig 5.1 the *m/z* 88 and *m/z* 103 peak intensities at 875K add up to about 40% of the intensity of *m/z* 79, while in Fig 5.3 (b) the *m/z* 56 peak at 875K has an intensity 30% that of *m/z* 76.

(2) the onset of bond homolysis of MTBE-d_3 in helium begins to be detectable at 950K (Fig 5.3 (a)), at which temperature *m/z* 15 and *m/z* 18 are both seen, as expected on the basis of Scheme 5.1 (some additional *m/z* 15 comes from thermal decomposition of acetone at this temperature);

(3) in helium, the peaks characteristic of homolysis of MTMB-d_6 – *m/z* 15, *m/z* 46 and 64, and *m/z* 56 and 57 (as expected on the basis of Scheme 2) – begin to appear at 850 K. Under these conditions the peaks corresponding to molecular elimination – *m/z* 88 and 103 – cannot be seen until above 900K and never become as intense as the peaks from bond homolysis.

Taking carrier gas effects into consideration, we conclude that homolytic bond cleavage of MTMB-d_6 overtakes molecular elimination as the predominant thermal dissociation pathway around 900K.

CALCULATIONS

Two thermal decomposition precedents can be compared with the results for MTMB. The homogeneous gas phase cleavage of hexamethylethane (HME; X=Y=CH_3 in Eqn 1) has been closely studied.[13] Thermal cleavages of the dimethyl ethers of tertiary *vic*-diols have also been examined.[14] While the simplest example, pinacol dimethyl ether (PDME; X=Y=OCH_3 in Eqn 1), has not been reported, extrapolation from its higher homologues predicts an activation energy approximately 45-50 kJ mol^{-1} lower than that of HME. Homolyses of HME and of tertiary *vic*-diol dimethyl ethers are reported to have Arrhenius preexponential factors on the order of 10^{17} s^{-1}. It is not obvious *a priori* whether cleavage of the central bond of MTMB should be much easier than that of HME (as it is for PDME). This question has been addressed by means of computation.

(1)

HME: X=Y=CH_3
PDME: X=Y=OCH_3
MTMB: X=CH_3, Y=OCH_3

Computations were explored using three levels of theory using the GAUSSIAN98 and GAUSSIAN03 program suites, all based on geometries optimized using density functional theory (DFT) at B3LYP/6-31(2df,p): DFT, G3X, and coupled clusters (CCSD) using single and double excitations. G3X theory represents a composite approach; it makes use of DFT zero point energies (scaled by a factor of 0.9854) and single-point electronic energies calculated at several higher ab initio levels The G3X energy is determined by sums and differences of those single point energies, including the scaled

zero point energy and a higher level correction.[22,23] In the case of HME, DFT optimization with no symmetry constraint gives the lowest electronic energy, but the geometry with D_{3d} symmetry possesses a lower zero point energy, which makes the D_{3d} structure energetically more favorable. MTMB was optimized with no symmetry constraint, while MTBE and the methoxythexyl radical ($MeOCMe_2CMe_2^{\cdot}$) preferred C_s symmetry. Methyl and *tert*-butyl radicals were optimized with C_{3v} symmetry constraints, but no constraint was imposed in the optimization of 2-methoxyisopropyl radical ($MeOCMe_2^{\cdot}$) or $tBuCMeOMe^{\cdot}$. Table 5.2 summarizes the results calculated for homolyses of HME, MTMB, and MTBE.

At the DFT level the 0K bond dissociation energy (D_0) of HME is calculated to be 246 kJ mol^{-1}, considerably lower than the reported experimental 300K bond dissociation energy of 322 kJ mol^{-1}.[24] Consideration of basis set superposition error (which is neglected here) would lower the calculated DFT value even further. By contrast, G3X theory predicts a D_0 value of 332 kJ mol^{-1} for HME, while CCSD gives a value of D_0 = 313 kJ mol^{-1} when unscaled zero point energies are taken into account.

Formula	Abbreviated	B3LYP	ZPE	G3X(0K)	CCSD
$(CH_3)_3CC(CH_3)_3$	HME	-315.729545	639	-315.359376	-314.905854
$(CH_3)_3CC(CH_3)_2OCH_3$	MTMB	-390.941418	650	-390.533186	-389.973150
$(CH_3)_3COCH_3$	MTBE	-272.998803	428	-272.717508	-272.330985
$(CH_3)_3C$ radical	tBu·	-157.812298	305	-157.616387	-157.387834
$(CH_3)_2COCH_3$ radical	MeOCMe·	-233.023958	320	-232.790851	-232.455274
CH_3 radical	Me·	-39.8433562	78	-39.792981	-39.720503
$(CH_3)_3CC(CH_3)OCH_3$ rad	tBuCMeOMe·	-350.972148	542	-350.612575	-350.102174
$(CH_3)_2CC(CH_3)_2OCH_3$ rad	$MeOCMe_2CMe_2$·	-350.965188	539	-350.608212	

Table 5.2 DFT electronic energies (a.u.), unscaled zero point energies (kJ mol^{-1}), G3X energies (a.u.), and CCSD energies (a.u.) of HME, MTMB, MTBE, and selected homolysis fragments using geometries optimized at B3LYP/6-31G(2df,p).

G3X theory gives a 0K bond dissociation energy for the central bond of MTMB of D_0 = 330 kJ mol^{-1}, while CCSD predicts a value of 316 kJ mol^{-1}. That is to say, both computational levels predicts the homolyses of the 2,3-bonds of HME and MTMB in eqn 1 to have nearly the same endothermicities. The value for homolysis of a methyl radical off of the *tert*-butyl group of MTMB (the 3,4-bond) to form a methoxythexyl radical ($MeOCMe_2CMe_2$·) is much higher, for which G3X theory predicts D_0 = 354 kJ mol^{-1}.

G3X and CCSD give quite different estimates of the enthalpy changes for cleavage of α–methyl groups. For homolysis of the 1,2-bond of MTBE (breaking apart the *tert*-butyl group) G3X theory predicts D_0 = 351 kJ mol^{-1} and CCSD predicts D_0 = 377 kJ mol^{-1}. Homolysis of the 1,2-bond of MTMB to give tBuCMeOMe· (2-methoxy-3,3-dimethylbutyl radical) corresponds to 0K bond dissociation energies of D_0 = 335 kJ mol^{-1} at G3X and D_0 = 365 kJ mol^{-1} at CCSD. Despite the fact that the D_0 values vary markedly between CCSD and G3X, both levels of theory estimate that the α–cleavage of methyl is less endothermic for MTMB than for MTBE (by 12 and 16 kJ mol^{-1}, respectively), as would be expected on the basis of steric hindrance.

While G3X calculations confirm the expectation that the 2,3-bond of MTMB is the one most easily cleaved, this level of theory gives calculated D_0 values for the two possible α–cleavages that are closer together than might have been anticipated. If the activation energies for 1,2-bond homolysis and 2,3-bond homolysis of MTMB were truly separated by only 5 kJ mol^{-1}, *m/z* 18 (from photoionization of CD_3 radicals) should have been observed in Figure 5.2 with an intensity roughly one-half that of *m/z* 15. Since *m/z* 18 is barely detectable, either the activation barriers are much further apart than the calculated G3X difference in D_0 values, or else the Arrhenius preexponential factors differ greatly.

The D_0 values calculated at CCSD/6-31G(2df,p)//B3LYP/6-31G(2df,p) using single and double excitations differ markedly from those at G3X. The 0K dissociation energy of the 2,3-bond of MTMB has a value of $D_0 = 316$ kJ mol^{-1}, while the calculated value for the 1,2-bond is $D_0 = 365$ kJ mol^{-1}. In other words, CCSD gives a difference in D_0 (49 kJ mol^{-1}) that is more consistent with the experimental results reported here.

DISCUSSION

When the hydrocarbon mixture used as a motor fuel autoignites in an automobile cylinder, engine knock results, and it becomes necessary to add antiknock agents. The two most prevalent antiknock compounds used in the twentieth century, tetraethyllead and MTBE, have now been banned in many locales, the former on the basis of its toxicity and the latter because of its solubility in water. Other methyl *tert*-alkyl ethers (higher homologues of MTBE) also exhibit antiknock properties. Table 5.1 summarizes the decrease in water solubility with increasing carbon number, the qualitative trend that one would expect. The biggest jump occurs in going from *tert*-hexyl methyl ether (MDMB) to the title compound, MTMB.

The antiknock properties of alkyl ethers have been ascribed to their facile molecular elimination of alcohol. It has been hypothesized that the resulting alkenes inhibit radical chain reactions in the fuel/air mixture on the uncombusted side of the

advancing flame front.[25] Hydrogen atom abstraction produces allylic radicals, which are thought to be less reactive in initiating ignition. Consistent with this model, a variety of fuel oxygenates with easily abstracted hydrogens, including 2-methylfuran, furfuryl alcohol, and *p*-cresol[26] are among the candidates proposed as viable antiknock additives, in addition to simple aliphatic alcohols,[27] as well as the *tert*-alkyl ethers TAME,[1] TOME,[2,3] MDMB,[6] ethyl *tert*-butyl ether (ETBE), and isopropyl *tert*-butyl ether (IPTBE).[28]

If this model is correct, the pyrolysis/supersonic jet expansion/118.2 nm photoionization TOF mass spectroscopic experiments reported here imply that MTMB ought to be a poor antiknock agent. Unlike MTBE or TOME, MTMB tends to produce free radicals under pyrolysis conditions, in preference to molecular elimination. Many potential fuel additives have been explored and found to be proknock.[2] The propensity of MTMB to undergo the homolysis drawn in Scheme 5.2 suggests that it may belong to this category.

The homolysis of MTMB appears to be highly specific for the 2,3-bond, yielding *tert*-butyl and methyl radicals, along with acetone-d_6. No cleavage of the 1,2-bond is seen, as attested by the virtual absence of CD_3^+ (*m/z* 18) in the photoionization mass spectra. The very tiny amount of *m/z* 18 that can be seen at the highest temperature in

Figure 5.2 can be ascribed to thermal dissociation of acetone-d_6 under the pyrolysis conditions.

The choice of carrier gas affects the pyrolytic pathways observed in the present experiments. The longer contact time provided by argon allows lower temperature decompositions to be seen. Comparison of Figure 5.1 with Figure 5.3 (b) shows that MTMB and MTBE exhibit similar propensities for molecular elimination below 900K, where not much bond homolysis is seen. At temperatures $\geq$900K, however, homolysis of the central bond of MTMB overtakes molecular elimination as the predominant pathway. The shorter contact time achieved using helium as carrier gas allows the homolysis products (methyl radical, acetone, and *tert*-butyl radical) to be detected. A shorter contact time has the advantage that subsequent dissociations of these products can be minimized.

Three levels of computation have been compared, which make very different predictions regarding bond homolyses. G3X theory gives dissociation energies for the 1,2- and 2,3-bonds of MTMB that are so close to one another that, if correct, CD_3 radicals ought to have been seen in the pyrolysis of MTMB-d_6. By contrast, CCSD calculations predict that the D_0 values differ by 49 kJ mol^{-1}, in agreement with the experimental observation that only the 2,3-bond cleaves.

Pyrolysis of isobutylene (C_4H_8)

Isobutylene was obtained and diluted in argon to 3% without further purification. Figure 5.4 presents a stack plot of mass spectra from the pyrolysis of isobutylene. In the room temperature trace a large molecular ion peak is observed at *m/z* = 56 (IE = 9.19 eV[29]). An isotope peak at *m/z* = 57 is observed with approximately 4% the intensity of the molecular ion, as would be expected. A small $–CH_3$ photoionization fragment at *m/z* = 41 is detected (AE = 11.33 eV[30]) and a much smaller –H photoionization peak is perhaps detectable at *m/z* = 55 (AE = 11.26 eV[29]). Both the $–CH_3$ and –H photoionization fragments have reported AEs of ~ 11.3 eV. Here it appears that expulsion of the alkyl group is preferred over hydrogen atom ejection. Additionally, it indicates that there is a small amount of higher energy ionization occurring, whether it be EI from the photoelectric effect or multi-photon in origin. There are poorly defined peaks in the vicinity of *m/z* = 39 and *m/z* = 23 which are believed to be an anomalous electronic artifacts. As the nozzle is heated to a temperature of 695 K there is a slight attenuation of signal due to a reduced number density. The relative intensity of *m/z* = 41 seems largely unaffected. As the microreactor is heated further to 1080 K a small peak at *m/z* = 15, CH_3 radical, is detected and another new peak is found at *m/z* = 40. The *m/z* = 15 peak is not a photoionization fragement and is characteristic of bond homolysis. That being the case, it seems likely the *m/z* = 40 peak is formed thermally as hydrogen atom is lost from the C_3H_5 radical resultant from the homolysis. The *m/z* = 55 and *m/z* = 41

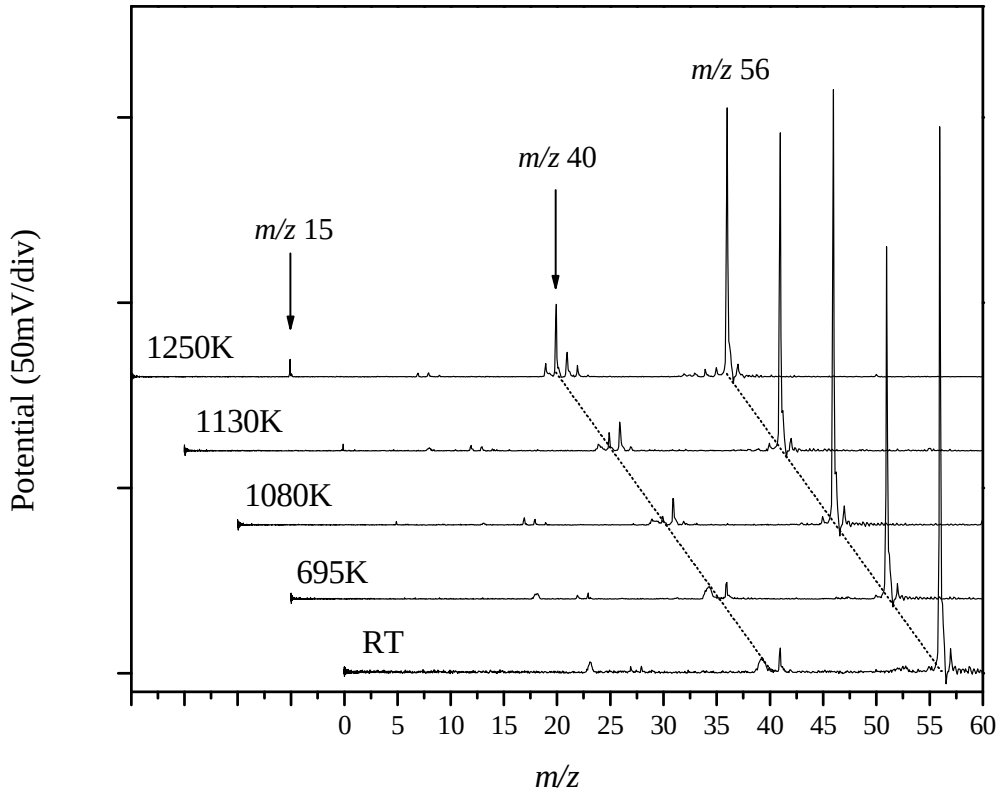

Figure 5.4 Stackplot of mass spectra for the pyrolysis of isobutylene (3%) in argon.

signal may be slightly more intense in this trace. In the hottest traces presented here, 1130 K and 1250 K, the signal of the parent molecule at *m/z* = 56 is not as intense while the remaining peaks grow, most notably *m/z* = 15, CH_3 radical, and *m/z* = 40, C_3H_4 (allene). Small new peaks at *m/z* = 39 and *m/z* = 54 are observed. From the above stated information it is concluded that 1) there is a small occurrence of higher energy ionization 2) of the resultant photoionization fragments methyl expulsion is favored over hydrogen

atom loss and 3) ≥ ~1100K isobutylene undergoes C-C bond homolysis and likely, to a smaller extent, C-H cleavage.

Pyrolysis of ethylene glycol tert-butyl ether

The pyrolysis of ethylene glycol *tert*-butyl ether (a.k.a. *t*-butyl cellosolve) was studied to examine the of pyrolysis experiments with less volatile component. In this case, the ethylene glycol unit imparts the ability to act as a solubilizer in fuels, effectively sequestering water that inevitably contaminates fuel storage tanks, preventing phase separation with subsequent oxidation of the tank leading to leakage. *t*-butyl cellosolve was obtained from TCI America (99+%) and diluted in helium. Scheme 5.3 presents the expected photo-ionization fragments for *t*-butyl cellosolve. Figure 5.5 presents a stack plot of mass spectra traces for the low to intermediate temperatures in the pyrolysis of *t*-butyl cellosolve. The molecular ion at *m/z* 118 was not observed while the fragments depicted below all were detected with *m/z* 103 being dominant. A large peak at *m/z* 68 is observed as a memory effect from previous experiments pyrolyzing isoprene. At a nozzle temperature of 850 K the intensity of the peaks all diminish with the exception of *m/z* 56 which more than triples in intensity, a modest new peak at *m/z* 57, and the detection of a small peaks at *m/z* 44 and 62. The trend continues as the nozzle is heated further to 920, 990, and 1060 K except for the peak at *m/z* 57 which diminishes in intensity. New small peaks emerge at *m/z* 15 and 31, methyl and hydroxymethyl radicals,

indicative of homolysis. Over this temperature region the decomposition of *t*-butyl cellosolve is expected to proceed by molecular elimination from the tertiary center to produce isobutylene (*m/z* 56) and ethylene glycol (*m/z* 62). The transition state energy for that process, DE_0 = 52.1 kcal/mol. The energy barrier calculated for the elimination of water is DE_0 = 63.2 kcal/mol and the transition state for elimination of vinyl and *t*-

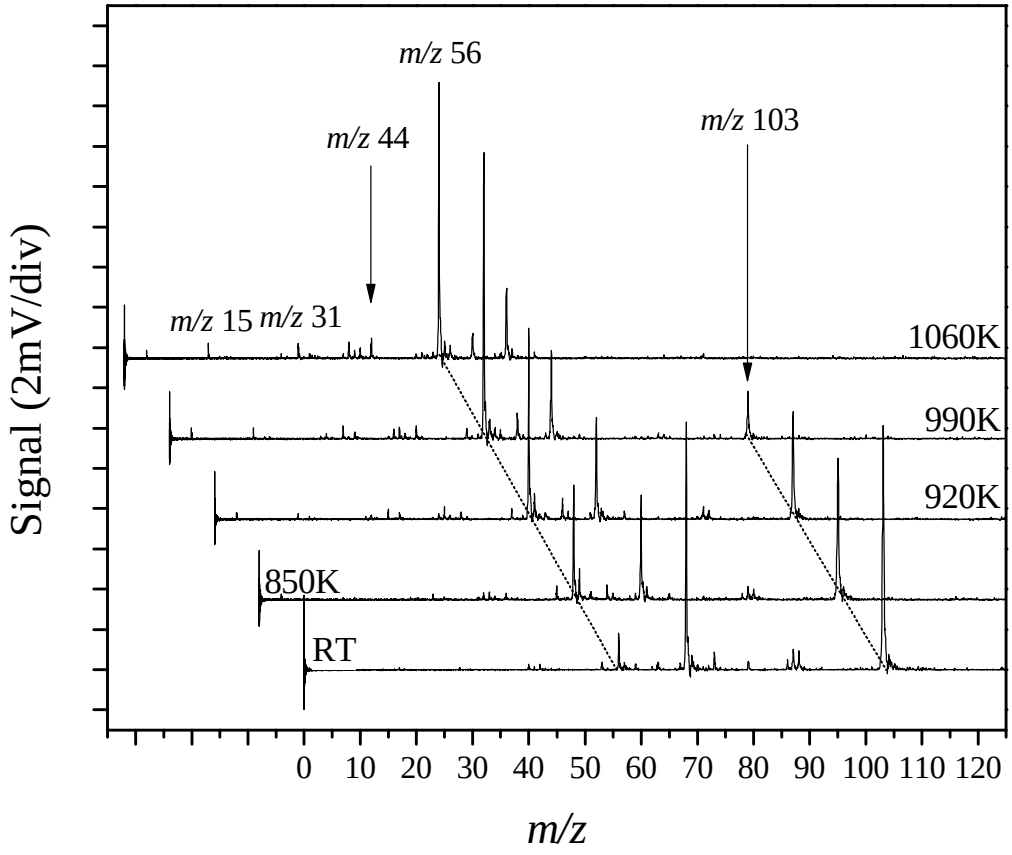

Figure 5.5 Stack plot of mass spectra for the pyrolysis of *t*-butyl cellosolve with unheated nozzle (RT) and over the temperatures from 850 – 1060 K. The traces are shifted for clarity.

butyl alcohols was not located, the potential energy well of the product complex proving shallow and the hydrogen bound OH groups proving to stable. Although a peak at *m/z* 44is observed which could correspond to vinyl alcohol, the corresponding *t*-butyl alcohol is not detected and neither is the vinyl ether product at *m/z* 100 expected from elimination of water. These factors all indicate that the molecular elimination of ethylene glycol to form isobutylene is the dominant process over intermediate temperatures ~800 – 1100 K. Figure 5.6 presents the stack plot of mass spectra for the pyrolysis of *t*-butyl cellosolve over the nozzle temperatures of 1130 – 1300 K.

As the nozzle is heated to a temperature of 1130 K the peaks at *m/z* 15 and 40 significantly increase signal intensity. The *m/z* 56 peak remains the dominant peak in the spectrum and the m/z signal of ethylene glycol at *m/z* 62 is clearly discernible. Upon further heating to 1200, 1235, then 1300 K the signals at *m/z* 15 and 40 continue to grow as does the *m/z* 44 peak. The small peaks at *m/z* 52 and 54 also exhibit growth in these spectral traces. The peaks at m/z 31, 39, 41, 42, 51,53 and 68 are found to have similar intensities over this temperature range, with the exception of *m/z* 39 increasing in intensity at the highest temperature trace presented corresponding to a nozzle temperature of 1300 K. The peak at *m/z* 62 is found to diminish over this temperature region.

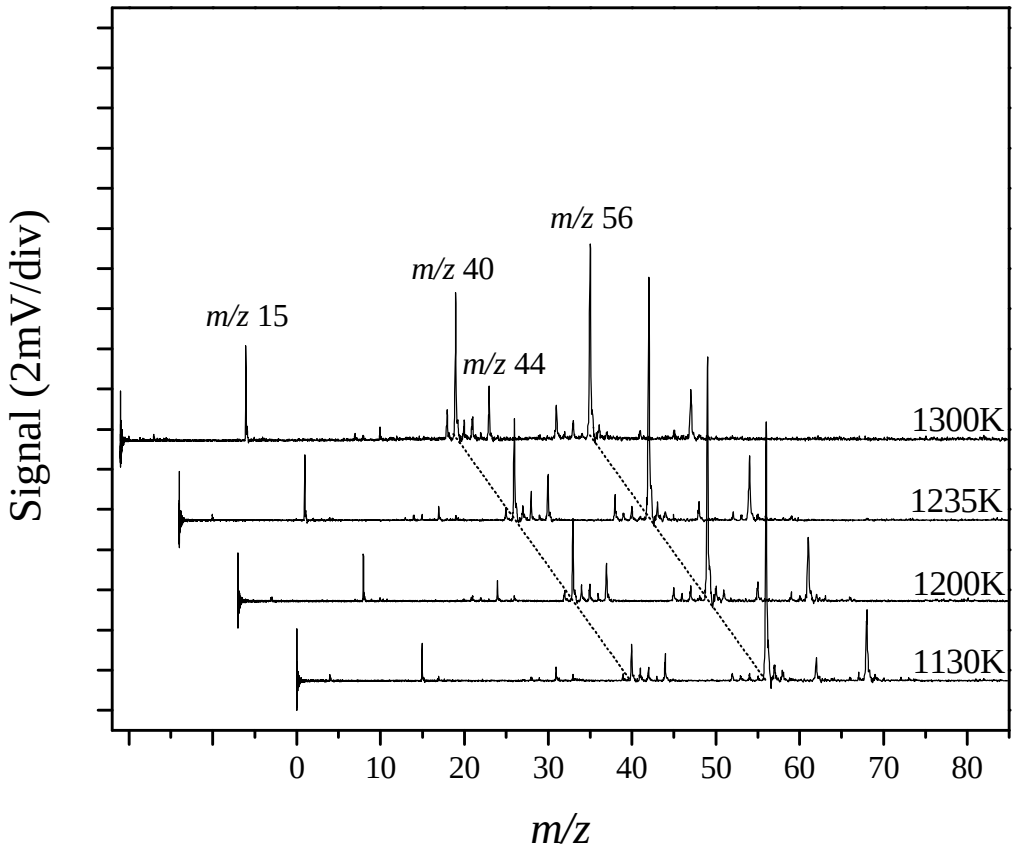

Figure 5.6 Stack plot of mass spectra for the pyrolysis of *t*-butyl cellosolve with nozzle temperatures from 1130 – 1300 K. The traces are shifted for clarity.

It was previously established that the molecular elimination of ethylene glycol to form isobutylene is the dominant process over the intermediate (800-1100 K) temperature region. The decreasing signal at *m/z* 62 is indicative of secondary pyrolysis of the

ethylene glycol molecular elimination product. The growth of *m/z* 15 is definitely indicative of homolysis of *t*-butyl cellosolve. As can be seen from Scheme 5.5 (path 1) the radical at *m/z* 103 is formed concomitantly with methyl cleavage. The *m/z* 103 radical is not observed in the spectra but presumably quickly decomposes to acetone at *m/z* 58, which is observed, and CH_2CH_2OH radical which could decompose to vinyl alcohol at *m/z* 44, also observed. From Scheme 5.5 the bond strength of the C1-C2 bond is 72.2 kcal/mol. Cleavage of the *t*-butyl-O bond (path 2) is predicted to have a slightly more accessible bond strength of 68.6 kcal/mol which would result in *t*-butyl radical at *m/z* 57 and ethylene glycol radical at *m/z* 61. The *t*-butyl radical (*m/z* 57 is observed) rapidly decomposes to isobutylene at *m/z* 56 for which there is a large signal. Although there is no *m/z* 61 signal it may be possible that the ethylene glycol radical rapidly decomposes to formaldehyde (not observable in this systeme) and CH_2OH radical at *m/z* 31 (also observed). The β-C-C decompositions of saturated alkoxy radicals are well known. Cleavage on the other side of the ethereal bond to form *t*-butoxy radical (path 3) and CH_2CH_2OH radical is predicted by DFT methods to be 71.2 kcal/mol. A very small *m/z* 73 peak is detectable in these spectral traces and the *t*-butoxy radical would presumably decompose to methyl radical at *m/z* 15 and acetone at *m/z* 58, all observed signals. The ethylene C-C bond (path 4) is predicted to be nearly isoenergetic with path 3 and would result in a *t*-butoxy methylene radical (*m/z* 87) and CH_2OH radical (*m/z* 31). While a signal is observed at *m/z* 31 no *m/z* 87 is detected. It may be the case that the t-butoxy methylene radical undergoes rapid decomposition to form formaldehyde, CH_2O, not detectable in this system, acetone at *m/z* 58, and a methyl radical at *m/z* 15. All of

these processes would be consistent with observed spectral features. In fact, paths 1-4 are all in a narrow energy range of 3.6 kcal/mol. This result couples with the experimental spectral traces suggest that all of these homolysis pathways may be in competition with each other at higher temperatures (>1100 K). The cleavage of the hydroxyl radical (path 5) is predicted to be prohibitive in comparison with a predicted energy value of 85.4 kcal/mol which leads to the conclusion that the contribution of path 5 is negligible.

CONCLUSIONS

The results of the experiments presented here lead to the following conclusions:

(1) With argon as carrier gas, MTMB and MTBE display comparable levels of molecular elimination of methanol at up to 875 K.

(2) With helium as carrier gas, MTMB exhibits homolytic cleavage of the 2,3-bond to a much greater extent than molecular elimination at temperatures $\geq$875K.

(3) With helium as carrier gas, homolysis of the 2,3-bond of MTMB takes place with no competition from homolysis of the 1,2-bond in the temperature domain 875-950K.

REFERENCES

[1] A. F. Diaz, D. L. Drogos (eds.), Oxygenates in Gasoline: Environmental Aspects, American Chemical Society (Oxford University Press), Washington, DC, 1979.

[2] M. J. Papachristos, J. Swithenbank, G.H. Priestman, S. Stournas, P. Polysis, E. Lois, J. Inst. Energy 64 (1991) 113.

[3] L. K. Rihko-Struckmann, R. S. Karinen, A. O. I. Krause, K. Jakobsson, J. R. Aittamaa, Chem. Eng. Processing 43 (2004) 57.

[4] L. K. Rihko, A. O. I. Krause, Indus. Eng. Chem. Res. 35 (1996) 2500.

[5] J. Liu, S. Wang, J. A. Guin, Fuel Proc. Technol. 69 (2001) 205.

[6] D. E. Hendrickson, U.S. Patent Application WO9516763 (1995).

[7] L. A. Smith, Jr., H. M. Putman, H. J. Semerak, C. S. Crossland, U.S. Patent 6,583,325 (2003).

[8] T. Evans, K. R. Edlund, U.S. Patent 2,010,356 (1935).

[9] J. Ignatius, H. Jaervelin, P. Lindqvist, Hydrocarbon Proc. 74(2) (1995) 51.

[10] S. Hoogasian, C. H. Bushweller, W. G. Anderson, G. Kingsley, J. Phys. Chem. 80 (1976) 643.

[11] J. C. Traeger, T. H. Morton, J. Phys. Chem. A 109 (2005) 10467.

[12] L. F. Fieser, M. Fieser, Advanced Organic Chemistry, Reinhold Publishing, New York, 1961, pp 249-251.

[13] J. A. Walker, W. Tsang, Int. J. Chem. Kinet. 11 (1979) 867.

[14] H. Birkhofer, H.-D. Beckhaus, C. Rüchardt, Chem. Ber. 126 (1993) 1023.

[15] H. W. Biermann, G. W. Harris, J. N. Pitts Jr., J. Phys. Chem. 86 (1982) 2958.

[16] S. D. Chambreau, J. Zhang, J. C. Traeger, T. H. Morton, Int. J. Mass Spectrom. 199 (2000) 17.

[17] J. E. Taylor, D. A. Hutchings, K. J. Frech, J. Am. Chem. Soc. 91 (1969) 2215.

[18] V. D. Knyazev, I. A. Dubinsky, I. R. Slagle, D. Gutman, J. Phys. Chem. 98 (1994) 5279.

[19] D. W. Kohn, H. Clauberg, P. Chen, Rev. Sci. Instrum. 63 (1992) 4003.

[20] H. Clauberg, D. W. Minsek, P. Chen, J. Am. Chem. Soc. 114 (1992) 99.

[21] http://webbook.nist.gov/chemistry

[22] L. Curtiss, P. C. Redfern, K. Raghavachari, J. A. Pople, Chem. Phys. Lett. 359 (2002) 390.

[23] L. Curtiss, K. Raghavachari, Theor. Chem. Acc. 108 (2002) 61.

[24] J. B. Pedley, R. D. Naylor, S. P. Kirby, Thermochemical Data of Organic Compounds, 2nd ed, Chapman and Hall, New York, 1986.

[25] A. Goldaniga, T. Faravelli, E. Ranzi, P. Dagaut, M. Cathonnet, 27th Symp Combustion (1998) 353.

[26] S. Gouli, E. Lois, S. Stournas, Energy Fuels 12 (1998) 918.

[27] W. J. Piel, Fuel Reformulation 4(2) (1994) 28.

[28] J. F. Knifton, P. -S. E. Dai, J. M. Walsh, J. Chem. Soc. Chem. Commun. (1999), 1521.

[29] Traeger, J. C. J. Phys. Chem. 90 (1986) 4114.

[30] Treager, J. C. Int. J. Mass Spectrom. Ion Processes 58 (1984) 259.

CHAPTER 6

ISOPRENE AND ISOMERS

INTRODUCTION

Isoprene (2-methyl-1,3-butadiene) is the major product obtained from thermal degredation of isoprenoids[1] and is an important precursor for the formation of polyaromatic hydrocarbons (PAH) in combustion processes.[2-4] Despite this, the pyrolysis of isoprene has been relatively little studied.[5,6] Badger *et al* found the pyrolysis of isoprene to produce large amounts of benzene, toluene, and xylenes in addition to a wide variety of PAH.[5] The major product recovered, toluene (22%), was believed to be formed by reaction of a two-carbon unit (vinyl radical or ethylene) with an isoprene radical or isoprene itself. Benzene (15%) was thought to be formed in a similar manner, the reaction of four-carbon and two-carbon units, and the *meta* and *para* xylenes (15%) formed through dimerization of isoprene units, presumably followed by subsequent loss of C_2H_2. The C2-C5 σ bond, being the weakest bond, was proposed to undergo homolytic cleavage to form CH_3 and C_4H_5 radicals that then abstract hydrogen from isoprene creating C_5H_7 radicals. It was demonstrated how all products observed could be formed, ultimately, from the reactions of isoprene, the four possible C_5H_7 radicals (I, II, III, IV), the –Me C_4H_5 radical (V), and radicals resulting from homolysis of the C2-C3 bond, C_3H_5 and C_2H_3. The free radicals and energetics of isoprene dissociation calculated in this work are presented in Figure 6.1. Perhaps consistent with that mechanism methane, propylene, ethene, and acetylene were all detected as products, however, without quantification. The work indicated the importance of isoprene and

fragment units in the formation of aromatic rings. However, many possibilities were not considered and mechanistic details were not elaborated on. The work of Oro *et al* followed the variation in PAH populations as a function of pyrolytic conditions, yet mechanisms were not specifically discussed.[6]

Energy economy and health concerns have prompted considerable work on thermal decompositions of hydrocarbons to gain insight on mechanisms for PAH, and ultimately soot, formation.[7] Of particular interest are compounds believed to be involved in formation of an aromatic ring, that process widely being considered the crucial rate limiting step in PAH formation. In this regard, the 1,3-butadiene (1,3-BD) system has been particularly well studied[8-17] and is expected to have relevance to the isoprene system. The primary initiation step for 1,3-BD pyrolysis was originally proposed to be cleavage of the C-C single bond, forming two vinyl radicals.[9-11] This mechanism, however, did not accurately account for ethylene production and unimolecular decomposition to form ethylene and acetylene[12,13] was suggested. Disagreement with experiment was still encountered until the isomerizations to 1,2-butadiene and 2-butyne was considered. These isomerizations have now been shown to be much faster than decomposition at high temperatures,[8] and previous work from this lab directly observed the isomerization pathway by detection of methyl and propargyl radicals under pyrolytic conditions.[17] In light of the recent advancements made on the 1,3-BD system, the pyrolysis of isoprene, the 2-methyl derivative of 1,3-BD, appeared to be ripe for further investigation. In this

work we examine the ability of isoprene to isomerize and elucidate the alterations in mechanistic pathways resulting from the additional methyl group. Due to the larger photoionization cross sections of the molecular fragments of isoprene, the molecular elimination channel(s) can be assessed, along with the contribution of direct homolysis channels(s).

As in the pyrolysis of 1,3-BD, the experimental approach of flash pyrolysis coupled to supersonic expansion and vacuum ultraviolet (VUV) photoionization mass spectrometry offers several advantages: short reaction times to examine the initial steps of the thermal decomposition; supersonic cooling to quench the reaction and minimize recombination of the initial products and intermediates; and minimized ion fragmentation due to the "soft" VUV photoionization.[17-19] Quantum chemistry calculations of the transition state barriers for isomerization reactions and product energetics are also carried out, and possible mechanisms are discussed.

EXPERIMENTAL

Isoprene (2-methyl-1,3-butadiene) was obtained from Fisher Chemicals (99%) and diluted to 15% and 1.5% in argon, without additional purification. This was accomplished by bubbling the Ar noble carrier gas through the liquid at ice/water or acetonitrile/dry ice bath temperatures. The backing pressure of the gas mixture was kept at ~1.5 atm for all measurements. The isomerization and decomposition energetics for

isoprene were calculated using quantum chemistry methods. Geometries were optimized using the hybrid density functional theory method of Becke three-parameter functional with nonlocal correlation provided by Lee, Yang, and Parr (B3LYP) and the 6-31+G(2df,p) basis sets.[21,22] The vibrational frequencies were calculated at the same level of theory for characterizing the nature of structures and used for computing zero-point energy corrections. All calculations were performed using the Gaussian 98 program suite.[23] Relative energies of the compounds and pertinent transition states were listed on the basis of the enthalpies of formation at 0 K . The energetics of the dissociative pathways of isoprene are shown in Figure 6.1 and Figure 6.2.

RESULTS

Relative energetics of select species involved in the pyrolysis of isoprene are presented in Figure 6.1. Potential energies for isomerization and homolysis of isoprene and isomers are presented in Figure 6.2. A stack plot of isoprene (15%) in argon carrier gas composed of spectral traces at room temperature (295 K) and nozzle temperatures of 700, 865, 1015, and 1140 K is presented in Figure 6.3 (a). A large molecular ion peak at *m/e* 68 is observed at 295 K; the very small peaks observed at *m/e* 67, 53, 42, and 40 at 295 K have respective appearance energies (AE) of 10.54—10.93 eV[24-26], 11.44—11.93 eV[26,27], 12.39 eV[26], and 12.76 eV[26], indicating a minimal amount of multiphoton or electron impact ionization. The multiphoton ionization could be caused by a VUV (focused 118.2 nm) photon + a UV (divergent 355 nm) photon, with a total energy of

13.98 eV. The occurrence of photoelectron generation by scattered light and subsequent electron impact ionization in the photoionization region in this apparatus and the efforts made to eliminate the effect have been described previously.[17] With a nozzle temperature

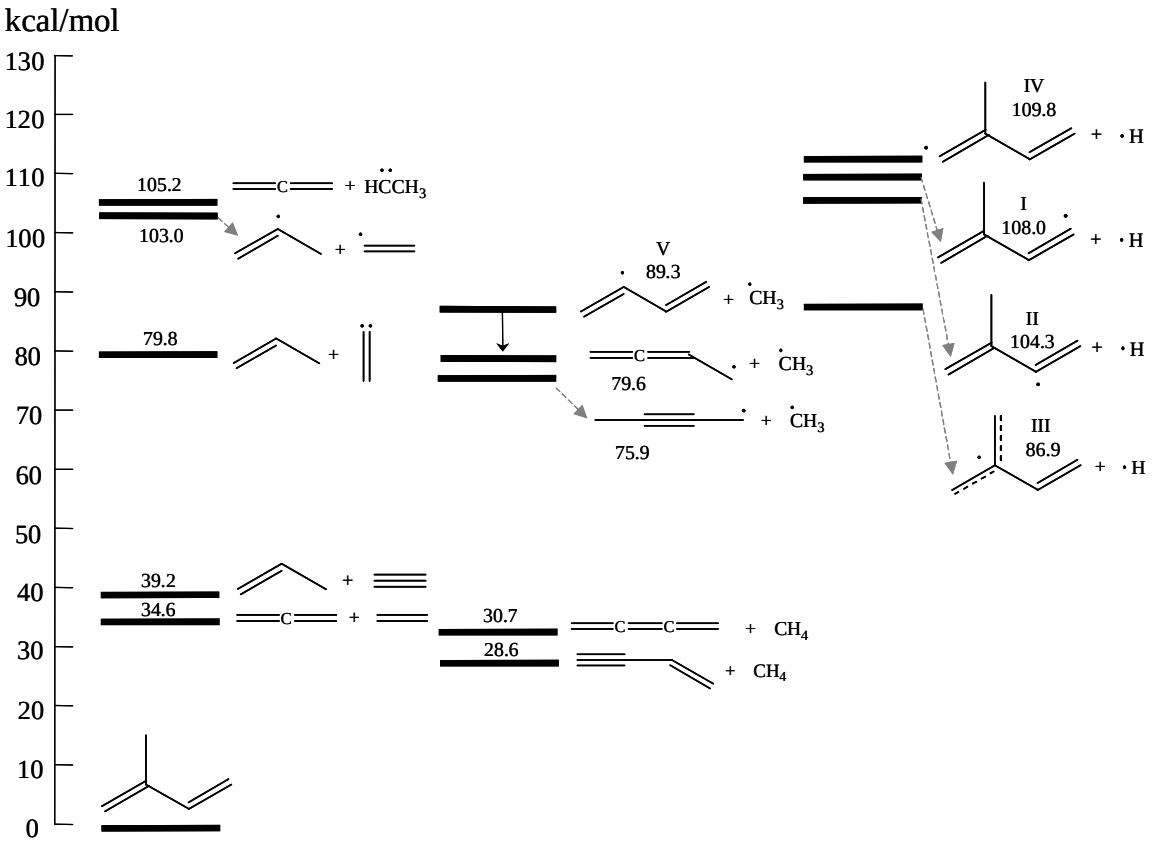

Figure 6.1 Relative energies of the species involved in the pyrolysis of isoprene (values determined from zero-point energy corrected heats of formation at 0 K) calculated at the B3LYP/6-31+G(2df,p) level of theory. The C_4H_5 radical V is stabilized to *i*-C_4H_5 radical by a 9.7 kcal/mol resonance energy.

of 700 K a decrease in the parent *m/e* 68 signal is observed due to drop in number density, and two small new peaks at *m/e* 41 (AE = 14.04 eV[26]) and *m/e* 39 (AE = 14.55 eV[26]) are

discernible. As the nozzle is increased to 865, 1015, and then 1140 K, the peaks at m/e 53 and 67, as well as the peaks at m/e 39-42, are found to grow in relative intensity.

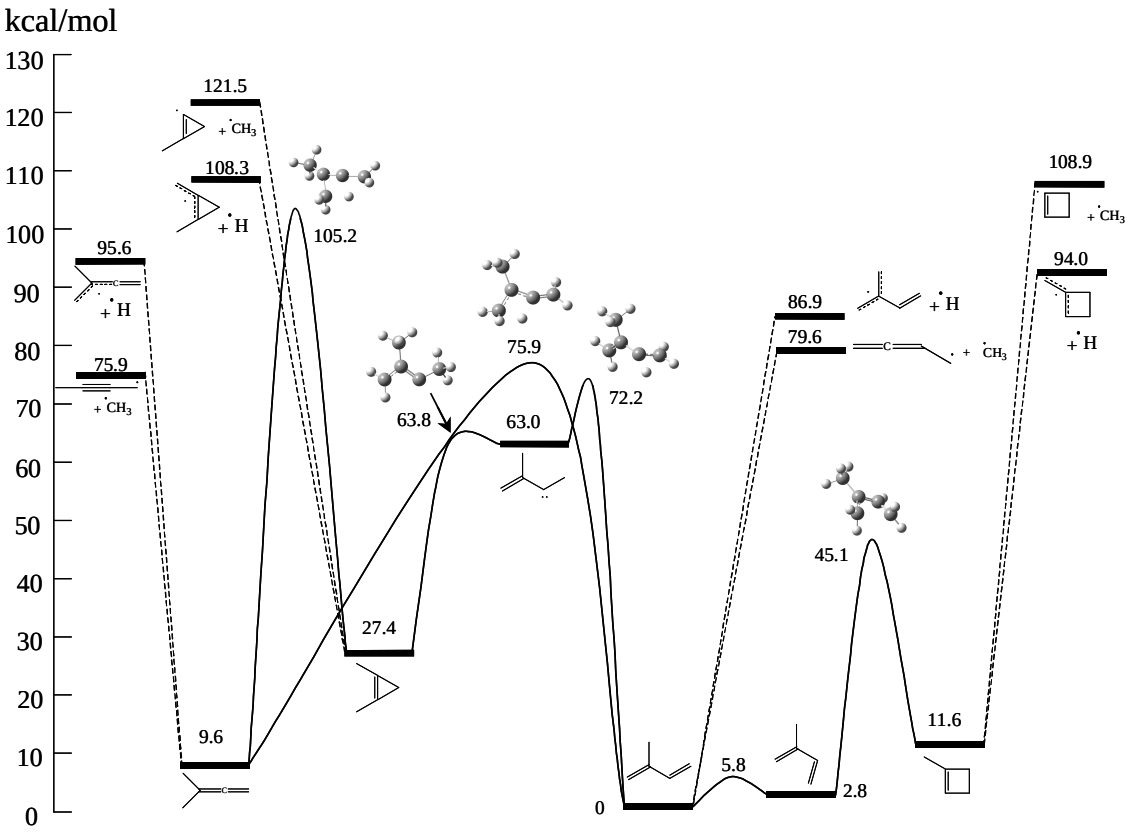

Figure 6.2 Energetics of the isomerization and dissociation pathways of isoprene. Enthalpies of formation and transition state energies are calculated at 0 K using the B3LYP/6-31+G(2df,p) level of theory. Vibrational frequencies were calculated at the same level of theory for computing zero-point energy corrections and verification of transition state structures.

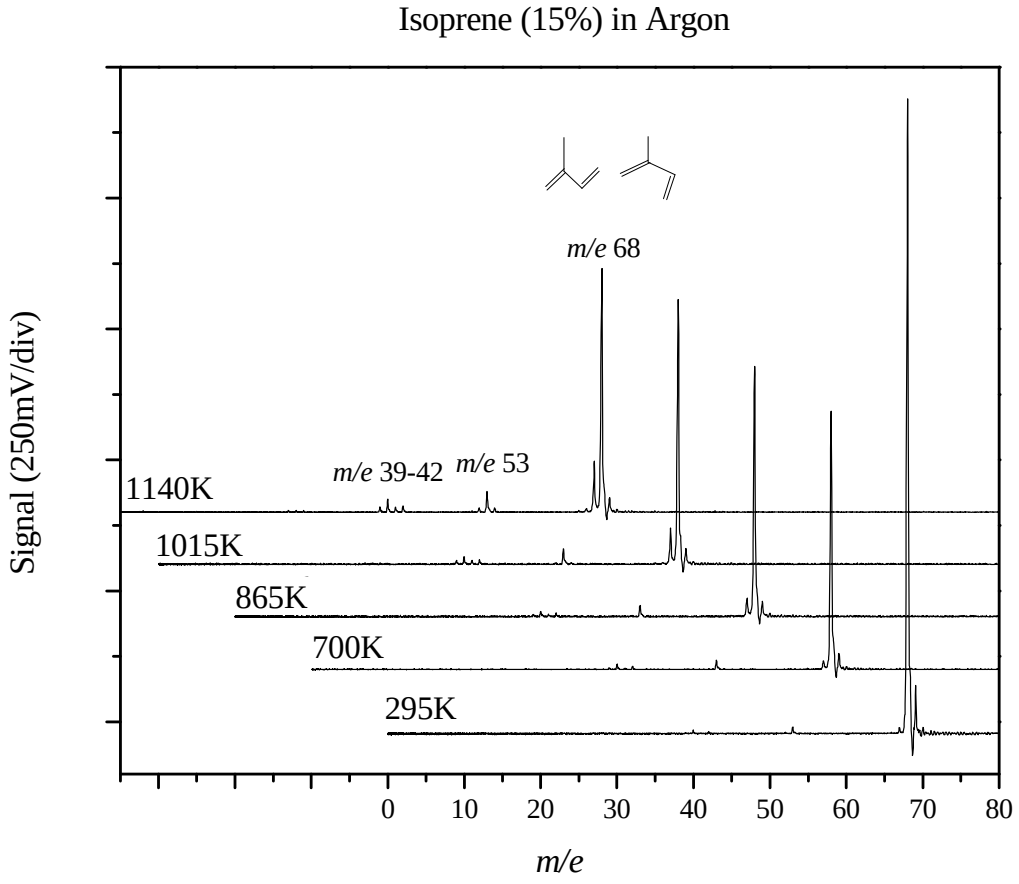

Figure 6.3 (a) Stack plot of mass spectra for pyrolysis of isoprene (15% in Ar) with internal nozzle temperatures from room temperature (295 K) to 1140 K.

A stack plot of mass spectra for isoprene (15%) in argon carrier gas with nozzle temperatures of 1215, 1255, 1300, 1340, and 1400 K is presented in Figure 3b. At 1215 K the parent ion continues to decrease in intensity with concomitant increases in all the previous observed peaks. The growth of the peak at *m/e* 40 is significantly greater than

the others in the *m/e* 39-42 region. Two new peaks are observed at m/e 52 and *m/e* 54, along with the slightly growing *m/e* 53 peak. In the 1255 K trace, the peaks at m/e 40, 52, and 54 continue to increase in relative intensity. Peaks at *m/e* 15, 28, 66 and 78 are now clearly detected. At 1300 K, the trend continues with *m/e* 40 and 52 displaying the greatest augmentation of intensity, and at 1340 K the peak at *m/e* 52 is nearly equal to the parent peak at *m/e* 68, while the *m/e* 53 peak starts to decrease. At this temperature new peaks at *m/e* 50 and 65 are observed. At a nozzle temperature of 1400K, the highest temperature presented, the parent peak continues to diminish as the relative intensities of other peaks increase.

A stack plot of mass spectra for isoprene (1.5%) in argon carrier gas with nozzle temperatures of 1200, 1230, 1310, 1330, and 1390 K is presented in Figure 6.3 (c). The concentration was reduced by an order of magnitude to evaluate the extent of secondary reactions in gas phase and surface reactions. The pyrolysis mass spectra are essentially the same in both experiments, except with the diluted sample the amount of *m/e* 15 and *m/e* 39 observed increases while the *m/e* 78 peak is attenuated. This indicates that the surface reactions and secondary gas-phase reactions are not significant in the ~100 μs short time scale of the flash pyrolysis.

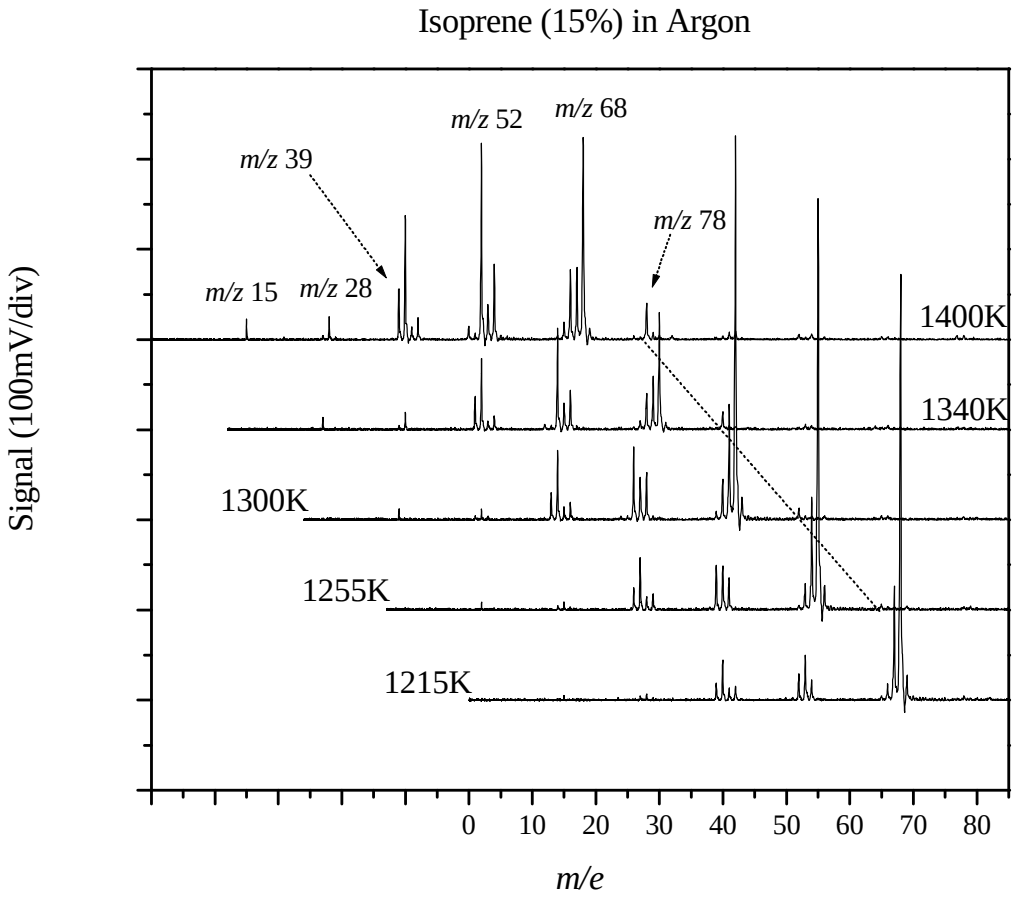

F

Figure 6.3 (b) Stack plot of mass spectra for pyrolysis of isoprene (15% in Ar) with internal nozzle temperatures from 1215 K to 1400.

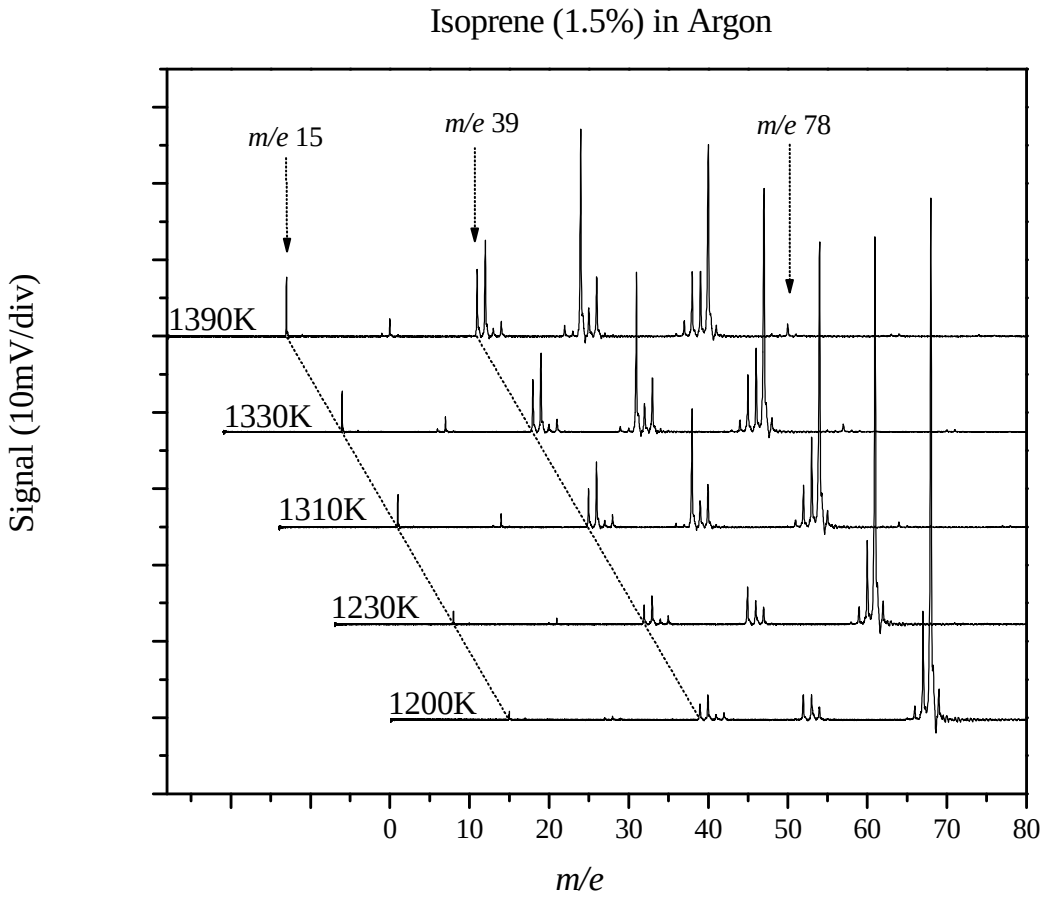

Figure 6.3 (c) Stack plot of mass spectra for pyrolysis of isoprene (1.5% in Ar) with internal nozzle temperatures from 1200 K to 1390 K. Mass spectra are shifted for clarity.

DISCUSSION

Equilibrium Structures and Isomerization

Energies of C_5H_8 isomers and their transition states of formation were calculated to characterize the reaction profile and elucidate the lowest energy pathways in the pyrolysis of isoprene. The results are presented graphically in Figure 6.2. The molecular parameters of isoprene calculated here in this work were found to be consistent with prior calculations.[28-30] The trans isomer is found to lie 2.8 kcal/mol below the gauche conformation with a 5.8 kcal/mol barrier to rotation. As can be seen from the figure, several isomers are readily accessed. The gauche conformation of isoprene can undergo electrocyclic ring closure by surmounting a 42.3 kcal/mol barrier to produce 1-methyl cyclobutene, 11.6 kcal/mol higher in energy than the reference trans isoprene. The conrotary ring opening of methylcyclobutene has activation energy calculated in this work of 33.5 kcal/mol, in reasonable agreement with the experimental value of 35.1 kcal/mol.[31]

Similar to 1,3-BD,[17] both conformers of isoprene are expected to be capable of undergoing 1,2 hydrogen shift across the C3-C4 bond of isoprene to produce a singlet carbene intermediate. The transition state for that process was calculated to be 72.2 kcal/mol above trans isoprene. Carbene moieties are not stable and are known to readily form corresponding cyclopropenes. 1,2-dimethylcyclopropene was found to lie 27.4 kcal/mol above isoprene and the barrier to its formation, in reference to the carbene compound, is only 0.8 kcal/mol. In 1,3-BD the carbene/cyclopropene intermediate can

isomerize further via a sequential 1,2 hydrogen shift to 1,2-BD or to 2-butyne.[17] In the case of isoprene, however, the absence of a vinylic hydrogen by CH_3 substitution significantly retards the rates of similar processes and therefore tend to undergo ring opening rather than further isomerization.[32] The 1,3 hydrogen shift is also known to be relatively facile and the barrier to directly forming dimethylallene in this manner was calculated to be 75.9 kcal/mol. Alternatively, dimethylallene can be formed from the carbene or cylclopropene intermediates. In this work, the transition from dimethylcyclopropene to dimethylallene was calculated to be 105.2 kcal/mol indicating that pathway is unlikely. Dimethylallene has a heat of formation of 9.6 kcal/mol relative to trans isoprene.

C_4H_4, C_4H_5, and C_4H_6 Production

The *m/e* 53 peak appears and increases at relatively low temperatures, and above 1200 K, the growth of the *m/e* 15 peak also becomes visible, suggesting production of the C_4H_5 and CH_3 species via homolytic dissociation of isoprene. The heats of reaction for the radicals produced by the homolytic cleavage of a methyl group from the isoprene isomers were calculated and are presented in Figure 6.1 and Figure 6.2. For the simple homolytic cleavage of methyl from isoprene, the *i*-C_4H_5 radical + CH_3 radical product channel is found to be 79.6 kcal/mol higher in energy relative to trans isoprene, with the C_4H_5 radical V significantly stabilized by a resonance energy of at least 9.7 kcal/mol. For the homolysis of dimethylallene minus methyl radical, the heat of reaction is only

75.9 kcal/mol above isoprene due to a propargyl-type resonance in the methylallenyl radical product. This work predicts that the methylallenyl radical is 3.7 kcal/mol more stable than the *i*-C_4H_5 radical, which is larger than the 2.4 kcal/mol predicted by Hansen *et al.*[33] Heat of reaction for homolysis of the methylcyclobutene isomer to produce the methyl and cyclobutene radicals is 108.9 kcal/mol relative to trans isoprene. The heat of reaction of the methylcyclopropene and methyl radicals from homolysis of dimethylcyclopropene is calculated to be 121.5 kcal/mol. Therefore, the likely mechanism for methyl loss in isoprene is isomerization via C3-C1 1,3 hydrogen shift to dimethylallene and subsequent dissociation to CH_3 and methylallenyl radicals. Compared to 1,3-BD, the CH_3 substitution in isoprene provides a possible direct CH_3 loss pathway. However, the CH_3 substitution removes one vinylic hydrogen and raises the energetics for subsequent 1,2 CH_3 shift to isomerize to dimethylallene (analog to 1,2-BD in 1,3-BD isomerization) or the alkyne (analog to 2-butyne in 1,3-BD isomerization). Consequently, the 1,3 hydrogen shift isomerization to dimethylallene becomes the more favorable isomerization pathway and leads to CH_3 loss.

The prominent peak at *m/e* 52 in the pyrolysis of isoprene presumably comes from overall loss of CH_4. This could occur by bond homolysis of isoprene to produce CH_3 and C_4H_5 radicals with subsequent loss of a hydrogen atom forming C_4H_4, or by direct molecular elimination of methane. The subsequent loss of hydrogen atom from methylallenyl and *i*-C_4H_5 radicals were calculated to be endothermic by 57.1 and 53.4 kcal/mol for butatriene and for vinylacetylene 58.4 and 51.1 kcal/mol respectively, indicating these as facile processes. The direct molecular elimination of methane from

isoprene to form butatriene was calculated to have a heat of reaction of 30.7 kcal/mol, while the same process to form vinylacetylene is 28.6 kcal/mol (Figure 6.1); however, the direct molecular elimination of methane is known to have activation energies above the simple bond enthalpies. In this work the activation energies for formation of vinylacetylene or butatriene by molecular elimination of methane are 107.1 and 103.1 kcal/mol, respectively, consistent with previous calculation.[34] These results indicate that σ bond homolysis of isoprene is favored over molecular elimination of methane, and the C_4H_4 product at *m/e* 52 is produced by subsequent H loss of the methylallenyl radicals.

The peak at *m/e* 54 observed in the pyrolysis cannot be the result of molecular elimination of CH_2. The heats of formation are calculated to be prohibitive, 114.8 kcal/mol from isoprene, and additionally the CH_2 created would be detectable with an ionization energy of 10.35 eV.[35] C_4H_6 can be formed by H-abstraction by C_4H_5 radicals, however, the relative intensity observed at *m/e* 54 displays no concentration dependence and therefore it may be that *m/e* 54 is largely a photoionization fragment. The ionization energies for cyclopropene and cyclobutene are 9.67 eV and 9.1 eV, resepectively,[36] and photofragments of that type have apparently been observed from photo-oxidized surfaces of methylcyclobutene and dimethylcyclopropene derivatives.[36]

C_3H_4 and C_2H_4 Production

Direct molecular eliminations resulting in the cleavage of the C2-C3 bond were considered and relative energies are presented in Figure 6.1. Two such molecular

elimination pathways possible for isoprene are molecular elimination of acetylene to produce propene, or elimination of ethylene to produce allene (shown in Figure 6.1) and/or propyne. The heat of reaction for the C_2H_2 + propene product channel is found to be 39.2 kcal/mol above trans isoprene, while the C_2H_4 + allene channel is more favorable by 4.6 kcal/mol at an energy of 34.6 kcal/mol. The elimination pathway for acetylene is believed to proceed through a vinylidene species,[10] and when the vinylidene intermediate is considered the energy level is increased to 79.8 kcal/mol (Figure 6.1). In a similar manner, one could envision the molecular elimination of ethene to proceed through a methyl carbene intermediate; this consideration leads to a product energy level of 105.2 kcal/mol. As can be seen in Figure 6.3, the amount of *m/e* 42, corresponding to propene from molecular elimination of acetylene, is less in comparison to the *m/e* 40 peak, for the C_3H_4 species; the molecular product channel producing ethene and C_3H_4 (allene and/or propyne) is more important. The transition state energy barrier for the ethene molecular elimination process to form allene was calculated in this work to be 74.0 kcal/mol, which is slightly smaller than those of CH_3 bond homolysis. The molecular elimination of ethene should be a favorable channel, and the growth of *m/e* 40 at elevated temperatures can then be attributed to this process.

The C2-C3 bond homolysis channel of isoprene to produce C_2H_3 and C_3H_5 radicals is 103.0 kcal/mol above trans isoprene (Figure 6.1). The absence or very minor peak growth at *m/e* 27 and *m/e* 41 indicates that these radicals are not formed in

appreciable amounts, as a prior work on nitroethylene pyrolysis has demonstrated that the vinyl radical produced in pyrolysis under these conditions should be readily detected. Therefore, isoprene does not undergo C2-C3 homolysis to an appreciable extent, consistent with the higher energy requirement.

All these features indicate that cleavage of the C2-C3 bond in isoprene is not homolytic and that the molecular elimination of C_2H_4 to produce C_3H_4 is the dominant molecular elimination pathway.

C_5H_6 and C_5H_7 production

The energy values of the possible -H radicals from equilibrium trans isoprene structure are presented in Figure 6.1. The -H radicals of isomers are presented in Figure 6.2. Radicals I, II, and IV are vinylic radicals with fairly similar energetics, lying 108.0, 104.3, and 109.9 kcal/mol above the trans isomer of isoprene (H atom energy considered). The allyl radical III has a weaker C-H bond with an energy of 99.6 kcal/mol, and when allowed to delocalize to the most stable conformation a value of 86.9 kcal/mol is obtained. The minus hydrogen radical of methylcyclobutene has a heat of reaction, 94.0 kcal/mol (delocalized), while dimethylcyclopropene minus hydrogen atom was found to be 108.3 kcal/mol relative to trans isoprene (Figure 6.2). The allylic radical of dimethylallene is slightly higher energy than for methylcyclobutene, 95.6 kcal/mol. The peak observed at

m/e 67 corresponds to C_5H_7. Since it is found to be unaffected by changes in concentration, it is likely the result of H elimination by thermolysis, presumably via the lowest energy pathway, H + allyl radical III. Alternatively, H-abstraction from isoprene by radicals such as CH_3 and C_4H_5 could also produce C_5H_7.

The peak at *m/e* 66 could be the result of molecular elimination of H_2 from isoprene. The heat of formation of 2-methyl-buta-1-ene-3yne is calculated to be 39.8 kcal/mol. As mentioned previously this process has been observed in the pyrolysis of 1,3-BD with an estimated transition state of 94.7 kcal/mol[8]. The peak at m/e 66 may also be the decomposition of the isoprenyl radical (allyl radical III), *m/e* 67.

C_3H_3 and C_6H_6 production

The formation of *m/e* 78 is an indication that combinations are indeed occurring in this experimental regime. Two general pathways are accepted as playing a role in the production of C_6H_6, (1) four carbon plus two carbon reactions and (2) three carbon self combination. In this experiment, the following possible routes to C_6H_6 are conceivable.

$C_4H_4 + C_2H_2 \rightarrow HCCCHCHCHCH_2$ (a)

$C_4H_2 + C_2H_4 \rightarrow HCCCHCHCHCH_2$ (b)

$C_3H_3 + C_3H_3 \rightarrow C_6H_6$ (c)

The amounts of C_4H_2 and C_2H_2 in this pyrolysis are not sufficient for pathways (a) and (b) to be plausible. The self reaction of C_3H_3, pathway (c) has been well studied[39] and is believed to be most facile in production of an aromatic ring. A noticeable delineation of the data collected at lower concentrations is the increased levels of CH_3 and C_3H_3 radicals, which implicates the involvement of these species in secondary reactions.

The heat of reaction to form C_3H_3 radical and hydrogen from C_3H_4 (allene) is calculated to be 88.6 kcal/mol, the weakest C-H bond predicted in this system. The C_3H_3 radical can be produced from the pyrolysis of allene at elevated temperatures. In addition, allene can readily isomerize to propyne,[32] which could also decompose to H + C_3H_3 radical. Alternatively, hydrogen abstraction by the CH_3 radicals from allene/propyne can also generate C_3H_3. As the isoprene precursor concentration increases, the amount of CH_3 detected diminishes as it abstracts hydrogen from allene/propyne to form methane, not detectable by this apparatus. The created C_3H_3 radicals then combine to produce an increase in *m/e* 78 intensity and overall diminishment of *m/e* 39. Experiments with

propargyl bromide confirm the propensity for C_3H_3 radicals to self-combine producing *m/e* 78 in this experimental regime.

Allene (H_2CCCH_2)

The pyrolysis of allene was accomplished at assist interpretation of isoprene pyrolysis data. Allene from liquid carbonic (97%) was used without purification and diluted to 3% in argon gas. A small amount of isobutylene was incorporated into the

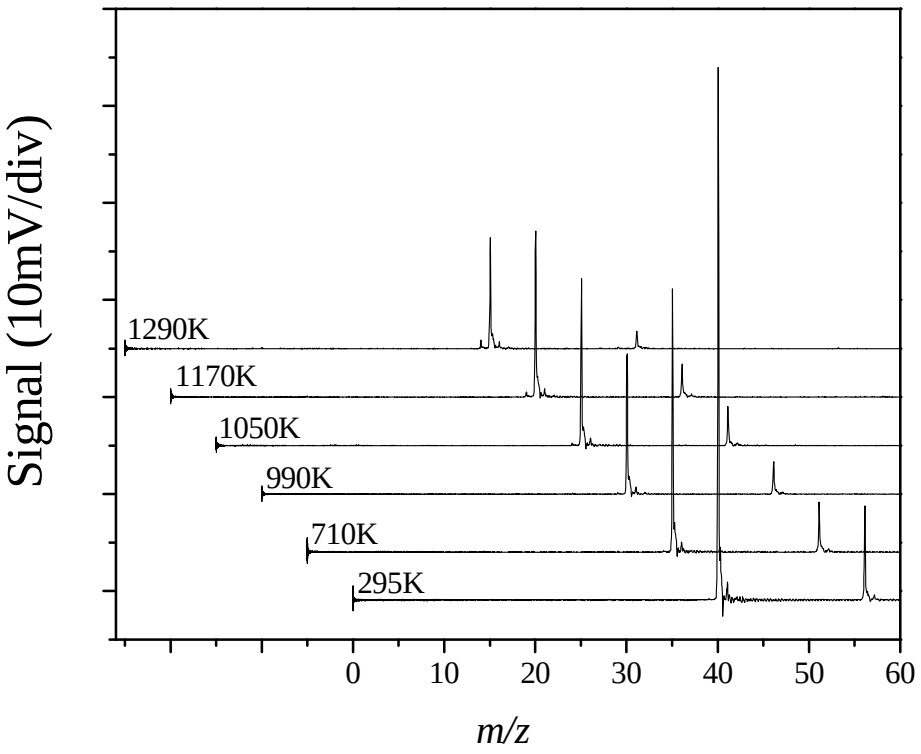

Figure 6.4 Stack plot of mass spectra from pyrolysis of allene and isobutylene.

sample to served as an internal thermometer. Figure 6.4 displays spectral traces obtained from the pyrolysis of allene. In the room temperature trace (RT) a strong molecular ion peak is observed for allene (IE = 9.961 eV[40]) at *m/z* 40 while the molecular ion of isobutylene is observed at *m/z* 56. As the nozzle is heated to 710 K then 990 K there is attenuation of the molecular ion observed due to a decrease in the number density. As the nozzle is successively heated to the higher temperatures of 1050, 1170, and then 1290 K the molecular ion peaks remain essentially the same, until the hottest trace of 1290 K where signal again diminishes, while a small new peak is observed at *m/z* 39. The reported AE of *m/z* 39 is 11.60 eV[40], much to high to be observed as a photoionization fragment. Therefore, the signal at *m/z* 39 is likely caused by the thermal loss of H atom to form propargyl radical. The C-H bond of allene is calculated to be on the order of 88 kcal/mol. While one might expect to observe evidence of homolysis at a lower temperature with such a weak bond energy, it must be considered that allene readily isomerizes to the more stable propyne either directly via a 1,3 H migration or through a vinylmethylene to cyclopropene pathway.[41,42] Over the intermediate temperatures allene is likely isomerizing first, that pathway having a lower energy barrier than homolysis (a 42.8 kcal/mol energy barrier for isomerization to vinylmethylene), with loss of H atom from propyne. The isobutylene in the sample does not undergo thermal decomposition over these temperatures.

CONCLUSIONS

Isoprene undergoes fast isomerizations to several different species at elevated temperatures. At ≥~1200 K in this pyrolytic system thermal bond decomposition is observed producing C_4H_5 and CH_3, in addition to the unimolecular elimination of C_2H_4 to produce C_3H_4. Quantum chemistry calculations indicate that σ bond homolysis to form methylallenyl and *i*-C_4H_5 radicals may be competing processes. Molecular elimination of acetylene to form C_3H_6 was found to be a very minor pathway and direct homolysis of C2-C3 bond was not observed at any temperatures. The C_3H_3 radicals observed could be produced from the pyrolysis of C_3H_4 or via the hydrogen abstraction from C_3H_4 by the CH_3 radicals created in the σ bond homolysis. At temperatures ≥ ~1250K production of C_6H_6 is observed due to the C_3H_3 self combination reaction. Combinations of C_4H_5 radicals are not prominent and therefore must be much slower than the corresponding process for C_3H_3 radicals.

REFERENCES

[1] L. J. Wall, J. Res. Natn. Bur. Stand. 41 (1948) 315.

[2] H. Staudinger, R. Endle, J. Herold, Ber. Dt. Chem. Ges. 46 (1913) 2466.

[3] E. L. Kennaway, Brit. Med. J. ii (1925) 1.

[4] E. Gil-Av, J. Shabtai, Nature 197 (1963) 1065.

[5] G. M. Badger, J. K. Donnelly, T. M. Spotswood, Aust. J. Chem. 19 (1966) 1023-43.

[6] J. Oró, J. Han, A. Zlatkis, Analytical Chem. 39 (1967) 27.

[7] M. Frenklach, Phys. Chem. Chem. Phys. 4 (2002) 2028-2037.

[8] T. Hidaka, T. Higashihara, N. Ninomiya, H. Masaoka, T. Nakamura, H. Kawano, Int. J. Chem. Kinet. 28 (1996) 137.

[9] J. H. Kiefer, K. I. Mitchell, H. C. Wei, Int. J. Chem. Kinet. 17 (1985) 225.

[10] J. H. Kiefer, K. I. Mitchell, H. C. Wei, Int. J. Chem. Kinet. 20 (1988) 787.

[11] S. W. Benson, G. R. Haugen, J. Phys. Chem. 71 (1967) 1735.

[12] G. B. Skinner, E. M. Sokolowski, J. Phys. Chem. 64 (1960) 1028.

[13] V. S. Rao, K. Takeda, G. B. Skinner, Int. J. Chem. Kinet. 20 (1988) 153.

[14] W. Tsang, V. Mokrushin, Proc. Combust. Institute 28 (2000) 1717.

[15] R. D. Kern, H. J. Singh, C. H. Wu, Int. J. Chem. Kinet. 20 (1988) 731.

[16] T. Hidaka, T. Higashihara, N. Ninomiya, T. Oki, H. Kawano, Int. J. Chem.Kinet. 27 (1995) 331.

[17] S. D. Chambreau, J. M. Lemieux, L. Wang, J. Zhang, J. Phys Chem. A 109 (2005) 2190.

[18] K. H. Weber, J. Zhang, D. Borchardt, T. H. Morton, Int. J. Mass Spectrom. 249-250 (2006) 303.[19] D. W. Kohn, H. Clauberg, P. Chen, Rev. Sci. Instrum. 63 (1992) 4003.

[20] A. V. Friderichsen, J. G. Radziszewski, M. R. Nimios, P. R. Winter, D. C. Dayton, D. E. David, G. B. Ellison, J. Am. Chem. Soc. 123 (2001) 1977.

[21] C. Lee, W. Yang, R. G. Parr, Phys. Rev. B 37 (1988) 785.

[22] A. D. Becke, J. Chem. Phys. 109 (2001) 9287.

[23] M. J. Frisch, G. W. Trucks, H. B. Schlegel, G. E. Scuseria, M. A. Robb, J. R. Cheeseman, V. G. Zakrzewski, J. A. Montgomery, R. E. Stratmann, J. C. Burant, S. Dapprich, J. M. Millim, A. D. Daniels, K. N. Kudin, M. C. Strain, O. Farkas, J. Tomasi, V. Barone, M. Cossi, R. Cammi, B. Mennucci, C. Pomelli, C. Adamo, S. Clifford, J. Ochterski, G. A. Petersson, P. Y. Ayala, Q. Cui, K. Morokuma, D. K. Malick, A. D. Rabuck, K. Raghavachari, J. B. Foresman, J. Cioslowski, J. V. Ortiz, B. B. Stefanov, G. Liu, A. Liashenko, P. Piskorz, I. Komaromi, R. Gomperts, R. L. Martin, D. J. Fox, T. Deith, M. A. Al-Laham, C. Y. Peng, A. Nanayakkara, C. Gonzalez, M. Challacombe, P. M. W. Gill, B. G. Johnson, W. Chen, M. W. Wong, J. L. Andres, M. Head-Gordon, E. S. Replogle, J. A. Pople, Gaussian 98/03; Gaussian, Inc.: Pittsburgh, PA, 1998.

[24] F. P. Lossing, J. C. Traeger, J. Am. Chem. Soc. 97 (1975) 1579.

[25] J. L. Holmes, Org. Mass Spectrom. 8 (1974) 247.

[26] J. -P. Puttemans, J. C. Delvaux, Ing. Chim. Brussell 55 (1973) 7.

[27] F. P. Lossing, J. L. Holmes, J. Am. Chem. Soc. 106 (1984) 6917.

[28] X. Gong, H. Xiao, Int. J. Quantum Chemistry 69 (1998) 659-667.

[29] I. L. Alberts, F. Schaefer III, Chem. Phys. Lett. 161 (1989) 375-382.

[30] Bock, Ch.W.; Panchenko, Yu.N. *J. Mol. Struct.* 160 (1989) 337.

[31] (a) E. N. Marvell, Thermal Electrocyclic Reaction, Academic Press, New York, 1980 p.136 (b) H. M. Frey, Trans. Faraday Soc. 58 (1962) 957.

[32] (a) R. Walsh, Chem. Soc. Rev. 34 (2005) 714; (b) M. S. Baird, Chem. Rev. 103 (2003) 1271.

[33] N. Hansen, S. J. Klippenstein, C. A. Taatjes, J. A. Miller, J. Wang, T. A. Cool, B. Yang, R. Yang, L. Wei, C. Huang, J. Wang, F. Qi, M. E. Law, P. R. Westmoreland, J. Phys. Chem. A 110 (2006) 3670.

[34] S. Wolfe, C. -H. Kim, Isr. J. Chem. 33 (1993) 295-305.

[35] W. Reineke, K. Strein, Ber. Bunsen – Ges. Phys. Chem. 80 (1976) 343.

[36] V. V. Takhstove, D. A. Ponomorev, Org Mass Spectrom 29 (1994) 395.

[37] (a) I. N. Domnin, Eur. Mass Spec. 5 (1999) 169-182 (b) I. N. Domnin, Eur. Mass Spec. 4 (1998) 151.

[38] H. -Y. Lee, B. B. Kislov, S. -H. Lin, A. M. Mebel, D. M. Neumark, Chem.-Eur. J. 9 (2003) 726.

[39] W. Tang, R. S. Tranter, K. Brezinsky, J. Phys. Chem. A 110 (2006) 2165.

[40] R. Stockbauer, K. E. McCulloh, A. C. Parr, Int. J. Mass Spectrom. Ion Phys. 31 (1979) 187.

[41] R. Walsh, Chem. Soc. Rev. 34 (2005) 714.

[42] M. Yoshimine, J. Pacansky, N. Honjou, J. Am. Chem. Soc. 111 (1989) 4198.

CHAPTER 7

CYCLOPENTADIENE, METHYLCYCLOPENTADIENE, CYCLOPENTENE, CYCLOHEXENE, AND 1,4-CYCLOHEXADIENE

INTRODUCTION

Combustion provides the majority of the global energy budget and will continue as an important source of energy in the future. Increasing concern over the health effects and global warming from pollutant emissions[1-5] has stimulated interest in an improved knowledge of combustion chemistry with a long-term goal of improving energy economy and reducing environmental impact. In particular, the formation of polyaromatic hydrocarbons (PAHs) and ultimately soot, resulting from imperfect combustion, has been an active area of research. A critical step in PAH production is formation of the "first aromatic ring" which includes first and foremost benzene and can be thought to include indene and naphthalene.[6-8] Benzene is formed through multiple pathways not limited to (1) acetylene (C_2H_2) addition (2) propargyl (C_3H_3) self-combination and (3) reaction of cyclopentadienyl radical (c-C_5H_5) with methyl radical (CH_3). There has been debate over the relative contributions of these reactions in the formation of benzene[9-14] and although the even carbon pathways involving C_2H_2 addition have been identified by kinetic simulations of C_2H_2 pyrolysis,[15] subsequent kinetic studies,[16-18] and numerical simulations,[19] the self-combination of C_3H_3 resonance-stabilized radicals (RSRs) is established[20-30] and seems to be the primary route to benzene in the majority of flames.[6,10,27] RSRs frequently play a key role in the formation of aromatics[31] and the

cC_5H_5 RSR is believed to be a critical PAH precursor in fuel rich flames.[32-37] The *c*C_5H_5 radical can be formed by the reaction of C_3H_3 RSR with C_2H_2,[38,39] loss of H atom from cyclopentadiene (Cp),[40-42] and loss of CH_3 radical from methylcyclopentadiene (MeCp).[43-45] The direct self-combination of *c*C_5H_5 RSRs to form naphthalene (spiran mechanism) was first proposed by Melius *et al*.[46] and more recently studied by Kislov and Mebel.[47] The formation of indene in the pyrolysis of Cp has lead to investigation of the *c*C_5H – cylcolpentadiene radical-neutral reaction[48,49] as well as successive C_2H_2 additions to the *c*C_5H_5 RSR.[50,51]

The pyrolysis of Cp and ensuing decomposition of the *c*C_5H_5 RSR has been studied experimentally.[40-42] The thermal decomposition is initiated by C-H bond fission producing *c*C_5H_5 which then undergoes a 1,2 H shift and ring opening to a linear C_5H_5 species. This intermediate can then undergo C-C bond fissure resulting in RSR C_3H_3 and C_2H_2. In addition to the radical thermal decomposition pathway, theoretical calculations have indicated that the direct molecular eliminations of acetylene to form either allene or propyne may be viable.[52] The pyrolysis of MeCp has received attention from various groups.[43-45] The shock tube study performed by Lifshitz et al.[44] produced products, in decreasing abundance, Cp, benzene, methane, ethane, naphthalene, acetylene, ethylene, C_4H_4, toluene, C_3H_4, and indene. MeCp can readily isomerize between 1, 2, and 5 position isomers on both the neutral[46] and minus H radical[53] potential energy surface. From the work of Dubnikova and Lifshitz[53] it has been concluded that isomerization to

form 5-(1,3-cyclopentadienyl)methyl radicals is the rate limiting step in the H-assisted expansion of fulvene (a critical intermediate in the C_6H_6 isomerization, to benzene).[54] Also, MeCp should be capable of undergoing similar molecular eliminations and ring opening/C-C bond fissures as for Cp, although to our knowledge no such studies have been conducted to investigate that process to this date.

Combustion and pyrolysis are complex processes dominated by the chemistry of free radicals and despite extensive study the mechanisms require further improvement. Despite the large amount of work on the pyrolysis of cyclopentadiene and methylcycopentadiene the mechanistic pathways need further characterization. The experimental approach of flash pyrolysis coupled to supersonic expansion and vacuum ultraviolet (VUV) photoionization mass spectrometry provides short reaction times to examine the initial steps of pyrolysis, supersonic cooling to minimize recombination and reactions of products and intermediates, and minimized ion fragmentation due to the low ionization photon energy.[55-57] Also, the bond fission and molecular elimination pathways in the initial stage of pyrolysis can be directly observed *simultaneously* in this work, with minimum complication from subsequent reactions.

EXPERIMENTAL

1,4-cyclohexadiene (97+%) and cyclopentene (99%) was obtained from Aldrich and cyclohexene (99%) was from Acros Organics. Cyclopentadiene and methyl-

cyclopentadiene were obtained by destructive distillation of the dimers dicylopentadiene (95%) from Fisher Scientific and dimethylcyclopentadiene (93%) from Sigma Aldrich. The compounds studied were used without further purification and diluted to 1-4% in argon or helium by bubbling the noble carrier gas through the liquid at acetonitrile/dry ice or ice/water bath temperatures. The backing pressure of the gas mixture was maintained at ~ 1.5 atm for all experiments.

RESULTS

(1) 1,4-cyclohexadiene, cyclopentene, and cyclohexene. As mentioned previously, in order to further establish the utility of the apparatus employed in these experiments, the pyrolyses of 1,4-cyclohexadiene, cyclopentene, and cyclohexene were performed their chemistries being well known. The decomposition of 1,4-cyclohexadiene to form benzene and hydrogen is known to be unimolecular in nature,[60,61] having an activation energy of 42.7 kcal/mol, proceeding through a disrotary transition state as predicted by Woodward and Hoffman symmetry rules. A stack plot of mass spectra for the pyrolysis of 1,4-cyclohexadiene with nozzle temperatures of 295, 705, 815, 930, 985, 1030, and 1165 K is presented in Figure 7.1 (a). Note that in the room temperature spectral trace, small peaks are observed at *m/e* 78 and *m/e* 79, the result of minimal photoionization fragmentation, in addition to the molecular ion ($M^{+\bullet}$) at *m/e* 80. In attempt to access the

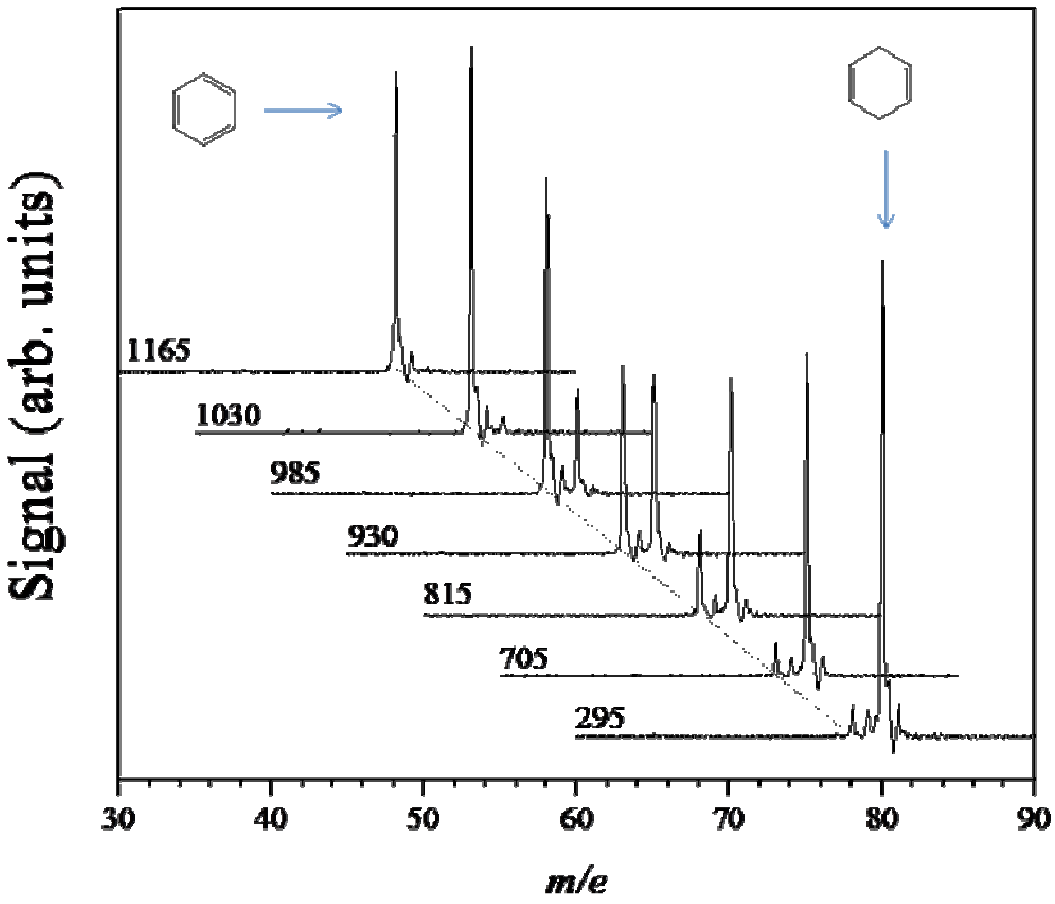

Figure 7.1 (a) Stack plot of mass spectra for the pyrolysis of 1,4-cyclohexadiene diluted in argon.

photoionization fragment producing a fairly consistent signal across a range of nozzle temperatures. The *m/e* peak at 78, however, increases dramatically in intensity beyond ~800 K as can be seen from the comparison of relative intensities presented in Figure 7.1 (b). This observation is consistent with the reported activation energy of 42.7 kcal/mol[61]

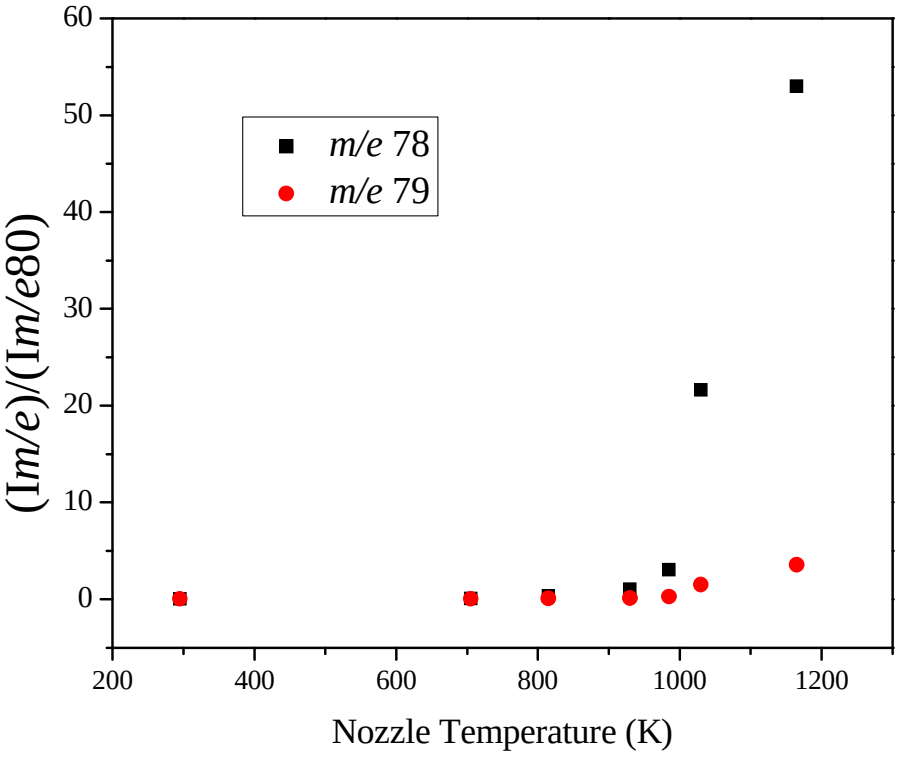

Figure 7.1 (b) Intensities of select *m/e* signals relative to the molecular ion.

for molecular elimination of hydrogen. Figure 7.2 (a) presents a stack plot of mass spectra from the pyrolysis of cyclopentene with nozzle temperatures of 295, 845, 980, 1065, 1195, and 1385 Kelvin. Eliminations of hydrogen from isotopically labeled cyclopentene has been studied by Baldwin[62] and shown to have a 10:1 preference for 1,4 over 1,2 elimination. The consumption channels of reaction with H atoms to create cyclopentenyl radicals plus hydrogen[31] is not observed here, however, the H-atom

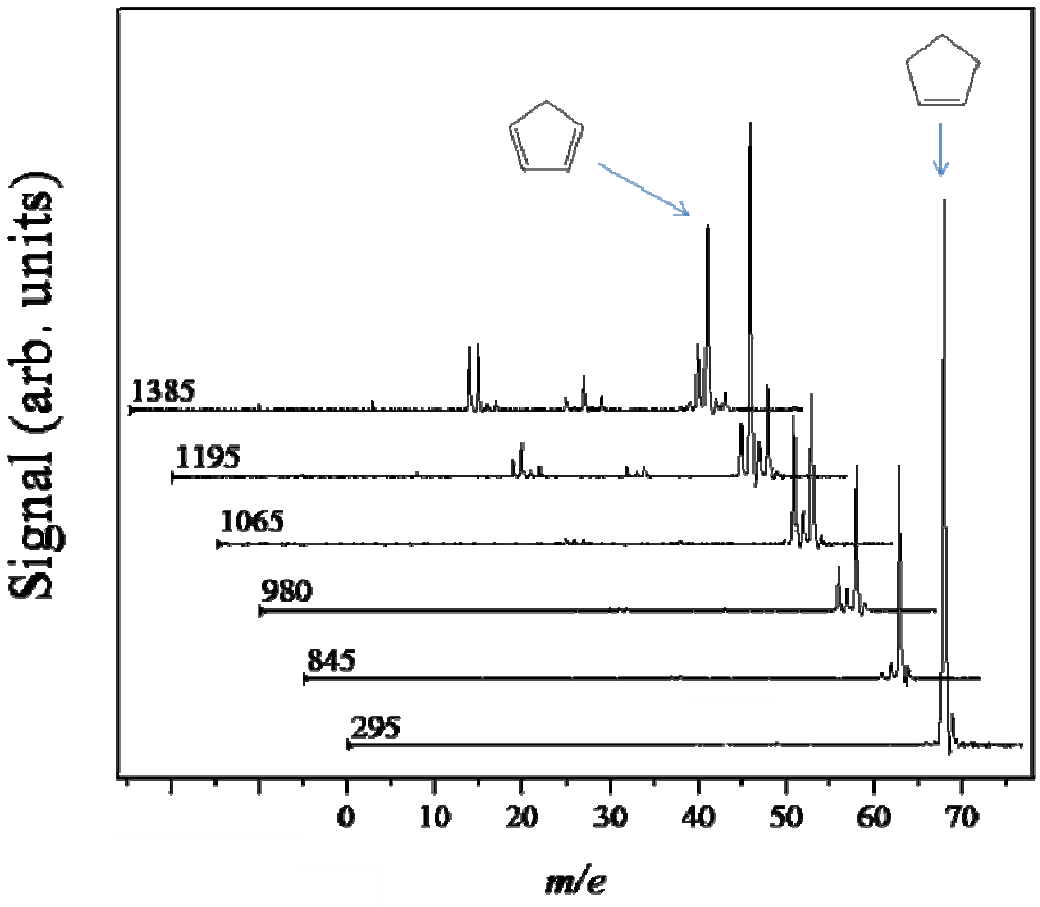

Figure 7.2 (a) Stack plot of mass spectra for the pyrolysis of cyclopentene diluted in argon. Reported nozzle temperatures are in units of Kelvin (K).

addition then decomposition that produces allyl radical and ethylene[32] may be observed at higher temperatures as *m/e* 42 and 28 peaks. A photoionization fragmentation plot of *m/e* number relative to the $M^{+\bullet}$ signal was prepared for the pyrolysis of cyclopentene and the result is displayed in Figure 7.2 (b). It seems plausible the *m/e* 67 peak is mainly

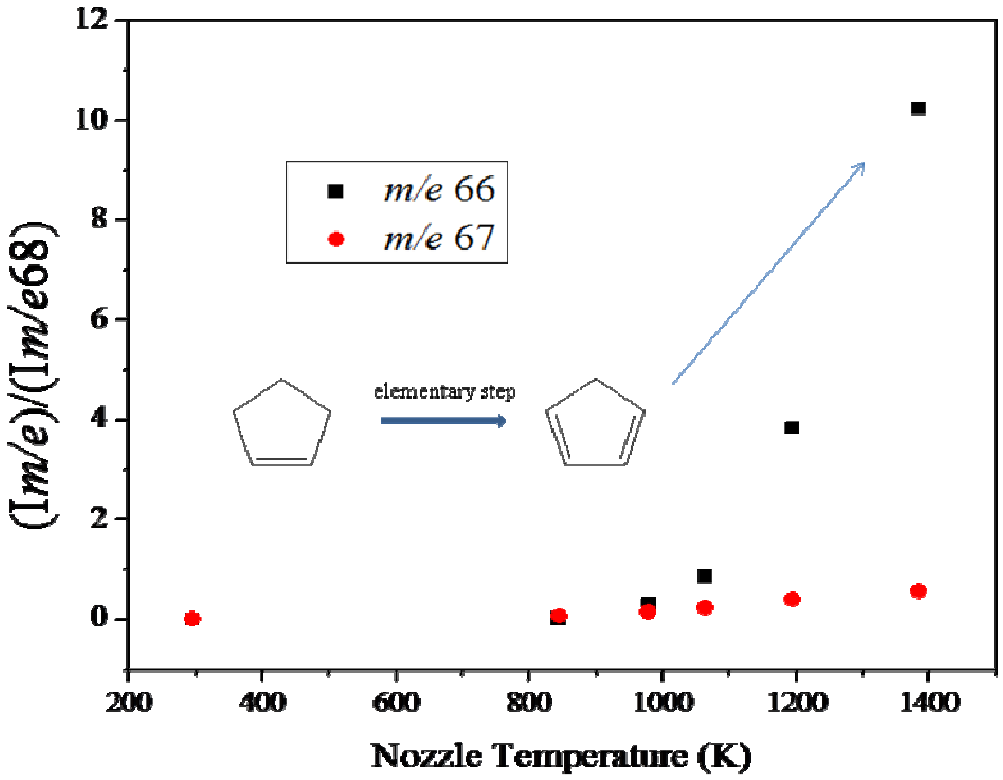

Figure 7.2 (b) Intensities of select *m/e* signals relative to the molecular ion.

attributed to photoionizaton fragmentation. The *m/e* 66 signal corresponds to thermally generated cyclopentadiene, expected over this temperature range. At elevated temperatures *m/e* peaks at 65, 50-52-54, 39-42, and 28 are detectable. The peak at *m/e* 65 results from the decomposition of cyclopentadiene into H atom and the *c*C_5H_5 RSR. The reported energy barriers for C-H fission differ from another, ranging from 77 kcal/mol[41] to 84 kcal/mol[42]. The *c*C_5H_5 RSR can then undergo a critical 1,2 H shift (activation energy of 55.0 kcal/mol, 61.9 kcal/mol) then C-C bond cleavage to ring open then further decompose to propargyl (*m/e* 39) and acetylene (not observable due to high ionization

energy). The transition states for ring opening are reported to be 76.9 (TS1) or 77.1 kcal/mol[41] 76.2 (TS1)or 79.7 (TS2) kcal/mol[42]. A signal at *m/e* 42 is not observed in the cyclopentadiene pyrolysis and may therefore here it appears to be a result of the H-atom addition/ decomposition reaction. Stack plots of mass spectra for the pyrolysis of cyclohexene is presented in Figure 7.3 (a) with spectral traces with nozzle heater temperatures of 295, 820, 970, 1020, and 1060 K are presented. In the ambient

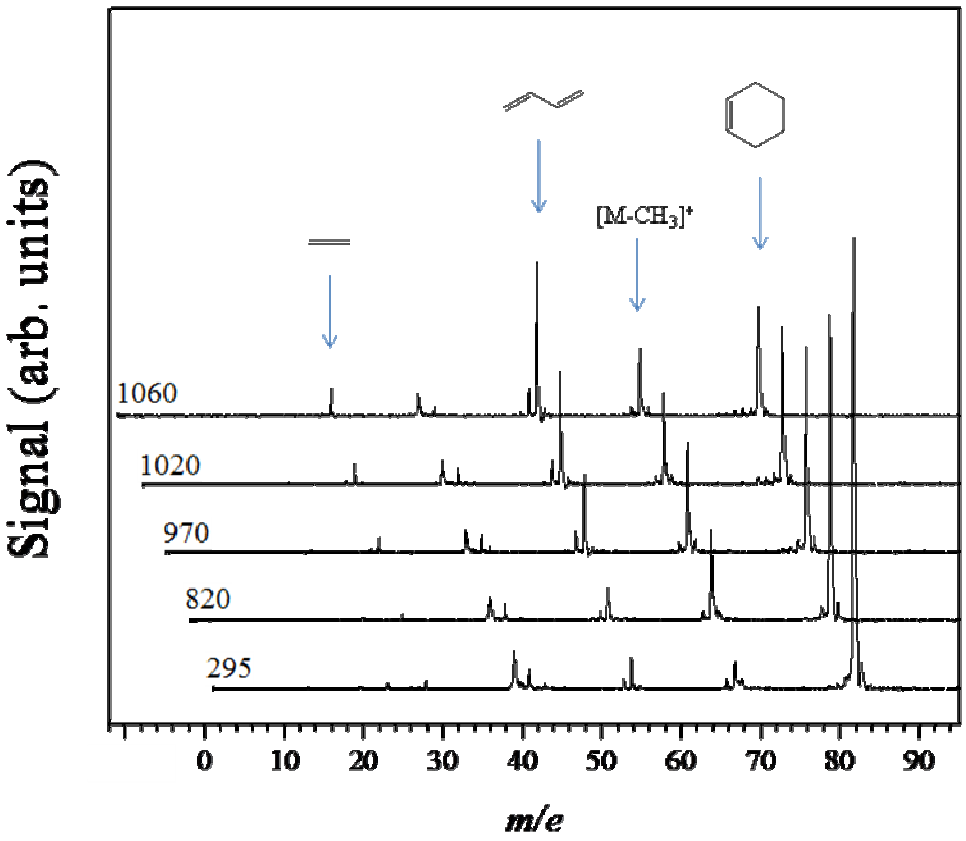

Figure 7.3 (a) Stack plot of mass spectra for the pyrolysis of cyclohexene with nozzle temperatures up to 1060 K.

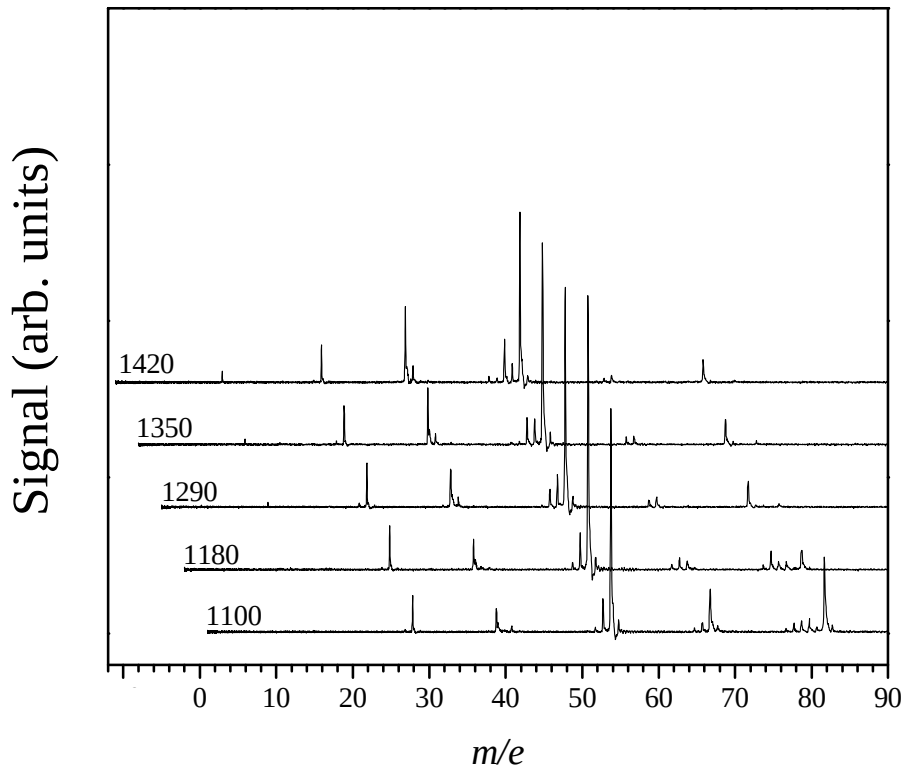

Figure 7.3 (b) Stack plot of mass spectra for pyrolysis of cyclohexene with nozzle temperatures ranging from 1100 – 1420 K.

temperature nozzle spectra a large molecular ion peak is observed at *m/e* 82. Smaller peaks at *m/e* 39, 41, 53, 54, 66, and 67 are observed as photoionization fragments. The next spectral trace with a heater temperature of 820 K demonstrates a complication in the interpretation of these pyrolytic spectra. Many photoionization fragments are not sensitive to internal energy content and produce a fairly constant signal due to the efficacy of the jet-cooling. This is not the case for the *m/e* 67 signal which displays a dramatic increase in intensity at higher nozzle temperatures. This signal is not the result of thermolysis, however, as the CH_3 radical created concomitantly would be easily detected in this apparatus, and it is not. As the nozzle is heated up through to 1060 K the

peaks at *m/e* 28 and 54 show consistent growth in relation to the other peaks resulting from the retro Diels-Alder reaction. Figure 7.3 (b) displays mass spectra for nozzle temperatures ranging from 1100 – 1420 K. In the lower two traces (1100K and 1180K) we see the last remnants of the parent cyclohexene. Although the retro Diels-Alder reaction is predominant, cyclohexene can also have 1,4 elimination of hydrogen to create 1,3-cyclohexadiene. 1,3-cyclohexadiene is more resistant to heat that 1,4-cyclohexadiene and will decompose to benzene by successive loss of H radicals.[60,61] Consistent with the molecular elimination of hydrogen followed by radical H loss are the peaks at *m/e* 82, 80 and then *m/e* 79 and 78. As the heat in increased to 1290, 1350 and 1420 K very little cyclohexene is observed to survive the pyroysis chamber. The peaks at *m/e* 41 and 67 are no longer observed, further indicating them as fragment ions of the parent compound. A new peak is observed at *m/e* 52, possibly vinylacetylene produced from the 1,3-butadiene created. The pyrolysis of 1,3-butadiene has been well studied by this group.[55] It is known to isomerize and then decompose into RSR propargyl (C_3H_3) and methyl radical, both being observed at elevated temperatures in these traces. The peak at *m/e* 78 could have a small contribution from the propargyl self-combination reaction but the features of the spectra lack characteristics consistent with self-combination. It is likely, therefore, that the *m/e* 78 signal observed is benzene and is formed by the 1,4 molecular elimination of hydrogen from cyclohexene to form 1,3-cyclohexadiene which then decomposes to benzene *via* a radical mechanism.

Cyclopentadiene

A stack plot of mass spectra from the pyrolysis of cyclopentadiene is presented in Figure 7.4 with nozzle temperatures of 295, 1060, 1160, 1240, 1280 and

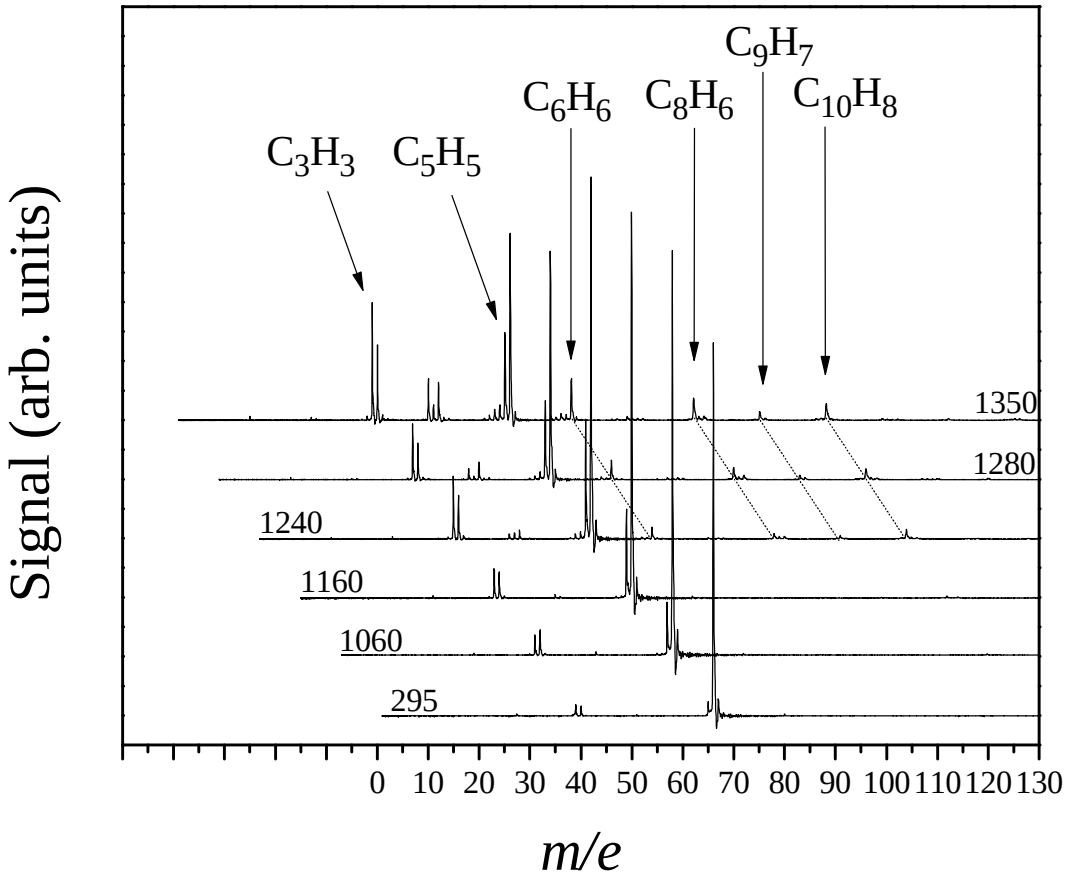

Figure 7.4 Stack plot of mass spectra for the pyrolysis of cyclopentadiene up to 1350 K.

1350 K. For the room temperature trace the molecular ion ($M^{+\bullet}$) at *m/e* 66 produces a strong signal with very small peaks at *m/e* 39, 40, and 65 being detectable. As heat is

applied bringing the reactor nozzle to temperatures of 1060 and 1160 K the peak at *m/e* 65 grows from 3% to 13% then 23%. It is likely that *c*C_5H_6 is undergoing C-H bond fission to form *c*C_5H_5 at these temperatures with a reported bond energies of 77[41] or 84 kcal/mol.[42] The previously observed peaks at *m/e* 39 and 40 show a modest increase in relative intensity to the parent ion growing from 2.5% at room temperature to ~7% at1060 and 1160 K. With the nozzle temperature being increased to 1240, 1280, and then 1350 K new peaks are observed while the peaks at *m/e* 39 and 40 (C_3H_3 and C_3H_4) increase dramatically. At the same time the *m/e* 65 peak continues to grow. Peaks at *m/e* 50, 51, and 52 are clearly discernible as is a prominent *m/e* 78 peak. Additionally, there is activity in the *m/e* 102-104, *m/e* 115-116, and *m/e* 128-130 regions of the spectra. At the hottest temperature trace 1350 K some activity may be in the *m/e* 91-92 region but the signal to noise ratio is poor. Note that there are small peaks at *m/e* 75, 76, and 77. This feature has been found to be consistent with C_6H_6 formed from propargyl self-combination in control experiments. The small peaks at *m/e* 63 and 64 may be an indication of the cyclic C_5H_5 undergoing ring opening to linear C_5H_5.

Methyl-cyclopentadiene

A stack plot of mass spectra from the pyrolysis of methyl-cyclopentadiene is presented in Figure 7.5with nozzle temperatures of 295, 1070, 1150, 1220, 1320 and 1460 K. In the room temperature trace the base peak is the molecular ion ($M^{+\bullet}$) at *m/e* 80. Also present are peaks *m/e* 39-41, *m/e* 51-54, *m/e* 66, 77, and 79. A small peak is detected at *m/e* 43 arising from the small amount of *n*-propyl iodide used as internal

calibrant. As the nozzle temperature is increased to 1070 K much of the spectra is similar to the room temperature spectra, however, a peak at *m/e* 15 (CH_3 radical) is detected as is a large peak at *m/e* 65 (C_5H_5). Additionally, there are peaks detected at *m/e* 128 and 130 as well as a new *m/e* 78 peak. As the nozzle is heated further to a temperature of 1150 K

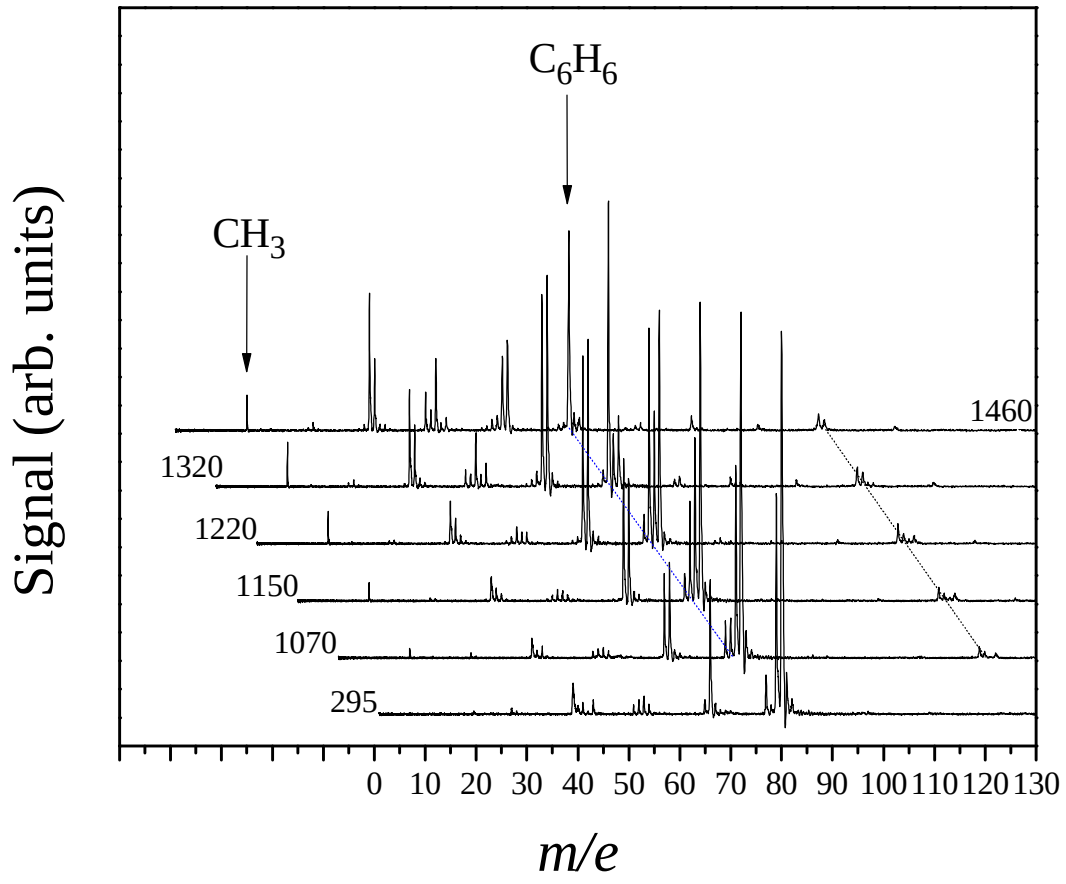

Figure 7.5 Stack plot of mass spectra for the pyrolysis of methyl-cyclopentadiene.

the intensities of the 15, 39, and 78, corresponding to methyl and propargyl radicals and C_6H_6 respectively, steadily increase while the peaks at *m/e* 128 and 130 display slight

augmentation. Successively heating the nozzle to temperatures of 1220, 1320, and 1460 K the parent peak at *m/e* 80 drastically diminishes until at *m/e* 1460 K is barely detectable as does the signal at *m/e* 79. Meanwhile, the C_6H_6 peak at *m/e* 78 is found to dominate the spectra, the base peak. The peaks at *m/e* 65 and 66, cyclopentadienyl and cyclopentadiene, are prominent peaks in these traces being of similar intensity to each other, approximately equal to the base peak intensity for the 1220 K trace and <50% of the base peak in the 1460 K trace. The signals at *m/e* 39 and *m/e* 40 continue to increase, however, the intensity of *m/e* 39 grows at a more rapid rate than *m/e* 40. The *m/e* 15 peak displays growth over 1220 -1320 then is found to produce an equally intense signal in the 1460 K trace. The signals at *m/e* 50 and 52 both show rapid onset of growth over this temperature range. In the higher *m/e* recombination region new peaks are found at *m/e* 91 and 92, perhaps corresponding to C_7H_7 chemistry. A strong peak at *m/e* 102 is clearly detected and is found to increase in intensity as the temperature is increased. A peak at *m/e* 115 is also detected which has an approximately constant intensity as does the peak at *m/e* 128. The *m/e* 130 signal decreases over this temperature range until in the 1460 K trace it is no longer detected.

DISCUSSION

(1) Thermal Degragredations. Figure 7.6 (a) presents the relative intensities of *m/e* 39, 40, 65 (corresponding to C_3H_3, C_3H_4, and C_5H_5) to the parent compound, cyclopentadiene, at

m/e 66. From this data interpretation it appears that at temperatures >1000 K cyclopentadiene is undergoing thermal loss of hydrogen to form *c*C_5H_5 (eq. 1).

$$cC_5H_6 \rightarrow cC_5H_5 + H \quad \text{(eq. 1)}$$

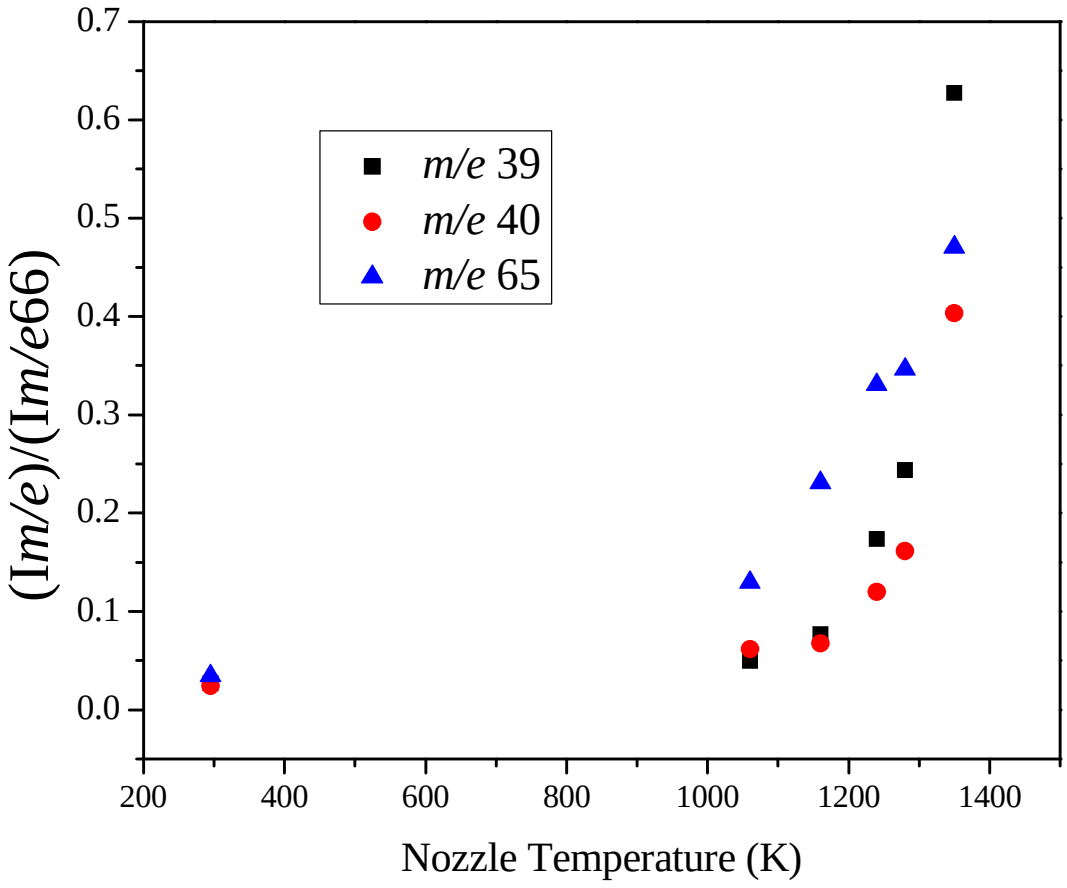

Figure 7.6 (a) Relative intensities of select ions for the cyclopentadiene pyrolysis.

At temperatures >1200 K propargyl radicals are present from the decomposition of the *c*C_5H_5 as further evidenced by the onset of the C_6H_6 combination peak at *m/e* 78. To

decompose the *c*C_5H_5 radical must undergo a ring opening *via* a 1,2-H migration to form linear radicals $CH_2CCHCHCH$, $CHCCH_2CHCH$, and $CH_2CHCHCCH$. Breaking of a C-C bond in the first two of these radicals results in C_2H_2 and C_3H_3.

$$cC_5H_5 \rightarrow C_5H_5 \rightarrow C_3H_3 + C_2H_2 \quad \text{(eq. 2)}$$

Recent calculations[39] estimate the 1,2-H migration and ring opening process to have energy barriers of 65.7 and 75.8 kcal/mol. The subsequent C-C bond breaking was found to be 91.7 kcal/mol relative to *c*C_5H_5. The rise in intensity of the peak at *m/e* 40 could imply that thermal decomposition on the neutral surface is occurring at elevated temperatures. Three pathways from *c*C_5H_6 to C_2H_2 and C_3H_4 were explored by Bacskay and Mackie.[52] A pathway proceeding through a cyclic carbene intermediate was found to have a 94.0 kcal/mol energy barrier to propyne and acetylene. A pathway that proceeds through allyl-vinylidene to produce allene and acetylene was found to have a 93.3 kcal/mol barrier. Lastly, a pathway that proceeds through a diradical intermediate was found to have a 102.4 kcal/mol barrier. It should be noted that Roy et al.[41] discounted the production of acetylene directly from C_5H_6 as it is produced after longer reaction times at high temperatures.

Figure 7.6 (b)-(d) presents relative intensities of select *m/e* peaks compared to the molecular ion for methylcyclopentadiene. In Figure 7.6 (b) the relative intensities of *m/e* 39, 40, and 41. As found in the cyclopentadiene pyrolysis the onset of both *m/e* 39 and 40 onset at the same time at approximately at 1200 K. In the methylcyclopentadiene

pyrolysis, however, the amounts of *m/e* 39 and 40 are far greater compared to the cyclopentadiene levels in Figure 7.6 (a). The *m/e* 41 peak is found to be constant over this temperature range and is attributed to a photoionization fragment. Figure 7.6 (c) presents intensities relative to the molecular ion for *m/e* 50-54. Over this

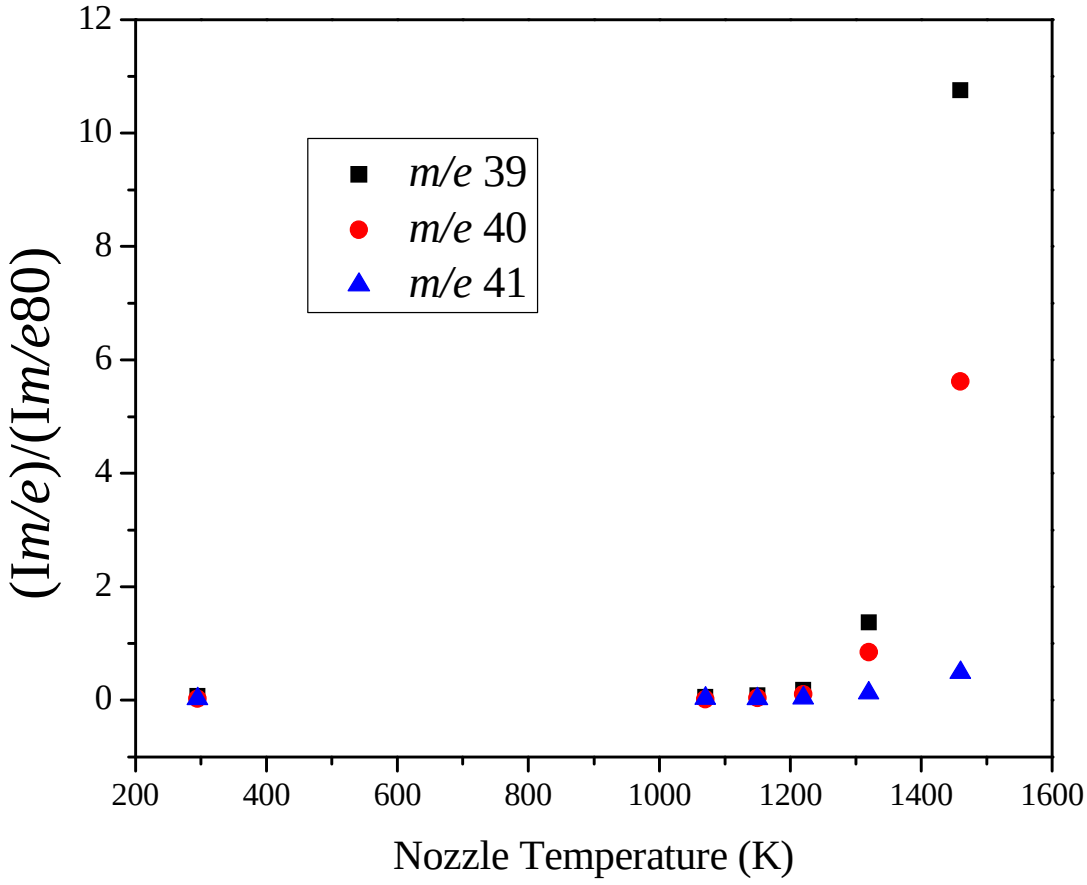

Figure 7.6 (b) Select relative intensities for the pyrolysis of methylcyclopentadiene.

temperature range all of these peaks increases in intensity beyond ~1200 K. The amount of *m/e* 52 is found to be significantly elevated from the intensities observed in the cyclopentadiene pyrolysis. Previous work with methylpropargyl radical in this apparatus has demonstrated that it will rapidly produce *m/e* 52 by loss of H atom, whether it be by thermolysis or photoionization fragmentation is not clear. Also, a peak at *m/e* 54 is

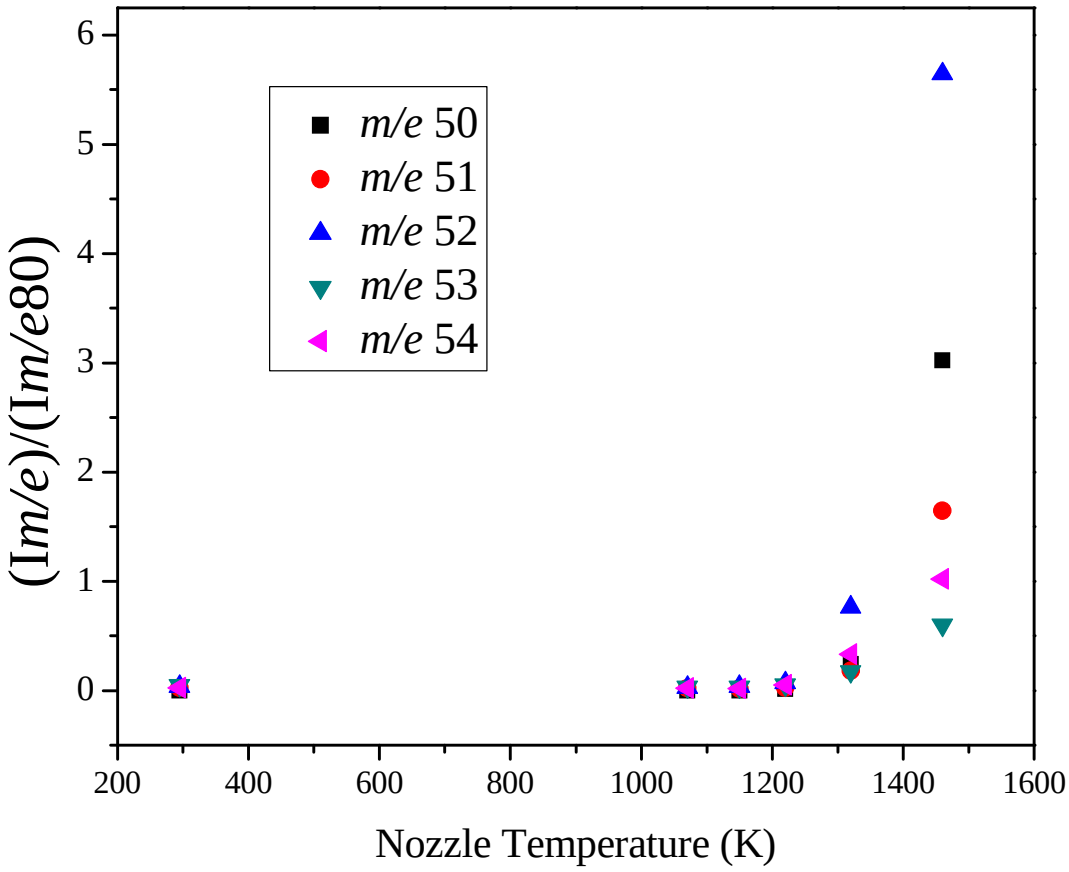

Figure 7.6 (c) Select relative intensities for the pyrolysis of methylcyclopentadiene.

observed in this pyrolysis which is not found in the cyclopentadiene pyrolysis. These spectral features coupled with the enhanced propargyl radical production are indicative of ring opening with subsequent C-C bond cleavage to form propargyl RSR and C_3H_4 or methylpropargyl RSR and acetylene. Figure 7.6 (d) present intensities relative to the parent signal at *m/e* 80 for the peaks at *m/e* 65, 66, 77, and 79. At temperatures above

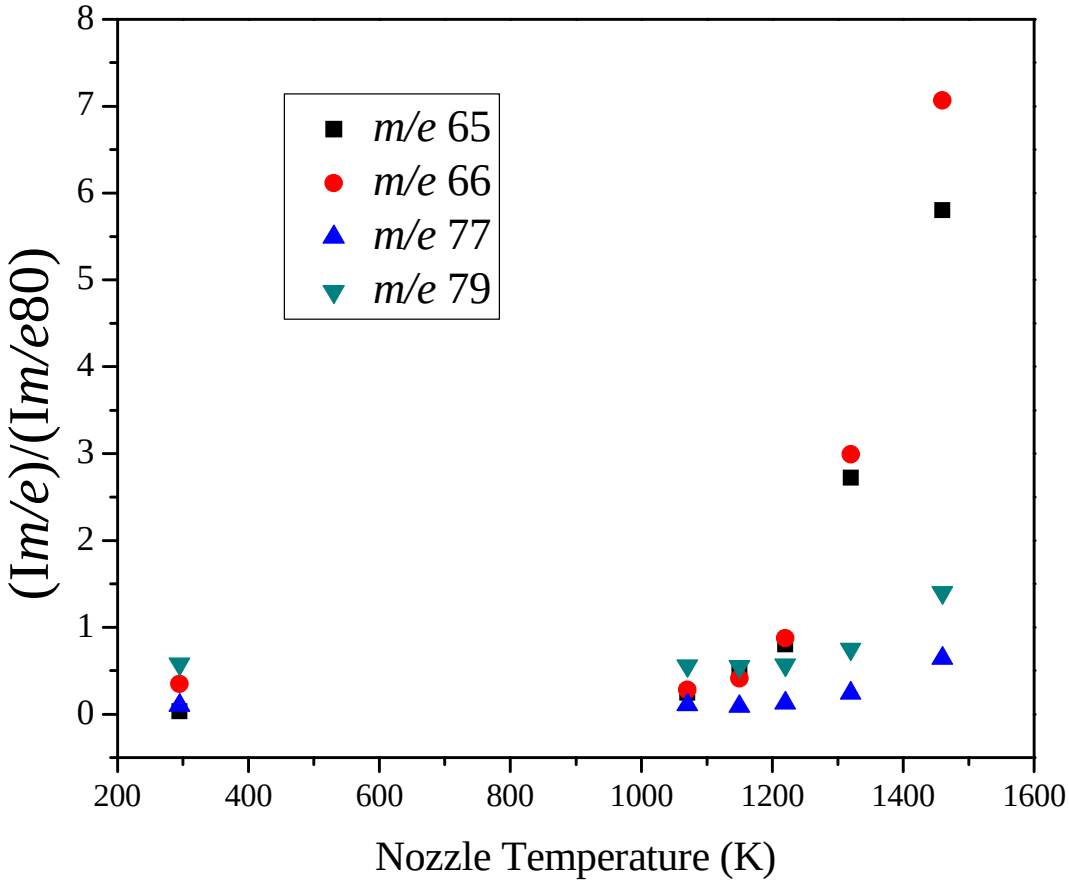

Figure 7.6 (d) Relative intensities of select ions in the pyrolysis of methycyclopentadiene.

1200 K the intensities of both *m/e* 65 and 66 both display marked growth indicating that both are produced by thermal processes. Cyclopentadiene is known to be a major product of methylcyclopentadiene pyrolysis and although a molecular elimination of cyclopentadiene has been observed in the similar *t*-butylcyclopentadiene,[54] here a molecular elimination is believed to be prohibitive and therefore Cp is likely produced by H-abstraction by cyclopentadienyl radicals. The intensities of *m/e* 77 and 79 are found to only increase slightly at temperatures greater than 1200 K. From Figure 7.6 (d) it is clear that these peaks are photoionization fragments at lower temperatures. At the higher temperatures *m/e* 79 would correspond to the –H radical of MeCP. Although the intensity does not increase significantly it seems plausible that the –H radical is unstable and rapidly decomposes either thermally or by photoionization to *m/e* 78. The peak at *m/e* 77 dissappears at the same time as the parent peak leading to the conclusion that it is mainly a photoionization fragment associated with the parent compound.

Initial Combinations in the Formation of Aromatics

Figures 7.7 (a) and (b) present a comparison of the aromatic growth region of the mass spectra for pyrolysis of cyclopentadiene and methyl-cyclopentadiene respectively. In Figure 7.7 (a) small peaks at *m/e* 78 from self-combination of C_3H_3 radicals, in addition to peaks at 128 and 130 from self-combination of cC_5H_5, are barely discernible in the 1160 K spectral trace. At a nozzle temperature of 1240 K the peaks at *m/e* 78 and 128 are now clearly observed with small new peaks at *m/e* 76 and 77, which from

previous experiments has been identified as characteristic for C_6H_6 formation (benzene rings do not produce such signals). Signals at *m/e* 102-104, and 115 are detected. The cross combination of C_3H_3 and cC_5H_5 radicals, to our knowledge, have not been previously reported. It would appear that if the signal at *m/e* 104 is the cross-combination product it rapidly dehydrates to *m/e* 102. It may be possible that this product is a precursor to phenylacetylene which has been identified as a key intermediate in PAH growth. The peak observed at *m/e* 115 could be the indenyl radical and the very small *m/e* 116 peak could be the +H product resulting from H addition to indenyl radical. The detection of indene in the products from Cp pyrolysis led to theoretical work on the Cp plus Cpdyl radical addition potential energy surface. The work referenced here[48] predicts that the Cp plus Cpdyl adduct (at *m/e* 131, not observed) would quickly isomerize and either lose H atom to form methyl indene at *m/e* 130 (also not observed) or alternatively, the loss of methyl radical to directly afford indene at *m/e* 116. The energy barriers for these processes are predicted to be 45 kcal/mol or 56 kcal/mol depending on the mechanistic pathway.[48] Alternatively, indene has been theoretically shown to form from

the reaction of propargyl radical with benzene.[49] This would lead to a *m/e* 117 adduct

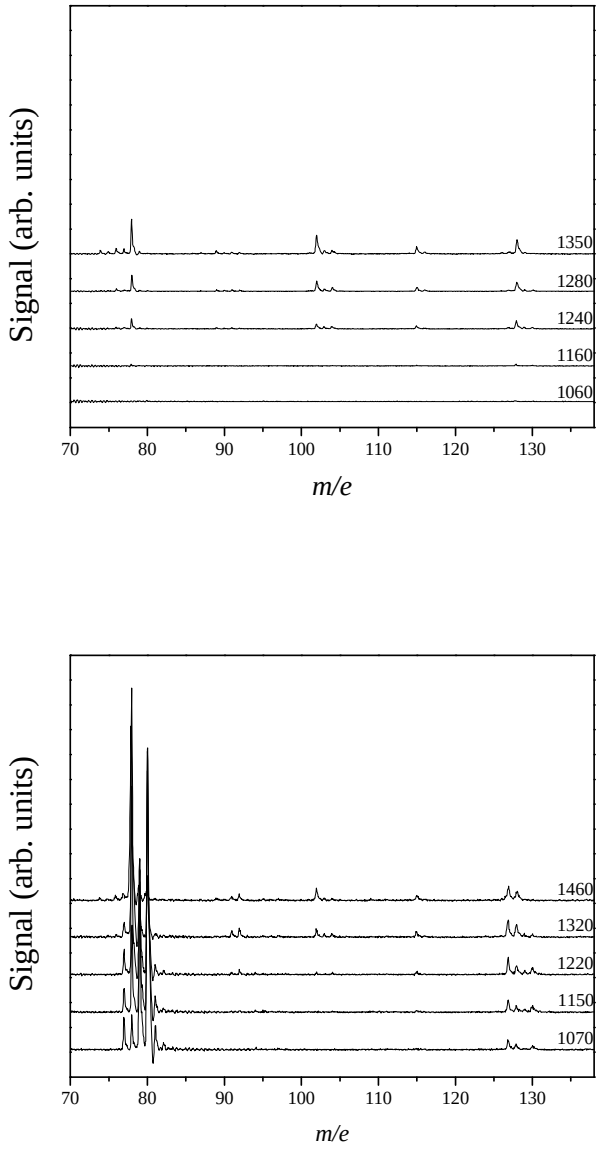

Figure 7.7 Comparison of the aromatic growth region of the mass spectra for the pyrolysis of (a) cyclopentadiene and (b) methyl-cyclopentadiene.

with subsequent H loss to form indene via multiple pathways. A *m/*e 117 signal is not observed in these pyrolyses.

To assist with interpretation of the data the pyrolysis of propargyl bromide was performed and presented in Figure 9. Pyrolysis of this compound produces propargyl radicals at lower temperatures due to the weaker C-Br bond, thereby allowing for a

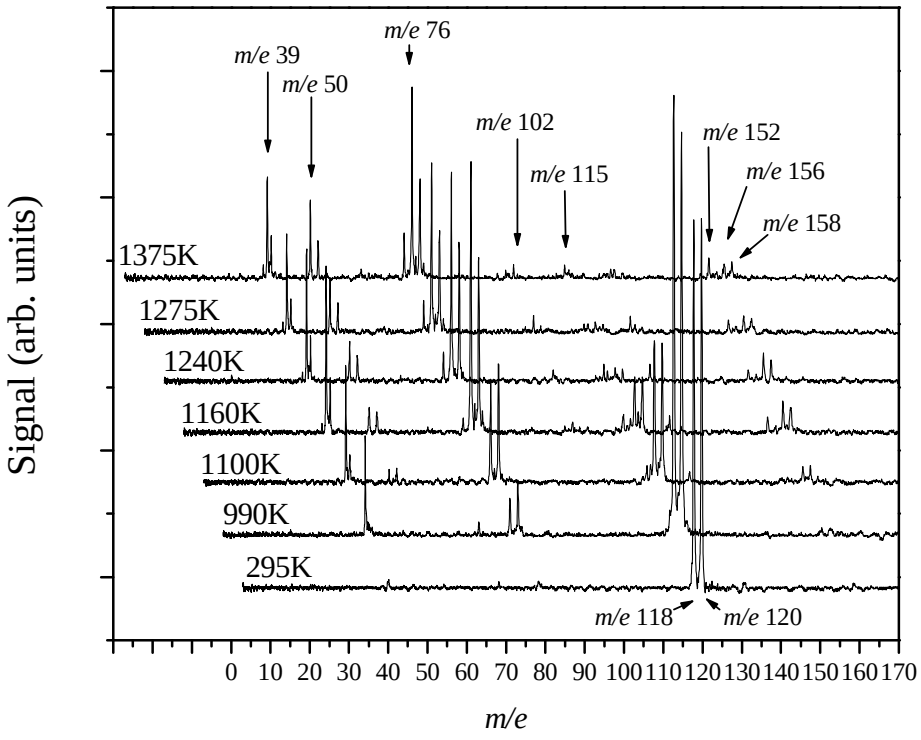

Figure 7.8 Stack plot of mass spectra for the pyrolysis of propargyl bromide.

longer time period for (re)combination. In this work the created propargyl radicals quickly pick up hydrogen producing a peak at *m/e* 40, while at the same time the C_6H_6

isomer peak looses hydrogen to produce peak from *m/e* 74-78 with the dominate peaks being at even *m/e* ratios (74, 76, 78). Significant peaks are observed at *m/e* 50 and 52 which may correspond to di and vinyl acetylene, known soot precursor. Small peaks are observed at *m/e* 102 and 104, with the peak at 102 being most stable, indicating that they may be combination products of *m/e* 50 and 52, in a process that assumedly is similar to the acetylene to vinylidene isomerization with subsequent addition as in the pyrolysis of acetylene. The intensities of the *m/e* 102 peak is, however, much less intense than observed in the Cp and MeCp pyrolyses therefore it is most likely that the contribution of this process is only minor compared to a $C_3H_3 + C_5H_5$ reaction in those experiments. In the propargyl bromide pyrolysis a small peak is observed at *m/e* 115 as in the Cp and MeCp pyrolyses. It seems plausible that propargyl radicals add to C_6H_5 and/or C_6H_4 to produce this signal. Again, the intensity observed is not great enough to completely explain the *m/e* 115 signal in the Cp and MeCp pyrolyses. This fact coupled with the observation that the *m/e* 115 peak seems to be associated with *m/e* 130 and 128 production leads to the conclusion that this peak may be, at least in part, a photoionization fragment of a higher order combination product, namely the C_5H_5 self-combination.

CONCLUSIONS

At temperatures ≥ 1100 K cyclopentadiene undergoes C-H bond fission resulting in H atom and *c*C_5H_5 RSR which then decomposes further to produce C_3H_3 RSR and C_2H_2 (acetylene). C_3H_3 RSR self-combinations produce C_6H_6 and *c*C_5H_5 self-

combinations produce $C_{10}H_8$ (naphthalene). Additions of both C_2H_2 and C_3H_3 to $c$$C_5H_5$ RSR are observed while neutral C_5H_6 additions to $c$$C_5H_5$ are not detected. The contribution of molecular eliminations from the neutral cyclopentadiene potential energy surface was found to be negligible. Methylcyclopentadiene undergoes C-CH_3 bond fission with temperatures > 1000 K in addition to H atom loss for temperatures ≥ 1100 K. Isomerization/decomposition to form benzene is the primary process observed for methylcyclopentadiene thermolysis while the C-CH_3 bond cleavage results in $c$$C_5H_5$ RSR chemistry.

REFERENCES

[1] J. Hansen, M. Sato, R. Ruedy, A. Lacis, V. Oinas, Proc. Natl. Acad. Sci. U.S.A. 97 (2000) 9875.

[2] M. Z. Jacobson, Nature 409 (2001) 695.

[3] M. F. Denissenko, A. Pao, M. S. Tang, G. P. Pfeifer, Science 274 (1996) 9875.

[4] J. L. Durant,W. F. Busby, A. L. Lafleur, B. W. Penman, C. L. Crespi, Mutat. Res. 371 (1996) 123.

[5] V. Ramanathan, G. Carmichael, Nature Geosci. 1 (2008) 221.

[6] H. Richter, J. B. Howard, Phys. Chem. Chem. Phys. 4 (2002) 2038.

[7] J. A. Miller, C. F. Melius, Combust. Flame 91 (2002) 21.

[8] M. Frenklach, Phys. Chem. Chem. Phys. 4 (2002) 2028.

[9] P. R. Westmoreland, A. M. Dean, J. B. Howard, J. P. Longwell, J. Phys. Chem. 93 (1989) 8171.

[10] J. A. Miller, C. F. Melius, Combust. Flame 91 (1992) 21.

[11] K. Kohse-Hoinghaus, B. Atakan, A. Lamprecht, G. G. Alatorre, M. Kamphus, T. Kasper, N. N. Liu, Phys. Chem. Chem. Phys. (2002) *4*.

[12] B. Atakan, A. Lamprecht, K. Kohse-Hoinghaus, Combust. Flame 133 (2003) 431.

[13] S. P. Walch, J. Phys. Chem. 103 (1995) 8544.

[14] N. Hansen, S. J. Klippenstein, C. A. Taatjes, J. A. Miller, J. Wang, T. A. Cool, B. Yang, L. Wei, C. Huang, J. Wang, F. Qi, M. E. Law, P. R. Westmoreland, J. Phys. Chem. A 110 (2006) 3670.

[15] M. Frenklach, D. W. Clary, W. C. Gardiner Jr., S. E. Stein, Proc. Combust. Inst. 20 (1985) 887.

[16] M. Frenklach, D. W. Clary, T. Yuan, W. C. Gardiner Jr., S. E. Stein, Combust. Sci. Technol. 50 (1986) 79.

[17] M. Frenklach, J. Warnatz, Combust. Sci. Technol. 51 (1987) 265.

[18] M. Frenklach, T. Yuan, M. K. Ramachandra, Energy Fuels 2 (1988) 462.

[19] J. D. Bittner, J. B. Howard, Proc. Combust. Inst. 18 (1981) 1105.

[20] U. Alkemade, K. H. Z. Homann, Phys. Chem. 161 (1989) 19.

[21] C. L. Morter, S. K. Farhat, J. D. Adamson, G. P. Glass, R. F. Curl, J. Phys. Chem. 98 (1994) 7092.

[22] D. B. Atkinson, J. W. Hudgens, J. Phys. Chem. A 103 (1999) 4242.

[23] A. Fahr, A. Nayak, Int. J. Chem. Kinet. 32 (2000) 118.

[24] S. Scherer, T. Just, P. Frank, Proc. Combust. Inst. 28 (2000) 1511.

[25] J. A. Miller, S. J. Klippenstein, J. Phys. Chem. A 105 (2001) 7254.

[26] J. D. DeSain, C. A. Taatjes, J. Phys. Chem. A 107 (2001) 4843.

[27] J. A. Miller, S. J. Klippenstein, J. Phys. Chem. A 107 (2003) 7783.

[28] E. V. Shafir, I. R. Slagle, V. A. Knyazev, J. Phys. Chem. A 107 (2003) 8893.

[29] W. Y. Tang, R. S. Tranter, K. Brezinsky, Phys. Chem. A 109 (2005) 6056.

[30] E. B. Jochnowitz, X. Zhang, M. R. Nimlos, M. E. Varner, J. F. Stanton, G. B. Ellison, J. Phys. Chem. A 109 (2004) 3812.

[31] N. Hansen, T. Kasper, S. J. Klippenstein, P. R. Westmoreland, M. E. Law, C. A. Taatjes, K. Kohse-Hoinghaus, J. Wang, T. A. Cool, J. Phys. Chem. A 2007.

[32] R. P. Lindstedt, K. A. Rizos, Proc. Combust. Inst. 29 (2002) 2291.

[33] N. M. Marinov, W. J. Pitz, C. K. Westbrook, A. E. Lutz, A. M. Vincitore, M., S. S. Proc. Combust. Inst. 27 (1998) 605.

[34] N. M. Marinov, W. J. Pitz, C. K. Westbrook, A. M. Vincitore, M. J. Castaldi, S. M. Senkan, C. F. Melius, Combust. Flame 114 (1998) 192.

[35] C. F. Melius, M. E. Colvin, N. M. Marinov, W. J. Pitz, S. M. Senkan, Proc. Combust. Inst. 26 (1996) 685.

[36] L. V. Moskaleva, A. M. Mebel, M. C. Lin, Proc. Combust. Inst. 26 (1996) 521.

[37] C. J. Pope, J. A. Miller, Proc. Combust. Inst. 28 (2000) 1519.

[38] V. D. Knyazev, I. R. Slagle, J. Phys. Chem. A 106 (2002) 5613.

[39] L. V. Moskaleva, M. C. Lin, Comput. Chem. 21 (2000) 415.

[40] A. Burcat, M. Dvinyaninov, Int. J. Chem. Kinet. 29 (1997) 505.

[41] K. Roy, C. Horn, P. Frank, V. G. Slutsky, T. Just, Twenty-Seventh Symposium (International) on Combustion/The Combustion Institute (1998) 329.

[42] R. D. Kern, Q. Zhang, J. Yao, B. S. Jursic, R. S. Tranter, M. A. Greybill, J. H. Kiefer, Twenty-Seventh Symposium (International) on Combustion/The Combustion Institute (1998) 143.

[43] E. Ikeda, R. S. Tranter, J. H. Kiefer, R. D. Kern, H. J. Singh, Q. Zhang, Proceedings of the Combustion Insititute 28 (2000) 1725.

[44] A. Lifshitz, C. Tamburu, A. Suslensky, F. Dubnikova, Proc. Combust. Inst. 30 (2005) 1039.

[45] L. V. Moskaleva, A. M. Mebel, M. C. Lin, Twenty-Sixth Symposium (International) on Combustion/The Combustion Institute (1996) 521.

[46] C. F. Melius, M. E. Colvin, N. M. Marinov, W. J. Pitz, S. M. Senkan, Twenty-Sixth Symposium (International) on Combustion/The Combustion Institute (1996) 685.

[47] V. V. Kislov, A. M. Mebel, J. Phys. Chem. A 111 (2007) 9532.

[48] D. Wang, A. Violi, D. H. Kim, J. A. Mullholland, *J. Phys. Chem. A.*

[49] V. V. Kislov, A. M. Mebel, J. Phys. Chem. A 111 (2007) 3922.

[50] S. Fascella, C. Cavallotti, R. Rota, S. Carra, S. J. Phys. Chem. A 109 (2005) 7546.

[51] C. Cavallotti, S. Mancarrela, R. Rota, S. Carra, J. Phys. Chem. A 111 (2007) 3959.

[52] G. B. Bacskay, J. C. Mackie, Phys. Chem. Chem. Phys. 12 (2001) 2467.

[53] F. Dubnikova, A. Lifshitz, J. Phys. Chem. A 106 (2002) 8173.

[54] W. S. McGivern, J. A. Manion, W. Tsang, J. Phys. Chem. A 110 (2006) 12822.

[55] S. D. Chambreau, J. M. Lemieux, L. Wang, J. Zhang, J. Phys. Chem. A 109 (2005) 2190.

[56] K H. Weber, J. Zhang, D. Borchardt, T. H. Morton, Int. J. Mass Spectrom. 249-250 (2006) 303.

[57] K. H. Weber, J. Zhang, J. Phys. Chem. A 111 (2007) 11487.

[58] D. W. Kohn, H. Clauberg, P. Chen, Rev. Sci. Instrum. 63 (2007) 4003.

[59] A. V. Friderichsen, J. G. Radziszewski, M. R. Nimios, P. R. Winter, D. C. Dayton, D. E. David, G. B. Ellison, J. Am. Chem. Soc. 123 (2001) 1977.

[60] R. J. Ellis, H. M. Frey, J. Chem. Soc. A (1966) 553.

[61] S. W. Benson, R. Shaw, J. Amer. Chem. Soc. 89 (1967) 5351.

[62] J. E. Baldwin, Tetrahedron Letters (1966) 2953.

CHAPTER 8

METHYCYCLOHEXANE AND METHYLCYCLOHEXENE PYROLYSIS

INTRODUCTION

Naphthenes (cycloalkanes) represent an important class of fuel hydrocarbons whose pyrolysis and oxidation has received scant attention until recently. Naphthenes are found in many fuels (e.g. gasoline) and jet fuels such as Jet-A are composed of up to 20% cycloalkane[1] and the JP-8 family of fuels are mostly comprised of naphthenes.[2] Fuels such as methylcyclohexane (MCH) are known to cool supersonic vehicles from the intense heat they generate during operation and in the presence of a platinum catalyst can be endothermically dehydrogenated to toluene and hydrogen[3] approximately doubling the total heat-absorbing ability of MCH.[4] Needles to say, characterization of the oxidation and decomposition of naphthenes is vital to the combustion community. The pyrolysis of cyclohexane (CH), one of the simplest naphthenes, was first studied by Wing Tsang[5] with a shock tube coupled to GC/FID. He concluded that the only reaction of note around 1100 K was isomerization to 1-hexene *via* a diradical intermediate.

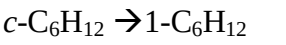

c-C_6H_{12} → 1-C_6H_{12} (1)

Subsequently, cyclohexane decomposition was investigated by Aribike et al.[6,7] in an annular flow reactor over 1000-1300 K and the following reactions were introduced:

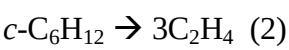

c-C_6H_{12} → $3C_2H_4$ (2)

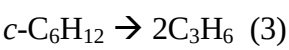

c-C_6H_{12} → $2C_3H_6$ (3)

c-C_6H_{12} → $C_4H_6 + C_2H_4 + H_2$ (4)

Brown et al.[8] studied the cyclohexane pyrolysis using very low pressure pyrolysis (VLPP) over the temperature range of 900-1200 K. The results supported Tsang's proposed diradical mechanism although the measured rate constant was not in agreement. The cyclohexane pyrolysis was next studied by Billaud et al.[9] at approximately 1100 K with a plug flow reactor. They observed copious amounts of butadiene and ethene with little cyclohexene. Voisin et al.[10] employed a jet stirred reactor (JSR) over 750 – 1100 K to study the oxidation of cyclohexane and introduced a C-H bond fission channel.

c-C_6H_{12} → *c*-C_6H_{11} + H (5)

El-Bakali et al.[11] also studied cyclohexane oxidation in a JSR over the temperature range of 750-1200 K using varying equivalence ratios. They suggested that the ethylene production channel, equation 2, proceeds through a diradical to molecular pathway

c-C_6H_{12} → $C_2H_4 + C_4H_8$ (2a)

C_4H_8 → $2C_2H_4$ (2b)

They also present a detailed kinetic mechanism where ring opening of the cyclohexyl radical is dominated by dehydrogenation. The pyrolysis of cyclohexane and oxidation of both cyclohexane and methylcyclohexane was studied by Granata and co-workers.[12] Under pure pyrolysis conditions they find the product distribution of ethylene, pentadiene, propene, butadiene, and cyclohexene to be invariant with respect to temperature. The kinetic model presented pays particular attention to the competition

between internal isomerization and β-decompositions. McEnally and Pfefferle[13] investigated the pyrolysis of cyclohexane in a coflowing, nonmixed CH4/air flame over 400 – 2000 K. Their interpretation of results suggested that pathways 1, 2, and 5 were in operation, that is isomerization to 1-hexene, ethylene production and cyclohexyl radical formation respectively. Braun-Unkhoff et al.[14] examined cyclohexane pyrolysis with H-atom atomic resonance absorption spectroscopy over 1200 – 1900 K with the conclusion that pathways 2 and 5 were the dissociation channels. Theoretical work by Sirjean et al. indicates that the ring-opening of cyclohexane does in fact proceed through a diradical intermediate which internally abstracts a H atom to afford the isomerization product, 1-hexene. Other diradical decompositions were considered including the decomposition of the diradical to ethene and C_4H_8 diradical (equation 2a) and were found to make a negligible contribution to the overall decomposition. Most recently, Kiefer and co-workers[15] studied the cyclohexane and 1-hexene pyrolyses using a combination of shock tube and RRKM theory. They find that cyclohexane decomposes simply to 1-hexene which subsequently produces propyl (C_3H_7) and allyl (C_3H_5) radicals. Using these two reaction pathways they are able to satisfactorily model the experimental data. The resulting k values agreed well with the values produced by Brown et al.[8] and Sirjean et al.[16] but not well with the value reported by Tsang.[5] They speculate that the large quantities of C_2H_4 product observed are produced by the primary dissociation pathway for propyl radicals producing ethene and methyl (CH_3) radicals. The production of H-atoms observed by Braun-Unkjoff[14] is conjectured to be from H atom loss from both allyl (C_3H_5) and propyl (C_3H_7) radicals. The (secondary) pyrolysis of 1-hexene was studied

previously by both Tsang[5] and King[17] who found the dominant pathway to be the dissociation into allyl (C_3H_5) and propyl (C_3H_7) radicals with activation energies of 70.8 and 70.7 kcal/mol respectively. A retro-ene pathway involving a 1,5 H-atom shift was identified as contributing 10 – 20% to the decomposition with activation energies of 57.7 and 57.4 kcal/mol. In the more recent work by Kiefer et al.[15] the retro-ene pathway is not observable and is not modeled as are the ethene and H atom concentration profiles. Additionally, the production of 1,3-butadiene and cyclohexene are not considered.

Methylcyclohexane (MCH) is often used as a model compound for naphthene chemistry. The pyrolysis of MCH was first accomplished by King and Brown[18] using very low pressure pyrolysis (VLPP) over the temperature range of 860-1220 K. Unlike CH which can only undergo one type of ring opening, MCH can ring open adjacent to the methyl group (A = 10^16.4 s-1, Ea = 345 kJ/mol) or non-adjacent (A = 10^16.7 s-1, Ea = 360 kJ/mol). In addition, MCH can undergo methyl cleavage to produce cyclohexyl and methyl radicals (A = 10^16.1, Ea = 368 kJ/mol). Pyrolysis and oxidation of MCH and blend of MCH with toluene as observed by turbulent flow reactor over the temperatures 1050 – 1200 K was reported by Zeppieri and co-workers.[19] Major products for both oxidation and pyrolysis included methane, ethylene, propene, 1,3-butadiene, and isoprene. Aromatics (benzene and toluene) were among the minor products as well as ethane, cyclopentadiene, cyclohexene, isobutene, allene, acetylene, and propyne. Granata et al.[12] modeled the kinetics of the pyrolysis and

oxidation of naphthenes, expanding the combustion properties of CH and MCH. This expansion was accomplished by adding the CH and MCH propagation reactions to an existing mechanism already validated for the pyrolysis and combustion of such hydrocarbon fuels as *n*-heptane and isooctane.[20-22] Recently, Orme et al.[23] studied MCH pyrolysis and oxidation using a shock tube or flow reactor over 1200 – 2100 K and provide a detailed chemical kinetic mechanism to simulate experiment, with good agreement. They find that at a temperature of 1250 K ~ 10% of MCH decomposes to cyclohexyl and methyl radicals. The cyclohexyl radical is proposed to ring open to the hex-1-en-6-yl radical with exclusion to other processes. The hex-1-en-6-yl radical then decomposes to give 90% but-1-en-4-yl radical plus ethane. From there, the but-1-en-4-yl radical can produce 1,3-butadiene (~78%) or decompose to ethene and ethenyl radical (21%).

EXPERIMENTAL

Methylcyclohexane (99%) was obtained from Aldrich and methylcyclohexene (99%) was from Acros Organics. The compounds studied were used without further purification and diluted to 1-4% in argon or helium by bubbling the noble carrier gas through the liquid at ice/water bath temperatures.

RESULTS

As in the pyrolysis of cyclohexane, the isomerization products of methylcyclohexane are expected to undergo bond fission where RSR will form. In the case of 1-heptene the products would be allyl radical and n-butyl radical. For 2-heptene the products expected are 2-buteneyl and *n*-propyl radical. Isobutenyl and *n*-propyl radicals are expected from the pyrolysis of 2-methyl-1-heptene and allyl ant *t*-butyl radical from 5-methyl-heptene. 3-methyl-heptene could decompose to methyl and hexen-3-yl radicals or buane-4yl and

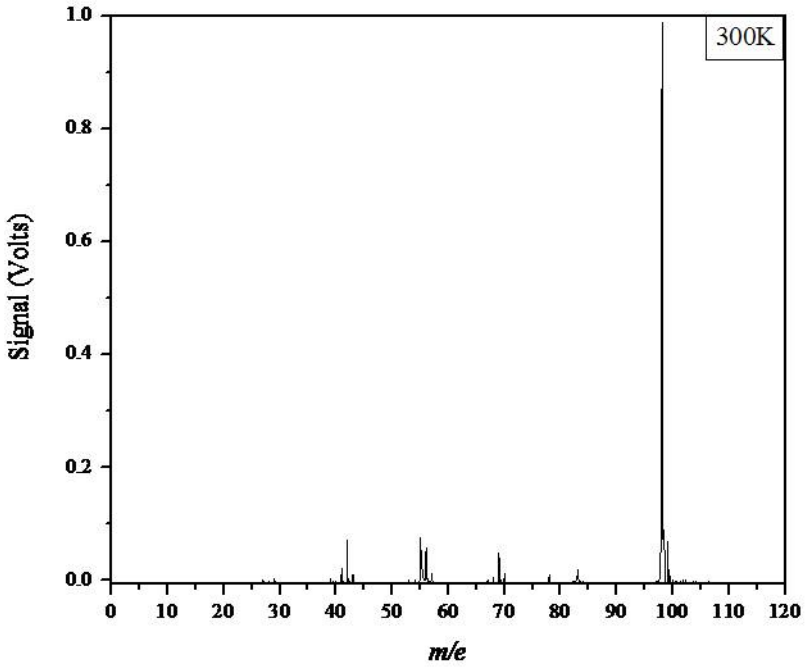

Figure 8.1 (a) Room temperature trace for MCH

n-propyl radicals. Figure 8.1 (a),(b),(c), and (d) present mass spectra for the pyrolysis of methylcyclohexane collected with nozzle temperatures of 300, 1090, 1155, and 1220 K

respectively. In the spectral trace where the nozzle is not heated (Figure 8.1 (a)) a large $M^{+\bullet}$ peak at *m/e* 98 is observed (IE = 9.85 eV)[27]. Small peaks are observed at *m/e* 42, 55, 56, and 69 as photoionization fragments. The reported M-CH_3^+photoionization fragment (AE = 10.95 eV)[28] is barely visible in this trace. In the trace where the nozzle is heated to a temperature of 1090 K, Figure 8.1 (b), the M-CH_3 photoionionization fragment at *m/e* 83 is now the base peak with the $M^{+\bullet}$ peak being ~75% of the fragment intensity. A new small peak is detected at *m/e* 15 corresponding to methyl radical which would be produced thermally as opposed to an ionization fragment. The creation of methyl radical necessitates the concomitant production of cyclohexyl radical also at *m/e* 83. The peaks at *m/e* 42, 55 and 69 increase in intensity while peaks at *m/e* 41, 56, 68, 70 and 82 show

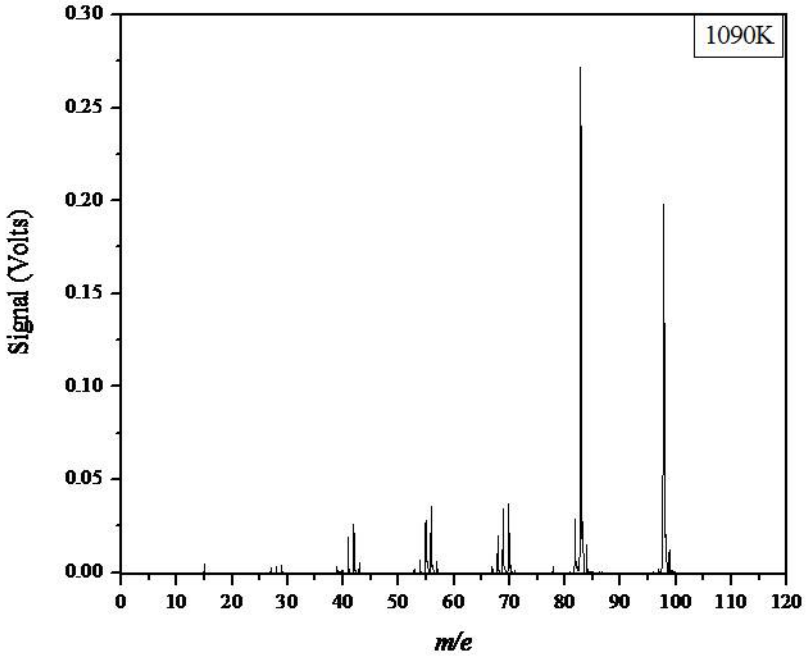

Figure 8.1 (b) Pyrolysis of MCH spectral trace with a nozzle temperature of 1090 K.

dramatic increases in intensity. Some activity around *m/e* 28 is barely detectable in this trace. At a nozzle temperature of 1155 K (Figure 8.1 (c)) the peak at *m/e* 83 is again the base peak with ~70% of the $M^{+\bullet}$ parent peak. The methyl radical peak at *m/e* 15 has increased to an intensity comparable to the peaks found below *m/e* 83. The peak at *m/e* 28, ethene, is now clearly visible. Peaks in the region of *m/e* 39-43 have all intensified retaining the basic relative intensities within that grouping. In the region of *m/e* 53-57 have also increased in intensity, however, the relative intensity of *m/e* 54, C_4H_6, has become the most significant peak within the grouping. The *m/e* 67-70 region has kept essentially the same relative intensities within the grouping, being more intense relative

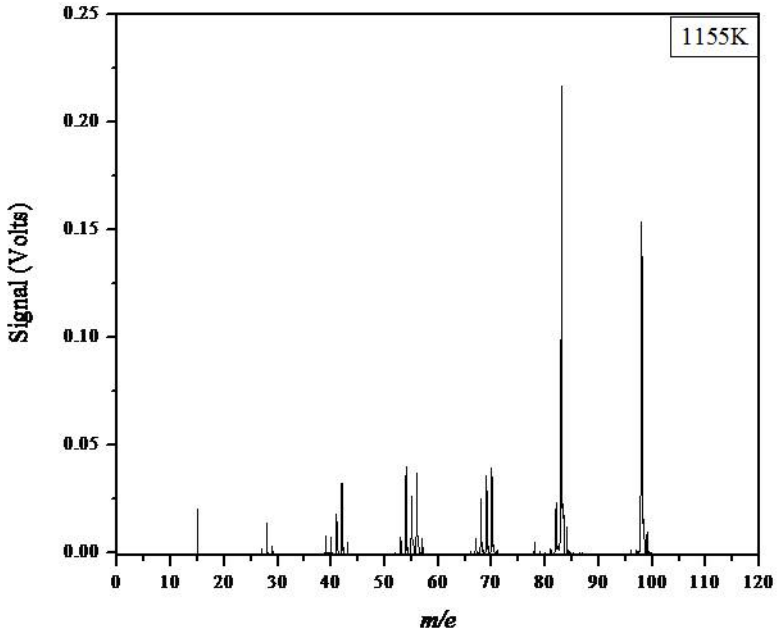

Figure 8.1 (c) Pyrolysis of MCH spectral trace with a nozzle temperature of 1155 K.

to the $M^{+\bullet}$ parent. A new peak is observed at *m/e* 78 being barely detectable. The *m/e* 82 peak is again found to be ~10% of the base peak at *m/e* 83. In the 1220 K spectral trace presented in Figure 8.1 (d) the relative intensities of the observed spectral peaks are markedly different than the general pattern observed in the preceding spectra. The C_4H_6 peak at *m/e* 54 is now the dominant base peak with the parent $M^{+\bullet}$ peak at *m/e* 98 giving rise to a signal with ~27% of the base peak. The next most intense peak is the *m/e* 15 methyl radical peak being ~63% the *m/e* 54 base peak intensity. The peaks at *m/e* 40 and 28 are now approximately equal in intensity, a little less than half the base peak intensity. The peaks at *m/e* 39 and 42 are now prominent with the *m/e* 41 signal increasing slightly. The peaks from *m/e* 55-57 exhibit attenuation of signal in this trace with the signal at *m/e* 57 being barely detectable. A new small peak is just discernible at *m/e* 51 and the *m/e* 52

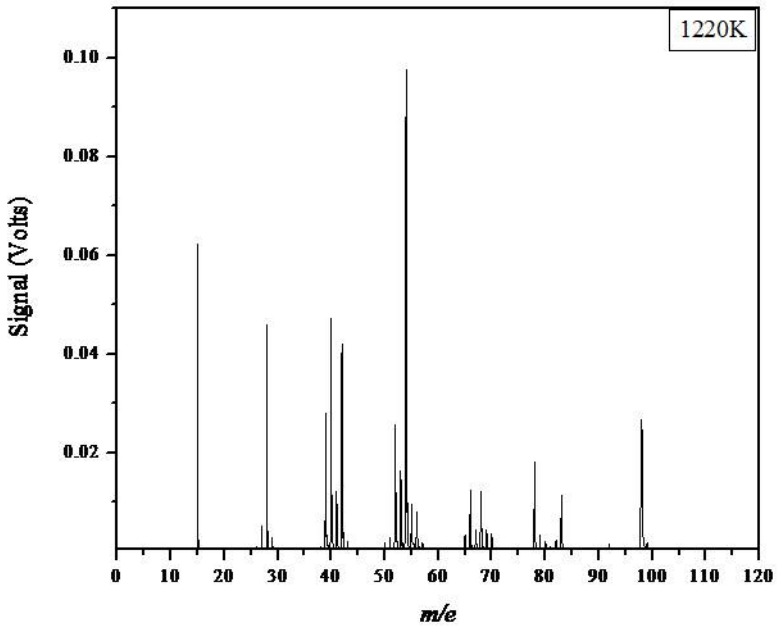

Figure 8.1 (d) Pyrolysis of MCH spectral trace with a nozzle temperature of 1220 K.

and 53 peaks have grown significantly. In the *m/e* 65-70 region of the spectra the peaks at *m/e* 69 and 70 have diminished significantly while the peak at *m/e* 66 has grown to approximately the same intensity as *m/e* 68, ~10% the base peak intensity. The *m/e* 78 signal has increased tremendously, rising to ~20% intensity relative to base peak *m/e* 54. Perhaps the most dramatic change in this higher temperature spectra, besides the increase in *m/e* 54 intensity, is the reduction of *m/e* 83 signal, which is at this point ~10% the base peak and 40% of the $M^{+\bullet}$ signal. The parent $^{M+\bullet}$ peak is observed to be diminished to 27% relative to the base peak, to 30mV compared to the original 1V signal.

Figure 8.2 (a)-(d) present mass spectra from the pyrolysis of methylcyclohexane from 1290 K to 1450 K. In the 1290 K trace presented in Figure 8.2 (a) the spectral features remain essentially unchanged from the 1220 K spectra displayed in Figure 8.2 (d). The 1355 K trace (Figure 8.2 (b), however, is significantly different. The *m/e* 54 peak remains the base as the $M^{+\bullet}$ parent peak at *m/e* 98 decreases to 10% relative intensity. The signals at *m/e* 28 and 40 rise to similar intensities as exhibited my the *m/e* 15 CH^3 radical signal, approaching 80% the base peak intensity. The signal at *m/e* 52 has

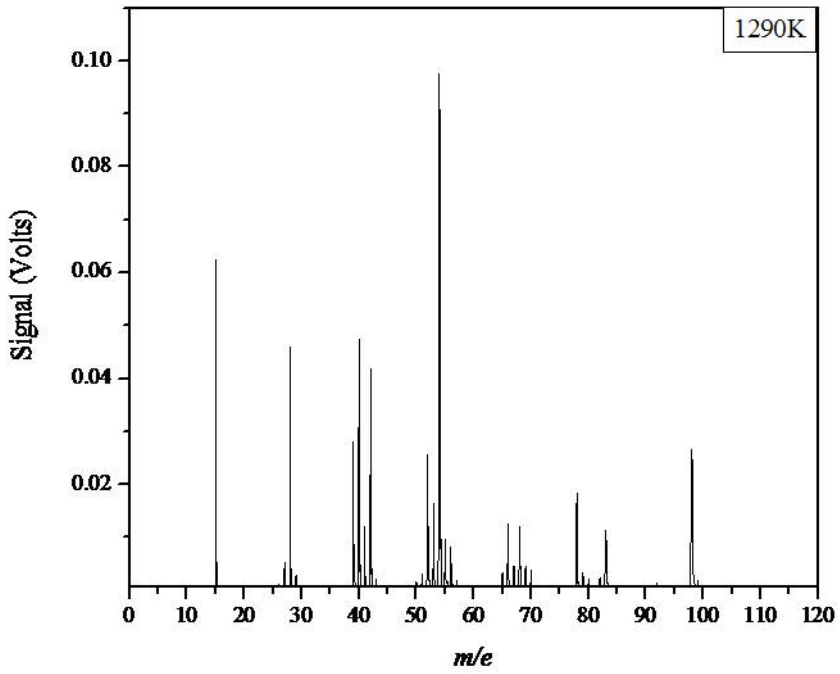

Figure 8.2 (a) Pyrolysis of MCH spectral trace with a nozzle temperature of 1290 K.

grown to about 2.5 times the intensity it possessed in the 1290 K trace (Figure 8.2 (a)). In the *m/e* 39-42 region of the spectra the *m/e* 39 peak, C_3H_3, has risen in intensity to an intensity comparable to the *m/e* 42 peak, about half the intensity relative to base peak. In the *m/e* 50-56 region, new *m/e* 50 and 51 peaks are observed accompanying the *m/e* 52

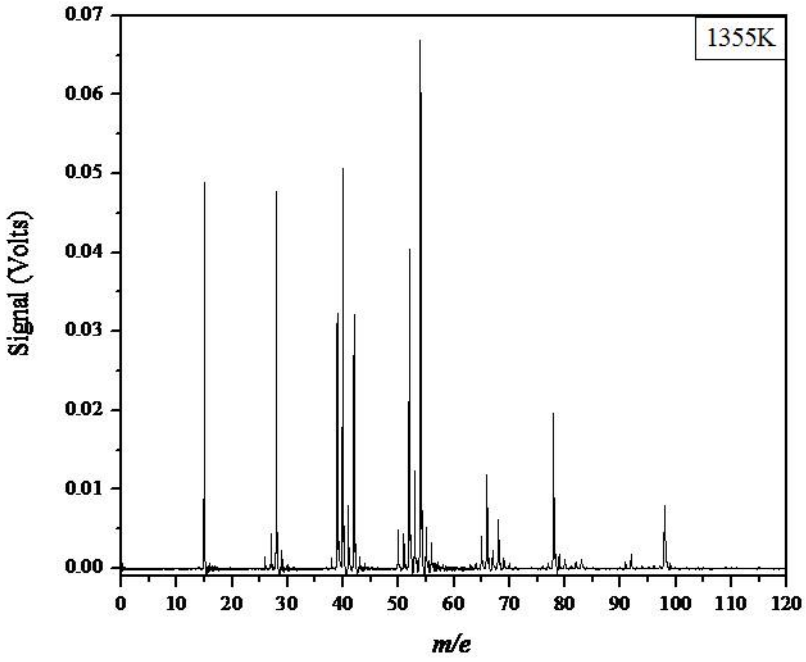

Figure 8.2 (b) Pyrolysis of MCH spectral trace with a nozzle temperature of 1355 K.

growth. The *m/e* 65-70 region is altered as evidenced by the increase in *m/e* 66 intensity while the *m/e* 69 and 70 are hardly discernible. The *m/e* 78 peak, C_6H_6, exhibits marked growth while at the same time small new peaks at *m/e* 91 and 92 are noted. Figure 8.2 (c) presents the 1425 K pyrolytic trace for methylcyclohexane. In this trace the parent peak $M^{+\bullet}$ at *m/e* 98 is reduced to 7% the *m/e* 54 peak, which continues to be the base peak. The peaks at *m/e* 15, 28, 40, and 52 have all risen to nearly the intensity level of the base

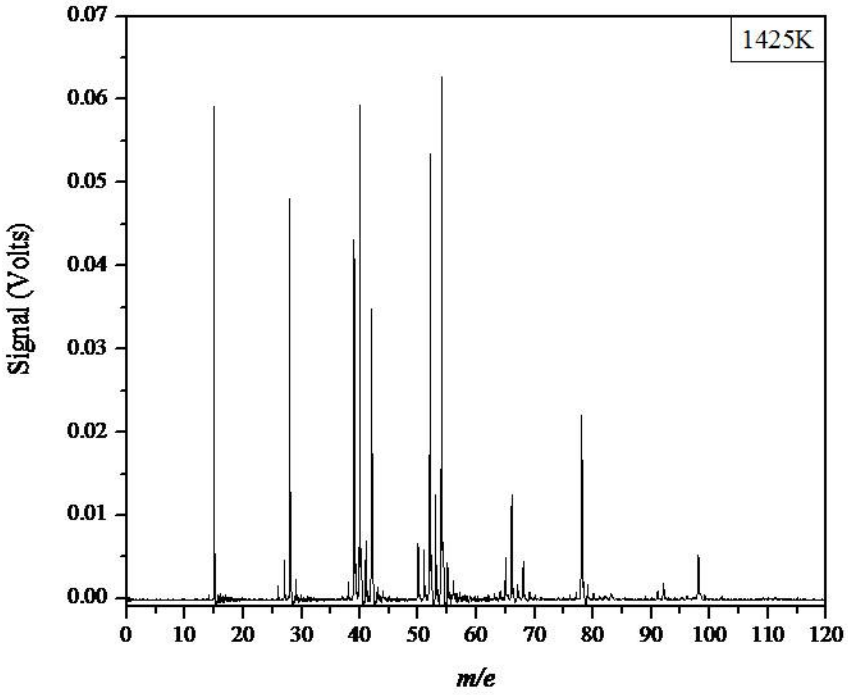

Figure 8.2 (c) Pyrolysis of MCH spectral trace with a nozzle temperature of 1425 K.

peak while the *m/e* 39 and 42 signals are slightly less intense. Peaks at *m/e* 41, 50, 51, and 53 are still noted. In the *m/e* 65-70 region of the spectra *m/e* 66 is still prominent with small peaks at *m/e* 65 and 68 being detected. Although the peaks at *m/e* 91 and 92 remain essentially unchanged the peak at *m/e* 78 continues modest growth. In the hottest trace presented here with a nozzle temperature of 1450 K, Figure 8.2 (d) the spectral features are relatively unchanged. Noticeable deviations are the increases in *m/e* 40 and *m/e* 52 intensities.

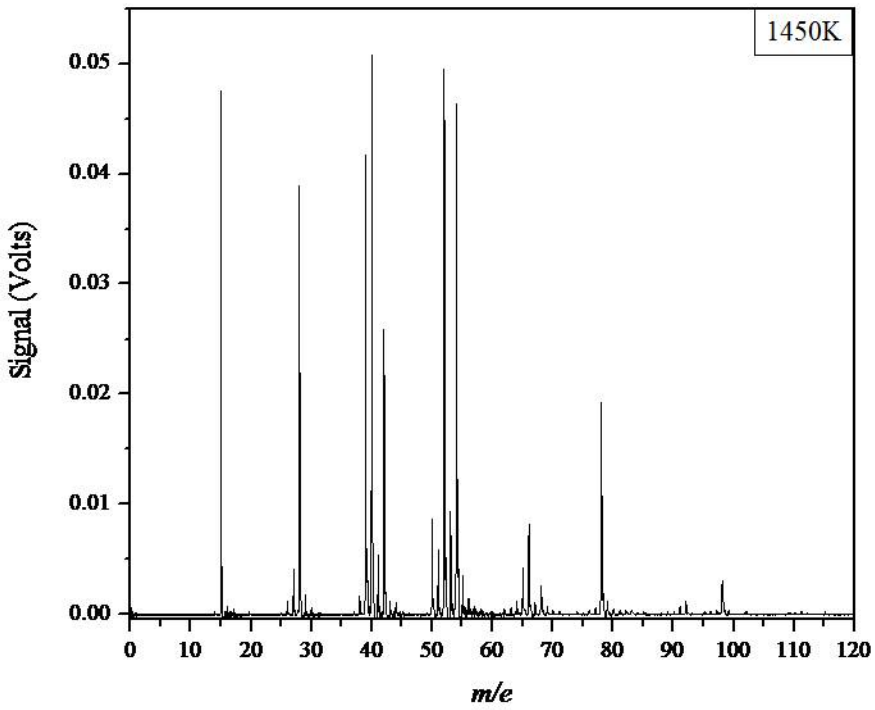

Figure 8.2 (d) Pyrolysis of MCH spectral trace with a nozzle temperature of 1450 K.

Figure 8.3 (a) presents a stack plot of mass spectra for the pyrolysis of 1-methylcyclohexene with the lower range nozzle temperatures of 295, 920, 1020, 1085, and 1150 K. In the spectral trace with an unheated nozzle, 295 K a large molecular ion, $M^{+\bullet}$, peak is observed an *m/e* 96 (IE = 8.67 eV) refx. Small peaks at *m/e* 40, 67, 68 and 81 are observed. The peaks at *m/e* 67,68, and 81 should correspond to the reported photoionization fragments with AEs of 10.47, 10.56, and 10.27 eV respectively. The *m/e* 40 peak is not a reported photofragment and is likely a memory effect from C_3H_4

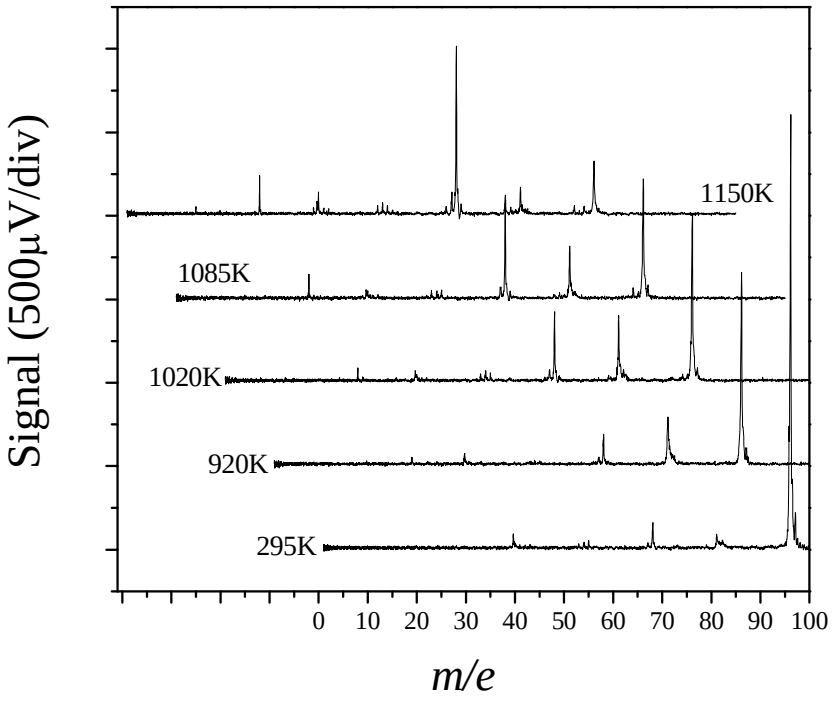

Figure 8.3 (a) Stackplot of mass spectra for the pyrolysis of methylyclohexene.

production (see below). As the heater temperature is increased to 920 K the parent M+• peak at *m/e* 96 experiences a significant drop in intensity due to the decrease in number density. The *m/e* 68 photoionization peak retains the same intensity, thus growing in intensity relative to the molecular ion. The M-CH_3^+ photoionization fragment at *m/e* 81 is observed to be almost four times the intensity found for the unheated nozzle trace being in this trace 25% of the parent peak intensity. This peak at *m/e* 81 is entirely due to photoionization fragmentation as the thermal loss of methyl radical would produce a signal at *m/e* 15 and no such signal is observed. As the nozzle temperature of 1020 K is

reached the *m/e* 81 signal remains basically constant as does the parent *m/e* 96 peak. The peak at *m/e* 68 is found to dramatically increase in intensity matching the signal intensity for *m/e* 81. Accompanying this augmentation of *m/e* 68 intensity is a clear *m/e* 28 peak corresponding to ethene, C_2H_4. At a nozzle temperature of 1085 K the parent $M^{+\bullet}$ peak diminishes along with the *m/e* 81 M-CH_3^+ fragment signal. The peaks at *m/e* 28 and 68 continue to become more intense and a small peak at *m/e* 94 is detectable. In the 1150 K trace the $M^{+\bullet}$ peak at *m/e* 96 is less than 15% the unheated nozzle spectra intensity. The M-CH_3^+ fragment at *m/e* 81 continues to attenuate while the peaks at *m/e* 28, 40, and 68 continue to grow.small peaks are discernible at *m/e* 92 and 94.

Figure 8.3 (b) presents a stack plot of mass spectra for the higher temperature region in the pyrolysis of 1-methylcyclohexene with nozzle temperatures of 1200, 1290, 1340, 1375, and 1420 K. In the 1200 K trace the molecular ion, $M^{+\bullet}$, at *m/e* 96 is found to be ~15% of the *m/e* 68 signal, the base peak. Small peaks are again detected at *m/e* 94 and 92 with a slight augmentation of the *m/e* 92 signal. A small peak at *m/e* 81 is observed with two smaller peaks at *m/e* 80 and 79. The *m/e* 78, C_6H_6, peak has grown to ~10% the base peak intensity. A peak at *m/e* 15, CH_3 radical, is clearly observed while the *m/e* 28, C_2H_4, peak is now larger than the parent *m/e* 96 peak, being ~20% relative to the base *m/e* 68 peak. A grouping of peaks is observed in the range of *m/e* 39-42 with the *m/e* 40 peak being dominant amongst the grouping. A series of peaks from *m/e* 52-54 is observed with similar intensities as the *m/e* 39-42 grouping. A small peak at *m/e* 66 and

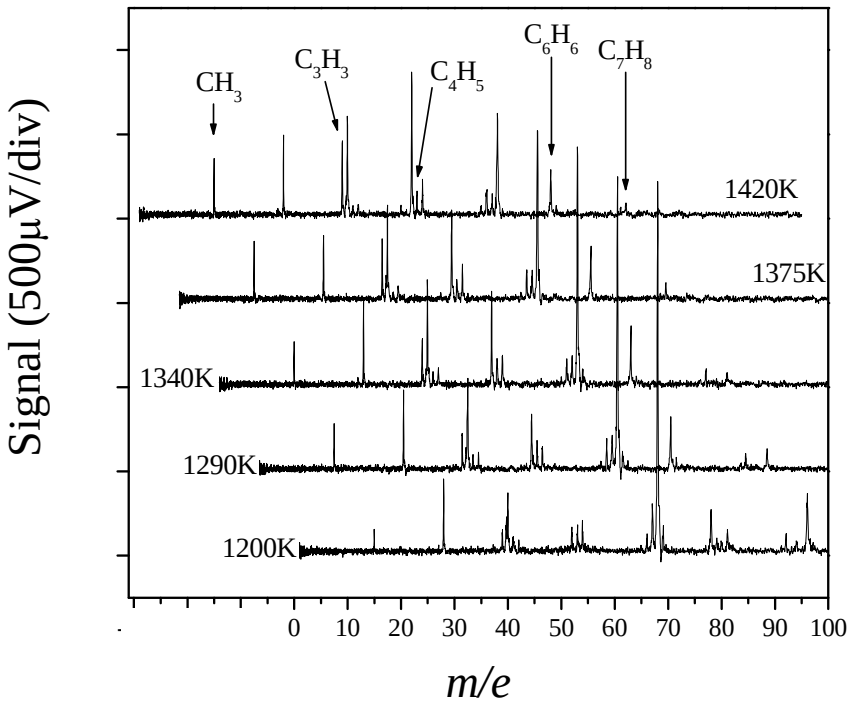

Figure 8.3 (b) Stack plot of mass spectra for the pyrolysis of methylcyclohexene.

modest signal at *m/e* 67 are also observed in this trace. As the nozzle is further heated to a temperature of 1290 K the peaks at *m/e* 92 and 96 are barely detectable and a *m/e* 94 peak is not observed. The *m/e* 15 signal is found to increase in intensity while the *m/e* 28, C_2H_4, peak remains fairly constant. The *m/e* 39 and 40 peaks are observed to increase in intensity as do *m/e* 52, 66, and 78. The *m/e* 80 and 81 peaks are also no longer discernible. The mass spectra obtained with a nozzle temperature of 1340 K is nearly identical to the 1290 K trace with the expection of the increase in relative intensity

observed for both *m/e* 39 and *m/e* 52. As the heater reaches a temperature of 1375 K the parent peak at *m/e* 96 is no longer visible. The intensity of the CH_3 peak at *m/e* 15 has increased to nearly the intensity of the *m/e* 28 peak continues to grow, in this trace now being ~75% of the *m/e* 40 signal. The remaining peaks remain essentially unchanged. In the highest temperature trace presented, 1420 K, the *m/e* 28 and *m/e* 52 peak continue augmentation.

DISCUSSION

The pyrolysis of MCH initially produces the various isomeric heptenes and methylhexenes. These compounds rapidly decompose to the corresponding RSRs and alkyl radicals. The RSRs are relatively stable, however they can undergo H atom reactions or decomposition to form stable products while the alkyl radicals rapidly decompose.

All of these features are observed as expected from previous work. Additional activity in the region of *m/e* 70 may be the detection of a direct decomposition without isomerization which was previously speculated about but was not required to model cyclohexane decomposition.

REFERENCES

[1] A. Violi, S. Yan, E. G. Eddings, A. F. Sarofim, S. Granata, T. Faravelli, E. Ranzi, Combust. Sci. Technol. 174 (2002) 399.

[2] J. Yu, S. Eser, Ind. Eng. Chem. Res. 34 (1995) 404.

[3] P. H. Taylor, W. A. Rubey, Energy Fuels 2 (1988) 723.

[4] L. E. Faith, G. H. Ackerman, H. T. Henderson, A. W. Ritchie, L. B. Ryland, Hydrocarbon Fuels for Advanced Systems - Technical Report No. AFAPL-TR-70-71, PART III; Shell Development Company: Ohio, 1972.

[5] W. Tsang, Int. J. Chem. Kinet. 10 (1978) 1119.

[6] D. S. Aribike, A. A. Susu, A. F. Ogunye, Thermochim. Acta 51 (1981) 113.

[7] D. S. Aribike, A. A. Susu, A. F. Ogunye, Thermochim. Acta 47 (1981) 1.

[8] T. C. Brown, K. D. King, T. T. Nguyen, J. Phys. Chem. 90 (1986) 419.

[9] F. Billaud, P. Chaverot, M. Berthelin, E. Freund, Ind. Eng. Chem. Res. 27 (1988) 759.

[10] D. Voisin, A. Marchal, M. Reuillon, J. C. Boettner, M. Cathonnet, Combust. Sci. Technol. 138 (1998) 137.

[11] A. El-Bakali, M. Braun-Unkhoff, P. Dagaut, P. Frank, M. Cathonnet, Proc. Combust. Inst. 28 (2000) 1631.

[12] S. Granata, T. Faravelli, E. Ranzi, Combust. Flame 132 (2003) 533.

[13] C. S. McEnally, L. D. Pfefferle, Combust. Flame 136 (2004) 155.

[14] M. Braun-Unkhoff, C. Naumann, P. Frank, Abstr. Pap.-Am. Chem. Soc. 227 (2004) U1096.

[15] J. H. Kiefer, K. S. Gupte, L. B. Harding, S. J. Klippenstein, J. Phys. Chem. A 113 (2009) 13570.

[16] B. Sirjean, P. A. Glaude, M. F. Ruiz-Lopez, R. Fournet, J. Phys. Chem. A 110 (2006) 12693.

[17] K. D. King, Int. J. Chem. Kinet.11 (1979) 1071.

[18] T. C. Brown, K. D. King, Int. J. Chem. Kinet. 21 (1989) 251.

[19] S. Zeppieri, K. Brezinsky, I. Glassman, Combust. Flame 108 (1997) 266.

[20] E. Ranzi, P. Gaffuri, T. Faravelli, P. Dagaut, Combust. Flame 103 (1995) 91.

[21] E. Ranzi, T. Faravelli, P. Gaffuri, A. Sogaro, A. D'Anna, A. Ciajolo, Combust. Flame 108 (1997) 24.

[22] E. Ranzi, M. Dente, A. Goldaniga, G. Bozzano, T. Faravelli, Prog. Energy Combust. Sci. 27 (2001) 99.

[23] J. P. Orme, H. J. Curran, J. M. Simmie, J. Phys. Chem. A 110 (2006) 114.

[24] K. H. Weber, J. Zhang, J. Phys. Chem. A 111 (2007) 11487.

[25] D. W. Kohn, H. Clauberg, P. Chen, Rev. Sci. Instrum. 63 (2007) 4003.

[26] A. V. Friderichsen, J. G. Radziszewski, M. R. Nimios, P. R. Winter, D. C. Dayton, D. E. David, G. B. Ellison, J. Am. Chem. Soc. 123 (2001) 1977.

[27] K. Watanabe, T. Nakayame, J. Mottl, J. Quant. Spectry. Radiative Transfer 2 (1962) 369.

[28] R. F. Pottie, A. G. Harrison, F. P. Lossing, J. Am. Chem. Soc. 83 (1961) 3204.

CHAPTER IX

CONCLUSIONS

The pyrolysis of ethyl and propyl iodides, *t*-butyl ethers TAME and MTMB, isoprene, cyclopentadiene and methylcyclopentadiene, and naphthalene methyl-cyclohexane have been conducted providing mechanistic insights into their decompositions. In the pyrolysis of ethyl anad propyl iodides the bond fission pathway is preferred over molecular elimination for the primary ethyl and propyl iodides. For the secondary isopropyl iodide the molecular elimination is preferred. The molecular eliminations here are shown to proceed exclusively via a 1,2 vicinal mechanism. In the pyrolysis of TAME the decomposition proceeds predominately by molecular elimination while at higher temperatures (>950 K) the various bond fissions compete. In contrast, the pyrolsis of MTMB proceeds almost exclusively via bond fission, contradictory to semi-ion transition state theory. The first compound pyrolyzed to study aromatization, isoprene, is shown to proceed mainly through two pathways. The molecular elimination of ethene to form allene is found to be particularly facile, quickly losing H atom (likely abstraction by CH_3 or the surface) to form propargyl radicals. Second, the isomerization to form dimethyallene has a slightly lower energy barrier and can then lose methyl radical to form methylpropargyl. Propargyl radicals are found to quickly combine to form C_6H_6. The pyrolysis of cyclopentadiene proceeds by an initiatory C-H bond fission with subsequent decomposition into C_2H_2 (acetylene) and C_3H_3 (propargyl). The C_5H_5 radicals combine to form $C_{10}H_8$ (naphthalene) or bond with propargyl to make styrene

then phenylacetylene. Propargyl radicals are found to rapidly combine in this system as well and the reaction of acetylene with propargyl radical may be detected. In contrast, methylcyclopentadiene decomposes primarily via isomerization and H loss to form C_6H_6. The loss of methyl from the parent compound is detected and the resulting C_5H_5 radical undergoes the same type of chemistry as in cyclopentadiene. Finally, the decomposisiton of methylcyclohexane proceeds primarily by isomerization to a heptene isomer or methylhexene which decomposes to a resonantly stabilized radical (RSR) and alkly radical pair. The RSRs are fairly stable and may abstact H atom or decompose to produce H atom and in one case decomposing to produce methyl radical. A direct β-decomposition pathway may be observed to be of importance. In the above experiments the "first ring" aromatizations are found to originate from RSR combinations although other pathways are known to exist.

CHAPTER X

FUTURE WORK

Diesels

Deisel fuels are complicated mixtures of compounds that represent an important source of combustion energy. To better regulate pollutant emissions a modeling of diesel fuel kinetics is advantageous. Due to their complexity, they are often modeled with surrogate fuels containing a small family of components. For a recent review of surrogate use see ref. 1. Typically, *n*-alkanes and aromatic hydrocarbons are employed for this purpose.[2] To this end the compounds *n*-heptane, 2-methylheptane, *n*-decane, and *n*-dodecane could be pyrolyzed in this system to shed further light on mechanistic details.

Fuels from Biomass

Increasing concerns over carbon neutral fuels and energy security have precipitated the development of fuels derived from biomass. For a recent review on biofuel chemistry see ref. 3. Lignin is present in all vascular plants and provides an important source of fuel. Being a complex polymer, it's chemistry is difficult to model. For this reason, model compounds that represent the important structural features of lignin are often used to develop the chemical understanding. The linkages in lignin is most commonly arylglycerol-β-aryl (β-O-4) most simply represented as phenethyl phenyl ether (PPE).[4] Pyrolysis of PPE and analogues could be studied in this system.

REFERENCES

[1] J. T. Farrell, N. P. Cernansky, F. L. Dryer, D. G. Friend, C. A. Hergart, C. K. Law, R. M. McDavid, C. J. Mueller, A. K. Patel, H. Pitsch, SAE paper 2007-01-0201 (2007).

[2] K. Mati, A. Ristori, S. Gail, G. Pengloan, P. Dagaut, Proc. Combust. Inst. 31 (2007) 2939.

[3] K. Kohse-Hoinghaus, P. Oβwald, T. A. Cool, T. Kasper, N. Hansen, F. Qi, C K. Westbrook, P. R. Westmoreland, Angew Chem Int. Ed. 49 (2010) 3572.

[4] A. Beste, A. C. Buchanan III, R. J. Harrison, J. Phys. Chem. A 112 (2008) 4982.

APPENDIX A

ALIGNMENT OF LASER

(1) Alignment with He:Ne Laser (needed only for initial coarse alignment)

Remove the UV focus lens (for VUV generation by tripling) in front of the Xe cell. Remove Xe cell along with the MgF_2 lens and the front flange of the main chamber; remove NO cell along with the back flange. Use a He:Ne laser beam to determine the optical path through the ionization region, i.e., the center axis of the chamber: pass the He/Ne beam through the center of the back window and the small front hole to define the He:Ne beam to the center. Reposition iris 1 and iris 2 (outside the chamber) to pass the He:Ne beam through the their centers; now iris 1 and iris 2 also define the light path, without opening the chamber later.

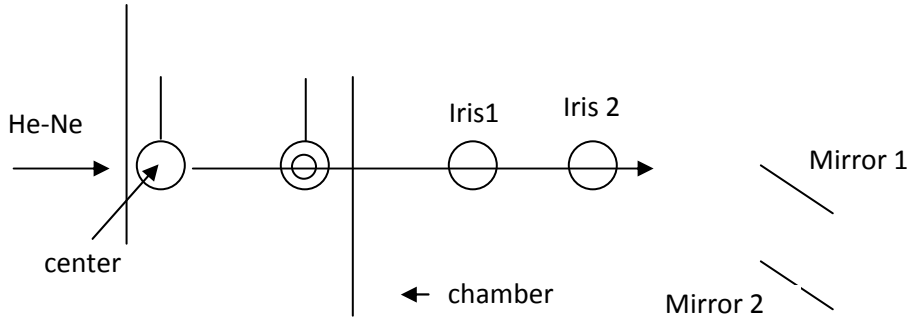

Figure A.1 Rough alignment with He/Ne laser.

(2) Alignment of the 355 nm Light

(a) Counter propagate 355 nm light from Nd:Yag with He-Ne beam or the light path. The most intense part of 355 nm should go through both iris1 and iris2.

- Adjust Mirror 2 to center the 355 nm beam on iris 2.
- Adjust Mirror 1 to center the 355 nm beam on iris 1.
- Repeat to meet both requirements. You may need open and close iris 1 and 2 during these procedures.
- Iris 1 and 2 serve as future reference; one can bring the 355 nm on the center light path using iris 1 and iris 2 and without opening the chamber.

(b) Reattach the front flange along with the Xe cell. Remount the UV focus lens; make sure the back reflection of the lens is closest to the beam axis (minimize change of light path). Inspect the 355 light on the exit of the chamber. Then reattach the back flange along with the NO cell; the shape of blue 355 nm spot should be approximately as an eclipsed sun and with maximum intensity.

A power meter is used to measure the laser energy output. The maximum (~330mW or 33 mJ/pulse) is found by adjusting the harmonic generating crystals and the half wave plate on the Nd:YAG laser.

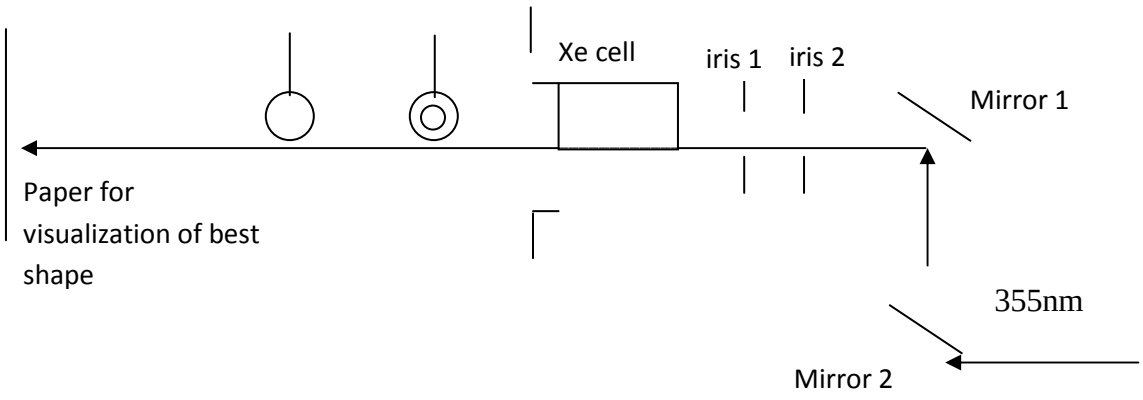

Figure A.2 Alignment of the 355nm light.

(3) Adjustment with NO Cell (Needed only for initial alignment)

Fill the NO cell with several Torr of NO and then pumped out by mechanical pump so that only a fraction of a Torr of NO remains in the cell. Fill the Xe cell with ~20-30 Torr. Maximize the photoionization signal of NO from the NO cell by adjusting the UV focus lens (between the Xe cell and iris 1) and optimizing the Xe pressure. The NO^+ signal is observed by placing a 145V-180V potential across the NO cell and monitoring the signal with an oscilloscope. For normal operation, 1 Meg ohm input impedance on the oscilloscope is required (with for the MCP detector of the TOFMS, 50 ohm impedance is used). The signal should be found somewhere within the 20-100 microsecond time scale. Adjust the vertical and horizontal positions of the UV focus lens to optimize NO^+ signal.

(4) Final Adjustment with TOFMS

Optimize mass signal while adjusting the UV lens vertical and horizontal. On the digital delay generator channel C is connected to the flashlamp of the laser and set to T_0. The Q-switch runs from channel D and is set to C + 3.220 milliseconds (adjusted to optimize the Nd:YAG laser output). The pulse valve driver runs from channel B set to D – 1.20000

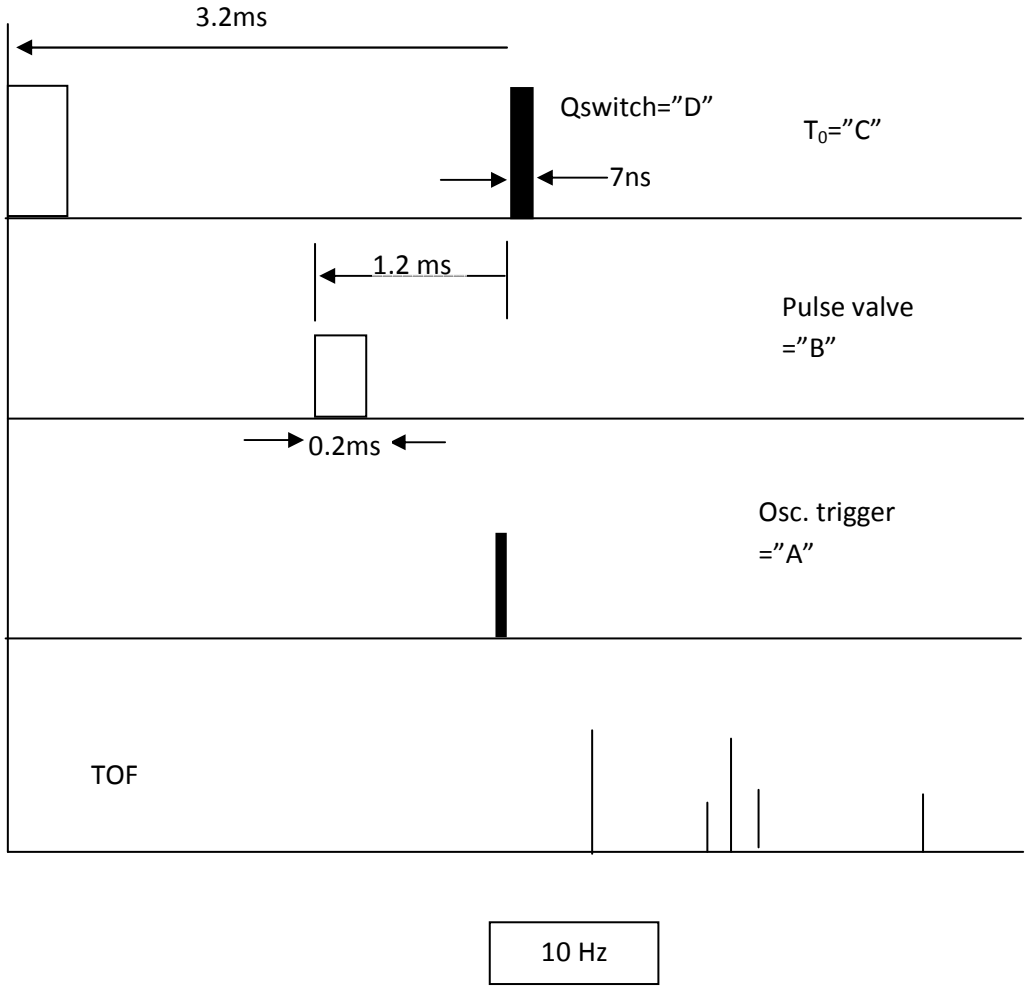

Figure A.3 Depiction of timing elements used in the experiments.

milliseconds. The oscilloscope trigger runs from channel A and is set to D – 0.000000250 seconds. These parameters can be altered to enhance signal. In particular the pulse valve driver (channel B) can be adjusted to "catch" the sample pulse that has a sharp onset and extended tail.

APPENDIX B

PULSE DRIVER UPKEEP

The pulse driver employed currently is the IOTA ONE (General Valve Corp.)

The duration of the opened valve should be at least 160 μs in duration. To check the actual performance of the timing circuitry of the valve driver one can use an oscilloscope to view the TTL sync output signal duration and the voltage magnitude. To be in a reasonable time domain it is desired to trigger from the flashlamp. Adjust the oscilloscope to appropriate time scale (200-400 μs per division) and potential scale (2-4 Volts per division). View the signal to make sure it is within the parameters listed above. Further check if the high voltage output might be needed.

After a period of usage, perhaps weeks or so, the pulse driver will need to be cleaned. This is accomplished by disconnecting the gas inlet tubing from the pulse valve assembly. Be careful of the metal tubing attached to the pulse valve as it can slide and change the position of the nozzle in relation to the skimmer. The side faceplate flange opposite the laser entrance (with NO cell) is removed and then electrical connections are removed from their electrodes on the main chamber. When setting the side flange down it is advised to place the machined face on cardboard or several paper towels. The faceplate with the pulse valve can then be removed, taking great care to not break wires. This faceplate will have the pulse valve assembly attached to it and is conveniently placed on

top of an appropriate sized bucket so the interior of the system can be inspected. The electric wires should be removed first before dissembling the valve. The actual pulse valve on the inside screws off. However, the assembly is a slide fit so the base where the pulse valve connects must be held in place. Once the pulse valve is disassembled it can wiped with methanol wet cotton applicator or KIM wipe. After, they can be sonicated in methanol for further cleaning. The tip should be inspected for damage and can be replaced (Parker Hannifin Corp – General Valve Corp). The connecting board which houses the electrodes for the electronics can be inspected. Clean in the same manner as above if necessary, ceramic parts can be sanded with very fine grit sandpaper.

When the pulse valve is reassembled and reattatched to it's faceplate one should adjust the tightness of the front plate. If the valve is attached too tightly the valve will not flow and if it is not tight enough the flow will be very poor. Start from the tightened assembly and while holding the base piece twist the nozzle board to a looser setting. Check the flow out put by applying a pressure gradient and operating the pulse valve. The pressure of the pulses can be monitored with your lips. Optimize.

Now the faceplate with pulse valve assembly and nozzle can be reattached (careful of those wires!) being sure not to pinch wires while fastening. Electrical connections are reestablished and the resistance across circuits is measured and checked against ground for shorts. In this instance the resistance across the thermocouple was 2 ohm, pulse valve

12 ohm, and across the heater 98 ohm. The heater to thermocouple resistances are measured to be 53 and 65 ohm, approximately half each of the total heater circuit.

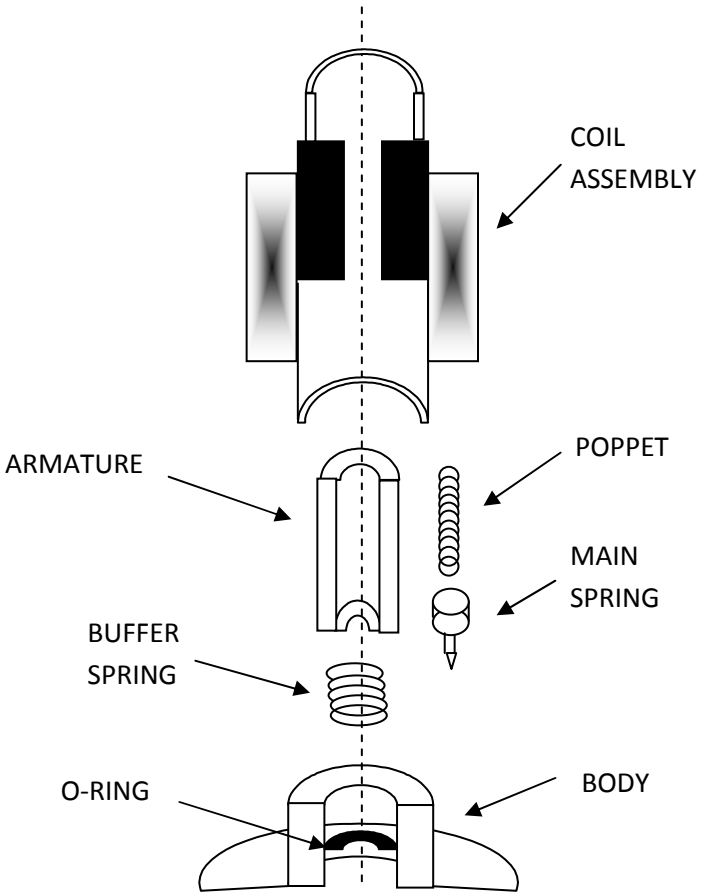

Figure B.1 Diagram of the pulse driver assembly

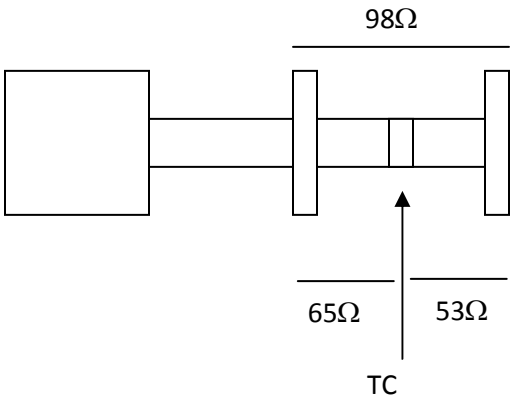

Figure B.2 Diagram of the nozzle heater resistances.